



# Films multicouches à base de polyélectrolytes biodégradables : caractérisation physico-chimique et interaction avec des cellules

Ludovic Richert

## ► To cite this version:

Ludovic Richert. Films multicouches à base de polyélectrolytes biodégradables : caractérisation physico-chimique et interaction avec des cellules. Biotechnologies. Université Henri Poincaré - Nancy 1, 2004. Français. NNT : 2004NAN11303 . tel-01776031

HAL Id: tel-01776031

<https://hal.univ-lorraine.fr/tel-01776031>

Submitted on 24 Apr 2018

**HAL** is a multi-disciplinary open access archive for the deposit and dissemination of scientific research documents, whether they are published or not. The documents may come from teaching and research institutions in France or abroad, or from public or private research centers.

L'archive ouverte pluridisciplinaire **HAL**, est destinée au dépôt et à la diffusion de documents scientifiques de niveau recherche, publiés ou non, émanant des établissements d'enseignement et de recherche français ou étrangers, des laboratoires publics ou privés.



## AVERTISSEMENT

Ce document est le fruit d'un long travail approuvé par le jury de soutenance et mis à disposition de l'ensemble de la communauté universitaire élargie.

Il est soumis à la propriété intellectuelle de l'auteur. Ceci implique une obligation de citation et de référencement lors de l'utilisation de ce document.

D'autre part, toute contrefaçon, plagiat, reproduction illicite encourt une poursuite pénale.

Contact : [ddoc-theses-contact@univ-lorraine.fr](mailto:ddoc-theses-contact@univ-lorraine.fr)

## LIENS

Code de la Propriété Intellectuelle. articles L 122. 4

Code de la Propriété Intellectuelle. articles L 335.2- L 335.10

[http://www.cfcopies.com/V2/leg/leg\\_droi.php](http://www.cfcopies.com/V2/leg/leg_droi.php)

<http://www.culture.gouv.fr/culture/infos-pratiques/droits/protection.htm>

2004/251

T/NCY/look/303  
(double)

04303

UNIVERSITE HENRI POINCARÉ - NANCY I  
FACULTE DE MEDECINE

183 069  
19 JUIL. 2005  
e  
C



N° attribué par la bibliothèque

███████████████████

THESE

pour obtenir le grade de

**DOCTEUR DE L'UNIVERSITE HENRI POINCARÉ**

*Discipline : Bioingénierie*

présentée et soutenue publiquement

par

**RICHERT Ludovic**

le 23 septembre 2004

Titre :

**FILMS MULTICOUCHES A BASE DE  
POLYELECTROLYTES BIODEGRADABLES :**

CARACTERISATION PHYSICO-CHIMIQUE ET INTERACTION AVEC DES CELLULES

Directeur de Thèse

Professeur Catherine PICART

JURY

Professeur Jean-François STOLZ (Président)  
Professeur Alain DOMARD (Rapporteur)  
Professeur Marcus TEXTOR (Rapporteur)  
Professeur Jean-Claude BLOCK (Examinateur)  
Professeur Catherine PICART (Examinateur)  
Professeur Jean-Claude VOEGEL (Examinateur)

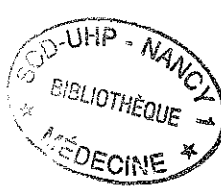


# Table des matières

<b>TABLE DES MATIERES .....</b>	<b>1</b>
<b>INTRODUCTION GENERALE.....</b>	<b>3</b>
<b>ABREVIATIONS ET SYMBOLES.....</b>	<b>5</b>
<b>CHAPITRE 1 : REVUE BIBLIOGRAPHIQUE.....</b>	<b>7</b>
<b>    1.1 : Traitement de surface des biomatériaux.....</b>	<b>8</b>
1.1.1. Propriétés physico-chimiques de la surface.....	8
1.1.2. Dépôt et greffage de molécules .....	10
1.1.3. Assemblages basés sur les interactions faibles. ....	10
<b>    1.2 : Films multicouches de polyélectrolytes : aspects physico-chimiques .....</b>	<b>11</b>
1.2.1. Principe de dépôt des films multicouches .....	11
1.2.2. Différentes méthodes de dépôt. ....	12
1.2.3. Nature des interactions .....	13
1.2.3.1. Interactions électrostatiques.....	14
1.2.3.2. Liaisons hydrogènes et interactions hydrophobes.....	14
1.2.4. Différents modes de croissance .....	15
1.2.4.1. Films à croissance linéaire.....	15
1.2.4.2. Films à croissance exponentielle.....	15
1.2.4.3. Exemples de paramètres pouvant être modulés .....	17
1.2.5. Renforcer la cohésion des films multicouches par la réticulation .....	18
<b>    1.3 : Applications des films multicouches au domaine des biomatériaux.....</b>	<b>21</b>
1.3.1. Mise au contact du milieu biologique .....	22
1.3.1.1. Adsorption de protéines.....	22
1.3.1.2. Adhésion cellulaire .....	23
1.3.2. Fonctionnalisation des films multicouches par des protéines et des peptides .....	25
1.3.2.1. Activité anticoagulante.....	26
1.3.2.2. Activité des protéines ou molécules enfouies au sein des films multicouches .....	26
1.3.2.3. Fonctionnalisation par couplage de peptides ou molécules.....	28
1.3.3. Encapsulation de cellules dans les films multicouches.....	28
<b>CHAPITRE 2 : MATERIELS ET METHODES.....</b>	<b>30</b>
<b>    2.1 : Matériels.....</b>	<b>31</b>
2.1.1. Polyélectrolytes .....	31
2.1.2. Construction des films multicouches de polyélectrolytes .....	33
<b>    2.2 : Méthodes.....</b>	<b>35</b>
2.2.1. Analyses physico-chimiques .....	35
2.2.1.1. Spectroscopie optique par guide d'onde.....	36
◆ Principe et description de la technique .....	36
◆ Dispositif expérimental.....	37
◆ Protocole expérimental.....	39
◆ Traitement du signal.....	40
2.2.1.2. Microbalance à cristal de quartz .....	41
◆ Principe.....	41
◆ Protocole expérimental.....	44
2.2.1.3. Mesure du potentiel d'écoulement .....	45
◆ La double couche électrique .....	45
◆ Dispositif expérimental.....	46
◆ Procédure de mesure .....	47
2.2.1.4. Microscopie de fluorescence .....	48
◆ Microscopie à épi-fluorescence.....	48
◆ Microscopie confocale.....	49

◆ Principe.....	51
◆ Mode image.....	52
◆ Mode force.....	54
<b>2.2.2. Analyses Biologiques.....</b>	<b>58</b>
2.2.2.1. Culture de chondrosarcomes.....	58
2.2.2.2. Culture des chondrocytes .....	58
2.2.2.3. Observation cellulaire .....	58
2.2.2.4. Dosage cellulaire.....	59
◆ Test MTT.....	59
◆ Dosage à la <sup>3</sup> H-thimidine.....	59
◆ Marquages fluorescents .....	59
2.2.2.5. Bactéries .....	60
2.2.2.6. Technique d'aspiration par micropipette.....	61
◆ Fabrication des micropipettes .....	61
◆ Mesure de la pression d'aspiration .....	61
◆ Chambre de mesure et dispositif expérimental .....	62
◆ Protocole de mesure de la force de détachement cellulaire.....	63
◆ Analyse statistique des données .....	64
<b>CHAPITRE 3 : FILMS MULTICOUCHES DE POLYPEPTIDES : RELATIONS ENTRE LES PROPRIETES PHYSICO-CHIMIQUES ET L'ADHESION CELLULAIRE.....</b>	<b>65</b>
<b>3.1 : Influence de l'épaisseur et de la couche terminale des films multicouches (poly(L-lysine)/acide poly(glutamique)) sur la force de détachement cellulaire.....</b>	<b>67</b>
3.1.1. Résumé 1 .....	67
3.1.2. Article 1.....	69
<b>3.2 : Influence du pH de construction des films multicouches sur leurs propriétés physico-chimiques et sur l'adhésion cellulaire.....</b>	<b>78</b>
3.2.1. Résumé 2 .....	78
3.2.2. Article 2.....	80
<b>CHAPITRE 4 : RETICULATION DES FILMS MULTICOUCHES DE (POLY(L-LYSINE)/HYALURONANE) : CONSEQUENCES SUR LES PROPRIETES PHYSICO-CHIMIQUES, MECANIQUES ET D'ADHERENCE DES FILMS.....</b>	<b>97</b>
<b>4.1 : Modification des propriétés physico-chimiques des films multicouches par réticulation.....</b>	<b>99</b>
4.1.1. Résumé 3 .....	99
4.1.2. Article 3.....	100
<b>4.2 : Propriétés mécaniques de films natifs et réticulés : relation à l'adhésion cellulaire. 111</b>	<b>111</b>
4.2.1. Résumé 4 .....	111
4.2.2. Article 4.....	112
<b>4.3 : Adhésion de chondrocytes sur des films natifs et réticulés : observations microscopiques. ....</b>	<b>121</b>
4.3.1. Résumé 5 .....	121
4.3.2. Article 5.....	122
<b>CHAPITRE 5 : FILMS MULTICOUCHES A BASES DE POLYSACCHARIDES (CHITOSAN/HYALURONANE) : PROPRIETES PHYSICO-CHIMIQUES ET BIOLOGIQUES. ....</b>	<b>135</b>
<b>5.1 : Résumé 6.....</b>	<b>136</b>
<b>5.2 : Article 6 .....</b>	<b>137</b>
<b>CONCLUSION ET PERSPECTIVES.....</b>	<b>148</b>
<b>BIBLIOGRAPHIE.....</b>	<b>152</b>
<b>ARTICLES PUBLIÉS AU COURS DE LA THÈSE .....</b>	<b>159</b>

# **Introduction générale**

---

L'intégration d'un implant dans son environnement biologique est un phénomène complexe qui va dépendre des propriétés de surface du matériau et de celles du tissu hôte. Durant ces dernières années, les efforts de nombreux chercheurs se sont tournés vers le traitement de surface du matériau afin de lui conférer de nouvelles propriétés. L'objectif est de contrôler la réaction cellulaire au contact du matériau implanté. Ainsi, on peut rechercher à contrôler la réaction inflammatoire, à créer des surfaces résistantes à la formation de biofilms bactériens...

Les films multicouches de polyélectrolytes font partie des nouveaux traitements de surface utilisés pour modifier les propriétés d'un matériau. En effet, il apparaît possible, à l'aide de ces films auto-assemblés de polyélectrolytes, d'influencer fortement le comportement cellulaire à leur contact. C'est précisément dans cette perspective que se situe ce travail de thèse, l'objectif principal étant la mise au point de plusieurs types de films à base de polypeptides et de polysaccharides et d'évaluer le comportement cellulaire sur ces films.

Le chapitre 1 sera consacré à l'état des travaux et des connaissances dans le traitement de surface et, plus particulièrement, dans l'utilisation des films multicouches pour fonctionnaliser la surface des biomatériaux. Dans le chapitre 2 seront décrites les différentes techniques utilisées lors de la réalisation des travaux. Dans le chapitre 3, nous nous intéresserons à des films à base de polypeptides et étudierons les propriétés d'adhésion de chondrosarcomes en fonction de l'épaisseur du film multicouche. Des tests d'adhésion quantitative par micromanipulation ont été mis au point pour mesurer la force de détachement des cellules sur les films multicouches.

Dans le chapitre 4, nous porterons notre attention sur des films à base de hyaluronane et de poly(L-Lysine). Nous montrerons qu'il est possible de réticuler ces films et que la réticulation a une grande influence sur l'adhésion cellulaire. Nous réaliserons également des mesures quantitatives par nano-indentation par AFM pour déterminer le module d'Young de ces films et montrerons que l'adhésion est directement reliée aux propriétés mécaniques du film. Nous étudierions également l'adhésion de cellules primaires de type chondrocytes sur ces films natifs et réticulés.

Dans le chapitre 5, nous nous focaliserons sur la réalisation de films à base de polysaccharides, le chitosane et le hyaluronane. Ces deux polysaccharides présentant des

propriétés biologiques et de biocompatibilité, il serait en effet intéressant de pouvoir déposer de tels films sur des matériaux. Nous avons recherché à déterminer les conditions optimales de construction pour ces films et nous avons également évalué leurs activités biologiques.

Enfin, nous conclurons ce travail et différentes perspectives permettant de poursuivre ce travail, seront présentés.

# Abréviations et symboles.

---

## Polymères:

Alg :	alginate
CHI:	chitosane
HA:	hyaluronane de sodium (appelé hyaluronane)
PAA:	acide poly(acrylique)
PAAm :	poly(acrylamide)
PAH:	poly(allylamine hydrochloridrique)
PDADMAC :	poly(diallyldimethylammonium)
PEG:	poly(éthylène glycol)
PEI:	poly(éthylène imine)
PGA:	acide poly(L-glutamique)
PLL:	poly(L-lysine)
PMA-P:	acide poly(maléique-co-propylène)
PSS:	poly(styrène sulfonate)
PVS:	sulfate de poly(vinyle)

## Protéines et enzymes

BMP :	protéine morphogénique osseuse : “ bone morphogenic protein ”
GA:	glucose amylase
GFP:	protéine fluorescente verte : “ green fluorescence protein ”
GOD:	D-glucose oxydase
HSA:	albumine sérique humaine : “ human serum albumin ”
IgG:	immunoglobuline G
$\alpha$ -MSH:	$\alpha$ -mélanocortine : “alpha-melanocyte stimulating hormone”
TNF $\alpha$ :	facteur de nécrose de tumeurs : ” tumoral necrose factor ”
VGF :	facteur de croissance vasculaire : “vascular growth factor ”
RGD :	Arginine - Glycine - Asparagine
GVGVP :	Glycine – Valine – Glycine – Valine – Proline
BDNF :	facteur neurotrophique : “ brain-derived growth factor ”

**Réactifs et solvants utilisés :**

EDC:	1-Ethyl-3-(3-diméthylamino-propyl) carbodiimide
Sulfo-NHS:	N-hydroxysulfo succinimide
MES :	acide 2-(N-morpholino) ethanesulfonique
Tris :	tris(hydroxy méthyle) aminométhane
FITC :	fluorescéine isothiocyanate
TR :	rouge Texas

**Appareils et techniques utilisés :**

OWLS:	spectroscopie optique par guide d'onde
QCM-D :	microbalance à cristal de quartz avec étude de la dissipation
CLSM :	microscopie confocale
FRAP :	mesure de fluorescence après photo-blanchiment
AFM:	microscopie à force atomique
FTIR:	spectroscopie infrarouge à transformée de Fourier

# **Chapitre 1 : Revue Bibliographique**

---

<b>1.1 : Traitement de surface des biomatériaux .....</b>	<b>8</b>
1.1.1. Propriétés physico-chimiques de la surface.....	8
1.1.2. Dépôt et greffage de molécules.....	10
1.1.3. Assemblages basés sur les interactions faibles.....	10
<b>1.2 : Films multicouches de polyélectrolytes : aspects physico-chimiques .....</b>	<b>11</b>
1.2.1. Principe de dépôt des films multicouches.....	11
1.2.2. Différentes méthodes de dépôt.....	12
1.2.3. Nature des interactions.....	13
1.2.3.1. Interactions électrostatiques.....	14
1.2.3.2. Liaisons hydrogènes et interactions hydrophobes.....	14
1.2.4. Différents modes de croissance .....	15
1.2.4.1. Films à croissance linéaire.....	15
1.2.4.2. Films à croissance exponentielle. ....	15
1.2.4.3. Exemples de paramètres pouvant être modulés.....	17
1.2.5. Renforcer la cohésion des films multicouches par la réticulation.....	18
<b>1.3 : Applications des films multicouches au domaine des biomatériaux.....</b>	<b>21</b>
1.3.1. Mise au contact du milieu biologique .....	22
1.3.1.1. Adsorption de protéines.....	22
1.3.1.2. Adhésion cellulaire .....	23
1.3.2. Fonctionnalisation des films multicouches par des protéines et des peptides.....	25
1.3.2.1. Activité anticoagulante.....	26
1.3.2.2. Activité des protéines ou molécules enfouies au sein des films multicouches .....	26
1.3.2.3. Fonctionnalisation par couplage de peptides ou molécules .....	28
1.3.3. Encapsulation de cellules dans les films multicouches.....	28

---

## 1.1 : Traitement de surface des biomatériaux

Dans tout processus de contact entre un biomatériau et un tissu intervient une cascade d'évènements, conséquence notamment de l'adsorption de protéines puis de l'adhésion (ou non) de diverses cellules (plaquettes, cellules inflammatoires...) à la surface du solide. Ces phénomènes initiaux sont primordiaux car ils conditionnent les évènements ultérieurs à l'interface biomatériau/tissu et notamment l'organisation, la prolifération et la motilité cellulaire (Ratner et al., 1996). Le contrôle des phénomènes interfaciaux est crucial en implantologie où le matériau est susceptible d'induire des phénomènes de proximité, comme l'adhésion de bactéries (Van Loosdrecht et al., 1990). Ceux-ci peuvent entraîner des modifications tissulaires ou des modifications de la surface du biomatériau qui peuvent favoriser ou compromettre la bonne intégration de l'implant (Gristina, 1994).

Désormais, on ne recherche donc plus uniquement à ce que les matériaux soient inertes ou biocompatibles, comme peut l'être le titane par exemple, mais de nombreux travaux visent à rendre la surface des matériaux bioactive et à modifier les interactions entre le matériau et les tissus environnants (Healy, 1999; Hubbell, 1999). Les premiers phénomènes d'interaction font intervenir les protéines et les cellules.

Dans le but de modifier ces surfaces, diverses approches peuvent être utilisées :

- la modulation des propriétés physiques telles que la mouillabilité, la charge de surface, la topographie ou la rugosité.
- le greffage de molécules en surface du matériau ou le dépôt par adsorption de molécules, en vue de former des films « biomimétiques ».
- le dépôt de films auto-assemblés de polyélectrolytes, appelés films multicouches de polyélectrolytes.

Selon les applications recherchées, le recouvrement de surface devra être stable dans le temps ou il pourra être dégradé rapidement, selon que l'action doit se poursuivre sur plusieurs mois voire années, ou sur quelques heures.

### 1.1.1. Propriétés physico-chimiques de la surface

De nombreux paramètres sont reconnus influencer l'adsorption protéique et l'adhésion cellulaire. Parmi ceux-ci, on peut citer :

- la mouillabilité de la surface : le caractère hydrophobe/hydrophile d'une surface joue un rôle sur l'adsorption des protéines et sur l'étalement cellulaire. Ainsi, les travaux de Vogler (Vogler et al., 1999), (Figure 1-1) montrent qu'il y a une zone

d'angle de contact et de tension de surface dans laquelle l'étalement cellulaire est optimum, que ce soit en présence ou en absence de sérum. Les conditions extrêmes, très forte hydrophilie ou très forte hydrophobie, sont en revanche défavorables.

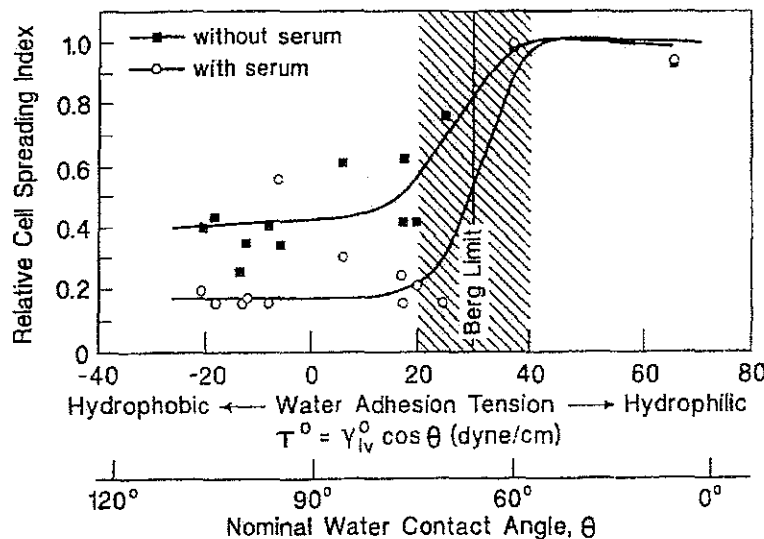


**Figure 1-1 : Evolution de l'étalement cellulaire de fibroblastes en fonction de la tension de surface et de l'angle de contact du substrat (plastique et verre) en présence ou en absence de sérum dans le milieu de culture (Vogler et al., 1999) (la référence 100% étant l'étalement cellulaire sur une surface avec un angle de contact de l'eau à 60°)**

- la charge de surface : il est reconnu que la charge de surface influence l'adsorption protéique, puisque des protéines sériques ont globalement une charge (pour la plupart négatives à pH physiologique). Il semblerait également que la charge influence l'adsorption d'ions calciums et phosphates, qui eux-mêmes peuvent jouer un rôle sur l'adhésion cellulaire. (Qiu et al., 1998) ont montré sur des surfaces d'oxyde d'indium et d'étain dont la charge était électriquement modulée que les cellules adhèrent plus sur les surfaces positives. En revanche, leur étalement et leur différentiation sont moindre.
- La topographie et la rugosité de surface : la topographie de surface et en particulier sa rugosité ont une grande importance vis-à-vis de l'adsorption protéique et de l'adhésion cellulaire. Ainsi, la « nano-rugosité » conditionne l'adsorption protéique : selon, Kasemo (Kasemo, 1998), une rugosité de l'ordre d'une cinquantaine de nanomètres favoriserait une adsorption stable des protéines, en raison de la présence de « niches » permettant un bon ancrage des protéines. En revanche, une rugosité inférieure à 30 nm serait moins favorable à l'adsorption protéique et à l'adhésion cellulaire (Dalby et al., 2002) .
- En ce qui concerne la « micro-rugosité », elle peut permettre une meilleure

adhésion de certains types cellulaires (Cooper, 2000) mais peut aussi être à l'origine d'une forte adhésion bactérienne et des macrophages (Salthouse, 1984) avec le risque associé de réactions inflammatoires chroniques.

### **1.1.2. Dépôt et greffage de molécules**

Divers types de molécules peuvent être déposés à la surface des matériaux. Voici quelques exemples d'activation de surfaces, qui ne constituent pas une liste exhaustive :

- des molécules de polyéthylène glycol peuvent être greffées pour limiter l'adsorption protéique et l'adhésion bactérienne (Park et al., 1998; Zhang et al., 1998).
- des monocouches auto-assemblées (SAMs) contenant des groupements fonctionnels différents peuvent également contribuer à modifier l'adhésion cellulaire en modifiant l'énergie de surface et leur caractère hydrophile/hydrophobe (Margel et al., 1993).
- lorsqu'il s'agit de favoriser l'ancre osseux, de l'hydroxyapatite peut être déposée, notamment sur des prothèses de titane (Ohgaki et al., 2001).
- des composants de la matrice extracellulaire ou des molécules naturelles, notamment collagène, acide hyaluronique, héparine, alginat... sont souvent utilisés pour fabriquer des films biomimétiques et moduler les propriétés d'adhésion cellulaire et de coagulation (Baldwin and Saltzman, 1998; Bos et al., 1999).
- des peptides d'adhésion ou des facteurs de croissance (par exemple basic fibroblast growth factor) peuvent aussi être mis à profit. Le plus connu des peptides est sans doute le peptide RGD dont le greffage peut être réalisé des surfaces modèles (Rezania and Healy, 1999), sur des polymères (Shu et al., 2004) ou sur d'autres types de surfaces.

Généralement, les techniques de greffage qui ne sont pas basées sur une adsorption simple requièrent un traitement préalable de la surface, c'est-à-dire son activation. Une silanisation peut ainsi être nécessaire sur des surfaces métalliques.

### **1.1.3. Assemblages basés sur les interactions faibles.**

L'attraction électrostatique a été mise à profit pour la préparation de films autoassemblés. Cette approche simple consiste à adsorber sélectivement des espèces

anioniques et cationiques à partir de solutions aqueuses. Dès 1966, Iler (Iler, 1966) avait démontré l'intérêt de l'interaction électrostatique pour préparer des multicouches constituées de particules colloïdales anioniques et cationiques. Cette idée est tombée dans l'oubli, certainement à cause du manque d'équipements adéquats pour la caractérisation des films. D'autre part, à l'époque, on pensait que le dépôt de polyélectrolytes de charges opposées s'arrêtait quand les charges du polycation avaient exactement compensé les charges du polyanion.

Gölander et al. (Gölander et al., 1982) ont ensuite préparé des films présentant des propriétés anti-thrombotiques sur des surfaces de polyéthylène, par adsorption successive de colloïdes biologiques cationiques et d'héparine. Toutefois, après un dépôt de cinq à six paires de couches, les auteurs observaient un phénomène de flocculation en surface.

A la suite de ces travaux, ce n'est qu'au début des années 1990 que les travaux de Decher ont véritablement mis en valeur la méthode d'assemblage couche par couche, appliquée en particulier à des polyélectrolytes chargés (Decher, 1997; Decher et al., 1998; Decher and Hong, 1991; Decher et al., 1992; Lvov et al., 1993).

## 1.2 : Films multicouches de polyélectrolytes : aspects physico-chimiques

### 1.2.1. Principe de dépôt des films multicouches

La méthode de dépôt couche par couche (LbL de l'anglais « Layer by Layer ») est basée essentiellement sur les interactions électrostatiques qui existent entre des espèces anioniques et cationiques qui sont adsorbées alternativement sur un support. Son principe est décrit schématiquement dans la Figure 1-2. Un substrat chargé négativement est mis au contact d'une solution de polycation pendant un temps donné (typiquement 5 à 30 min). Les polycations s'adsorbent sur la surface et les molécules non adsorbées sont éliminées par simple rinçage. Après rinçage, la surface est chargée positivement car il y a surcompensation de charges lors de l'adsorption (Caruso et al., 1998; Ladam et al., 2000a). Par conséquent, lorsque le substrat est mis au contact avec une nouvelle solution de polyanions, ceux-ci peuvent également interagir et s'adsorber sur la surface. Cette adsorption est suivie d'une étape de rinçage à l'issue de laquelle la surface est chargée négativement. La surcompensation de charge après chaque dépôt a été mise en évidence par des mesures du potentiel zéta

(Caruso et al., 1998; Hoogeveen et al., 1996) (Ladam et al., 2000a) et constitue le moteur de la construction des films multicouches.

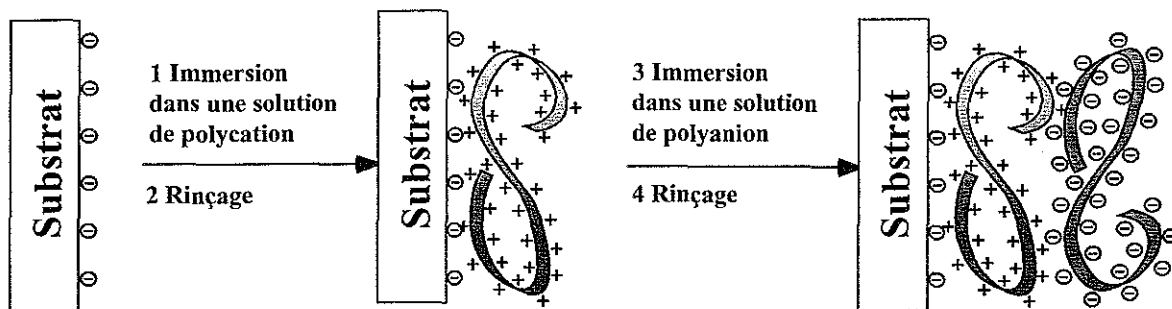


Figure 1-2 : Schéma simplifié de la construction d'un film multicouche de polyélectrolytes par adsorptions successives de polycations et de polyanions sur un substrat. Le substrat (ici chargé négativement) est initialement immergé dans une solution contenant un polycation (1) après rinçage (2) l'ensemble est alors immergé dans une solution polyanionique (3) et de nouveau rincé (4). Le cycle peut-être reproduit n fois jusqu'à l'obtention d'un film d'épaisseur désirée (Decher, 1997).

### 1.2.2. Différentes méthodes de dépôt.

La méthode « traditionnelle » de dépôt est celle du procédé d'immersion en solution, ou « dip-coating », dans laquelle il s'agit de tremper un substrat dans un bain de polyanions ou polycations. Cette méthode permet facilement de varier les temps de trempage et de rinçage. De même, il est possible de faire varier le taux de sel ou le pH des solutions, de sécher ou non le film après dépôt de chaque couche... Cependant, le procédé d'immersion en solution peut être responsable de désordre local au niveau de l'interface entre deux couches déposées (Schmitt et al., 1993). Ce désordre n'est pas désiré lorsque l'on recherche à construire un film fortement stratifié et structuré, comme c'est le cas pour la préparation de cellules photovoltaïques (Kim and Sandman, 2001).

D'autres techniques de dépôt ont été étudiées en vue de changer la structuration des films ou de les déposer plus rapidement. Ainsi, les polyélectrolytes peuvent être déposés à l'aide d'un procédé aérosol, le spray, contenant alternativement des polycations et polyanions. Schlenoff et al (Schlenoff et al., 2000) ont ainsi construit des films à base de PSS/PDADMAC en présence de sel (1M) en effectuant un rinçage entre chaque couche. Les auteurs ont comparé ces films à ceux réalisés par immersion et montrent que les spectres infrarouges ainsi que la perméabilité aux ions est identique. De même, pour des temps de contact similaires, les épaisseurs mesurées par ellipsométrie sont similaires.

Une autre possibilité consiste à utiliser la méthode de « spin coating ». Il s'agit de déposer une gouttelette de polyélectrolytes sur une surface en rotation qui est étalée par force centrifuge lorsque la surface est mise en mouvement. Le temps de dépôt d'une seule couche peut être ainsi réduit à quelques secondes (Chiarelli et al., 2001). En utilisant des solvants très volatiles, il est donc possible de construire des films sans rinçage entre les dépôts de polyélectrolytes. Les films déposés par cette méthode présentent une stratification homogène (Figure 1-3).

Enfin, on peut citer une autre technique de dépôt qui permet de réaliser des réseaux microgravés des films multicouches. Guo et al (Guo et al., 2002) ont déposé des films à base de PAH/PAA sur un substrat en polyéthylène téréphthalate en utilisant un dépôt par jet d'encre.

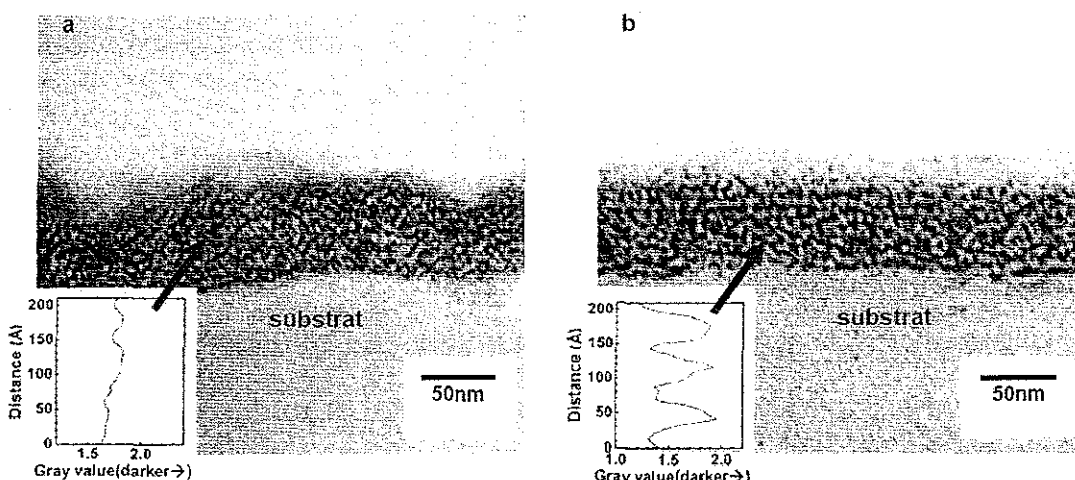


Figure 1-3 : Observation et comparaison de la structure des films multicouches  $(\text{PSS/PAH})_{20}$  construit par immersion (a) et par spin coating (b) observés par microscope électronique à transmission. En encart est représenté le niveau de gris en fonction de la position normale dans le film, le film obtenu par immersion présente un niveau de gris relativement constant quelque soit la position en z. En revanche, pour le film obtenu par spin coating, on observe une forte stratification. (Cho et al., 2001)

### 1.2.3. Nature des interactions

Outre les interactions électrostatiques, des forces secondaires à courte distance ont également une influence sur l'épaisseur et la morphologie finales. Des études récentes ont permis d'approfondir la compréhension du rôle des interactions électrostatiques et de leurs combinaisons avec d'autres types d'interaction, comme les interactions hydrogènes et hydrophobes.

### 1.2.3.1. *Interactions électrostatiques.*

Pendant longtemps, les études ont porté sur le comportement de polyélectrolytes fortement chargés dont on peut écraner les charges en augmentant la force ionique. Plus récemment, des polyélectrolytes faibles, dont la densité de charge change avec le pH, ont été étudiés. Par exemple, la densité de charges d'un polyanion augmente avec le pH car les groupements acides se déprotonent. L'équipe de Rubner a plus spécifiquement étudié le système PAA/PAH composé de deux polyélectrolytes faibles (Mendelsohn et al., 2000; Shiratori and Rubner, 2000; Yoo et al., 1998). Ces polyélectrolytes ont respectivement un pKa de 5 et 9 en solution. Shiratori et al (Shiratori and Rubner, 2000) ont représenté l'épaisseur des films PAA/PAH en fonction du pH. Ainsi, à pH 7, ces polyélectrolytes s'assemblent en couches très interpenetrées où les chaînes adoptent une conformation plate. L'épaisseur est de 3 à 5 Å par paire de couche. Si le pH des solutions est proche d'un des pKa, l'épaisseur des couches augmente alors de manière importante. Ainsi, à pH 5, l'augmentation d'épaisseur est de 80 Å pour le PAH et de 45 Å pour le PAA, ce qui peut être expliqué par la présence de boucles et de repliement des polymères.

Outre la modulation d'épaisseur des films, le changement de pH a pour effet de moduler la tension de surface (Yoo et al., 1998) et la micro-porosité par changement de pH après construction du film (Mendelsohn et al., 2000). Pour plusieurs systèmes de multicoques, il a été montré que les films présentent un rapport stœchiométrique de 1 : 1 entre les groupes anioniques et cationiques. Cependant, il semblerait que le rôle des contre ions soit primordial et puisse modifier la stœchiométrie entre les charges des polyélectrolytes. Ainsi, Salomaki et al. (Salomaki et al., 2004) ont montré que des films (PSS/PDADMAC) formés en présence d'ions chaotropiques ( $\text{Br}^-$ ,  $\text{NO}_3^-$ ) sont environ trois fois plus épais que des films construits en présence de  $\text{F}^-$  et d'acide acétique. Cette augmentation d'épaisseur serait attribuée à la désorganisation des polyélectrolytes par les ions chaotropiques qui favoriseraient une structure désordonnée dans le film, les polyélectrolytes adoptant une conformation en boucle. Cependant, le rôle exact des contre-ions est encore l'objet de nombreuses études (Schönhoff, 2003).

### 1.2.3.2. *Liaisons hydrogènes et interactions hydrophobes.*

Les liaisons hydrogènes peuvent être impliquées dans l'assemblage des polyélectrolytes (Sukhishvili and Granick, 1998; Wang et al., 2000). Ainsi, la cohésion des films multicoques à base de poly(acrylamide) et d'acide poly(acrylique) construits à pH 3 reposeraient essentiellement sur les liaisons hydrogènes, car la plupart des groupements acides du

polyacrylamide sont non ionisés. Le problème de ces films est alors leur stabilité lorsque le pH est élevé, ce à quoi les auteurs pallient en procédant à leur réticulation par voie thermique (90°C pendant 8H).

Plusieurs études ont examiné le rôle des interactions hydrophobes dans l'élaboration des films multicouches. Il semblerait que des polyélectrolytes hydrophobes puissent former des multicouches relativement stables (Cochin and Laschewsky, 1999). De plus, il est possible de construire des films multicouches sur des surfaces polymériques très hydrophobes et non chargées (Delcorte et al., 1997).

#### **1.2.4. Différents modes de croissance**

##### *1.2.4.1. Films à croissance linéaire.*

Ce type de films est caractérisé par une épaisseur constante pour chaque paire de couche déposée. Dans ces films, les polyélectrolytes interagissent avec les polyélectrolytes de charge opposée constituant la surface externe du film (Decher, 1997). Le système poly(allylamine hydrochloride)/poly(styrene sulfonate) (PAH/PSS) en est sans doute l'exemple le plus largement étudié. Des analyses réalisées par réflexion de RX et neutrons ont montré que ces films sont pseudo-stratifiés, en raison de la présence de pic de Bragg en réflectivité de neutrons lorsque les polyélectrolytes sont deutérés (Decher, 1997; Lösche, 1997). Il existe donc une inter-pénétration entre couches adjacentes, conférant au film une homogénéité de structure et de distribution de charges (Decher et al., 1994; Schmitt et al., 1993). Plusieurs paramètres caractérisant ces films à croissance linéaire peuvent être contrôlés tels que l'épaisseur, la densité, et leur structure. Par exemple, le choix de différents polycations et polyanions, faibles ou forts, permet de moduler l'épaisseur des films, de même que l'augmentation de la force ionique en solution. En effet, la conformation des polyélectrolytes dépend du taux de sel en solution : à faible concentration, il existe une grande longueur de persistance en raison des répulsions entre les charges du polyélectrolyte alors qu'à forte concentration, l'écrantage des charges lui confère une conformation plus repliée. L'épaisseur des films formés à fort taux de sel est donc plus grande.

##### *1.2.4.2. Films à croissance exponentielle.*

En augmentant le taux de sel en solution, certains auteurs ont observé une croissance plus rapide que la croissance linéaire, qu'ils ont appelée « super linéaire » (McAloney et al., 2001; Ruths et al., 2000). Ils ont relié cette augmentation d'épaisseur à une augmentation de

la rugosité du film. En effet, l'augmentation de la rugosité entraîne une augmentation de l'aire de la surface d'adsorption et, par conséquent, de la quantité de matière déposée. D'autres études portant sur des polypeptides et polysaccharides ont mis en évidence une croissance exponentielle de l'épaisseur. En 1999, Elbert et al (Elbert and Hubbell, 1998) ont montré pour le système PLL/Alg que son épaisseur à sec atteint 150 nm après dépôt de 15 paires de couches. Ils ont attribué la croissance du film à la présence de complexes coacervats formés progressivement au cours du dépôt des couches. Par la suite, au sein de notre laboratoire, d'autres films à croissance exponentielle ont été mis en évidence : des films construits à base de polypeptides comme les systèmes PLL/PGA (Lavalle et al., 2002) et à base d'un polypeptide et d'un polysaccharide, le hyaluronane (PLL/HA) (Picart et al., 2001b) en sont deux exemples types. L'épaisseur des films peut atteindre un à plusieurs micromètres après dépôt d'une vingtaine de paires de couches. Ces épaisseurs permettent d'utiliser la microscopie confocale pour visualiser la structuration en *z* du film après marquage fluorescent d'un des polyélectrolytes. Ainsi, il a été mis en évidence que la croissance exponentielle est liée à la diffusion d'au moins l'un des deux polyélectrolytes constituant le film, à chaque étape de dépôt (Picart et al., 2002). Le mécanisme de construction associé à la diffusion est schématisé sur la Figure 1-4 pour le système PLL/HA dans lequel le PLL diffuse.

Dans un premier temps, les molécules de PLL diffusent dans le film au moment du dépôt de la solution de PLL (Fig. 1-4, B et C). Lors du rinçage, ces molécules de PLL « libres » ne seront que partiellement éliminées car une partie seulement diffuse vers la surface du film et sort du film (Fig. 1-4, D). En effet, toutes les molécules ne sortent pas en raison de l'existence d'une barrière de potentiel en surface du film. Lors de l'addition de HA, ces molécules de PLL peuvent à nouveau diffuser hors du film mais au contact de la solution de HA, elles vont complexer et s'adsorber en surface du film pour en constituer la couche supérieure (Fig. 1-4, E). Le nombre de molécules de PLL piégées dans le film est en première approximation proportionnel à l'épaisseur du film. Cela entraîne une augmentation de l'épaisseur de la couche de HA en fonction du nombre de couches déposées et conduit ainsi à un régime de croissance exponentielle (Lavalle et al., 2004). De tels films possèdent des caractéristiques physico-chimiques proches de celles d'un hydrogel notamment en raison de leur forte teneur en eau.

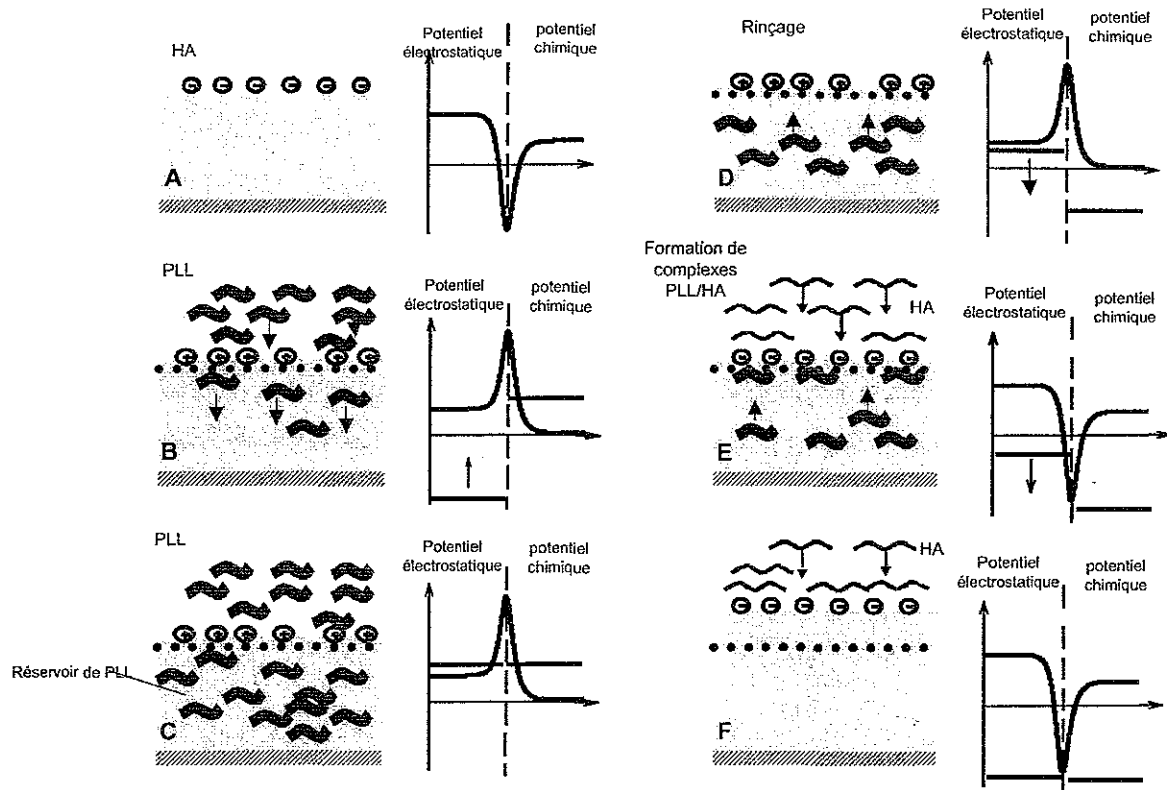


Figure 1-4 : Schéma du mécanisme de construction d'un film multicouche (PLL/HA), basée sur la diffusion du polycation: (A) le mécanisme proposé débute par un film s'achevant par une couche de HA chargée négativement, (B,C) le film est mis en contact avec la solution de polycation (PLL) ; la majeure partie des molécules de PLL diffuse dans le film; quelques chaînes s'adsorbent sur le film, rendant sa charge de surface positive; (D) après le rinçage, quelques chaînes de PLL polycations libres restent dans le film; (E) Lors de l'adsorption de HA, les molécules de PLL libres diffusent à l'interface et se complexent avec le HA présent en solution qui s'adsorbe sur le film; (F) En fin d'étape E, la surface est de nouveau chargée négativement et une grande partie des molécules de PLL libres a été utilisée pour complexer le HA. Le cycle d'adsorption peut alors recommencer (Picart et al., 2001b)

#### 1.2.4.3. Exemples de paramètres pouvant être modulés

Un grand nombre de paramètres caractérisant les films multicouches peuvent être modulés :

- leur épaisseur dépend des polyélectrolytes utilisés, de la force ionique des solutions et de leur pH
- la charge de surface dépend de la couche terminale (polyanion, polycation), de la nature des polyélectrolytes et des conditions ioniques
- la rugosité dépend du nombre de couches, des polyélectrolytes, et de la force ionique
- la perméabilité dépend de la possible présence de pores au sein du film et de la répartition des charges, des contre ions...

- le taux de recouvrement du substrat dépend de la présence ou non de couches « précurseurs » et des propriétés d'étalement et de complexation des polyélectrolytes.
- la densité des films dépend de la nature de la nature des polyélectrolytes et des conditions d'édification (pH...)

**Tableau 1-1 : Paramètres modifiables sur les films multicouches de polyélectrolytes.**

Propriétés modifiables	Paramètres utilisés pour la modification	Publication
Charge de surface	Couche terminale	(Decher, 1997)
Rugosité	Nombre de couches	(McAloney et al., 2003)
Tension de surface/hydratation	pH des solutions	(Yoo et al., 1998)
Densité	pH des solutions	(Mendelsohn et al., 2003)
Porosité	pH des solutions	(Hiller et al., 2002)
Taux de recouvrement du substrat	Nombre de couches	(Picart et al., 2001b)
Perméabilité	Masse molaire des polyélectrolytes	(Brissava et al., 1998)
Propriétés mécaniques	Action de solvants	(Lulevich et al., 2004)

### 1.2.5. Renforcer la cohésion des films multicouches par la réticulation

Certains films multicouches sont très fragiles et peu résistants à des changements de pH. C'est le cas, par exemple, des films à base de poly(acrylamide) dont nous avons déjà parlé (cf 1.2.3.2). En vue de conserver l'intégrité du film après un changement de pH, il est possible de les réticuler par la chaleur (Tableau 1-2). D'autres films peuvent présenter des problèmes de stabilité lorsqu'ils sont mis au contact de solvants ou que la force ionique du milieu est changée. De plus, il apparaît possible de moduler certaines propriétés des films multicouches par la réticulation, comme par exemple modifier leur perméabilité (Dai et al., 2002). Ainsi, on peut constater que plusieurs travaux ont porté sur les procédés de réticulation des films multicouches en vue de changer leurs propriétés physico-chimiques (Tableau 1-2).

Tableau 1-2 : Différentes techniques de réticulation utilisées sur les films multicouches de polyélectrolytes.

Techniques de réticulation	Avantages	Inconvénients
Réticulation thermique entre groupements amine et carboxylique (Harris et al., 1999) et entre groupements imine et carboxylique (Lee and Kunitake, 1994)	Facile à mettre en œuvre pour des groupes réactionnels bien identifiés Applicable théoriquement à de nombreux systèmes	Nécessite une stabilité des films à haute température et un séchage préalable des films
• 130 °C (Harris et al., 1999) • 90°C (Mendelsohn et al., 2003)		
Couplage chimique :		
• Glutaraldehyde : appliquée à des films héparine/albumine (Brynda and Houska, 1996)	Possibilité de réticuler des films sans groupement réactif.	Risque de toxicité
• Tetraethyl orthosilicate (TEOS) : Mis au contact de films PDADMAC/laponite, à la fin de la construction, en vue de leur gélification (Rouse et al., 2000)	Réalisable à température ambiante.	Risque de dénaturation de composés actifs éventuellement inclus dans le film
• Carbodiimide : applicable sur des groupes réactifs amine et carboxylique (Schuetz and Caruso, 2003)	Possibilité de contrôler le taux de réticulation	
Photo-réticulation		
• Films contenant une diazoxyne (polycation réactif à l'UV) et du PSS, réaction entre les groupes N <sup>2+</sup> et SO <sup>3-</sup> (Chen et al., 1999)	Contrôle spatial de la réticulation avec possibilité de motifs réalisés avec des masques	Possible dénaturation liée à la réaction chimique et à l'exposition lumineuse
• Poly(diallylaminium) couplé à un groupement styrène sensible à 254 nm et laponite (fabrication dans le DMSO) (Vuillaume et al., 2002).		

Les procédés peuvent être répartis en trois catégories :

- la réticulation thermique, qui consiste à placer le film à haute température pendant une certaine durée : elle peut être appliquée à des polyélectrolytes contenant des groupements amine et imine, qui en réagissant avec des groupements carboxyliques vont former des liaisons amides ou imides (Harris et al., 1999; Lee and Kunitake, 1994) .
- la réticulation chimique utilise différentes molécules en vue de réaliser des points chimiques entre les groupements chimiques des polyélectrolytes. Selon l'agent de couplage (glutaraldéhyde, tetraethyl orthosilicate), les groupements réactifs ne sont pas les mêmes. Ainsi, le glutaraldéhyde a été utilisé pour réticuler des films à base d'héparine et d'albumine (Brynda and Houska, 1996) mais la chimie précise de couplage est mal connue. Ce plus, ce produit peut se révéler toxique. Le tetraethyl orthosilicate est quant à lui un précurseur sol/gel couramment utilisé dans la formation de la silice. Une hydrolyse partielle des orthosilicates se produit pour former Si(OH)<sub>n</sub>(OEt)<sub>4-n</sub> et de l'éthanol, et la condensation entre les groupes silanols ou entre les groupes silanols et silyethoxy

permettent la gélation. On peut citer également les carboimidés qui permettent la formation de liaisons amides entre les groupements acide carboxylique et amine (Schuetz and Caruso, 2003). C'est cette méthode que nous utiliserons, nos travaux ayant été menés sans avoir connaissance de ce de Schuetz et Caruso.

- la photo-réticulation fait intervenir un agent photo-sensible qui est soit incorporé dans le film ou couplé à un des polyélectrolytes. Dans ce cas, le film est réticulé lorsque l'agent est irradié à la longueur d'onde convenable (Chen et al., 1999; Vuillaume et al., 2002). Ce type de réticulation permet d'envisager la réalisation de motifs gravés en utilisant des masques.

#### **1.2.6 Une large variété de substrats pour déposer les films multicoches de polyélectrolytes**

Les supports le plus souvent utilisés sont des surfaces planes ou des particules colloïdales, qui sont adaptées à un certain nombre de techniques expérimentales. Cependant, au cours des dernières années sont apparus des substrats destinés à des applications médicales et donc de forme, nature chimique, et rugosité différente. Les matériaux les plus largement employés sont de type verre, quartz, mica, silicium et or. Les films ont aussi été déposés sur des métaux et alliages métalliques en Ti (Vautier et al., 2003), NiTi (Thierry et al., 2003), et acier inox (Tan et al., 2003), notamment utilisés dans les domaines dentaires, cardio-vasculaires et orthopédiques. Des polymères non chargés de type polypropylène, polystyrène, polyéthylène, téflon et silicone permettent également la construction des films. Pour ceux-ci, des interactions de type VDW et/ou hydrophobe assurent vraisemblablement l'adsorption du polyélectrolyte sur le support. La construction des films peut aussi être réalisée sur des substrats dégradables afin d'obtenir des capsules creuses (Donath et al., 1997) ou des membranes auto-supportées (Kotov, 1999). Dans le tableau 1-3 sont regroupé un certain nombre de matériaux

Outre la possibilité de déposer les films sur des substrats de géométrie variable, voire des matrices poreuses, il est possible de déposer sélectivement les films dans des structures microgravées afin de leur conférer une géométrie confinée(Berg et al., 2003; Clark and Hammond, 2000).

Tableau 1-3 : Substrats utilisés pour la construction des films multicouches de polyélectrolytes.

Inorganiques	Organiques
Lames de verre (Decher, 1997).	Poly(propylène) (Delcorte et al., 1997)
Quartz (Lvov et al., 1995).	Poly(styrène) (Donath et al., 1997)
Mica (Kim et al., 1999).	Poly(éthylène) (Greene et al., 2004)
Argent (Yamada and Shiratori, 2000).	Thermanox (Mendelsohn et al., 2003)
Titane fritté (Vautier et al., 2003)	Acide poly(lactique) (Zhu et al., 2004)
NiT <sub>i</sub> (Thierry et al., 2003)	SAMs (Cheng et al., 1999).
Silicium (Sukhorukov et al., 1996b).	Silicone (Ai et al., 2003).
Particules de Calcium (Gao et al., 2001)	Téflon (Chen and McCarthy, 1997)
Acier inox (Tan et al., 2003)	Collagène (Thierry et al., 2003)
	Latex (Schuetz and Caruso, 2002)
	Dacron (Brynda and Houska, 2000)

## 1.3 : Applications des films multicouches au domaine des biomatériaux

Les films multicouches présentent de nombreuses applications potentielles dans le domaine des biomatériaux, en raison de la grande variété de choix des polyélectrolytes, de la modulation de leurs propriétés physico-chimiques et de la possibilité de les fonctionnaliser. Fonctionnaliser signifie conférer au film une ou des propriété(s) spécifique(s) soit en le modifiant chimiquement ou physiquement, par insertion de protéines ou peptides actifs.

### 1.3.1. Mise au contact du milieu biologique

Les premiers événements se produisant quand le matériau est mis au contact d'un milieu biologique sont l'adsorption protéique et l'adhésion cellulaire.

#### 1.3.1.1. Adsorption de protéines.

Les protéines sériques sont pour la plupart chargées négativement à pH physiologique et vont s'adsorber préférentiellement sur un film de charge opposée.

Des études d'adsorption de différentes protéines sur des films de type PAH/PSS ont montré que les quantités adsorbées sont plus importantes quand la charge globale de la protéine est opposée à celle de la multicouche. Ainsi, les protéines chargées positivement s'adsorbent préférentiellement sur un film terminé par PSS alors que celles chargées négativement s'adsorbent préférentiellement sur un film terminé par PAH (Ladam et al., 2000a; Ladam et al., 2001). Cependant, la quantité de protéines négatives adsorbées sur des films terminés par PSS n'est pas négligeable.

Certains films multicouches présentent des propriétés de très faible adsorption vis-à-vis des protéines. Ainsi, Müller et al. (Müller et al., 2001) ont suivi l'adsorption d'albumine sérique humaine (HSA) et de fibrinogène sur des films multicouches à base de PEI et de PAA, d'acide poly(maléimique-co-propylène) et de sulfate de polyvinyle (PVS). Les influences du type de polymère, de la force ionique et du pH des solutions ont été étudiées. Il apparaît que les films terminés par les polyanions faibles ont des propriétés anti-adsorbantes à pH 7.4 alors que ceux terminés par le polyanion fort, PVS, présentent une adsorption protéique. D'autre part, la diminution du pH augmente l'adsorption en HSA sur les films finissant par le PAA.

Plus récemment, Gergely et al. (Gergely et al., 2004) ont montré que l'adsorption d'albumine sur un film (PLL/PGA) dépend de la couche terminale, l'adsorption étant plus

grande pour les films terminés par PLL. De plus, le pH des solutions lors de la construction et de l'adsorption joue également un rôle sur celle-ci, la plus faible adsorption étant observée à pH 7.4.

#### *1.3.1.2. Adhésion cellulaire*

Dans la perspective d'applications biomédicales des films multicouches de polyélectrolytes, de nombreuses études ont porté ces dernières années sur le comportement de cellules sur les films multicouches.

La première étude est celle de Elbert et al (Elbert et al., 1999) qui ont déposé des multicouches de (PLL/Alg) sur des supports de gélatine, de matrice extra-cellulaire produite par des fibroblastes et de collagène type I. Ces films sont un premier exemple de multicouche à croissance exponentielle possédant des propriétés de bioinertie vis-à-vis des fibroblastes humains. En effet, les films construits sur des substrats, initialement favorables à l'adhésion cellulaire, sont anti-adhésifs pour les fibroblastes.

Plus récemment, Mendelsohn et al (Mendelsohn et al., 2003) ont montré que des films multicouches à base de PAH et PAA possèdent des propriétés d'adhérence modulable vis-à-vis d'une lignée de fibroblastes (NR6WT). Le principe de modulation repose sur le changement de pH des solutions de polyélectrolytes lors de la construction du film (en absence de sel). Ainsi, lorsque les films sont construits à pH 6.5 (condition dans laquelle les polyélectrolytes sont fortement chargés), les cellules adhèrent normalement. Ces films sont minces et peu hydratés. Les films construits à pH 2 (pH auquel le PAA est très peu ionisé) sont en revanche cinq fois plus épais (pour un nombre équivalent de couches) et totalement résistants à l'adsorption cellulaire. Un comportement similaire a été observé quand le PAA est remplacé par l'acide poly(méthacrylique). Ces auteurs ont de plus mis en évidence une corrélation directe entre le caractère non adhérent des films et leur capacité de gonflement en solution aqueuse. L'ensemble de ces résultats suggère fortement que le caractère non adhérent d'une multicouche est directement relié à son degré d'hydratation. En revanche, la quantité de protéines adsorbées sur les films construits aux différents pHs ne semble pas être reliée à l'adhésion cellulaire. Ce résultat remet en cause une croyance largement répandue selon laquelle l'adsorption protéique est directement reliée à l'adhésion cellulaire.

Les films non adhérents décrits par l'équipe du professeur Rubner peuvent de plus être rendus adhérents pour les fibroblastes par greffage d'un peptide d'adhésion (RGD). L'adhésion est alors sélective aux domaines sur lesquels le peptide a été greffé (Berg et al.,

2003). L'adhésion non spécifique de cellules ne possédant pas de récepteurs RGD est ainsi évitée.

Sans rechercher à moduler la capacité de gonflement des films, il est possible de moduler l'adhésion cellulaire en jouant sur la nature des polyélectrolytes et en particulier sur la couche terminale. Ceci est valable surtout pour les films minces d'épaisseur 20 à 50 nm. Il est à noter cependant que différents types cellulaires ne réagissent pas de la même façon sur des films pourtant identiques.

Tryoen-Toth et al (Tryoen-Toth et al., 2002) ont comparé l'adhésion d'ostéoblastes humains (SaOS-2) et de fibroblastes primaires du ligament periodontal (PDL) sur des films multicouches formés d'une couche précurseur PEI-(PSS/PAH)<sub>2</sub> et terminés soit par PSS, PSS-PAH, PGA, ou PGA-PLL. L'étude montre que l'adhésion aux temps courts (20 min) est liée à la nature de la couche terminale et dans une moindre mesure à la charge de surface. En effet, les surfaces terminées par PLL (+), PGA (-) et PAH (+) favorisent l'adhésion cellulaire à l'inverse des films terminés par PSS (-) et PEI (+).

Vautier et al. (Vautier et al., 2003) ont également montré que la couche terminale joue un grand rôle sur la morphologie de chondrosarcomes HCS-2/8. Sur un film précurseur de PEI-(PSS/PAH)<sub>2</sub>, ils ont déposé deux paires de couches de (PSS/PAH) ou (PGA/PLL) et rajouté une couche pour obtenir des films terminés par les polyanions PSS et PGA. Les cellules adoptent une forme plus étalée et présentent des points focaux d'adhésion préférentielle sur les films terminés par PSS et PGA. Lorsque les films sont déposés sur des structures 3D en titane fritté (billes de diamètre 500 µm), les cellules cultivées sur les films terminés par PSS et PGA présentent de longs pseudopodes de plusieurs centaines de micromètres alors que celles déposées sur les films à terminaison positive (PLL) ne présentent plus de protusions et possèdent une morphologie ramassée. Cette étude s'inscrit dans le cadre d'une collaboration avec le service ORL du CHU de Strasbourg (Prof Debry) pour recouvrir des prothèses en titane fritté par les films multicouches.

La structure macroporeuse en titane permet déjà une re-colonisation de la prothèse. Le dépôt de films multicouches sur la prothèse devrait permettre le contrôle du phénotype cellulaire et la fonctionnalisation de la prothèse par un agent anti-inflammatoire (Schultz et al., In Press).

Les polyélectrolytes synthétiques de type PEI, PSS, et PAH sont souvent utilisés pour élaborer des films minces et favoriser l'adhésion cellulaire. Boura et al (Boura et al., 2003) ont ainsi démontré que des cellules endothéliales adhèrent et prolifèrent mieux sur des films PEI-(PSS/PAH)<sub>3</sub> que sur une monocouche de PAH. L'équipe de Kotov (Grant et al., 2001) a

également construit des films en utilisant du collagène de type I et du PSS. Ces films permettent une bonne croissance de cellules de myoblastes (C2C12) mais ne permettent pas le développement de phéochromocytomes (PC12). Cette équipe a réussi également à cultiver des myoblastes sur une surface initialement cytotoxique de CdTe en la recouvrant d'un film multicouche (PDAMAC/collagène de type I).

Plusieurs études visent une application à la neurologie et plus particulièrement à la régénération des connexions nerveuses lésées. La laminine, protéine de la matrice extracellulaire, a été utilisée dans les films multicouches pour faciliter la croissance de motoneurones (Ai et al., 2003; Bataille et al., 1998). Il est également possible d'insérer un facteur de croissance neurotrophique comme le BDNF (brain-derived growth factor) dans des films (PSS/PAH) ou (PLL/PGA) pour favoriser la formation et la croissance d'axones. Les films terminés par PSS se sont révélés être très favorables au développement des axones.

### 1.3.2. Fonctionnalisation des films multicouches par des protéines et des peptides

Les films multicouches peuvent être fonctionnalisés soit par insertion de protéines (identiques ou différentes) à un ou plusieurs niveaux de l'édifice, soit par couplage d'un peptide à un polyélectrolyte suivi de l'insertion dans ou en surface du film (Figure 1-5).

Dans le cas de protéines, il est possible de concevoir des films entièrement à base de protéines, ou des films à base de protéines et de polyélectrolytes.

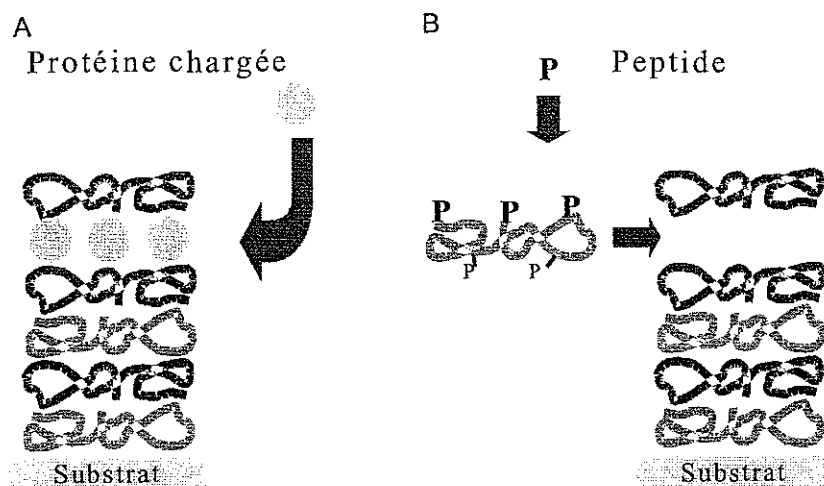


Figure 1-5 : Schéma de fonctionnalisation de films de multicouches de polyélectrolytes (A) soit par l'intégration dans le film d'une protéine active (Lvov et al., 1996), (B) soit par l'utilisation d'un polyélectrolyte couplé à un principe actif (Chluba et al., 2001).

### 1.3.2.1. Activité anticoagulante.

Plusieurs équipes ont utilisé des polyélectrolytes possédant déjà une activité anticoagulante et notamment des polysaccharides de type héparine ou dextran. Ainsi, Bryanda et al (Brynda and Houska, 2000) ont préparé des films destinés au recouvrement d'implants médicaux. Ils ont associé l'héparine à de l'albumine et réalisé un film multicouche aux propriétés anticoagulantes notamment quand l'héparine est en couche terminale. Cependant, l'inconvénient de l'héparine est qu'elle favorise l'activation du système du complément et la fixation des immunoglobulines. Les films s'achevant par l'albumine, qui présentent une activité moindre mais résistent très fortement à l'adsorption d'immunoglobulines G, seraient donc préférables car ils ne sont pas pro-inflammatoires. Ces auteurs ont également montré que ces films sont stables *in vivo* pendant trois semaines sur des prothèses en Dacron.

Dans la même optique, Tan et al (Tan et al., 2003) ont déposé des films à base d'héparine et de PEI sur un support en acier inoxydable (matériau couramment utilisé pour la réalisation de stents). Ces auteurs ont démontré qu'un tel film conserve une activité anticoagulante pendant trois semaines.

L'activité anti-coagulante des films peut être modulée en utilisant des polysaccharides notamment chitosan et dextran et en faisant varier la force ionique. L'augmentation de la concentration saline conduit à une augmentation de l'épaisseur par couche déposée, ainsi qu'à une augmentation de l'excès de charges négatives observer après dépôt de dextran. Ainsi, à partir de trois paires de couches déposées et pour une teneur en sel supérieure à 0.5M, les films terminés par le dextran sulfate sont anti-coagulants alors que ceux terminés par le chitosan sont pro-coagulants. Les propriétés anti-coagulantes sont expliquées par l'excès de charge introduit par la couche externe de dextran. Pour les autres conditions (taux de sel plus faibles et films plus minces), les films ont un comportement anti-coagulant quelque soit la couche terminale. Lorsque l'héparine remplace le dextran sulfate, les films possédant des propriétés anti-coagulantes pour des taux de sel supérieurs à 1M, quelque soit la nature de la couche externe. Thierry et al (Thierry et al., 2003) ont montré que des films multicouches à base de chitosane et de hyaluronane déposés sur des stents NiTi possèdent une activité anticoagulante.

### 1.3.2.2. Activité des protéines ou molécules enfouies au sein des films multicouches

Caruso et al ont montré que des films peuvent contenir des immunoglobulines (IgG) (Caruso et al., 1997) tout en préservant leur activité. Ils ont associé les IgG en multicouche avec du PSS. Dans de tels films, l'anti-IgG enfoui dans le film restent fonctionnel et conserve

sa capacité de reconnaissance spécifique vis-à-vis de l'IgG. Inversement, les anti-IgG reconnaissent toujours l'IgG lorsque celui-ci est enfoui dans un film (PSS/IgG).

L'activité peut en outre être modulée en faisant varier le nombre de couches d'anti-IgG déposées, la réponse étant proportionnelle à ce nombre.

Afin que les protéines restent actives dans le film, il est important d'éviter leur dénaturation. Des analyses par spectroscopie infrarouge à transformée de Fourier ont montré la conservation de la structure secondaire des protéines insérées dans les architectures de polyélectrolytes (Schwinté et al., 2002; Schwinté et al., 2001). L'enfouissement de protéines présente l'avantage de les stabiliser thermiquement en empêchant la formation de feuillets  $\beta$  intermoléculaires. D'autre part, il a été montré que des enzymes, comme la glucose oxydase, la glucose amylase incluses dans les films conservent toute leur activité enzymatique (Onda et al., 1996).

Outre les enzymes, des capsules virales ou d'autres molécules comme l'ADN, peuvent être incorporées dans les films (Lvov et al., 1995). En effet, l'ADN est une macromolécule chargée qui peut se substituer à un polyanion pour construire un film multicouche de polyélectrolytes en association avec du PLL (Sukhorukov et al., 1996a) et pour obtenir une surface permettant la transfection directe de cellules (Shi et al., 2002). L'utilisation de l'ADN est également étudiée pour la réalisation de biocapteurs avec l'incorporation de DNase inactivé (sans Mg<sup>2+</sup>) dans un film de (ADN/PDADMAC) (Serizawa et al., 2003). La présence d'ions Mg<sup>2+</sup> dans le milieu (par exemple lors d'une inflammation) active la DNase qui dégrade alors progressivement le film. Si celui-ci contient un médicament, la dégradation du film va entraîner une délivrance localisée de médicament.

Plus récemment, il a été démontré que des cellules peuvent communiquer avec une protéine, la protéine A, enfouie au sein des films multicouches. Jessel et al (Jessel et al., 2003) ont ainsi inséré la protéine A (à activité anti-tumorale) dans des films multicouches de type (PLL/PGA) puis ont déposé des myocytes. La réponse cellulaire a été analysée en mesurant la production d'une cytokine pro-inflammatoire, le TNF $\alpha$  (facteur de nécrose tumorale) en réponse à l'interaction cellule/protéine A. Quand la protéine A est recouverte de dix paires de couches, la production de TNF $\alpha$  est maximale après une durée de contact de 2H et atteint un plateau après cette durée. Ces auteurs ont pu visualiser un film constitué de vingt paires de couches en co-marquant la protéine A en rouge et la PLL-FITC en vert : ils ont montré que la protéine reste localisée dans le film. Ils ont pu également observer des dégradations locales du

film par les macrophages ainsi que le développement de pseudopodes. Ces pseudopodes permettraient à la cellule d'atteindre la protéine A enfouie.

#### *1.3.2.3. Fonctionnalisation par couplage de peptides ou molécules*

Une autre voie de fonctionnalisation consiste à inclure dans l'architecture un polyélectrolyte modifié par couplage covalent à un peptide ou à une autre molécule. Les premiers travaux dans ce domaine sont ceux de Chluba et al. (Chluba et al., 2001) qui ont évalué la réponse de mélanocytes (cellules de mélanomes) mises au contact de films (PLL/PGA) dont certaines couches de PLL étaient remplacées par de la PLL couplée à l'hormone  $\alpha$ -mélanocortine ( $\alpha$ -MSH). Cette hormone peptidique est un stimulateur potentiel de la mélanogénèse.

Ces auteurs ont tout d'abord vérifié que le peptide couplé (PLL- $\alpha$ -MSH) déposé en couche terminale du film conserve une activité similaire à celle de l'hormone libre. Ils ont montré que la profondeur d'enfouissement du peptide (peptide enfoui sous une à trente paires de couches) joue un rôle sur l'activité cellulaire surtout aux temps courts. La réponse aux temps longs n'est que peu affectée par la profondeur d'enfouissement. Une explication possible à cette observation est que la communication puisse être établie grâce à la diffusion de la PLL- $\alpha$ -MSH à travers tout le film, de façon similaire à ce qui a été montré pour les films (PLL/HA). Une autre origine pourrait être la dégradation du film par les cellules, mais l'insertion de couches de (PSS/PAH) non dégradables par les enzymes n'empêche pas totalement la communication cellulaire.

Une application plus récente vise à limiter l'adhésion bactérienne en mettant à profit des films multicouches fonctionnalisés par des PEG. Boulmedais et al. (Boulmedais et al., 2004) ont ainsi couplé du PEG à du PGA puis déposé les molécules de PGA-g-PEG au sein et en surface d'un film (PGA/PLL). Ils ont montré que l'adsorption protéique et l'adhésion bactérienne sont considérablement réduites quand une couche de PGA-g-PEG est déposée, le résultat étant encore amélioré quand trois couches sont déposées en alternance avec la PLL.

#### **1.3.3. Encapsulation de cellules dans les films multicouches.**

Récemment, plusieurs travaux ont porté sur l'encapsulation de cellules ou levures au sein des films multicouches.

Ainsi, Diaspro et al (Diaspro et al., 2002) ont réussi à encapsuler des levures de type *Saccharomyces cerevisiae* dans un film à base de PSS et de PAH. Le développement des levures dans leur « coque » de PSS/PAH semble normal. L'utilisation de polyélectrolytes

fluorescents dans la construction d'un tel film multicouche permet de marquer facilement la surface extérieure des levures. Par exemple, ce système a été utilisé par Krol et al (Krol et al., 2003) pour suivre le mécanisme de digestion des *Saccharomyces cerevisiae* par un protozoaire *Paramecium primaurelia*.

Ai et al (Ai et al., 2003) ont montré qu'il est possible d'encapsuler des plaquettes dans un film multicouche de type ((PSS/PAH)-nanosphères-(PSS/PAH)-IgG)<sub>n</sub>. Les nano-sphères permettraient de limiter l'auto-agrégation des plaquettes et les IgG permettraient un ciblage spécifique par le système multicouche. Selon ces auteurs, il serait même envisageable de rendre le film multicouche semi-perméable pour permettre une libération contrôlée de principes actifs secrétés par les plaquettes.

Par ailleurs, Schneider et al (Schneider et al., 2001) ont recouvert des îlots pancréatiques encapsulés dans des billes d'alginate par des films multicouches à base de PEI, PAA, carboxymethyl-cellulose et alginate. La membrane recouverte de polyélectrolytes (couche d'épaisseur 145 nm) ne détériore pas la biocompatibilité des capsules transplantées qui au contraire, présentent une meilleure stabilité mécanique. Cette stabilité mécanique dépend des combinaisons polycations/polyanions, qui ont également une influence sur la taille critique de filtration des molécules au passage de la membrane.

# Chapitre 2 : Matériels et Méthodes

---

<b>2.1 : Matériels .....</b>	<b>31</b>
2.1.1. Polyélectrolytes.....	31
2.1.2. Construction des films multicouches de polyélectrolytes.....	33
<b>2.2 : Méthodes.....</b>	<b>35</b>
2.2.1. Analyses physico-chimiques.....	35
2.2.1.1. Spectroscopie optique par guide d'onde.....	36
◆ Principe et description de la technique.....	36
◆ Dispositif expérimental.....	37
◆ Protocole expérimental .....	39
◆ Traitement du signal .....	40
2.2.1.2. Microbalance à cristal de quartz .....	41
◆ Principe.....	41
◆ Protocole expérimental .....	44
2.2.1.3. Mesure du potentiel d'écoulement.....	45
◆ La double couche électrique .....	45
◆ Dispositif expérimental .....	46
◆ Procédure de mesure.....	47
2.2.1.4. Microscopie de fluorescence .....	48
◆ Microscopie à épi-fluorescence .....	48
◆ Microscopie confocale.....	49
◆ Principe .....	51
◆ Mode image .....	52
◆ Mode force.....	54
2.2.2. Analyses Biologiques .....	58
2.2.2.1. Culture de chondrosarcomes.....	58
2.2.2.2. Culture des chondrocytes.....	58
2.2.2.3. Observation cellulaire.....	58
2.2.2.4. Dosage cellulaire .....	59
◆ Test MTT .....	59
◆ Dosage à la <sup>3</sup> H-thimidine .....	59
◆ Marquages fluorescents.....	59
2.2.2.5. Bactéries .....	60
2.2.2.6. Technique d'aspiration par micropipette .....	61
◆ Fabrication des micropipettes .....	61
◆ Mesure de la pression d'aspiration.....	61
◆ Chambre de mesure et dispositif expérimental .....	62
◆ Protocole de mesure de la force de détachement cellulaire.....	63
◆ Analyse statistique des données .....	64

---

## 2.1 : Matériels

### 2.1.1. Polyélectrolytes

Les polyélectrolytes sont préparés en solution aqueuse, par dissolution dans de l'eau ultra-pure (18.2 MΩ de résistivité) délivrée par un système Milli-Q-plus (Millipore), à une concentration de 1 mg/mL sauf indication contraire. Le pH est ajusté avec des solutions d'acide chlorhydrique et de soude. Plusieurs types de polyanions et polycations ont été utilisés. Leurs caractéristiques sont données respectivement dans les tableaux 2-1 et 2-2.

Tableau 2-1 : Polyanions utilisés.

Nom des polypeptides	Notation	Nature	pKa	Formule développée	Fournisseur	Masse molaire ( $M_w$ ) ( $10^3 \text{ g.mol}^{-1}$ )
Poly(L-glutamique de sodium)	PGA	Polypeptide synthétique dégradable	4.3 (Kyte, 1995)		Sigma	~55
Poly(4-styrène sulfonate de sodium)	PSS	Synthétique non dégradable	2 (Ahrens et al., 2000)		Aldrich	70
Acide Poly(acrylique)	PAA	Synthétique non dégradable	5 (Mendelsohn et al., 2003)		Aldrich	100
Hyaluronane de sodium	HA	Polysaccharide naturel dégradable	2.9 (Lapčík et al., 1998)		Bioiberica	400

Tableau 2-2 : Polycations utilisés.

Nom des polypeptides	Notation	Nature	pKa	Formule développée	Fournisseur	Masse molaire ( $M_w$ ) ( $10^3 \text{ g} \cdot \text{mol}^{-1}$ )
Poly(L-lysine)	PLL	Polypeptide synthétique dégradable	10.5 (Kyte, 1995)		Sigma	30
Poly(éthylène imine)	PEI	Synthétique non dégradable	Polybase forte		Aldrich	750
Poly(allylamine hydrochlorique)	PAH	Synthétique non dégradable	9 (Mendelsohn et al., 2003)		Aldrich	70
Chitosane	CHI	Polysaccharide naturel dégradable	6.5-7.4 (Denuziere et al., 1996)		FMC Biopolymer	110/128 272/460

**Tableau 2-3 : Réactifs utilisés.**

Nom du produit	Notation ou formule chimique	Fournisseur	Masse molaire (g/mol)
Sodium Dodecyl Sulfate	SDS	Sigma	288.4
N-hydroxysulfo succinimide	Sulfo NHS	Fluka	217.2
1-Ethyl-3- (3-diméthylamino-propyl) carbodiimide	EDC	Sigma	191.7
Acide chlorhydrique à 37%	HCl	Prolabo	36.5
Hydroxyde de sodium	NaOH	Prolabo	40
Chlorure de sodium	NaCl	Prolabo	58.4
Acide 2- (N-morpholino) ethanesulfonique	MES	Sigma	195.2
Tris (hydroxy méthyle) aminométhane	Tris	Merck	121.1
Chlorure de Magnesium	MgCl <sub>2</sub> • 2 H <sub>2</sub> O	Sigma	147
Chlorure de Calcium	CaCl <sub>2</sub> • 6 H <sub>2</sub> O	Sigma	203.3

### 2.1.2. Construction des films multicouches de polyélectrolytes

Les substrats utilisés pour les études sont généralement à base de silice qui est chargée négativement et présente une faible rugosité. De plus, sa transparence facilite les observations optiques. Ces différentes caractéristiques font donc du verre un bon support d'étude. Les résultats obtenus sur le verre sont facilement transposables, car les films multicouches de polyélectrolytes possèdent rapidement au cours de leur construction des caractéristiques indépendantes du substrat (Ladam et al., 2000b).

Pour les études en microscopie à force atomique et en microscopie confocale ainsi que pour les études cellulaires, les films multicouches de polyélectrolytes sont construits sur des lamelles de borosilicate de diamètre 12 ou 14 mm (VWR). Les lamelles sont préalablement nettoyées à l'aide de SDS 0.01 M (10 min, au bain-marie), puis mises dans du HCl 0.1 N (10 min, au bain-marie) et enfin, rincées abondamment à l'eau et séchées sous flux d'azote.

Les lamelles sont ensuite immergées dans la solution de polycations (à 1 mg/mL), la surface des lamelles de verre étant chargée négativement, (10 min). Puis les lamelles sont rincées avec une solution saline de concentration identique à la solution de polyélectrolytes. Le temps de rinçage est compris entre 5 et 10 min selon les études. L'ensemble est enfin plongé dans une solution de polyanion et rincé suivant le même protocole que pour le dépôt

du polycation. L'opération d'immersion successive dans le polycation et dans le polyanion est répétée jusqu'à l'obtention du nombre de couches souhaitées.

Pour la réalisation de films contenant un nombre élevé de couches, l'opération de dépôt est programmée à l'aide d'un bras automatisé (Dipping Robot DR3, Kriesten) déplaçant séquentiellement les portoirs à lamelles dans les différents bains de polyélectrolytes et de rinçage.

## 2.2 : Méthodes

### 2.2.1. Analyses physico-chimiques

L'étude physico-chimique des films multicouches de polyélectrolytes a été réalisée à l'aide de différentes techniques complémentaires (Figure 2-1). Elle a porté principalement sur la caractérisation d'épaisseur (OWLS, QCM-D, Microscope confocal, AFM mode image), l'indice de réfraction (OWLS), le potentiel  $\zeta$  de surface (mesure du potentiel d'écoulement), la topographie de surface (AFM mode image) et les propriétés rhéologiques (AFM mode force).

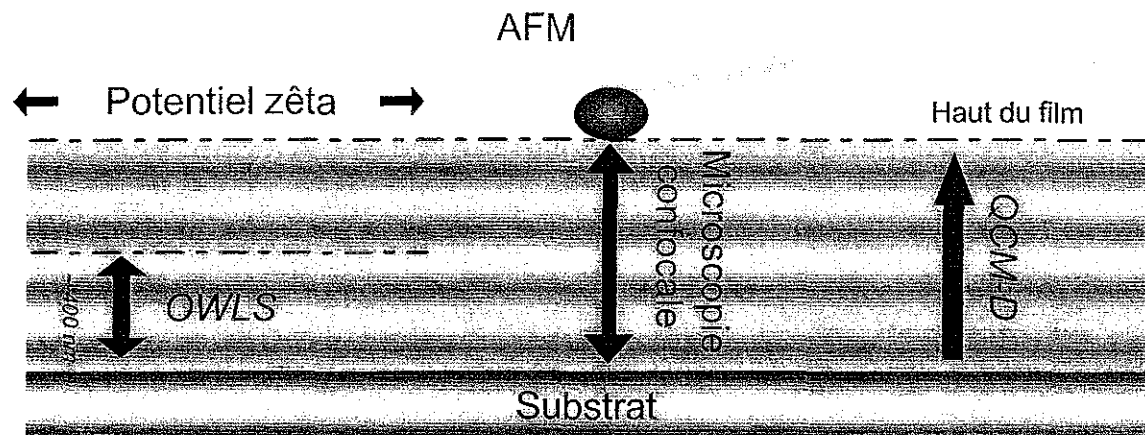


Figure 2-1 : Techniques d'analyses physico-chimiques utilisées pour caractériser physico-chimiquement les films multicouches de polyélectrolytes. La spectroscopie optique par guide d'onde (OWLS) permet de mesurer l'indice de réfraction et l'épaisseur de films multicouches jusqu'à environ 400 nm. La microbalance à cristal de quartz (QCM) informe sur la masse des films. La microscopie à force atomique (AFM) permet d'imager la topographie des films (mode image) et de mesurer leurs propriétés mécaniques (mode force). La microscopie confocale est utilisée pour imager la structure normale des films d'épaisseur micrométrique et la diffusion des polyélectrolytes libres. Enfin, la mesure du potentiel zéta informe sur la charge de surface des films multicouches.

### 2.2.1.1. Spectroscopie optique par guide d'onde

- ◆ Principe et description de la technique

La spectroscopie optique par guide d'onde (ou OWLS Optical Waveguide Lightmode Spectroscopy) (Tiefenthaler and Lukosz, 1989) est une technique optique permettant d'étudier *in situ* l'adsorption de macromolécules sur un substrat. La technique utilise les propriétés de réflexion de la lumière à l'interface guide/couche adsorbée pour déterminer l'épaisseur et l'indice de réfraction de cette couche. Un faisceau laser est dirigé sur le guide d'onde (généralement en oxyde métallique transparent de ~200 nm d'épaisseur et d'indice de réfraction supérieur à 1.7) sur lequel est gravé un réseau de diffraction. Pour un angle donné, appelé angle de couplage, le faisceau laser reste confiné au sein du guide d'onde par réflexion totale interne et se propage dans le guide (dans la direction x) jusqu'aux photodiodes disposées aux extrémités latérales du guide d'onde. (Figure 2-2).

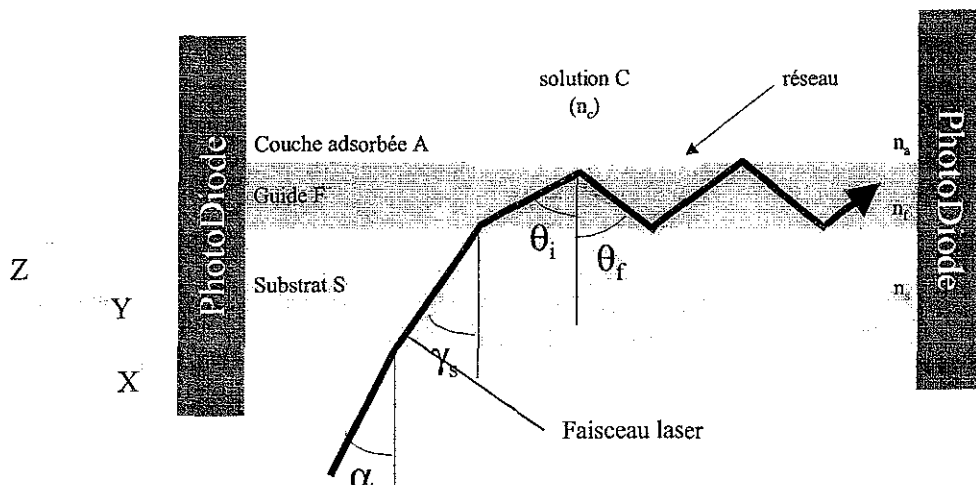


Figure 2-2 : Schéma de principe de la spectroscopie optique par guide d'onde

La propagation du faisceau dans le guide est obtenue lorsque l'équation des phases (2-1) est satisfaite :

$$2k_{z,F} d_F + \Phi_{S,F} + \Phi_{F,A,C} = 2\pi m \quad (2-1)$$

où  $m$  est un entier appelé l'ordre du guide,  $k_{z,F}$  représente la composante normale du vecteur d'onde de l'onde diffractée au niveau de la couche guide d'onde (F) qui est définie par la relation (2-2):

$$\begin{aligned}
 k_{z,F} &= -k_0(n_F^2 - N^2)^{1/2} = -k_0 f \\
 k_{z,S} &= -ik_0(N^2 - n_S^2)^{1/2} = -ik_0 s \\
 k_{z,C} &= -ik_0(N^2 - n_C^2)^{1/2} = -ik_0 c \\
 k_{z,A} &= -ik_0(N^2 - n_A^2)^{1/2} = -k_0 a
 \end{aligned} \tag{2-2}$$

avec  $k_0 = \frac{2\pi}{\lambda}$  et  $N$  l'indice de réfraction effectif obtenu par la relation suivante :

$$N = n_f \sin(\theta_f) = n_{air} \sin(|\alpha|) + \frac{l\lambda}{\Lambda} \tag{2-3}$$

où  $l$  est l'ordre de la diffraction,  $\lambda$  représente la longueur d'onde du faisceau incident et  $\Lambda$  représente le pas du réseau de diffraction.

Les expressions des déphasages  $\Phi_{S,F}$  et  $\Phi_{F,A,C}$  du faisceau aux interfaces silice/guide (S/F) et guide/couche adsorbée/solution (F/A/C) ont été tout d'abord développées pour un dépôt monocouche homogène et uniforme (Picart et al., sous presse ; Picart et al., 2001a) :

$$\Phi_{F,A,C} = 2 \arctan \left[ - \left( \frac{n_F a}{n_A f} \right)^{2\rho} \frac{\frac{c}{n_C^{2\rho}} + \frac{a}{n_A^{2\rho}} \tanh(k_0 a \cdot d_A)}{\frac{a}{n_A^{2\rho}} + \frac{c}{n_C^{2\rho}} \tanh(k_0 c \cdot d_A)} \right] \tag{2-4}$$

$$\Phi_{F,S} = -2 \arctan \left( \frac{n_F s}{n_S f} \right)^{2\rho}$$

avec  $\rho = 0$  ou  $1$  pour respectivement la composante électrique ou magnétique du faisceau laser. Ainsi l'équation de déphasage (2-1) est vérifiée pour deux angles correspondant respectivement aux composantes électrique et magnétique, ce qui permet de calculer les deux indices de réfraction effectifs  $N_{TE}$  et  $N_{TM}$ .

#### ♦ Dispositif expérimental

Le dispositif expérimental, mis au point au sein de l'unité par le Dr Frédéric Cuisinier, est schématisé sur la Figure 2-3. Un laser Hélium-Néon de 5 mW (Melles-Griot), de longueur d'onde 632.8 nm, est réfléchi par un miroir sur un guide d'onde en  $\text{Si}_{0.8}\text{Ti}_{0.2}\text{O}_2$  (Micro Vacuum Ltd) mono-mode ( $m=0$ ) permettant uniquement une réflexion du premier ordre ( $l=1$ ). Le guide est monté dans une cellule de mesure, deux photodiodes (Hamamatsu) sont disposées à chaque extrémité du guide. Un ordinateur pilote le déplacement d'un moteur (M-UTM Newport) permettant la rotation du guide sur une plage angulaire de  $-8^\circ$  à  $+8^\circ$  avec une

précision angulaire de  $3 \cdot 10^{-4}$  degrés. La résolution en indice de réfraction effective ( $\Delta N$ ) est alors de  $10^{-5}$ .

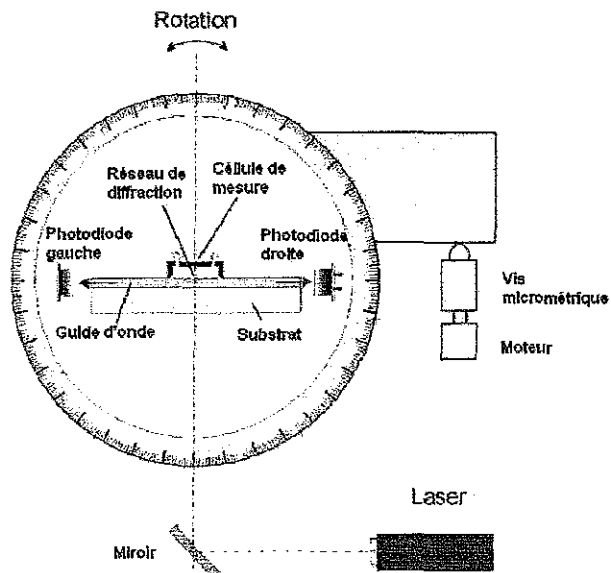


Figure 2-3 : Schéma de principe du spectroscope par guide d'onde comprenant un laser polarisé, un guide d'onde et deux photodiodes qui mesurent les intensités de couplage et un moteur qui permet d'effectuer un balayage d'angulaire (schéma repris de (Vörös et al., 2002))

Lorsque les conditions de couplage sont vérifiées, le faisceau diffracté par le réseau se propage jusqu'aux photodiodes où l'intensité est mesurée. Deux angles de couplage sont ainsi obtenus pour chaque photodiode (Figure 2-4). Le temps d'acquisition d'un point étant d'environ 1min 30s, il est ainsi possible de suivre la construction du film multicouche.

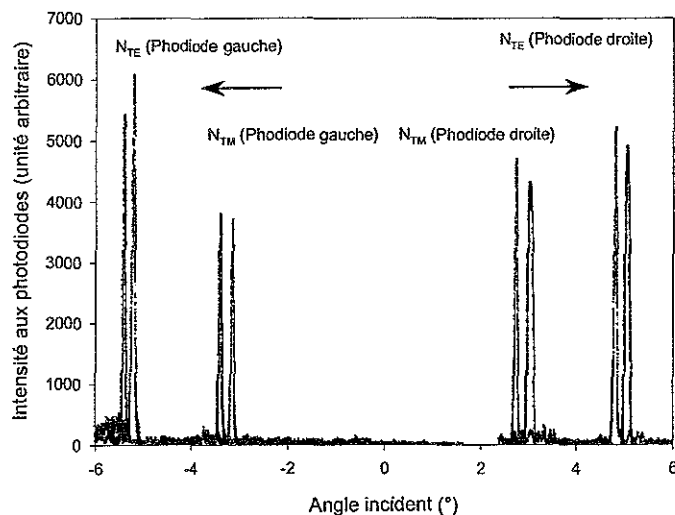


Figure 2-4 : Courbes caractéristiques de l'évolution de l'intensité lumineuse en fonction de l'angle incident  
Les angles de couplage correspondent aux angles pour lesquels l'intensité couplée est maximale La

construction d'un film multicouche entraîne un décalage des angles de couplage vers des valeurs plus élevées en raison de l'adsorption de matière (courbe grise)

Les guides d'onde ASI 2400 (MicroVacuum Ltd) sont en  $\text{Si}_{0.8}\text{Ti}_{0.2}\text{O}_2$ , ils sont déposés sur un substrat en silice pur, dont les caractéristiques sont décrites dans le tableau 2-4.

Tableau 2-4 : Caractéristiques techniques des guides ASI 2400 (MicroVacuum Ltd)

<b>Film guide d'onde</b>		
— Matériel	$\text{Si}_{(1-x)}\text{Ti}_x\text{O}_2$	$x=0.25 \pm 0.05$
— Indice de réfraction (25 °C)	$n_F$	$1.77 \pm 0.03$
— Epaisseur	$d_F$	170 – 220 nm
<b>Substrat</b>		
— Matériel	Silice ( $\text{SiO}_2$ )	
— Indice de réfraction (25 °C)	$n_s$	1.52578
— Epaisseur	$d_s$	0.55 mm
<b>Réseau de diffraction</b>		
— Localisation	Sur le film	
— Périodicité	2400 lignes/mm	0.4166 μm
— Ordre de diffraction		1
— Dimensions des lignes	Profondeur	20 nm
	Largeur	16 mm
— Orientation du réseau	Parallèle à la largeur du guide	
<b>Dimension totale</b>	Longueur	48 mm
	Largueur	16 mm

#### ♦ Protocole expérimental

Les solutions sont préalablement dégazées pendant 30 minutes. Cette opération est nécessaire pour éviter la formation de bulle d'air dans le montage.

L'indice de réfraction de la solution tampon ( $n_c$ ) est mesuré dans les conditions expérimentales avec un réfractomètre RFM 340 (Bellingham-Stanley).

Après réglage du laser pour avoir des pics symétriques et d'intensité maximale, la cellule de mesure est mise à l'équilibration pendant 30 min. Les guides d'ondes utilisés étant chargés négativement, la construction du film débute par l'injection de la solution de polycation (100μL) dans la cellule de mesure (37μL). L'ensemble est laissé au repos durant 10 min. Après le dépôt de la couche de polycation, la cellule est rincée sous flux (10mL/h) pendant 10 min avec la solution de rinçage. Les étapes d'injection et de rinçage des différents polyélectrolytes sont ensuite répétées selon le même schéma avec une alternance entre les polyélectrolytes chargés négativement et positivement. La construction de la multicouche est ainsi suivie *in situ*. Les adsorptions des protéines sériques sont quant-à-elles réalisées sur une durée minimale de 60 min.

♦ Traitement du signal

Les indices effectifs ( $N_{TE}$  et  $N_{TM}$ ) sont mesurés en fonction du temps. Avant le calcul de l'indice de réfraction de film ( $n_A$ ) et de son épaisseur ( $d_A$ ), il faut auparavant caractériser les propriétés optiques du guide d'onde : indice de réfraction ( $n_F$ ) et épaisseur ( $d_F$ ). En l'absence de film déposé (phase de rinçage initiale), la réflexion à l'interface guide/solution est totale. L'équation de couplage (2-1) est alors résolue en utilisant les équations de déphasages aux interfaces F/A/C et S/F (Tiefenthaler and Lukosz, 1989): (2-5)

$$\begin{cases} \Phi_{F,A,C} = -2 \arctan \left[ \left( \frac{n_F}{n_C} \right)^{2\rho} |k_{z,C}| / k_{z,F} \right] \\ \Phi_{F,S} = -2 \arctan \left[ \left( \frac{n_F}{n_S} \right)^{2\rho} |k_{z,S}| / k_{z,F} \right] \end{cases} \quad (2-5)$$

Dans ces conditions, la résolution de l'équation (2-1) donne les valeurs  $n_F$  et  $d_F$ . A l'aide de ces données, il est alors possible d'estimer numériquement les valeurs  $n_A$  et  $d_A$  en connaissant les valeurs expérimentales  $N_{TE}$  et  $N_{TM}$ . Cependant, l'équation de couplage (2-1) n'a pas de solution analytique explicite. En revanche, elle peut être représentée sous forme matricielle pour un nombre  $j$  de couches (2-6) (Picart et al., sous presse) et ainsi être résolue numériquement pour des films dont l'épaisseur est inférieure à la longueur d'onde du laser utilisé (pour notre système  $\lambda = 632.8$  nm) :

$$\begin{pmatrix} W_i \\ W_r \end{pmatrix} \propto I_F^{-1} I_1 L_1 I_1^{-1} I_2 L_2 I_2^{-1} \dots I_\kappa L_\kappa I_\kappa^{-1} I_C \begin{pmatrix} 1 \\ 0 \end{pmatrix} \quad (2-6)$$

avec  $\kappa$  le nombre de couches,  $W_i$  et  $W_r$  respectivement l'amplitude du champs électrique de

l'onde incidente et réfléchie,  $I_j = \begin{pmatrix} 1 & 1 \\ \frac{k_j}{n_j^{2\rho}} & -\frac{k_j}{n_j^{2\rho}} \end{pmatrix}$  et  $L_j = \begin{pmatrix} \exp(ik_j d_j) & 0 \\ 0 & \exp(-ik_j d_j) \end{pmatrix}$ .

$L_j$  définissant l'influence de la couche  $j$  sur l'onde et  $I_j^{-1} x I_l$  étant le déphasage de l'onde lors de son passage de la couche  $j$  à la couche  $l$ .

La précision de l'appareil ( $10^{-5}$  sur les indices effectifs) limite l'épaisseur maximale réellement mesurable à environ 400 nm d'épaisseur pour les films d'indice 1.5 (Picart et al., sous presse). Un programme de résolution numérique de l'équation (2-6) a été développé au sein du laboratoire. Pour l'analyse numérique, le film multicouche de polyélectrolytes est alors défini comme un film homogène et uniforme (donc  $j = 1$  dans l'équation 2-6).

A partir des grandeurs  $n_A$  et  $d_A$ , une formule approchée (2-8) donnant la masse adsorbée ( $q_A$ ) a été proposée par DeFetyer et al. (De Feijter et al., 1978):

$$q_A = \frac{Q_A \times 0.1}{dn/dc} \quad (2-8)$$

où  $dn/dc$  (en mL/g) est la variation d'indice de réfraction par rapport à la variation de concentration en polyélectrolyte dans le film avec :

$dn/dc = 0.197$  mL/g pour les polyélectrolytes (Huglin, 1972)

$dn/dc = 0.18$  mL/g pour les protéines (Huglin, 1972)

### 2.2.1.2. Microbalance à cristal de quartz

#### ◆ Principe

La microbalance à cristal de quartz (ou QCM pour Quartz Crystal Microbalance) développée dans les années 60 (Sauerbrey, 1959), est une technique utilisant les propriétés piézo-électriques d'un cristal pour mesurer la masse adsorbée sur ce cristal. La fréquence caractéristique de vibration d'un matériel piézoélectrique (cristal de quartz) est en effet reliée à la masse de l'objet déposée sur ce cristal. Des impulsions de courant alternatif sur les deux faces du cristal (électrodes, Figure 2-5) induisent des contraintes de cisaillement sur le cristal perpendiculairement au champ électrique. Inversement, les oscillations du cristal génèrent aux électrodes un signal électrique qui est collecté par l'appareil.

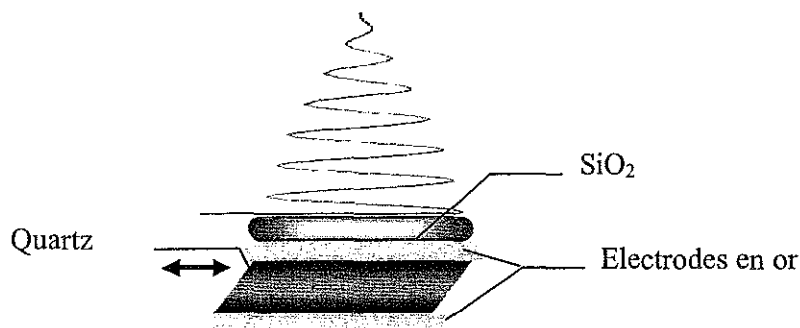


Figure 2-5 : Schéma des cristaux de quartz sur lesquels se trouvent deux électrodes en or et éventuellement une couche superficielle de  $\text{SiO}_2$  (QSX 303; Q-Sense)

Le cristal entre en résonance quand la relation (2-9) est vérifiée avec  $n$  un nombre entier impair,  $t_q$  l'épaisseur du cristal,  $v$  la vitesse de l'onde d'extension et  $v/f$  est la longueur d'onde.

$$f = \frac{nv}{2t_q} \quad (2-9)$$

L'adsorption de molécules sur le cristal augmente la masse oscillante et induit un changement de fréquence de résonance du cristal. Ce phénomène s'observe également aux harmoniques impaires. Pour ces fréquences, la sensibilité de la technique est augmentée.

Toutefois leur longueur de pénétration diminue avec l'augmentation de la fréquence étudiée. Le changement de fréquence dû à l'adsorption peut-être corrélé à la variation de masse pour des films fins, rigides et uniformes au contact de l'air ou sous vide grâce à la relation de Sauerbrey (2-10). Il est ainsi possible de convertir la variation de fréquence en masse.

$$\Delta m = -\frac{\rho_q t_q \Delta f}{nf_0} = -\frac{C \Delta f}{n} \quad \text{avec} \quad C = \frac{\rho_q t_q}{f_0} \approx 17.7 \text{ ng/cm}^2 \text{ Hz} \quad (2-10)$$

où  $\rho_q$ ,  $t_q$  et  $f_0$  sont respectivement la densité, l'épaisseur et la fréquence de résonance fondamentale et  $n$  le rapport entre la fréquence de l'harmonique et la fréquence fondamentale.

Cette relation a été développée pour un dépôt au contact avec le vide. Maramatasu et al (1988) ont montré que la mesure en solution liquide génère une résistance sur l'oscillation du cristal. Il a été récemment démontré que la relation de Sauerbrey s'applique également, mais de façon approchée, à un dépôt solide au contact d'un liquide (Rodahl and Kasemo, 1996), mais toujours pour des films fins, rigides et uniformes.

Or, les films multicouches étudiés sont très hydratés et possèdent généralement un comportement de gels lorsqu'ils deviennent épais. La relation de Sauerbrey n'est alors plus applicable. Les récentes évolutions techniques ont permis l'étude d'un nouveau paramètre : la dissipation. Le facteur de dissipation ( $D$ ) est inversement proportionnel au temps de vibration du cristal après son excitation. (Figure 2-6).

Le facteur de dissipation est lié aux propriétés viscoélastiques (module d'Young, et viscosité) du dépôt. Une analyse de l'évolution des fréquences et de la dissipation a été réalisée à partir du modèle proposé par Voinova et al. (Voinova et al., 1999). Ce modèle a été étendu par le Dr B. Senger (Inserm U 595) aux données obtenues à l'aide de la QCM-D (Q-Sense). Le programme détermine ainsi l'évolution de l'épaisseur sur plusieurs centaines de nanomètres ainsi que les propriétés mécaniques des films tels que la viscosité et le module élastique pour des films multicouches de polyélectrolytes (Zhang et al., 2004).

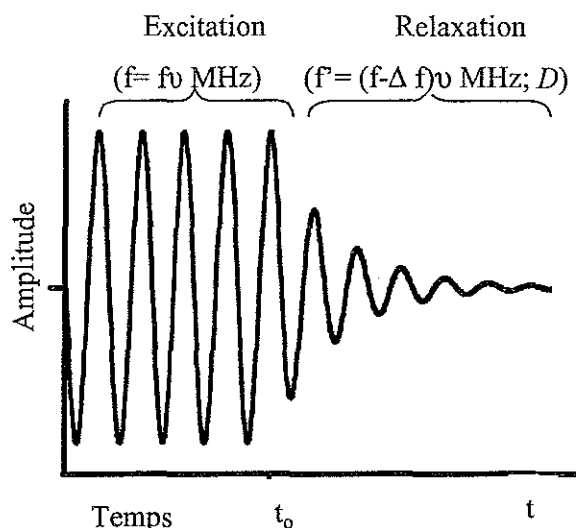


Figure 2-6 : Amplitude d'oscillation du cristal en fonction du temps  $A(t)$  lors d'une expérience en QCM : Première phase (jusqu'à  $t_0$ ), excitation du cristal à sa fréquence de résonance. Seconde phase, étude de la relaxation du cristal avec obtention de la nouvelle fréquence de résonance ( $f'=f-\Delta f$ ) et de la dissipation ( $D$ ) à l'aide des formules :  $A(t) = A_0 \sin(2\pi t \times f') \times e^{-t/\tau}$  et  $D = \frac{1}{\tau \pi f_0}$

La technique est sensible à la masse totale mise en mouvement lors de l'oscillation et notamment à l'eau emprisonnée dans le film. Ces deux phénomènes rendent une analyse quantitative du dépôt délicate et plus particulièrement pour la caractérisation mécanique du film.

Les cristaux utilisés sont de type QSX 303 (cristaux de cristal Quartz recouvert d'un film de SiO<sub>2</sub> de 100 nm (Q-Sense) (Figure 2-5)) et ils possèdent une fréquence de résonance fondamentale à 5 MHz et des fréquences harmoniques à 15, 25 et 35 MHz. Les fréquences de résonance du cristal sont mesurées avec une précision de 1 Hz. La sensibilité en masse de l'appareil dans ces conditions est de ~5 ng/cm<sup>2</sup> dans l'eau et de ~1 ng/cm<sup>2</sup> dans l'air à la fréquence de résonance fondamentale de 5 MHz.

◆ Protocole expérimental

Avant chaque expérience, le cristal est nettoyé *in situ*, avec une solution de Hellmanex à 2% pendant une demi-heure à température ambiante. Il est ensuite rincé avec du HCl 0.1N puis lavé à l'eau et séché à l'azote.

La suite de l'expérience se déroule de manière similaire à l'étude en OWLS par une injection alternée des solutions de polycations et de polyanions (10 min d'adsorption suivie de 10 min de rinçage) dans la cellule de mesure (Figure 2-7). Toutefois, il faut utiliser 2 mL de solution par dépôt : une expérience en QCM-D nécessite des quantités de produits plus importantes qu'une expérience réalisée par OWLS. La température de mesure est fixée à 25°C. Le temps séparant 2 mesures est de quelques secondes permettant ainsi d'observer les cinétiques de dépôt et de désorption.

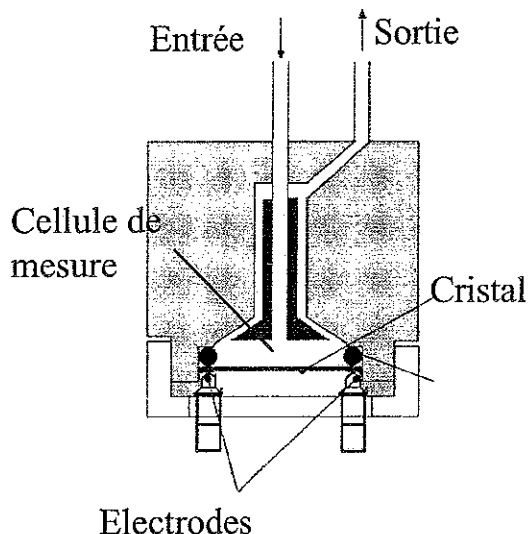


Figure 2-7 : Schéma de la cellule de mesure (Q-Sense). Les polyélectrolytes sont injectés par le port d'entrée et sortent par le port de sortie.

### 2.2.1.3. Mesure du potentiel d'écoulement

L'environnement ionique d'une surface s'organise pour maintenir l'électro-neutralité du système. Ainsi, les ions de charge opposée à celles de la surface sont attirés sous l'effet de la force d'attraction de Coulomb et les ions de charge identique sont repoussés. Combinées au mouvement Brownien, ces forces conduisent à une distribution des charges normale à l'interface. L'atmosphère ionique, fixée à la paroi, constitue ce qu'on appelle la double couche.

- ♦ La double couche électrique

Graham et al. (Graham, 1947) ont proposé un modèle à deux zones pour la distribution normale des ions à une surface chargée. Dans la première zone, seuls les ions de charge opposée à la surface sont présents, cela constitue la couche de Stern. Dans cette couche, les ions sont présents sous deux états : fortement liés à la surface, ils sont alors très peu hydratés et leur distance moyenne avec la surface définie le plan interne d'Helmholtz (PIH). Au-delà de ce plan, les ions sont hydratés et leur interaction à la surface est plus faible.

D'après le modèle, dans la seconde zone, il existe une distribution entre les anions et les cations qui suit le modèle défini par Chapman (Chapman, 1913). Ce modèle (Figure 2-8) définit l'évolution du rapport entre les espèces positives et négatives à partir de la couche de Stern jusqu'à l'équilibre à l'aide de considérations thermodynamiques. Ainsi, l'approximation de Debye-Hückel (2-11) permet d'estimer l'évolution du potentiel en fonction de la distance par rapport à la surface, pour des potentiels faibles, et s'écrit :

$$\bullet = \bullet_0 \exp(-\kappa x) \quad (2-11)$$

avec  $\psi_0$  le potentiel de la surface,  $x$  la distance normale à la surface et  $1/\kappa$  la longueur de Debye-Hückel.

Le potentiel zêta ( $\xi$ ) correspond au potentiel au niveau du plan de cisaillement entre la surface et un flux parallèle à la surface. Les ions de la couche de Stern sont fortement liés à la surface et ils ne sont pas arrachés par le flux. Le plan de cisaillement est généralement confondu avec le plan de Stern. Le potentiel zêta est défini par la relation de Smoluchowski (Smoluchowski, 1903; Smoluchowski, 1921) (2-12)

$$\Delta V = \Delta P \frac{(r^2 R_C \varepsilon \varepsilon_0 \pi \zeta)}{L \mu} \quad \text{d'où} \quad \zeta = \frac{\Delta V}{\Delta P} * R_C * \frac{L \mu}{(r^2 \varepsilon \varepsilon_0 \pi)} \quad (2-12)$$

où  $r$  est le rayon du capillaire (en m),  $L$  la longueur du capillaire (en m),  $R_C$  la résistance électrique du capillaire contenant l'électrolyte (en  $\Omega$ ),  $\varepsilon \varepsilon_0$  la permittivité de l'électrolyte et  $\mu$  la viscosité dynamique de l'électrolyte.

En mesurant  $\Delta V$  en fonction de  $\Delta P$ , il est ainsi possible de calculer le potentiel zéta de la surface du capillaire.

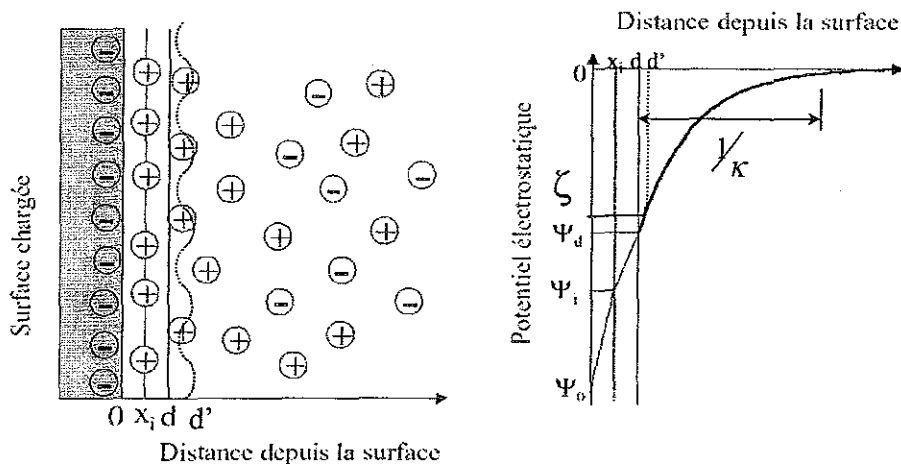


Figure 2-8 : Le modèle de Graham (Graham, 1947) Le plan interne de Helmholtz (PIH) est localisé à la distance  $x_i$  de la surface, alors que le plan externe de Helmholtz (PEH) ou plan de Stern est localisé à la distance  $d$  et le plan de cisaillement est proche du plan de Stern à une distance  $d'$  proche de  $d$  (Viallis-Terrisse, 2000)

Expérimentalement, la mesure consiste à appliquer un flux d'une solution d'électrolytes (solution tampon) dans un capillaire recouvert du film multicouche. La différence de potentiel ou potentiel d'écoulement ( $\Delta V$ ) aux extrémités du capillaire est mesurée en fonction de la différence de pression ( $\Delta P$ ) qui est appliquée aux extrémités du capillaire.

#### ♦ Dispositif expérimental

Le dispositif expérimental (Figure 2-9) est constitué de deux cellules de mesure reliées par un capillaire en silice de 20 cm, de longueur et  $530 \pm 12 \mu\text{m}$  de diamètre (SIN 2042-R10, Perichrom SARL). Les films multicouches de polyélectrolytes sont construits dans le capillaire. L'ensemble est relié par une extrémité à un réservoir de solution d'électrolytes qui peut être mise sous pression (1.2 bar) avec une bouteille d'azote. Au cours de l'expérience, les valeurs du potentiel d'écoulement ainsi que la différence de pression aux extrémités du

capillaire sont acquises en continu par un logiciel mis au point par J. Iss (Institut Charles Sadron, Strasbourg).

♦ Procédure de mesure

Après étalonnage de la résistance du capillaire ( $R_c$ ) et du circuit dans les conditions expérimentales (sans flux), le film multicouche est construit *in situ* dans le capillaire. 8 mL d'une solution de polycation sont injectés pour le dépôt de la première couche, laissés au repos pendant 20 min puis rinçés par 50 mL de solution d'électrolyte. Après le rinçage du film, le potentiel d'écoulement est mesuré à trois reprises en fonction de la pression aux extrémités du capillaire. La pression est contrôlée par l'application ponctuelle d'une pression de 1.2 bars à une extrémité du capillaire. La valeur moyenne de ces trois mesures (et l'écart type) est prise pour valeur du potentiel zéta.

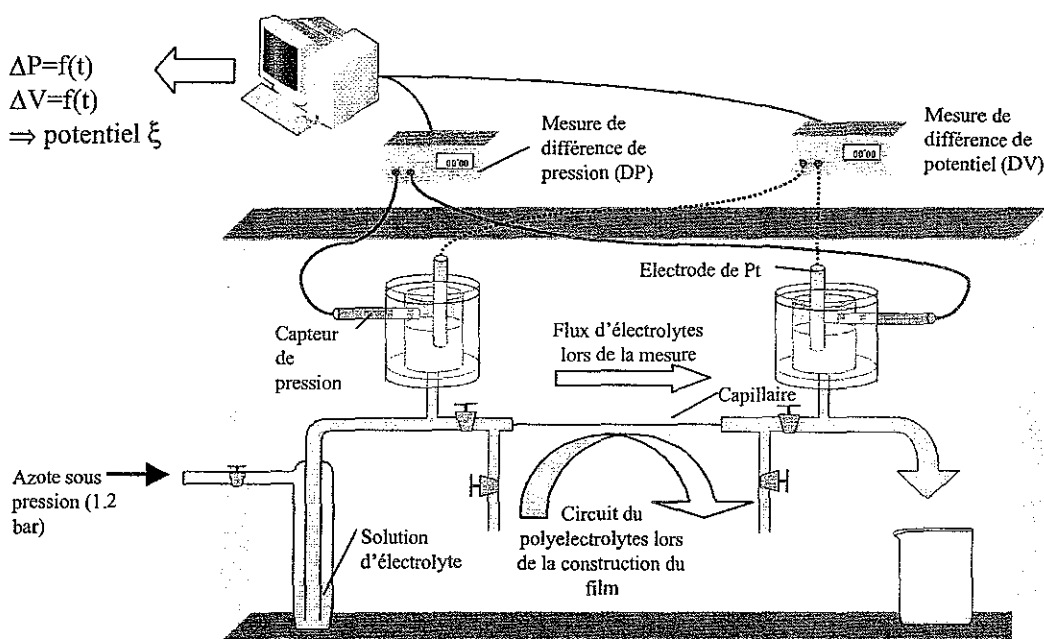


Figure 2-9 : Dispositif expérimental de mesure du potentiel d'écoulement. Le potentiel  $\xi$  est obtenu par analyse de la différence de pression et du potentiel d'écoulement aux extrémités du capillaire en fonction du temps lors de la mise en mouvement de la solution d'électrolyte à l'aide de la surpression dans le réservoir d'électrolyte. D'autre part, un circuit secondaire au niveau du capillaire permet d'injecter directement les polyélectrolytes dans le capillaire et de les rincer après chaque adsorption.

### 2.2.1.4. Microscopie de fluorescence

La fluorescence est la propriété d'une molécule à absorber un photon, puis à le ré-émettre à une longueur d'onde plus élevée (Diagramme de Jablonski, Figure 2-10). Soumise à une excitation lumineuse de longueur d'onde donnée, la molécule fluorescente est portée dans un état électronique excité ( $S_1'$ ). A température ambiante, la conversion interne entraîne une perte partiellement de l'énergie absorbée et la molécule se retrouve à un état excité moins élevé ( $S_1$ ). Le retour de la molécule à son état stable ( $S_0$ ) est associé à la libération d'énergie sous forme lumineuse. La perte d'énergie par conversion interne, se traduit par une longueur d'onde d'émission supérieure à la longueur d'onde d'absorption (Déplacement de Stocke).

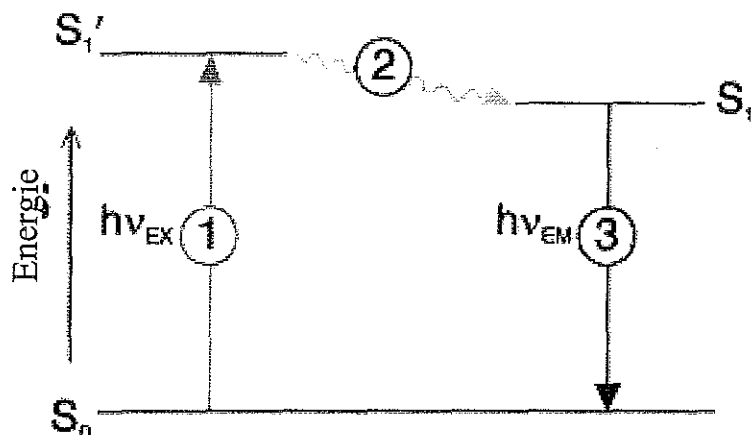


Figure 2-10 : Diagramme de Jablonski. Un électron du fluorophore adsorbe de l'énergie sous forme lumineuse (1) et se retrouve à l'état excité  $S_1'$ . Lors de la déexcitation, il y a tout d'abord perte de l'énergie par conversion interne (vibration, chocs...). La molécule se trouve à état d'excitation inférieur ( $S_1$ ) et retrouve son état stable ( $S_0$ ). Cette transition libère de l'énergie sous forme lumineuse, correspond à une longueur d'onde plus élevée (car l'énergie est plus faible).

#### ♦ Microscopie à épi-fluorescence

En microscopie à épi-fluorescence, la lumière est tout d'abord filtrée (filtre d'excitation) puis dirigée par un miroir dichroïque vers l'objectif qui sert d'abord de condensateur au faisceau d'excitation. L'objectif est ensuite utilisé pour collecter la fluorescence émise par l'échantillon. L'utilisation d'un tel dispositif (TE200 ; Nikon) associé à l'emploi d'un miroir dichroïque et d'un filtre d'émission limite l'incidence de la lumière excitatrice sur le signal collecté aux oculaires et fournit des images avec un bon signal/bruit. L'objectif collecte également la fluorescence provenant des plans non-focalisés et ne permet alors pas d'analyse volumétrique.

♦ Microscopie confocale

Le principe général de la microscopie confocale a été proposé par Minsky (1957). Il s'agit de diriger une lumière ponctuelle, généralement obtenue à partir d'un laser, sur un point précis (point focal) de l'échantillon à l'aide d'un microscope à épi-fluorescence. Cependant, le trajet du faisceau laser dans l'échantillon génère de la fluorescence en dehors du plan focal. Pour éliminer cette fluorescence parasite, un trou de filtrage (pinhole) (Figure 2-11) est placé en amont du détecteur, il ne laisse passer que la lumière en provenance du point focal. L'image ainsi obtenue présente un bon rapport signal /bruit. Le balayage de l'échantillon en XY par le laser fournit une image du plan focal. Ce balayage est obtenu à l'aide de miroirs motorisés disposés sur le trajet optique du laser. Pour le balayage en Z, l'objectif est monté sur un moteur piézo-électrique. Il est ainsi possible d'obtenir des images en provenance de différents plans focaux et ainsi reconstituer une structure en trois dimensions avec une résolution latérale et normale respective de  $0.15 \mu\text{m}$  et  $0.58\mu\text{m}$  pour un objectif ayant une ouverture numérique de 1.4 et l'utilisation d'une longueur d'onde de 500 nm (Stelzer and Lindek, 1994).. Cette caractéristique est particulièrement intéressante pour étudier la structure normale des films multicouches épais (micrométriques) en milieux aqueux.

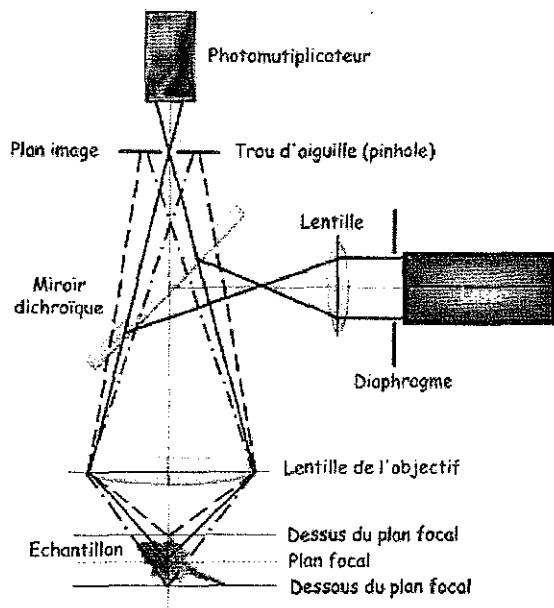


**Figure 2-11 :** Schéma de principe d'un microscope confocal en épi-fluorescence. La source laser est condensée par l'intermédiaire du miroir dichroïque et de l'objectif en un point focal. La fluorescence est ensuite recueillie par un photomultiplicateur. Pour éliminer la fluorescence parasite (ligne en pointillé), le trou de filtrage (pinhole) est disposé au niveau du plan image de l'objectif.

Le microscope confocal utilisé est de type LSM510 (Zeiss), monté sur un microscope AxioVert100M (Zeiss) associé à des lasers HeNe et Ar. Pour les visualiser, les films sont marqués à l'aide de fluorophores couplés aux polyélectrolytes, généralement à l'aide de fluorescéine isothiocyanate (FITC adsorption/émission 488nm/520nm) ou de TexasRed (596nm/620nm). Les polyélectrolytes marqués utilisés sont la Poly(L-Lysine)-FITC (PLL-FITC, Sigma), le Chitosan-FITC et le Hyaluronan-TexasRed (HA-TR) ces deux composés étant préparés par X. Shu du groupe de G. Prestwich (University of Utah).

Sur les films multicouches dont l'un au moins des polyélectrolytes diffuse, le dépôt d'un polyélectrolyte marqué qui diffuse à travers l'ensemble de la construction permet de visualiser l'intégralité du film (Figure 2-12). Pour obtenir un marquage complet du film, le polyélectrolyte est déposé en couche terminale pendant une durée minimale de 15 min pour la PLL-FITC (0.1 mg/mL).

Le microscope confocal utilisé disposant de plusieurs lasers, il est possible de co-marquer les films multicouches à l'aide de deux sondes fluorescentes différentes. Il est également possible d'observer le comportement cellulaire sur un film multicouche par un marquage distinct du film et des cellules (cf. culture cellulaire).

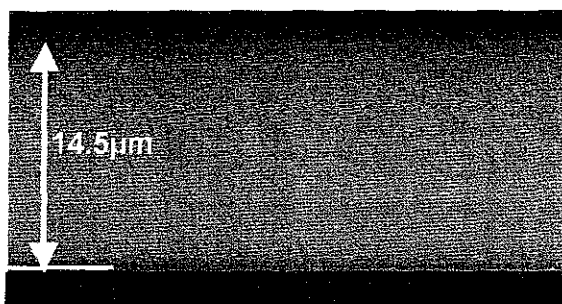
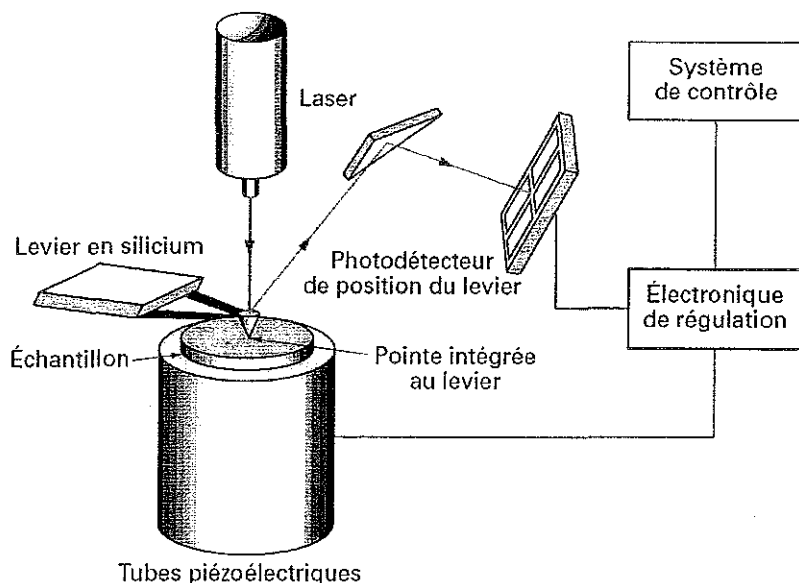


Figure 2-12 : Coupe normale en Z d'un film multicouche de  $(\text{PLL/HA})_{60}$ -PLL-FITC construit sur une lamelle de verre et observé avec un objectif X 40. La bande verte correspond à la diffusion de la PLL-FITC à travers tout le film et permet de mesurer l'épaisseur du film, ici 14.5  $\mu\text{m}$ .

### Microscopie à force atomique

La microscopie à force atomique (AFM, Atomic Force Microscopy) est un microscope à champ proche. Ce type de microscope a été développé dans les années 80 avec le microscope à effet tunnel (Binning et al., 1982) : l'AFM en est une variante destinée à l'observation de la topographie des surfaces non-conductrices (Binnig et al., 1986). Le principe consiste à balayer la surface de l'échantillon avec une pointe et à détecter les interactions entre cette pointe et la surface. L'AFM est ainsi utilisé pour imager les surfaces biologiques avec une résolution latérale de l'ordre de la dizaine de nanomètre et normale (en z) de l'ordre de l'Angstrom. Les évolutions des techniques AFM ont permis la cartographie de diverses propriétés : mécaniques (Burnham et al., 1990), électrostatiques et magnétiques (Martin et al., 1988).



**Figure 2-13 : Schéma d'un microscope à force atomique.** L'échantillon est fixé sur le tube piézo-électrique. La pointe du cantilever est approchée de la surface. Les interactions entre la pointe et la surface génèrent une déflexion du cantilever qui est mesurée optiquement. Un faisceau laser est réfléchi par l'extrémité de la pointe sur une photodiode. Le voltage mesure par la photodiode indique la déflexion du cantilever.

#### ♦ Principe

La technique consiste à balayer la surface de l'échantillon avec une sonde fixée à l'extrémité d'un levier à constante de raideur connue, l'ensemble formant le cantilever. L'échantillon est fixé sur un tube piézo-électrique 3D ce qui permet un mouvement de l'échantillon dans les 3 dimensions (Figure 2-13). Lors du balayage, les interactions de la sonde avec la surface génèrent la déflexion du cantilever. Pour mesurer la déflexion, un

faisceau laser est focalisé sur l'extrémité du cantilever (zone réfléchissante) et il est réfléchi sur une photodiode à quatre cadans (Figure 2-13). La différence de tension entre les différents quadrants indique avec précision la déflection du cantilever. Cette méthode de mesure de la déflection présente l'avantage de ne détecter que les variations angulaires du cantilever. En revanche, ce type de mesure est sensible à la dérive thermique et nécessite un temps d'attente avant l'obtention d'un signal stable. La déflection est reliée à la force ( $F$ ) exercée sur la pointe par la loi de Hooke (2-13)

$$F = -k_c \Delta d \quad (2-13)$$

avec  $k_c$  la constante de raideur du cantilever et  $\Delta d$  la déflection du cantilever

#### ♦ Mode image

L'image en AFM est obtenue par la mesure de la déflection du cantilever en chaque point (XY) de la surface. Le mode image a été initialement développé pour observer la topographie de l'échantillon. Lors du balayage de la surface, les propriétés physico-chimiques de la surface modifient la déflection de la pointe, différentes procédures ont été développées afin de cartographier et de quantifier ces propriétés comme le module d'Young (Radmacher et al., 1996).

#### ↳ Mode contact

Dans ce mode, la pointe est maintenue en contact avec la surface de l'échantillon, généralement avec une force constante de l'ordre de 10 nN. Une boucle de rétroaction ajuste en permanence la position en z de l'échantillon à l'aide du déplacement de la céramique piézo-électrique. Le déplacement vertical (en z) du tube piézo-électrique en fonction de la position XY donne alors l'image topographique de la surface. Si l'échantillon est très peu rugueux, il est possible de bloquer le déplacement vertical (hauteur constante) et de réaliser l'observation topographique en associant uniquement la déflection du cantilever à la position en XY.

#### ↳ Mode non-contact

En mode non-contact, le cantilever balaye la surface sans contact en oscillant au-dessus de la surface. L'interaction pointe/surface entraîne des modifications de la fréquence de résonance. Le déplacement normal sur la céramique piézo-électrique permet de retrouver la fréquence de résonance et de caractériser la surface. L'étude des variations de fréquence permet notamment de réaliser une cartographie des propriétés magnétiques ou électriques de la surface.

↳ Mode Tapping

Pour remédier aux problèmes liés à l'imagerie en mode contact (altération de la surface par friction, bruit par torsion de la pointe), Zhong et al. (Zhong et al., 1993) ont développé le mode Tapping. Ce mode consiste à faire osciller la pointe à proximité de la surface pour qu'elle touche l'échantillon à chaque oscillation mais avec une amplitude suffisante pour permettre son détachement de l'échantillon. Ce mode est surtout utilisé pour imager les échantillons fragiles. L'étude du déphasage entre la fréquence appliquée par le tube piézoélectrique et celle détectée à la photodiode permet d'extrapoler notamment les propriétés viscoélastiques de la surface (Radtmacher et al., 1996).

↳ Procédure en mode image

La réalisation d'images topographiques est effectuée sur un Nanoscope IV (Veeco) avec des pointes pyramidales ( $\alpha=35^\circ$ ) montées sur des cantilevers triangulaires de constante de raideur comprise entre 50 et 200 pN/nm (MLCT-AUHW, Veeco) (Figure 2-14). Les observations sont réalisées en mode contact à une fréquence de balayage d'environ 2 Hz.

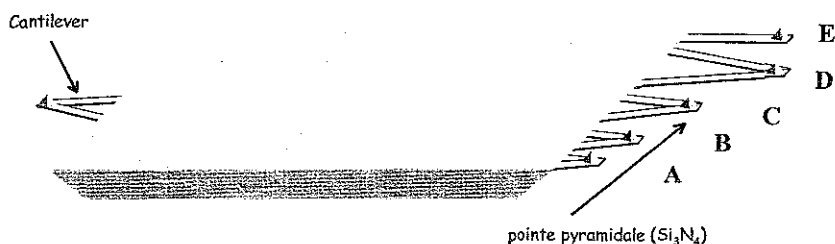


Figure 2-14 : Schéma d'un support de cantilevers à pointes pyramidales de constantes de raideur différentes (pointe de type MLCT-AUHW, Veeco). Généralement, seuls les pointes C et D sont utilisées pour la visualisation.

Les observations des films sont effectuées en phase liquide ou à sec. Pour l'observation à sec, les films sont d'abord rincés dans de l'eau ultra-pure pour éviter la formation de cristaux salins puis séchés à température ambiante pendant plusieurs heures. Les observations en milieu liquide sont réalisées dans la solution utilisée pour le rinçage des films.

Les observations des cellules sont effectuées à sec. Après fixation au glutaraldehyde (2.5%) dans du tampon phosphate salin (PBS 1X) pendant 25 min à température ambiante, les échantillons sont déshydratés progressivement avec des solutions éthanol de concentration croissance (50,75,90,100% v/v d'éthanol). Les échantillons sont finalement séchés à température ambiante avant d'être observés.

♦ Mode force

↳ Principe

En mode force, le but n'est plus d'acquérir une image mais d'étudier l'évolution de la force normale (en z) à l'échantillon en fonction de la distance entre la pointe et l'échantillon. Une expérience en mode force se déroule en deux phases : approche et retrait.

Dans un premier temps, le cantilever est approché de la surface (Figure 2-15). Il part d'un état initial (A) où il ne subit aucune interaction avec la surface.

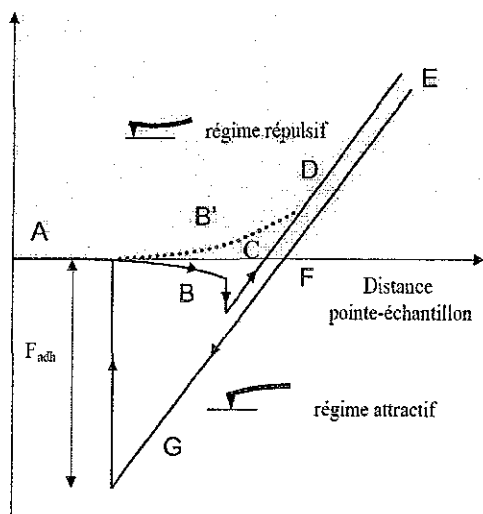


Figure 2-15 : Courbe de force caractéristique d'une expérience en AFM mode force: les flèches indiquent le sens du parcours de la courbe. L'expérience débute à l'équilibre (A). En approchant de la surface la pointe interagit avec la surface (B et B'). La pointe exerce ensuite une contrainte mécanique sur l'échantillon (D). Au cours du retrait, les forces d'adhésion maintiennent la pointe sur la surface (G). Lorsque la distance est suffisante, la pointe se détache et retrouve sa position d'équilibre.

Le cantilever est ensuite progressivement approché de la surface. La pointe commence à interagir avec la surface de façon attractive (B) ou répulsive (B'). Dans le cas d'une force attractive entre la pointe et la surface, la pointe entre au contact avec la surface pour une distance donnée (C). Ce saut fournit des informations sur les forces d'interaction entre la pointe et la surface et notamment sur la constante de Hamaker. A partir de la position C et jusqu'à E, la pointe exerce une contrainte sur l'échantillon.

Le mouvement du tube piézo-électrique est ensuite inversé quand la position E est atteinte. S'il n'y a aucune interaction entre la pointe et l'échantillon, la courbe de retrait sera identique à la courbe d'approche. Dans le cas contraire, la courbe de retrait présente une hystérésis par rapport à la courbe d'approche. Cette hystérésis (F et G) apporte des informations sur la force d'adhésion entre la pointe et la surface et plus particulièrement sur l'énergie de surface.

Initialement développée pour étudier les interactions électrostatiques (Ducker et al., 1992) ainsi que les phénomènes d'interaction protéine/surface, cette technique permet notamment de caractériser les propriétés mécaniques de surface.

#### ↳ Mesure du module d'Young

Le module d'Young ( $E$ ) (2-14) ou module élastique est défini comme le rapport d'une contrainte ( $\sigma$ ) sur une déformation relative ( $\varepsilon$ ) pour un échantillon homogène et isotrope.

$$E = \frac{\sigma}{\varepsilon} \quad (2-14)$$

Il est possible d'exercer une contrainte connue sur un échantillon à l'aide de la pointe de l'AFM et d'étudier la déformation du film. L'étude de l'approche entre A et E (Figure 2-15) permet d'obtenir une relation entre la déformation de l'échantillon et la force appliquée grâce à la relation de Hooke. Il est ainsi possible de caractériser les propriétés mécaniques de l'échantillon (module d'Young, viscosité,...). Par exemple, la loi de Hertz (2-15) relie la force exercée sur un objet ( $F$ ) à la l'indentation ( $\delta$ ) (distance de déformation de la pointe dans l'objet) par une fonction ( $K$ ) dépendant du module de Young de la surface (ici définie pour un contact élastique entre une sphère et une surface plane en l'absence d'adhésion) :

$$F = KR^{\frac{1}{2}}\delta^{\frac{3}{2}} \quad \text{avec} \quad K = \frac{4}{3} \left[ \frac{1-\nu_p^2}{E_p} + \frac{1-\nu_c^2}{E_c} \right]^{-1} \quad (2-15)$$

avec  $\nu_p$  et  $\nu_c$  les coefficients de Poisson,  $E_p$  et  $E_c$  le module d'Young caractéristique de la pointe et de l'échantillon et  $\delta$  l'indentation de la pointe dans le film (2-15)

$$\delta = \Delta d - (z - z_0) \quad (2-16)$$

Pour l'étude de films minces et mous comme les films multicouches de polyélectrolytes, l'emploi de pointes pyramidales génère des contraintes risquant d'endommager l'échantillon. Dimitriadis et al (Dimitriadis et al., 2002) ont également montré sur des gels de poly(vinyl alcool) que l'emploi de pointes pyramidales entraîne une surestimation significative des valeurs du module d'Young sur les films minces d'épaisseur micrométriques. Ils ont développé une technique de mesure du module d'Young en utilisant des pointes sphériques, afin de mieux préserver les échantillons. De plus, l'emploi de sphères de taille micrométrique permet d'exercer une contrainte sur une zone plus étendue rendant, la technique moins sensible aux hétérogénéités de surface.

#### ↳ Réalisation des expériences

La mesure du module d'Young a été réalisée au sein du laboratoire du professeur D. Discher (Université de Pennsylvanie) au moyen d'un microscope Asylum MFP-1D monté sur un microscope inversé (Axiovert 100, Zeiss).

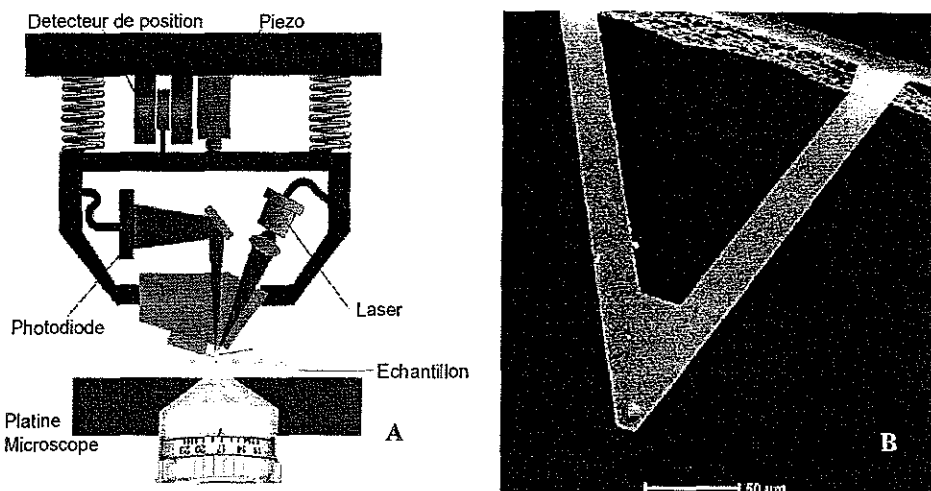


Figure 2-16 : (A) Schéma de l'AFM Asylum MFP-1D. (B) Image en microscopie électronique d'un cantilever avec une pointe colloïdale de 5 μm de diamètre (BioForce NanoScience).

Les mesures sont réalisées avec des particules de borosilicate de 5 μm de diamètre fixées sur des cantilevers triangulaires de constante de raideur de 60 pN/nm (BioForce Nanoscience) (Figure 2-16). Les films étudiés étaient déposés sur des lamelles de verre (24\*24 mm<sup>2</sup>) par trempage à l'aide d'un bras automatisé (Dipping Robot DR3, Kierstein). Les lamelles échantillons sont elles-mêmes fixées sur une lame de verre, le tout étant déposé sur la platine du microscope inversé. Dans la configuration de l'AFM d'Asylum Research, le cantilever est solidaire de la céramique piézo-électrique. (Figure 2-16). Avant chaque série d'expériences, la calibration du cantilever est effectuée dans l'air à l'aide d'un module d'analyse du bruit thermique (Thundat et al., 1994). Les courbes de distances sont ensuite réalisées à différents endroits de l'échantillon avec une vitesse d'approche constante de 2 μm/s. Plusieurs cycles d'approches retraits sont réalisés sur chaque zone de mesure.

#### ↳ Analyse des courbes

La force est exercée sur les films multicouches perpendiculairement à leur surface (axe z). Le module de Young ainsi calculé correspond au module d'Young apparent dans la direction perpendiculaire à la surface du film, qui sera noté ici  $E_{\perp}$ . L'analyse des courbes se déroule en deux temps. Dans un premier temps, le point de contact théorique ( $z_0$ ) entre la pointe et la surface est déterminé en utilisant une régression selon la méthode des moindres carrés de la fonction proposée par Domke et Radmacher (Domke and Radmacher, 1998).

Cette fonction (2-17) relie la distance entre la surface et la pointe ( $z$ ) à la déflexion du cantilever ( $d$ )

$$z = z_0 - b\sqrt{d} + d \quad (2-17)$$

Après avoir déterminé le point de contact,  $E_{\perp}$  est calculé pour chaque point avec la formule proposée par Dimitriadis (2-18), représentant le modèle de Hertz adapté à un objet indenteur sphérique. Cette formule est valable pour des mesures faites avec une pointe colloïdale sur un film d'épaisseur finie adhérent à la surface :

$$F = 4 \frac{4E}{3(1-\nu^2)} R^{1/2} \delta^{3/2} \left[ 1 - \frac{2\alpha_0}{\pi} \chi + \frac{4\alpha_0^2}{\pi^2} \chi^2 - \frac{8}{\pi^3} \left( \alpha_0^3 + \frac{4\pi^2}{15} \beta_0 \right) \chi^3 + \frac{16\alpha_0}{\pi^4} \left( \alpha_0^3 + \frac{3\pi^2}{5} \beta_0 \right) \chi^4 \right]$$

$$\alpha_0 = -\frac{1.2876 - 1.4678\nu + 1.3442\nu^2}{1-\nu} \quad (2-18)$$

$$\beta_0 = \frac{0.6387 - 1.0277\nu + 1.5164\nu^2}{1-\nu}$$

avec  $\chi = \frac{\sqrt{R\delta}}{h}$  où  $R$  est le rayon de sphère du cantilever,  $\delta$  l'indentation,  $h$  l'épaisseur

du film est dans notre cas déterminée par microscopie confocale,  $\nu$  le coefficient de Poisson est fixé à 0.5 (cette valeur est typique de films polymériques (Dimitriadis et al., 2002)). La formule est applicable uniquement pour des films dont l'épaisseur est inférieure à ~13 fois le rayon de la sphère d'indentation. De plus, l'indentation ne doit pas être réalisée sur plus de 10 % de l'épaisseur du film. La courbe de  $E_{\perp}$  en fonction de l'indentation dans le film est alors représentée. (Figure 2-17). La moyenne des valeurs obtenues au niveau du plateau est retenue comme la valeur du module d'Young.

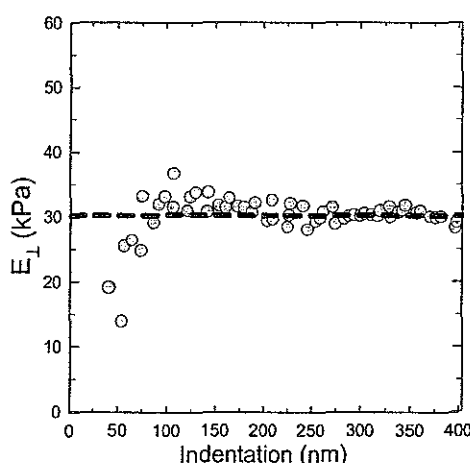


Figure 2-17 : Evolution du module d'Young en fonction de l'indentation pour un film multicouche (PLL/HA) 20.

## 2.2.2. Analyses Biologiques

### 2.2.2.1. Culture de chondrosarcomes

Les cellules de chondrosarcome humain HCS-2/8 (passage de 22 à 25) sont cultivées dans le milieu de culture « Minimum Essentiel Eagle » (MEM, GibcoBRL) supplémenté avec 10% de sérum de veau fœtal (FCS) et des antibiotiques (pénicilline, streptomycine respectivement 0.5 et 0.5% (GibcoBRL) dans une étuve thermostatée à 37°C sous une atmosphère de 5% de CO<sub>2</sub>. Pour le passage, les cellules sont détachées par trypsination (Trypsine/EDTA, Sigma à 0.5%) pendant 4 min à 37°C. Les cellules sont stockées par congélation (-80°C). Pour cette congélation, elle sont suspendues à 10<sup>6</sup> cellules par mL dans un milieu contenant du MEM, 20 % de sérum de veau fœtal (FCS GibcoBRL) et 20% de dimethyl sulfoxyde (DMSO, Sigma). La densité cellulaire est mesurée avec une cellule Neubauer.

Pour les études de prolifération cellulaire, les cellules sont déposées à une concentration comprise entre 10<sup>4</sup> et 10<sup>5</sup> cellules par mL. Le milieu est ensuite changé après 24 h puis tous les 2 jours.

### 2.2.2.2. Culture des chondrocytes

Les cellules de chondrocytes de rats ont été fournies par Dr L. Grossin du laboratoire de Physiopathologie et Pharmacologie articulaire de la faculté de médecine de Vandoeuvre-Lès-Nancy. Elles sont extraites de capsules de têtes fémorales de rats âgés de 8-10 semaines. Les capsules sont découpées en petits morceaux et digérées à l'aide de pronase (Sigma) à raison de 4 mg dans 5 mL de 0.9% de NaCl pour 100mg de capsule pendant 2 h à 37 °C.

Après centrifugation (1200 tpm, 10 min), les prélèvements sont digérés par de la collagénase (Boehringer) à raison de 4 mg dans 5 mL de MEM (GibcoBRL) pour 100mg de capsules fraîches pendant 12 h à 37 °C. Après centrifugation (1200 tpm 10 min), les cellules sont mises en culture dans leur milieu DMEM/F12, complété par les éléments suivants : glutamate, (12%), pénicilline (50 U/mL), streptomycine (50 U/mL), sérum de veau fœtal (11%) et à la fongizone (1 %) (GibcoBRL). Les études de prolifération sont faites dans les mêmes conditions que pour les chondrosarcomes, en se limitant toutefois à deux passages.

### 2.2.2.3. Observation cellulaire

Les observations cellulaires sont effectuées avec un microscope TE200 (Nikon) équipé en champ clair et en épi-fluorescence (lampe au mercure 100W et filtre pour la FITC

(495/520nm) et la rhodamine (560/590 nm). Les images sont capturées à l'aide d'une caméra numérique DMX1200 (Nikon) associée à un logiciel de capture d'images (Lucia).

#### *2.2.2.4. Dosage cellulaire*

- ◆ Test MTT

Ce test informe sur la viabilité cellulaire en mesurant l'activité mitochondriale des cellules. Le test MTT est réalisé selon la méthode décrite par Mosmann (1983). Le principe du test MTT consiste à mesurer l'activité de la succinate déshydrogénase mitochondriale uniquement présente chez les cellules vivantes. Cette enzyme, par coupure du cycle tétrazolium, transforme le MTT, ou Bromure de 3-(4,5-diméthylthiazol-2-yl)-2,5-diphényltétrazolium de couleur jaune, en cristaux de formazan bleus. Le MTT est déposé à raison de 1 mg/mL de MEM sans sérum. Après incubation (3h, à 37 °C), les cristaux de formazan sont solubilisés dans une solution de n-propanol (1/6 v/v) et 5 N de HCl (15 min à 37°C sous agitation). La quantité de formazan est ensuite évaluée par une lecture spectrophotométrique à 550 nm (par rapport à une référence à 650 nm), la densité optique étant directement proportionnelle au nombre de cellules vivantes.

- ◆ Dosage à la  $^{3}\text{H}$ -thimidine

Le dosage à la  $^{3}\text{H}$ -thymidine permet d'obtenir la quantité de cellules capables d'incorporer de la thymidine extra-cellulaire et est représentative des cellules qui sont en phase de synthèse d'ADN. Dans ce test, le milieu est complété avec de la  $^{3}\text{H}$ -thimidine (Perkin) (5  $\mu\text{Ci}/\text{mL}$ ) pendant 24 h. Les cultures sont ensuite lavées au PBS, puis trypsinizées et enfin lysées par des cycles de congélation/décongélation. Les lysats sont déposés dans du liquide à scintillation. La radioactivité totale est ensuite comptée par un scintillateur (Packard-Perkin-Elmer).

- ◆ Marquages fluorescents

- ↳ Marquage à la Rhodamine-Phalloïdine

La rhodamine-phalloïdine est un marqueur des filaments d'actine et permet d'observer le cytosquelette de la cellule. Elle donne ainsi des informations sur l'organisation et la morphologie de la cellule. Après lavage des cellules au tampon phosphate (PBS à 37°C). Les cellules sont fixées avec du paraformaldehyde (PFA, sigma) à 3.7 % v/v dans du PBS, pendant 15 min à température ambiante. Les cellules fixées sont perméabilisées avec une solution de 0.1% v/v de triton X-100 (t-Octylphenoxy Polyethoxyethanol, Sigma) et de PFA 3.7% v/v dans le PBS durant 10 min à température ambiante. Après, rinçage au PBS, la

Rhodamine-Phalloidine à 1 µg/mL est mise en contact des cellules durant 10 min à température ambiante. Finalement, l'ensemble est rincé au PBS et conservé à 4 °C dans le PBS jusqu'à l'observation. L'observation est réalisée avec le filtre (560/590nm) sur le microscope à épi-fluorescence TE200 Nikon.

#### ↳ Marquage au PHK26

Le marquage au PHK26 permet un marquage fluorescent du cytoplasme non toxique et rémanent (jusqu'à trois mois), permettant de suivre une culture cellulaire sur plusieurs semaines. Le marquage est réalisé avec un kit PHK26 (Sigma). Les cellules sont préalablement trypsiniées et mises en solution dans le MEM à une concentration de  $2 \times 10^7$  cellules par mL. La solution mère est diluée (4%) avec le diluant C du kit et mélangé avec un rapport 1/1 avec les cellules. Après 3 min à 37 °C, le marquage est stoppé avec l'ajout de sérum (1/1 v/v) pendant 15 min. La suspension cellulaire est lavée, dans un premier temps, au milieu sans sérum puis au milieu avec sérum (10 % v/v). Les cellules sont ensuite mises normalement en culture sans condition spécifique (MEM+10% FBS, 37°C, 5%CO<sub>2</sub>). L'observation est réalisée en épi-fluorescence (TE200 Nikon) avec le filtre (560/590nm).

#### 2.2.2.5. Bactéries

L'étude de l'adhésion bactérienne a été effectuée à partir d'une souche gram négative *d'Escherichia Coli* (Invitrogen). Cette souche a été transformée en utilisant un plasmide pFPV25 portant le gène de la protéine fluorescente verte (Green Fluorescent Protein, GFP) sous contrôle d'un promoteur de la protéine ribosomale de *S. typhimurium*. Ce plasmide portait également un gène de résistance à l'ampicilline, ce qui a permis la sélection des bactéries exprimant la GFP (plasmide généreusement donné par le Dr B. Lemaître, CNRS-CGM, Gif-sur-Yvette, France).

Pour chaque expérience, une colonie bactérienne est ensemencée en présence de milieu Luria Broth (LB, Difco). La culture est réalisée en aérobiose, à 37°C sous agitation (150 tpm) pendant environ 12h. Après repiquage, la croissance bactérienne est suivie régulièrement par mesure de la densité optique (DO) à 600 nm. Lors des tests d'adhésion, les cultures sont mises en contact avec les multicouches lorsque la phase exponentielle de croissance est atteinte, ce qui correspond à une DO comprise entre 0.3 et 0.6 à 600 nm. Les bactéries sont alors diluées afin d'obtenir une concentration de  $1.35 \times 10^6$  bactéries par mL, soit une DO de 0.1 à 600 nm. Après 30 minutes, les multicouches sont rincées trois fois avec du tampon phosphate, les bactéries adsorbées sur la surface sont visualisées par microscope à

fluorescence inversé (TE200, Nikon) et différents champs de la surface sont photographiés (DMX1200, Nikon) et le comptage des bactéries fluorescentes est effectué.

#### *2.2.2.6. Technique d'aspiration par micropipette*

Cette technique a été développée pour mesurer individuellement la force d'adhésion de cellules au contact d'une surface. Pour cela, après adhésion des cellules au contact du substrat étudié, une force obtenue par dépression est exercée sur chaque cellule par une micropipette afin de les détacher. Cette force de détachement est contrôlée par un système de manomètre.

##### ♦ Fabrication des micropipettes

Les micropipettes sont obtenues par un étirage à chaud d'un tube capillaire. Les tubes capillaires (WPI-100/4) de diamètre extérieur 1 mm, intérieur 0.5 mm, et de longueur 10.2 cm, sont tout d'abord nettoyés à l'éthanol. Ils sont ensuite étirés d'une étireuse (Sutter P-97, Sutter Instruments) possédant un filament en boîte de 2 mm de largeur (FB220B, Sutter Instruments). Les différents paramètres de l'appareil (la température de chauffage du filament (valeur du « ramp test »), la force (90 sur 255) et la vitesse (75 sur 255) exercées sur le tube capillaire, ainsi que la pression (500 sur 999) et le temps d'action (80 ms) du flux de refroidissement) ont été ajustés pour obtenir des micropipettes avec une pointe de 20 à 30 mm de longueur et un diamètre interne à l'extrémité de 2 à 3  $\mu\text{m}$ . Elles sont ensuite coupées à l'aide d'une micro-forge (Alcatel), la pointe est mise en contact avec une goutte de verre fondu maintenue sur le filament en platine iridium de la microforge. L'arrêt brutal du chauffage accompagné de la rétraction du filament, permet de briser la pointe au niveau du point de contact entre la pointe et la goutte de verre. Le diamètre final de l'extrémité  $D_p$  est ainsi adapté aux besoins : de l'ordre de 8 à 10  $\mu\text{m}$  pour les mesure de force d'adhésion cellulaire. Les micropipettes sont ensuite remplies sous vide d'eau ultra-pure pour éliminer les bulles d'air éventuellement présentes.

##### ♦ Mesure de la pression d'aspiration

Le système utilisé a été fabriqué au laboratoire en reproduisant un système déjà existant (Pr. Discher, Université de Pennsylvanie), lui-même conçu selon le principe décrit par Needham (1993). La micropipette est reliée à un manomètre constitué de deux réservoirs, un réservoir de référence et un réservoir de travail hermétique, la différence de pression entre ces deux réservoirs étant obtenue avec un capteur de précision (Validyne DP103 : 0-12 kPa, précision ~20 Pa) relié à un afficheur digital (Validyne CD 223) (Figure 2-18). L'afficheur est calibré à l'aide d'un manomètre à eau (tube en U) avec une précision de l'ordre du mm d'eau (~10 Pa) sur une hauteur de 1.20 m (~1.2 hPa correspondant à 100 % sur l'afficheur).

Les deux réservoirs sont montés sur une platine mobile dans l'axe vertical, ce qui permet d'ajuster la pression initiale à l'extrémité de la pipette.

La variation de pression à l'extrémité de la pipette est obtenue par compression ou décompression de l'air présent dans le réservoir de travail à l'aide d'une seringue. Afin d'obtenir une variation de pression uniforme, la seringue est montée sur un pousse-seringue programmable (Genie, Kent Scientific). Par exemple, une aspiration de 1 mL/min dans la seringue (50 mL) correspond à une variation de pression d'environ 200 Pa/min.

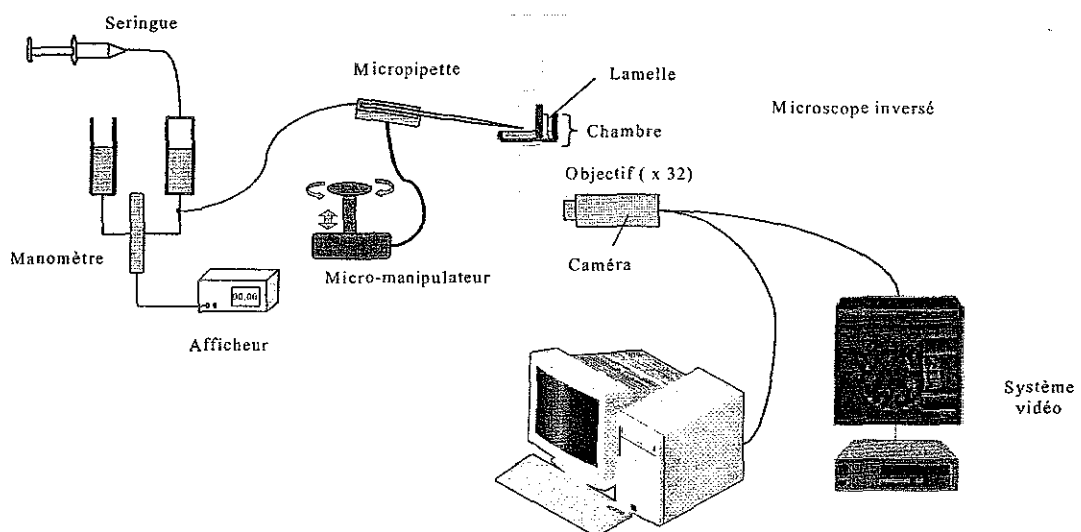


**Figure 2-18 :** Montage expérimental utilisé pour les expériences de micromanipulation comprenant : une chambre de mesure dans laquelle est placée une lamelle recouverte d'une multicoche de polyélectrolytes et des cellules, un microscope inversé équipé d'un micromanipulateur hydraulique, un système vidéo et un manomètre pour la mesure de la pression d'aspiration.

#### ◆ Chambre de mesure et dispositif expérimental

Une chambre de mesure (Figures 2-19) a été conçue spécialement pour l'expérience : elle est constituée d'une section de seringue de 50 mL en polypropylène fixée sur une lamelle de verre (diamètre 40 mm, 0.17 mm d'épaisseur) à l'aide d'une colle silicone. L'échantillon constitué d'une lamelle recouverte de la multicoche est fixé sur un support en T en plexiglas. L'échantillon est maintenu verticalement sur le support à l'aide de graisse silicone.

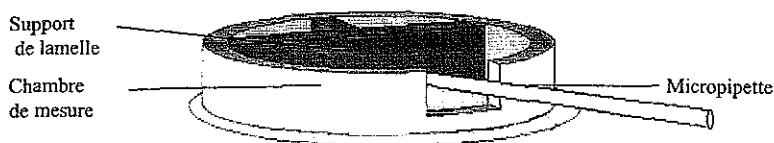


**Figure 2–19 : Schéma de la chambre de mesure utilisée pour les expériences de micromanipulation. Le support de lamelle est en forme de T en plexiglas. La chambre est ouverte sur le côté ce qui permet un passage facile de la micropipette en minimisant l'angle par rapport à l'horizontale.**

L'ensemble est monté sur une platine de microscope inversé (TE 200 Nikon) doté d'un objectif x40 à longue distance de travail et associé à un système de micromanipulation hydraulique tridimensionnel (Narishige). Le microscope est équipé d'un système acquisition numérique comportant une caméra numérique (DXM1200, Nikon) et un micro-ordinateur.

♦ Protocole de mesure de la force de détachement cellulaire

Une lamelle recouverte d'une multicoche est fixée sur le support en plexiglas et placée dans la chambre de mesure. La chambre est ensuite remplie avec 2 mL de milieu de culture avec ou sans sérum suivant les conditions d'études à température ambiante ( $\sim 23^{\circ}\text{C}$ ). Les cellules d'un diamètre moyen de  $\sim 18 \mu\text{m}$  sont ensuite déposées dans la chambre à raison de 5000-10000 cellules par mL. Après une phase d'équilibration (10 min), les cellules sont alors capturées une à une, à l'aide de la micropipette avec une légère dépression ( $\sim 50 \text{ Pa}$ ) et mises au contact de la multicoche pendant 10 s. Après suppression de la dépression et retrait de la micropipette, les cellules sont laissées au contact de la multicoche pendant 30 min.

Après cette phase d'adhésion, la micropipette est délicatement approchée de la cellule et une dépression est appliquée sur la membrane cellulaire. La platine motorisée du microscope est déplacée de quelques micromètres (5-15  $\mu\text{m}$ ) de façon normale à la micropipette, l'opération étant renouvelée avec une augmentation de la dépression (par pas de 120 Pa) jusqu'à obtenir le détachement de la cellule. La force d'adhésion pour la cellule est calculée à partir de la pression négative minimale nécessaire au détachement de la cellule (Figure 2-20). Chaque mesure d'adhésion est réalisée sur un minimum de 50 cellules pour chaque type de surface examinée.

Au cours de l'expérience d'autres paramètres tels que le diamètre de la micropipette, l'angle de contact, le rayon de contact de la cellule et de la multicoche, le rayon de la cellule, peuvent être éventuellement recueillis (Figure 2-20).

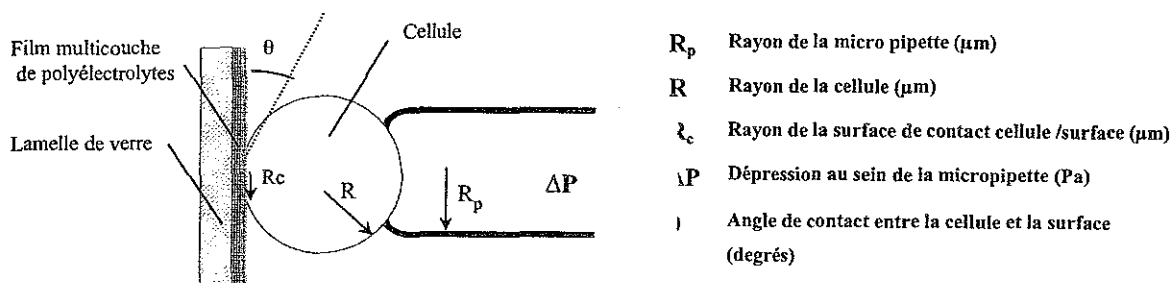


Figure 2-20 : Schéma indiquant les différents paramètres pouvant être mesurés au cours d'une expérience.

La force de détachement d'une cellule est déterminée à partir de la formule suivante (Ra et al., 1999) :

$$F = \Delta P * \pi * R_p^2 \text{ (en nN)}$$

où  $R_p$  représente le rayon de la micro-pipette et  $\Delta P$  la dépression mesurée.

♦ Analyse statistique des données

Les valeurs moyennes de force et d'énergie d'adhésion sont analysées soit deux par deux à l'aide du test sur la somme des rangs de Mann-Whitney, soit par comparaison de plusieurs ensembles de données à l'aide de la méthode Anova sur les rangs Kruskal-Wallis (Dunn). Le seuil de confiance est fixé à 95 % ( $p < 0.05$ ).

# **Chapitre 3 : Films multicouches de polypeptides : Relations entre les propriétés physico-chimiques et l'adhésion cellulaire**

---

Dans ce chapitre, nous nous sommes intéressés aux relations pouvant exister entre les propriétés physico-chimiques de films multicouches à base de poly(L-lysine) (PLL) et d'acide poly(L-glutamique) (PGA) et l'adhésion cellulaire. Ce type de film fait l'objet de nombreuses études au laboratoire et dans d'autres équipes, en raison des propriétés intrinsèques de ces polyélectrolytes et propriétés qu'ils peuvent avoir en étant combinés. Ces films possèdent des propriétés biologiques, notamment liées aux polyélectrolytes. Ces deux polyélectrolytes sont des homo-poly(amino acides) synthétiques, biodégradables, biocompatibles et solubles en milieu aqueux. Pour ces raisons, ils sont utilisés dans de nombreux domaines d'activité tels que l'industrie alimentaire, cosmétique et médicale. Dans ce dernier domaine, le PGA est notamment utilisé pour « transporter » et « délivrer » divers médicaments comme par exemple des anti-cancéreux tel que le paclitaxol (Li et al., 2000). La PLL permet également de transporter des médicaments tel que le methexitate (agent anti-métabolique), (Ryser and Shen, 1978). La PLL est également utilisée pour recouvrir des surfaces, favoriser l'adsorption protéique ou l'adhésion cellulaire. Les deux macromolécules portent des charges opposées, négatives pour le PGA via ces groupements carboxyles et positives pour la PLL par ces groupes amines. Elles peuvent donc être utilisées ensemble pour construire des films multicouches de polyélectrolytes (Tryoen-Toth et al., 2002). De plus, ces polyélectrolytes peuvent être facilement couplés à d'autres molécules, voire à des principes actifs, comme le PEG ((Boulmedais et al., 2004; Huang et al., 2001; Tosatti et al., 2004) ou l'α-MSH (Chluba et al., 2001).

Dans un premier travail (chapitre 3-1), nous avons déterminé de manière quantitative l'adhésion de cellules de chondrosarcomes (HCS-2/8) sur des films multicouches de type (PLL/PGA). Nous avons analysé, en particulier, l'influence du nombre de couches constituant le film multicouche sur l'adhésion cellulaire en présence ou non de sérum. Tout d'abord, nous avons caractérisé la croissance de ces films et l'adsorption de protéines sériques. Les cellules

HCS-2/8 ont été choisies car elles étaient notamment utilisées pour d'autres études au sein du laboratoire, notamment pour le recouvrement d'une prothèse laryngo-trachéale(Vautier et al., 2003).

Dans un second travail (chapitre 3-2), nous nous sommes intéressés à ces mêmes films, mais construits à des pH très différents, pour étudier l'influence de celui-ci sur les propriétés des films et notamment sur l'adhésion cellulaire. Toutes les mesures cellulaires ont été réalisées en présence de milieu physiologique. Il nous a donc tout d'abord fallu tester la stabilité de ces films à un pH de 7.4 et en présence de sels ( $\text{NaCl}$ ,  $\text{Ca}^{2+}$ ,  $\text{Mg}^{2+}$ ,  $\text{PO}_4^{2-}$ ).

### **3.1 : Influence de l'épaisseur et de la couche terminale des films multicouches (poly(L-lysine)/acide poly(glutamique)) sur la force de détachement cellulaire.**

#### **3.1.1. Résumé 1**

Cette étude a débuté par l'évaluation des propriétés physico-chimiques (épaisseur, topographie, charge de surface...) des films multicouches à base de poly(L-lysine) et d'acide poly(L-glutamique) et plus particulièrement leurs évolutions au cours de la construction. Puis, dans une seconde étape, ces propriétés ont été corrélées à l'adsorption protéique et l'adhésion à court terme de cellules de chondrosarcome.

L'étude a été menée dans des conditions proches des conditions physiologiques (0.15 M NaCl et pH ajusté à 7.4). La construction des films a notamment été suivie par OWLS et QCM-D. L'épaisseur évolue alors exponentiellement avec le nombre de couches déposées et correspond à ~1 pour la monocouche de PLL, 10 et 150 nm pour un dépôt de (PLL/PGA)<sub>2</sub>-PLL et de (PLL/PGA)<sub>9</sub>-PLL. Les mesures réalisées par QCM-D et par spectroscopie par guide d'onde ont montré que la quantité de protéines sériques déposées dépend de la couche terminale du film. L'adsorption de protéine est négligeable sur les films terminés par PGA et de l'ordre de 0.3 µg/cm<sup>2</sup> pour les films terminés par PLL indépendamment de l'épaisseur du film.

Les mesures d'adhésion cellulaire réalisées à l'aide de la technique d'aspiration par micropipette ont permis par ailleurs de quantifier l'adhésion cellulaire à court terme (30 min). Pour cela, nous avons d'abord mis au point un dispositif permettant de placer une lamelle recouverte d'un film multicouche et de mettre au contact une cellule avec le film multicouche. Après une trentaine de minutes d'adhésion, la cellule est progressivement aspirée au sein de la micropipette, en augmentant la dépression appliquée à l'aide d'une seringue. La dépression est mesurée en continu ce qui permet ensuite d'en déduire la force de détachement. En analysant environ 60 cellules par conditions, il est alors possible de tracer des histogrammes de force de détachement. Ces histogrammes ont été obtenus pour des films se terminant par PLL et des films se terminant par PGA pour un nombre de couches variant de 1 à 9. Nous avons montré que des cellules de chondrosarcomes (HCS-2/8) n'adhèrent pas sur les films terminés par PGA en absence de sérum au contraire des films terminés par PLL. Nous avons également montré que l'ajout de sérum dans le milieu entraîne une forte diminution, de 30 à

50%, de la force de détachement des cellules sur les films de PLL. D'autre part, l'ajout de sérum permet de mesurer une légère adhésion sur les films terminés par PGA mais les valeurs sont nettement plus faibles que celles obtenues avec les films terminés par PLL. Cette étude a également montré que le nombre de couches et donc l'épaisseur des films influence l'adhésion cellulaire à court terme. En effet, un film de (PLL/PGA)<sub>9</sub>-PLL est environ 30% moins adhérent qu'une monocouche de PLL, ceci indépendamment de la présence ou non de sérum.

Nous avons ainsi pu mettre en évidence qu'il est possible de moduler l'adhésion cellulaire sur des films multicouches de polyélectrolytes en faisant varier le nombre de couches déposées et en changeant la nature de la couche terminale. De plus, il a été mis en évidence que l'adsorption protéique n'est pas le seul paramètre modifiant l'adhésion cellulaire sur les films multicouches.

### 3.1.2. Article 1

## Cell Interactions with Polyelectrolyte Multilayer Films

L. Richert,<sup>†</sup> Ph. Lavalle,<sup>†</sup> D. Vautier,<sup>†</sup> B. Senger,<sup>†</sup> J.-F. Stoltz,<sup>‡</sup> P. Schaaf,<sup>§,||</sup>  
J.-C. Voegel,<sup>†</sup> and C. Picart<sup>\*,†,||</sup>

INSERM Unité 424, UFR d'Odontologie, Université Louis Pasteur, 11 rue Humann,  
F-67085 Strasbourg Cedex, France, Institut Charles Sadron (CNRS-ULP), 6 rue Boussingault,  
F-67083 Strasbourg Cedex, France, Ecole Européenne de Chimie, Polymères et Matériaux de Strasbourg,  
25 rue Bacquerel, F-67087 Strasbourg Cedex 2, France, and UMR CNRS 7563, Faculté de Médecine,  
54 500 Vandoeuvre-lès-Nancy, France

Received April 9, 2002; Revised Manuscript Received July 19, 2002

The short-term interactions of chondrosarcoma cells with polyelectrolyte multilayer films built up by the alternate adsorption of poly(L-lysine) (PLL) and poly(L-glutamic acid) (PGA) was studied in the presence and in the absence of serum. The films and their interaction with serum proteins were first characterized by means of optical waveguide lightmode spectroscopy, quartz crystal microbalance, and zeta potential measurements. In a serum-containing medium, the detachment forces measured by the micropipet technique were about eight times smaller on PGA-ending than on PLL-ending films. For these latter ones, the adhesion force decreased when the film thickness increased. In a serum-free medium, the differences between the negative- and positive-ending films were enhanced: adhesion forces on PLL-ending films were 40–100% higher, whereas no cellular adherence was found on PGA-terminating films. PGA-ending films were found to prevent the adsorption of serum proteins, whereas important protein adsorption was always observed on PLL-ending films. These results show how cell interactions with polyelectrolyte films can be tuned by the type of the outermost layer, the presence of proteins, and the number of layers in the film.

### Introduction

There is an increasing interest in developing new coatings to improve biocompatibility and to prepare biomaterial surfaces that can resist or enhance cellular adhesion by mimicking extracellular matrix components.<sup>1,2</sup> The most important step toward this end concerns the improvement at the nanometer to micrometer scales of material surface properties<sup>3</sup> in order to control cell adhesion, spreading, and growth. It has been shown that different parameters such as hydrophobicity and hydrophilicity,<sup>4,5</sup> surface charge,<sup>6</sup> roughness,<sup>7</sup> and free energy<sup>8,9</sup> affect protein adsorption and thereby subsequent cellular adhesion. The definition of general rules is not straightforward, and the observed cellular behaviors probably depend not only on a single parameter but also on a complex combination of different factors. Substrate properties somehow modulate the ability of adsorbed proteins to interact with cells.

Recently, a new type of tunable surface has been proposed for controlling the chemistry and the spatial order of a substrate. It consists of the alternate deposition of polyanions and polycations for the buildup of multilayered polyelectrolyte films<sup>10,11</sup> that can have a nanometer or even microme-

ter thickness.<sup>12,13</sup> Various types of polyelectrolytes can be used for building up the multilayers including polypeptides (i.e., poly(L-lysine)) and natural polyelectrolytes (e.g., hyaluronan, chitosan).<sup>13–15</sup> Indeed, proteins,<sup>16,17</sup> DNA,<sup>18</sup> or even colloids can be embedded in the film or deposited on the top of it. It has been shown that the film morphology and thickness depend mainly on the buildup conditions such as ionic strength<sup>19</sup> and pH of the solution.<sup>20</sup>

For certain plasma proteins deposited on the top of the multilayers, a preferential adsorption on oppositely charged polyelectrolyte films was found.<sup>21–24</sup> To our knowledge, there are no data available for the deposition on a polyelectrolyte multilayer of a mixture of proteins, such as serum, for which competitive adsorption should occur. At the cellular scale, only a few studies are concerned with the direct evaluation of cellular interactions with polyelectrolyte multilayers, although polyelectrolytes have already widely been used in the monolayer form, to render the substrate either adhesive, as for poly(L-lysine) (PLL), or nonadhesive, as for polyacrylic acid coupled to poly(ethylene glycol).<sup>25</sup> Elbert et al.<sup>26</sup> used PLL and alginate polyelectrolyte multilayer films in order to build a nonadhesive barrier. More recently, it was shown that cells can be deposited on a poly(L-lysine)/poly(L-glutamic acid) (PLL/PGA) multilayer and grown for several days in culture in a serum-free medium. These cells can specifically respond to a small peptide hormone bound to PLL and incorporated at different depths in the polyelectrolyte film.<sup>27</sup> The biocompatibility of such PGA- and PLL-ending films for SaOS-2 osteoblast-like cells and of PGA-

\* To whom correspondence may be addressed at INSERM Unité 424, Faculté de Médecine, Bât 3, 11 rue Humann, 67085 Strasbourg Cedex, France. Tel: 33-3-90-24-32-58. Fax: 33-3-90-24-33-79. E-mail: Catherine.Picart@medecine.u-strasbg.fr.

† INSERM Unité 424, UFR d'Odontologie, Université Louis Pasteur.

‡ UMR CNRS 7563, Faculté de Médecine.

§ Institut Charles Sadron (CNRS-ULP).

|| Ecole Européenne de Chimie, Polymères et Matériaux de Strasbourg.

B Richert et al.

Biomacromolecules

ending films for human periodontal ligament cells was also evidenced.<sup>28</sup>

The present study is aimed at quantifying by micromanipulation the short-term interaction of chondrosarcoma cells with polyelectrolyte multilayers built up with PLL and PGA. As the role of the adsorbed serum proteins in mediating the cell–multilayer interactions may be important, experiments were performed in serum-containing and serum-free media. The goals were the following: (i) to measure the adhesion forces of cells interacting with PLL- or PGA-ending films and to analyze their dependence with the number of layers in the film; (ii) to precisely determine the role of adsorbed serum proteins on cellular adhesion on multilayered polyelectrolyte films.

Quantitative force measurements of cell–substrate adhesion can be performed using different techniques. Since various techniques are sensitive to different aspects of adhesion, forces varying by orders of magnitude are reported in the literature. The first type of measurements concern assemblies of cells. The centrifugation method, the spinning disk,<sup>29</sup> and the flow chamber<sup>9</sup> belong to this type of experiment where the fraction of cells adhering more strongly than a critical discrimination value is estimated. A probability distribution is obtained by counting the number of cells that remain attached on the surface for an applied shear stress and a given exposure time. Other techniques based on the measurement of the adhesion forces of individual cells have been developed. A cytodetacher<sup>30</sup> and a modified atomic force microscope<sup>31</sup> have been used to measure the shear strength between a cell and a substrate by displacing horizontally the cells with a cantilever of given compliance. We have chosen the widely used approach employing the application of negative pressure onto single cells by micromanipulation.<sup>32–35</sup> A setup in which the force is applied perpendicularly to the substrate was already employed for the study of the adhesion of Jurkat cells on glass-supported LFA<sub>3</sub>–lipid layers<sup>32</sup> and of osteoblasts onto titanium surfaces.<sup>33</sup> More generally the micropipet aspiration technique has been used to determine the forces needed to separate ligament fibroblasts from a fibronectin-coated surface<sup>34</sup> and to peel muscle cells from narrow strips of collagen-coated glass.<sup>35</sup>

## Materials and Methods

**Materials. Polyelectrolyte Solutions.** Anionic PGA (MW = 54000) and cationic PLL (MW = 30300) were purchased from Sigma. Sodium chloride (purity = 99.5%) was purchased from Fluka. Tris(hydroxymethyl)aminomethane (Tris), 2-(N-morpholino)ethanesulfonic acid (MES), and sodium dodecyl sulfate (SDS) were purchased from Sigma. All the chemicals of commercial origin were used without further purification. All solutions were prepared using ultrapure water (Milli-Q-plus system, Millipore) with a resistivity of 18.2 MΩ·cm. Polyelectrolyte solutions were always freshly prepared by direct dissolution of the respective adequate weights in filtered buffer solution. The (PLL/PGA)<sub>i</sub> and (PLL/PGA)<sub>i</sub>–PLL films, where *i* corresponds to the number of layer pairs, were prepared in Mes–Tris (Mes 25 mM,

Tris 25 mM, pH = 7.4 containing 0.1 M NaCl). The final polyelectrolyte concentrations were of 5 mg/mL. For streaming potential experiments, since the experimental device is extremely sensitive to very slight pH changes, solutions were prepared in a Tris-HCl buffer (0.5 mM Tris, 0.1 M NaCl, pH 7.4).

**Analysis of the Film Growth and of Its Surface Charge.** The (PLL/PGA)<sub>i</sub> film buildup process and its subsequent contact with serum were followed by optical waveguide lightmode spectroscopy (OWLS) and by quartz crystal microbalance (QCM). Briefly, OWLS is sensitive to the penetration depth of an evanescent wave through the film near the waveguide surface and gives access to the optical properties of the films.<sup>36</sup> Details about the experimental setup<sup>12</sup> and the procedure can be found elsewhere.<sup>13</sup> For serum protein adsorption on the multilayer films, serum diluted at 10% in MES-Tris was injected and allowed to rest for 1 h. The solution was then put in contact with the buffer for an additional hour. The structure of the multilayers was analyzed using the homogeneous and isotropic monolayer model which allows the refractive index *n<sub>A</sub>* and the thickness *d<sub>A</sub>* to be determined.<sup>12</sup> For the protein adsorption, the homogeneous and isotropic bilayer model was used.<sup>12</sup> In this case, the refractive index and the thickness of the first layer constituting the bilayer, which corresponds to the polyelectrolyte multilayer, were fixed to the values found before protein adsorption, i.e., *n<sub>A</sub>* and *d<sub>A</sub>*, respectively. The refractive index and thickness of the protein film (*n<sub>B</sub>*, *d<sub>B</sub>*) were determined by solving the guided mode equations.<sup>12</sup> Mass data are calculated according to the De Feltjer formula<sup>37</sup> (adsorbed mass = (dn/dc)<sup>-1</sup>(*n<sub>B</sub>* – *n<sub>C</sub>*)*d<sub>B</sub>*, where (dn/dc) = 0.18 cm<sup>3</sup>/g and *n<sub>C</sub>* (=1.3350) is the refractive index of the buffer).

QCM (Q-Sense, Göteborg, Sweden) consists of measuring the changes in the resonance frequency of a quartz crystal<sup>38,39</sup> when material is brought from solution.<sup>40</sup> The crystal is excited at its fundamental frequency (about 5 MHz) and observation takes place at the third, fifth, and seventh overtones (corresponding to 15, 25, and 35 MHz, respectively). The details of the experimental setup have been previously presented,<sup>13</sup> except that the crystal used for the present study is coated with a thick ( $\approx$ 100 nm) SiO<sub>2</sub> film.

The streaming potential method was also used to characterize the surface. Measurements were carried out on a homemade apparatus developed by Zembala and Déjardin<sup>41</sup> that has been previously described.<sup>13,42</sup> The basic principle is to measure the pressure and the potential differences on both sides of a 530 μm radius capillary made of fused silica via two flasks containing four electrodes. Details about the procedure are given in Picart et al.<sup>13</sup>

**Preparation of the Polyelectrolyte Multilayer-Coated Glass Slides for Cell Adhesion Experiments.** For cell adhesion experiments, multilayer polyelectrolyte films were deposited on borosilicate glass slides (18 × 18 × 0.18 mm<sup>3</sup>) that had been cleaned with both 10 mM SDS and 0.1 N HCl for 15 min in a boiling water bath and extensively rinsed. PLL was first adsorbed onto glass slides by 15 min of immersion in a beaker followed by rinsing with buffer. Then, PGA was adsorbed and subsequently rinsed following the

## Biomacromolecules

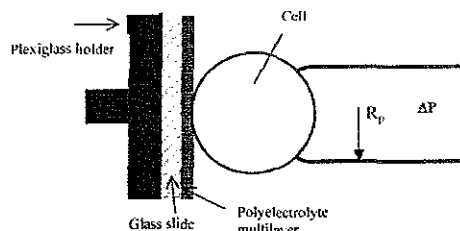


**Figure 1.** Schematic top view of the experiment:  $R_p$ , radius of pipet;  $\Delta P$ , depression applied to the cell membrane. A cell approaches a multilayer-coated glass slide which is held by a Plexiglas holder. After 30 min at rest, the cell is progressively detached by step increases in the depression applied to its membrane.

same procedure. Adsorption of polyelectrolyte layers was performed alternately until the desired multilayer film was built. Films were stored at 4 °C for no more than 4 days before use. The films are stable over this period of time, as was evidenced by atomic force microscopy (data not shown).

**Cell Culture.** HCS-2/8 human chondrosarcoma cells derived from a chondrocyte-like cell line<sup>43</sup> were routinely grown in Gibco BRL's minimum essential medium with Eagle's salts (MEM, Life Technologies), 10% fetal calf serum (FCS, Life Technologies), 50 U/mL penicillin, and 50 g/mL streptomycin (Bio-Whittaker) in a 5% CO<sub>2</sub> and 95% air atmosphere at 37 °C. A flask of cells was brought into suspension after incubating for 2.5 min in 0.5% trypsin (Bio-Whittaker). Following trypsinization, cells were washed twice by centrifugation to a pellet at 500g for 5 min and resuspended in 10 mL of fresh medium containing 10% FCS or without serum. Chondrosarcoma cells were stored at 37 °C for 1–4 h until seeding in the micropipet chamber.

**Quantification of Cell Adhesion by Micromanipulation.** **Microscopy and Micromanipulation.** The micropipet setup is similar to systems described in the literature.<sup>33,44</sup> For aspiration of cells, micropipets were pulled to a fine point (model 97, Sutter Instrument Co., Novato, CA) and fractured with a microforge (Alcatel, France) to inner radii of  $\approx 7 \mu\text{m}$ . The water pre-filled pipets were connected to a homemade manometer with pressure transducers (DP103, Validyne Eng., Northridge, CA) balanced against atmospheric pressure, as described elsewhere.<sup>33,45,46</sup> A micromanipulator (Narishige, Tokyo, Japan) was used to define the micropipet position. A homemade Plexiglas holder was designed to maintain the multilayer-coated glass slide vertically (Figure 1). The cell chamber consisted of a section of a polypropylene syringe mounted on a 40 mm diameter cover glass with silicone cement and with a window cut into its side to provide room for pipet micromanipulation.<sup>33</sup> The chamber is placed on an inverted light microscope (Zeiss Axiovert 10, Germany) equipped with a 32× dry objective, connected to a video camera (SSC-M3, Sony, Japan), S-VHS video recorder (NV-HS-900F, Panasonic, Sony), and monitor (SSM-125CE, Sony, Japan). Recorded images are digitized with a computer equipped with a frame grabber card (LG3; Scion Corp., Frederick, MD) and analyzed with the public domain software NIH Image v.1.6.

**Measuring Detachment Force Using a Micropipet.** The cells were first deposited at room temperature in the chamber containing either MEM with 10% FCS or only MEM. A

## Cell Interactions with Multilayer Films C

single chondrosarcoma cell was aspirated with a small negative pressure ( $\approx 50 \text{ Pa}$ ) within the micropipet and brought horizontally into the vicinity of the polyelectrolyte film. Then, the negative pressure was removed and the cell was left in this position for 15 s to allow it to attach to the film. The micropipet was slowly pulled away from the surface. After the seeding time (30 min), the micropipet was brought in contact with the cell and a small depression was applied to the cellular membrane. As the speed at which the cell is displaced might influence the force measured, due to the dependence of the rupture force on the retraction rate,<sup>47</sup> the micropipet was pulled away from the surface at a constant speed ( $\approx 3 \mu\text{m/s}$ ). If the negative pressure applied to the pipet was not sufficient to create a force that exceeds the cellular adhesion force, the procedure was repeated. The depression was successively increased (by  $-120 \text{ Pa}$  steps) by automatically pulling on an air-filled syringe connected to one of the water reservoirs (Programmable Syringe Pump, Genie-220, World Precision Instruments Ltd, Hertfordshire, U.K.), until the chondrosarcoma cell adhesion force was exceeded. More than 50 cells were tested for adhesion on each type of film. The pipet radius and the depression applied to the cell membrane were collected (Figure 1) in order to calculate the detachment force<sup>35,48</sup> according to

$$F = \pi R_p^2 \Delta P \quad (1)$$

**Statistics.** Comparison between groups was performed using the Mann–Whitney rank test to determine if any significant differences ( $p < 0.05$ ) existed.

**Experiments with Fluorescently Labeled PLL.** Experiments with PLL labeled with fluorescein isothiocyanate (PLL-FITC, MW = 50200, Sigma) were also undertaken: PLL-FITC (denoted here PLL\*) has been incorporated in (PLL/PGA)<sub>7</sub> films at the fourth pair of layers (i.e., PLL<sub>4</sub>\* ) or at the sixth pair of layers (i.e., PLL<sub>6</sub>\* ), or it has been deposited on the top of a (PLL/PGA)<sub>6</sub> film (i.e., PLL<sub>7</sub>\* ). Fluorescence images were taken with a 40× oil objective after cell adhesion and after cell detachment.

## Results

**Physicochemical Characteristics of the (PLL/PGA)<sub>n</sub> Films.** The buildup of the (PLL/PGA)<sub>n</sub> multilayer films was followed *in situ* step by step by OWLS before and after contact with serum. In a previous work,<sup>49</sup> the (PGA/PLL)<sub>n</sub> multilayers deposited on a precursor poly(ethyleneimine) layer have been characterized by *in situ* atomic force microscopy and by OWLS. The evolution of the thickness and of the adsorbed mass with the number of layers deposited was exponential. These layers formed extended structures that appear with a vermiculate pattern. In the present experiments, although the PLL is directly deposited on the waveguide surface without any PEI precursor layer, the growth is exponential too. This exponential growth of the multilayers was explained on the basis of polyelectrolyte diffusion:<sup>49</sup> when the architecture is in contact with a PLL solution, PLL diffuses in the film whereas PGA diffuses out. The diffusion of the polyanion out of the film leads to a

D. Richert et al.

Biomacromolecules

**Table 1.** Refractive Index,  $n_A$ , and Optical Thickness,  $d_A$  (nm), of the Different (PLL/PGA)<sub>i</sub> Films Used for the Cell Adhesion Experiments, As Measured by the OWLS Technique (mean  $\pm$  standard deviation)

multilayer film	$n_A$	$d_A$ (nm)
PLL	1.683 $\pm$ 0.030	1.01 $\pm$ 0.19
PLL/PGA	1.597 $\pm$ 0.020	2.04 $\pm$ 0.45
(PLL/PGA) <sub>2</sub> -PLL	1.443 $\pm$ 0.007	10.22 $\pm$ 1.35
(PLL/PGA) <sub>3</sub>	1.451 $\pm$ 0.008	15.54 $\pm$ 2.02
(PLL/PGA) <sub>6</sub> -PLL	1.425 $\pm$ 0.003	66.16 $\pm$ 6.53
(PLL/PGA) <sub>7</sub>	1.424 $\pm$ 0.003	75.87 $\pm$ 7.12
(PLL/PGA) <sub>9</sub> -PLL	1.424 $\pm$ 0.003	153.30 $\pm$ 15.5

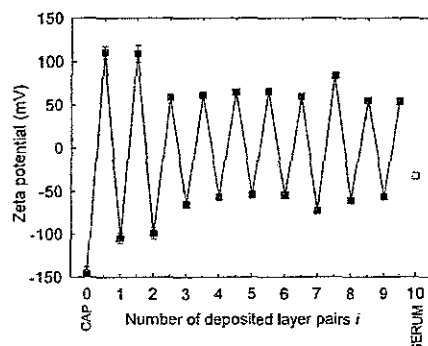


**Figure 2.** Evolution of the  $\zeta$  potential (mV) during the alternate deposition of PLL and PGA layers (closed symbols) and the ultimate adsorption of serum (open symbol) as a function of the number of deposited layer pairs  $i$  on a fused silica capillary (CAP). PLL and PGA were prepared in a 0.5 mM Tris-HCl buffer ( $\text{pH} = 7.4$ ) containing 0.1 M NaCl.

complexation with the incoming polycation, and vice versa. This complexation leads to an accumulation of large polyion complexes at the top of the film.

The mean refractive indices and thicknesses of the different architectures that have been used for cell adhesion studies are given in Table 1. Refractive indices of the films are of the order of 1.42 and indicate that these films are not as dense as other multilayer films.<sup>49</sup> Thicknesses vary from 1 nm for a PLL monolayer up to about 150 nm for a (PLL/PGA)<sub>9</sub>-PLL film.

The  $\zeta$  potential of the (PLL/PGA)<sub>i</sub> multilayers was also determined after deposition of each new polyelectrolyte layer of the film (Figure 2). The alternate adsorption of PLL and PGA causes a reversal of the  $\zeta$  potential after each new deposition up to 9.5 pairs of layers. When PGA forms the outermost layer, the  $\zeta$  potential is negative (-104 to -55 mV). Subsequent adsorption of PLL produces positive  $\zeta$  potentials (+54 to +110 mV) confirming the stepwise growth of the multilayer film. A decrease of the absolute value of the  $\zeta$  potential is observed after deposition of the two initial bilayers. Its absolute value remains constant thereafter.

**Interaction of Serum Proteins with the Films.** As most experiments with cells are performed in serum-containing media, the films were put in contact with serum and adsorption of proteins was studied by means of OWLS and QCM for films of various thicknesses (Figure 3). Protein adsorption was important on PLL-ending films but was negligible on PGA-ending ones. Indeed, it appears that,

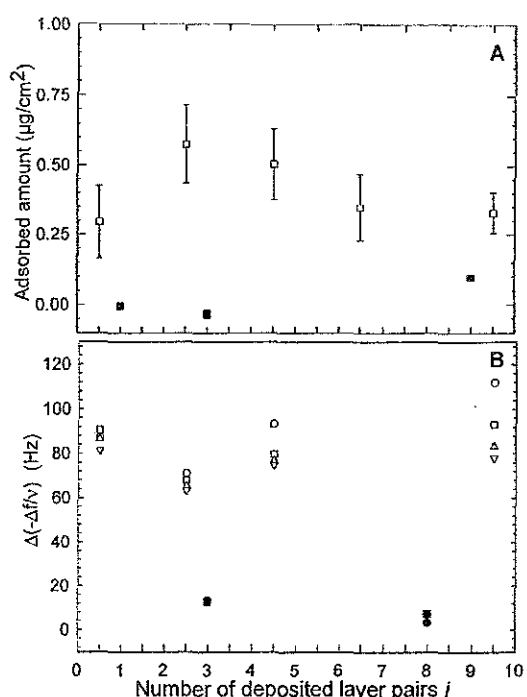


**Figure 3.** Serum adsorption onto the (PLL/PGA)<sub>i</sub> films as measured by OWLS and QCM. (A) Adsorbed amount in  $\mu\text{g}/\text{cm}^2$  as a function of the number of layer pairs in the film. Each point represents the mean  $\pm$  standard deviation of several experiments, on PLL-ending films (□) and on PGA-ending films (■). (B) Increment in the QCM frequency shifts  $\Delta(-\Delta f/v)$ ,  $v$  being the overtone number, which corresponds to the contribution of serum adsorption, plotted as a function of the number of deposited layers. Open symbols are for PLL-ending films and closed symbols are for PGA-ending ones. Data are given for the four harmonics at 5 (○), 15 (□), 25 (△), and 35 MHz (▽).

**Table 2.** Value of Zeta Potential (mV) of the Films at the End of Their Buildup and after Contact with Serum

film	$\zeta$ potential of the film (mV)	$\zeta$ potential of the film, after contact with serum (mV)
<b>positively ending films</b>		
PLL	+91.0	-51.2
(PLL/PGA) <sub>2</sub> -PLL	+70.3	-54.5
(PLL/PGA) <sub>9</sub> -PLL	+54.0	-32.3
<b>negatively ending films</b>		
PLL/PGA	-104.0	-69.0
(PLL/PGA) <sub>3</sub>	-95.8	-55.3

within the experimental accuracy, the adsorbed protein amount on PLL-ending films remains almost constant when the number of layers in the film is increased; it is on the order of 0.3  $\mu\text{g}/\text{cm}^2$  with a thickness of about 10–12 nm as determined by OWLS. QCM experiments gave qualitatively similar results for all the frequencies investigated since a decrease in the resonance frequency is associated, in a first approximation, to an increase of the mass coupled to the quartz.<sup>13</sup>

From the  $\zeta$  potential values after serum adsorption (Table 2), one can notice that the potential becomes negative after adsorption on PLL-ending films whatever the number of

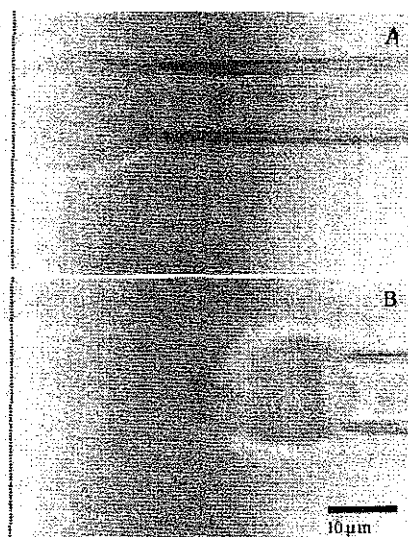


**Figure 4.** Cell detachment measurement. After the 30 min seeding time, a chondrosarcoma cell was pulled from the multilayer surface with step increases in aspiration depression (A). The pipet holding the cell with a minimum aspiration depression was moved by micromanipulation until the cell finally detached from the surface (B). (The dotted line represents the cell/film polyelectrolyte film interface.)

layers constituting the film. For the PGA-ending films, the  $\zeta$  potential remains negative but with a slightly lower absolute value. One can thus conclude that for all the types of films investigated and containing various numbers of layers, the  $\zeta$  potential was approximately constant and negative ( $\approx -55$  mV) after serum adsorption.

**Detachment Forces in a Serum-Containing Medium.** To measure the detachment forces, the cells were first put in contact with the films and allowed to rest for 30 min in a serum-containing medium. Then, the cells were progressively aspirated and peeled (Figure 4A) until they finally detached (Figure 4B).

The cell detachment forces were measured on PLL- or PGA-ending films consisting of different numbers of layers. These forces were also compared to those measured on cells in direct contact with glass slides. The histograms of the adhesion forces obtained with the different film architectures (more than 50 cells for a given film) and the glass are represented in Figure 5. First, it can be pointed out that the detachment forces were extremely low on all PGA-ending films whatever the number of layers constituting the film (parts B, D, and F of Figure 5). Some cells even detached spontaneously before being peeled off from the film surface. For PLL-ending films, the range of detachment forces and the shape of the distribution depended on the number of deposited layers. The most regular distribution was found for the  $(\text{PLL}/\text{PGA})_6$ -PLL film, whereas the widest range in the adhesion forces was obtained for the  $(\text{PLL}/\text{PGA})_9$ -PLL architecture (panels A, C, E, and G of Figure 5). The histogram corresponding to glass is given in Figure 5H.

The plot of the average detachment forces (Figure 6) indicated that chondrosarcoma cells adhered more strongly to a PLL monolayer than to the other positive films and that

the force decreased from 121 to 77 nN when the number of layers in the film increased. The differences between the different film architectures were statistically significant when compared altogether. The mean values for PGA-ending films were about 8-fold lower and were in the range 5–13 nN. For glass, the mean adhesion force was 26.5 nN. There were no statistical differences between the PGA-ending films, but these were significantly different from all the PLL-ending films and from glass.

**Force Histograms in the Absence of Serum.** To further understand the role of serum in mediating the cell/film interactions, several adhesion experiments were also performed in serum-free media. For the PGA-ending films, repulsion was so strong that cells did even not attach and no force could be measured. Regarding the PLL-ending films and the glass, the histograms of detachment forces cover a much wider range of forces than those obtained in the presence of serum (Figure 7). Average force values were much higher than those obtained in the serum-containing medium (Figure 6). For a PLL monolayer, an adhesion force of 266 nN was measured as compared to the 121 nN measured in the presence of serum. For a  $(\text{PLL}/\text{PGA})_6$ -PLL film, although the difference was not as pronounced, a 50% increase in the force (133 nN as compared to 89 nN for the same film in the presence of serum) was found. Again, the detachment force appeared to decrease when the film thickness increased. The mean detachment force measured on glass was 46 nN instead of 26 nN in the presence of serum.

**Experiments with Fluorescently Labeled PLL.** To investigate a possible film rupture during detachment, experiments were performed using fluorescently labeled PLL embedded at different depths in the film or deposited on the top of the film. These experiments were performed both in the absence and in the presence of serum. For films in which PLL-FITC was embedded (e.g.,  $\text{PLL}_4^*$  and  $\text{PLL}_6^*$ ), no fluorescence could be detected on the cell membrane after a 30 min adhesion time and after cell detachment. When PLL-FITC was adsorbed on the top of the film (e.g.,  $\text{PLL}_7^*$  films), around 85% of the cells in the absence of serum and 55% in the presence of serum were fluorescent after a 30 min cell adhesion and after detachment.

## Discussion

**Cell Adhesion on PLL- and PGA-Ending Films.** The  $\zeta$  potential values of the films in the absence of serum were dependent on the outermost layer: the  $\zeta$  potential was positive for PLL-ending films and negative for PGA-ending films. The forces were high for PLL-ending films (in the range 130–260 nN) whereas they were not measurable for PGA-ending ones. As cell membranes carry a negative charge in physiological conditions,<sup>50</sup> these results can be explained by pure electrostatic repulsion or attraction forces between the negatively charged chondrosarcoma cells and the ending layer of the architecture.

When serum is added to the medium, cell adhesion is modified: forces measured on PLL-ending films were 40–100% lower than those measured in the absence of serum.

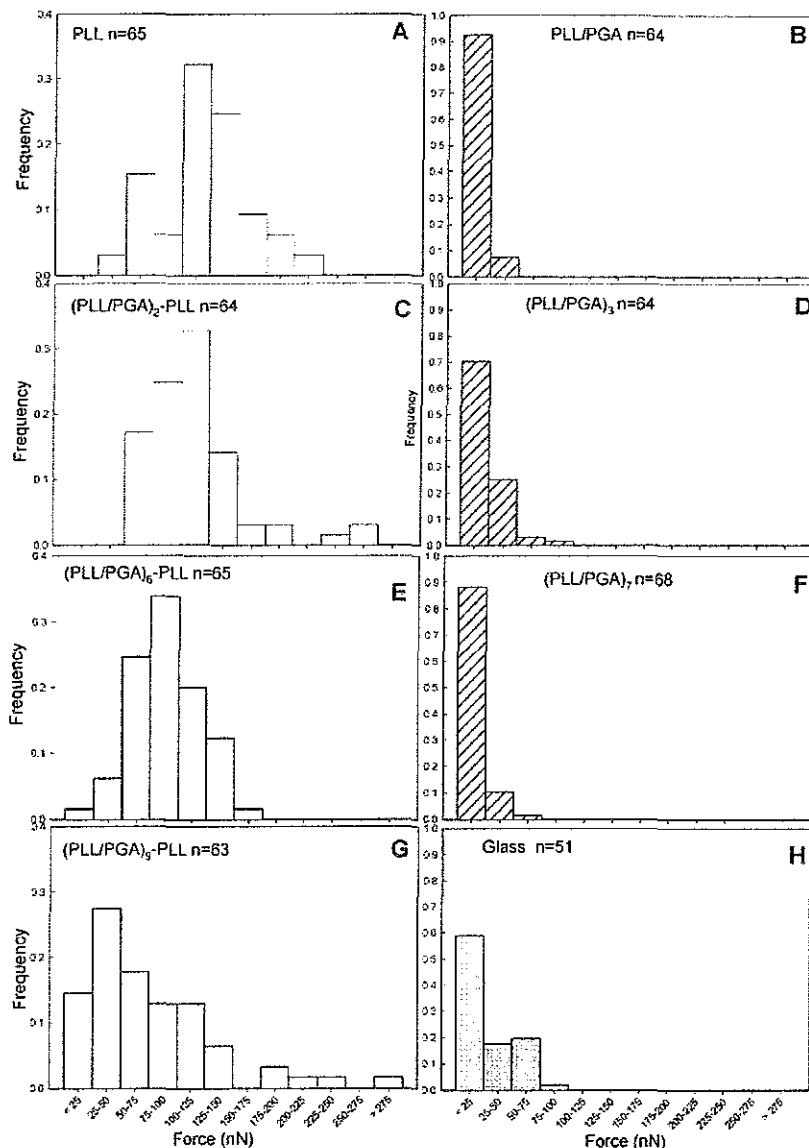


**Figure 5.** Histograms of cell detachment forces for seven different films containing an increasing number of layer pairs (up to 9.5) and compared to a glass slide: (A) PLL; (B) PLL/PGA; (C) (PLL/PGA)<sub>2</sub>-PLL; (D) (PLL/PGA)<sub>3</sub>; (E) (PLL/PGA)<sub>6</sub>-PLL; (F) (PLL/PGA)<sub>7</sub>; (G) (PLL/PGA)<sub>9</sub>-PLL; (H) glass. The histograms for PLL-ending films (white bars) are shown on the left-hand side, and those corresponding to PGA-ending films (hatched bars) as well as to glass (gray bars) are shown on the right-hand side. *n* means the number of cells detached in each experiment.

They were still very high compared to the ones on PGA that were measurable in these conditions (on the order of 10 nN). After contact with serum proteins, both surfaces present a similar  $\zeta$  potential value, even if protein adsorption could only be detected on PLL-ending films by OWLS and QCM (Figure 3.). Most serum proteins being negatively charged at pH 7.4, a larger amount of proteins is thus expected to adsorb on PLL-ending multilayers in accordance with the results obtained for individual proteins.<sup>24</sup> More unexpected is the fact that no detectable amount of proteins adsorbs on PGA-ending films whereas individual proteins were found to adsorb, even though in a smaller extent, to multilayers of similar charge.<sup>24</sup> Antifouling properties have, however,

already been evidenced for another weak polyelectrolyte, the poly(acrylic acid),<sup>21</sup> and were found to depend on the pH.<sup>22</sup> The  $\zeta$  potential is very sensitive even to very small amounts of adsorbed proteins, as long as they contribute to a change of the charge of the outer layer of the film. A possible explanation for this slight increase of the  $\zeta$  potential of the PGA-ending films could be that small amounts of positively charged proteins adsorb onto these films or that there may be an exchange between some PGA molecules and some incoming proteins, without any noticeable change in the optical properties of the film. Also, as proteins behave as dipoles, there could be some positive segments interacting with the PGA molecules such that the negative parts of the

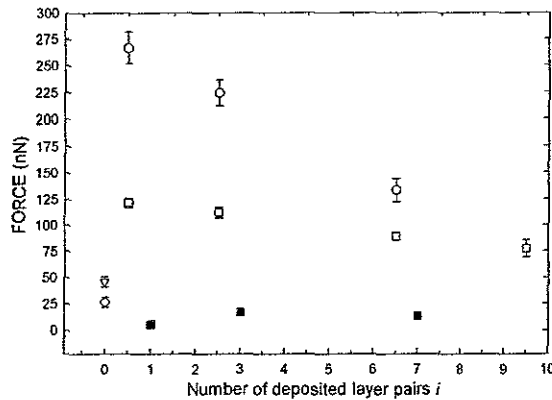


**Figure 6.** Average detachment force of chondrosarcoma cells seeded in the presence of serum and in a serum-free medium on several (PLL/PGA)<sub>*n*</sub> films as a function of the number of deposited layers. In the presence of serum, positively PLL-ending (□) and negatively PGA-ending (■) films are compared to a glass surface (○). The number of cells measured in each group is as given in Figure 5. In a serum-free medium, the PLL-ending films (○) are compared to a glass surface (▽). The number of cells measured in each group is as given in Figure 7. Error bars are standard error of the mean.

protein would point out of the film. Even such small adsorption could lead to a change in the value of the  $\zeta$  potential.

Whereas in the absence of serum, cells must interact with the PLL/PGA films through nonspecific electrostatic interactions, in the presence of serum, extracellular matrix (ECM) proteins may adsorb onto the film and specific cell adhesion may occur via these ECM proteins. Specific interactions are, however, usually stronger than nonspecific ones. This seems, at first glance, in contradiction with the observed reduction of the adhesion force between cells and PLL-terminating films once these films are put in contact with serum. The lower forces obtained in the presence of serum can easily be explained by a larger number of interactions in the nonspecific case than in the specific one.

**Influence of the Polyelectrolyte Multilayer Architecture.** For positive-ending films, one observes a continuous decrease of forces versus film thickness both in the presence and in the absence of serum.

In the absence of serum, several reasons can be suggested to explain this result. First, the initial  $\zeta$  potential for the PLL-coated surface is high and its slight decrease with respect to the layer number (from PLL to (PLL/PGA)<sub>*n*</sub>-PLL) can contribute to a decrease of the electrostatic interactions. One may also suggest that the roughness plays a role, but previous investigations showed that the surface roughness of the film becomes constant after deposition of the third pair of layers<sup>49</sup> thus excluding the role of this parameter. It may also be possible that the film viscoelastic properties change when the film thickness increases and that the cellular interactions depend on this parameter. Another explanation is based on the (PLL/PGA) multilayer architecture that has been previously examined by atomic force microscopy (AFM) and OWLS.<sup>49</sup> It was suggested that the diffusion of the polyelectrolytes associated to their complexation at the top of the film leads to an exponential growth. Therefore, if one assumes that the bindings between the different complexes

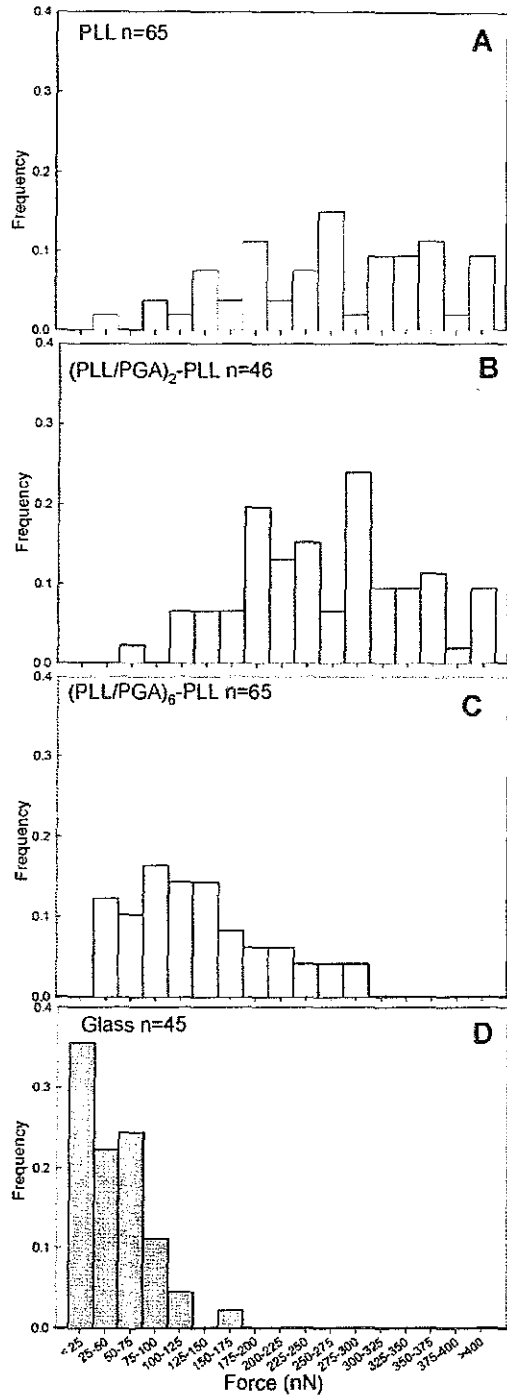


**Figure 7.** Histograms of cell detachment forces for different films and glass obtained in a serum-free medium: (A) PLL; (B) (PLL/PGA)<sub>2</sub>-PLL; (C) (PLL/PGA)<sub>6</sub>-PLL; (D) glass.

are weak, one can conjecture that the outer structure stability decreases with the number of deposited layers. As a consequence, during cell detachment, the rupture may occur in the upper part of the film (final adsorbed layer). However, as seen on Figure 8, cells become fluorescent even after

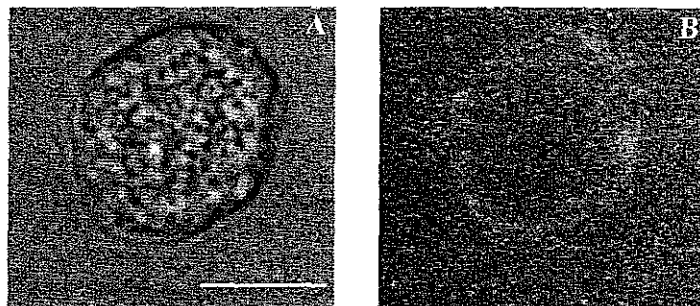


**Figure 8.** Bright field (A) and fluorescence images (B) of a cell that has adhered for 30 min on a (PLL/PGA)<sub>6</sub>-PLL<sub>7\*</sub> multilayer film in a serum-free medium. Some fluorescence is visible on the cell membrane. (Scale bar = 10  $\mu\text{m}$ .)

adhesion and before detachment. This observation indicates that PLL-FITC when adsorbed on the top of the film is able to diffuse and to adsorb on the cell membrane.

In the presence of serum, the rupture can take place at three different locations: inside the film, between the proteins and the film, and finally between the cell and the proteins. In any case, the rupture takes place at the weakest interaction point. If the rupture takes place inside the film, one would expect that the rupture forces should be independent of the protein adsorption consecutive to contact with serum. This is not observed. On the other hand the presence of fluorescence on detached cells after contact with the PLL-FITC ending film (PLL,<sup>\*</sup> architecture) does not imply that the rupture occurs at the PGA/PLL-FITC interface since fluorescence can again be due to the PLL-FITC diffusion. It is difficult to discriminate, in the presence of serum, between the two other possibilities (i.e., film/protein or protein/cell rupture).

The reduction of the adhesion force with the film thickness may be due to a change in the external structure of the multilayer which could influence protein adsorption. Viscoelastic properties of the film may also be responsible for the observed evolution of the rupture force. Further studies are necessary to get more insight into this problem. One should, in particular, try to determine which specific proteins adsorb on the film. With this information, one could use labeled proteins and verify if they are detached with the cell during the cellular detachment process.

### Conclusion

The short-term interaction of chondrosarcoma cells with (PLL/PGA) polyelectrolyte multilayers was investigated in a serum-containing medium and in a serum-free medium for films constituted by an increasing number of layers. Detachment forces were measured by micromanipulation both in the presence and in the absence of serum. We found that the detachment forces were significantly higher on PLL-ending films than on PGA-ending ones. The forces were higher in the absence of serum. In the presence of serum the detachment forces were almost undetectable on PGA-ending films that thus behave as nonadherent films. For PLL-ending films the detachment forces decrease with the number of deposited layers. This study reveals the importance of the multilayer structure and architecture to control the detachment force.

**Acknowledgment.** The authors wish to thank D. E. Discher (University of Pennsylvania, Philadelphia, PA) for assistance with the micromanipulation setup. C.P. is indebted to the “Université Louis Pasteur” for financial support. This work was supported by the program “Adhésion Cellules-Matiériaux” from INSERM-CNRS and by the Association pour la Recherche sur le Cancer (Project No. 7597).

### References and Notes

- (1) Healy, K. E. *Curr. Opin. Solid State Mater. Sci.* **1999**, *4*, 381–387.
- (2) Dillon, A. K.; Turrell, M. *Curr. Opin. Solid State Mater. Sci.* **1998**, *3*, 252–259.
- (3) Angelova, N.; Hunkeler, D. *Trends Biotechnol.* **1999**, *17*, 409–421.
- (4) Grinnell, F.; Feld, M. K. *J. Biol. Chem.* **1982**, *257*, 4888–4893.
- (5) Sagvolden, G.; Glaever, I.; Pettersen, E. O.; Feder, J. *Proc. Natl. Acad. Sci. U.S.A.* **1999**, *96*, 471–476.
- (6) Qiu, Q.; Sayer, M.; Kawaja, M.; Shen, X.; Davies, J. E. *J. Biomed. Mater. Res.* **1998**, *42*, 117–127.
- (7) Duffrêne, Y. F.; Marchal, T. G.; Rouxhet, P. G. *Langmuir* **1999**, *15*, 2871–2878.
- (8) Absalom, D. R.; Zingg, W.; Neumann, A. W. *J. Biomed. Mater. Res.* **1987**, *21*, 161–171.
- (9) Kapur, R.; Rudolph, A. S. *Exp. Cell Res.* **1998**, *244*, 275–285.
- (10) Decher, G.; Hong, J. D.; Schmitt, J. *Thin Solid Films* **1992**, *219*, 831–835.
- (11) Decher, G. *Science* **1997**, *277*, 1232–1237.
- (12) Picart, C.; Ladam, G.; Senger, B.; Voegel, J.-C.; Schaaf, P.; Cuisinier, F. J. G.; Gergely, C. *J. Chem. Phys.* **2001**, *115*, 1086–1094.
- (13) Picart, C.; Lavalle, P.; Hubert, P.; Cuisinier, F. J. G.; Decher, G.; Schaaf, P.; Voegel, J. C. *Langmuir* **2001**, *17*, 7414–7424.
- (14) Serizawa, T.; Yamaguchi, M.; Matsuyama, T.; Akashi, M. *Biomacromolecules* **2000**, *1*, 306–309.
- (15) Berth, G.; Voigt, A.; Dautzenberg, H.; Donath, E.; Möhwald, H. *Biomacromolecules* **2002**, *3*, 579–590.
- (16) Lvov, Y.; Ariga, K.; Ichinose, I.; Kunitake, T. *J. Am. Chem. Soc.* **1995**, *117*, 6117–6123.
- (17) Caruso, F.; Mohwald, H. *J. Am. Chem. Soc.* **1999**, *121*, 6039–6046.
- (18) Sukhorukov, G. B.; Montral, M. M.; Petrov, A. I.; Shabarchina, L. I.; Sukhorukov, B. I. *Biosens. Bioelectron.* **1996**, *11*, 913–922.
- (19) McAloney, R. A.; Sinyor, M.; Dudnik, V.; Goh, M. C. *Langmuir* **2001**, *17*, 6655–6663.
- (20) Yoo, D.; Shiratori, S. S.; Rubner, M. F. *Macromolecules* **1998**, *31*, 4309–4318.
- (21) Muller, M.; Rieser, T.; Lunkwitz, K.; Meier-Haack, J. *Macromol. Rapid Commun.* **1999**, *20*, 607–611.
- (22) Muller, M.; Rieser, T.; Dubin, P. L.; Lunkwitz, K. *Macromol. Rapid Commun.* **2001**, *22*, 390–395.
- (23) Ladam, G.; Gergely, C.; Senger, B.; Decher, G.; Voegel, J.-C.; Schaaf, P.; Cuisinier, F. J. G. *Biomacromolecules* **2000**, *1*, 674–688.
- (24) Ladam, G.; Schaaf, P.; Cuisinier, F. G. J.; Decher, G.; Voegel, J.-C. *Langmuir* **2001**, *17*, 878–882.
- (25) Amírpour, M. L.; Ghosh, P.; Lackowski, W. M.; Crooks, R. M.; Pishko, M. V. *Anal. Chem.* **2001**, *73*, 1560–1566.
- (26) Elbert, D. L.; Herbert, C. B.; Hubbell, J. A. *Langmuir* **1999**, *15*, 5355–5362.
- (27) Chluba, J.; Voegel, J. C.; Decher, G.; Erbacher, P.; Schaaf, P.; Ogier, J. *Biomacromolecules* **2001**, *2*, 800–805.

Biomacromolecules

PAGE EST: 8.3

- (28) Tryoen-Toth, P.; Vautier, D.; Haikel, Y.; Voegel, J.-C.; Schaaf, P.; Chluba, J.; Ogier, J. *J. Biomed. Mater. Res.* 2002, 60, 657–667.
- (29) Garcia, A. J.; Takagi, J.; Boettiger, D. *J. Biol. Chem.* 1998, 273, 34710–34715.
- (30) Athanasiou, K. A.; Thoma, B. S.; Lactot, D. R.; Shin, D.; Agrawal, C. M.; LeBaron, R. G. *Biomaterials* 1999, 20, 2405–2415.
- (31) Yamamoto, A.; Mishima, S.; Maruyama, N.; Sumita, M. *J. Biomed. Mater. Res.* 2000, 50, 114–124.
- (32) Tozeren, A.; Sung, K. L.; Sung, L. A.; Dustin, M. L.; Chan, P. Y.; Springer, T. A.; Chien, S. *J. Cell Biol.* 1992, 116, 997–1006.
- (33) Nugiel, D. J.; Wood, D. J.; Sung, K. L. P. *Tissue Eng.* 1996, 2, 127–140.
- (34) Sung, K. L.; Yang, L.; Whittemore, D. E.; Shi, Y.; Jin, G.; Hsieh, A. H.; Akeson, W. H.; Sung, L. A. P. *Natl. Acad. Sci. U.S.A.* 1996, 93, 9182–9187.
- (35) Ra, H. J.; Picart, C.; Feng, H.; Sweeney, H. L.; Discher, D. E. *J. Cell Sci.* 1999, 112 (Part 10), 1425–1436.
- (36) Tiefenthaler, K.; Lukosz, W. *J. Opt. Soc. Am. B* 1989, 6, 209–220.
- (37) De Peijter, J. A.; Benjamins, I.; Veer, F. A. *Biopolymers* 1978, 17, 1759–1772.
- (38) Rodahl, M.; Kasemo, B. *Rev. Sci. Instrum.* 1996, 67, 3238–3241.

Cell Interactions with Multilayer Films 1

- (39) Rodahl, M.; Kasemo, B. *Sens. Actuators, B* 1996, B37, 111–116.
- (40) Hook, F.; Rodahl, M.; Brzezinski, P.; Kasemo, B. *J. Colloid Interface Sci.* 1998, 208, 63–67.
- (41) Zembala, M.; Déjardin, P. *Colloids Surf., B* 1994, 3, 119–129.
- (42) Ladam, G.; Schaad, P.; Voegel, J. C.; Schaaf, P.; Decher, G.; Cuisinier, F. *Langmuir* 2000, 16, 1249–1255.
- (43) Tagikawa, M.; Tajama, K.; Pan, H. O.; Enmoto, M.; Kinoshita, A.; Suzuki, F.; Takano, Y.; Mori, Y. *Cancer Res.* 1989, 49, 3996–4002.
- (44) Tozeren, A.; Sung, K. L.; Sung, L. A.; Dustin, M. L.; Chan, P. Y.; Springer, T. A.; Chien, S. *J. Cell Biol.* 1992, 116, 997–1006.
- (45) Needham, D. *Methods Enzymol.* 1993, 220, 111–129.
- (46) Discher, D. E.; Mohandas, N.; Evans, E. A. *Science* 1994, 266, 1032–1035.
- (47) Evans, E.; Ritchie, K. *Biophys. J.* 1997, 72, 1541–1555.
- (48) Evans, E. A. *Methods Enzymol.* 1989, 173, 3–35.
- (49) Lavalle, P.; Gergely, C.; Cuisinier, F. G. J.; Decher, G.; Schaaf, P.; Voegel, J.-C.; Picart, C. *Macromolecules* 2002, 35, 4438–4465.
- (50) Alberts, B.; Bray, D.; Lewis, J.; Raff, M.; Roberts, K.; Watson, J. D. *Molecular biology of the cell*; Garland Publishing Inc: New York, 1994.

BM0255490

## 3.2 : Influence du pH de construction des films multicouches sur leurs propriétés physico-chimiques et sur l'adhésion cellulaire.

### 3.2.1. Résumé 2

Plusieurs travaux, notamment ceux de l'équipe du professeur Rubner, ont démontré l'existence d'une corrélation entre la capacité de gonflement et d'hydratation des films multicouches et l'adhésion cellulaire (Mendelsohn et al., 2003; Yang et al., 2003). Nous avons cherché à modifier le gonflement et l'hydratation des films multicouches à base de PLL et de PGA, notamment en modifiant le pH lors de la construction des films et pour voir quelle était l'incidence sur la force de détachement cellulaire. Pour cette étude, les polyélectrolytes ont été dissous dans des solutions sans sel.

Cette étude nous a ainsi montré que l'épaisseur des films est très sensible au taux de charge des polyélectrolytes lors de la construction. Les films construits avec les deux polyélectrolytes chargés (pH compris en 6 et 8) sont fins (moins de 30 nm après 5 paires de couches) et denses (indice de réfraction de l'ordre de 1.52). En revanche, les films construits avec l'un des polyélectrolytes faiblement chargé (pH inférieur à 5 ou supérieur à 9) sont au contraire épais (au moins 50 nm voire plus de 100 nm après 5 paires de couches) et moins denses (l'indice de réfraction inférieur à 1.45 après 5 bicouches).

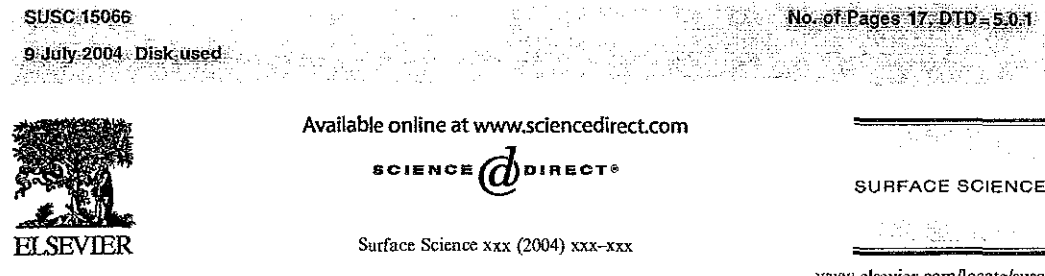
Les films construits à pH 4.4, lorsque le PGA est peu ionisé, sont également très sensibles aux modifications de taux de sel après la préparation du film. Ainsi, l'immersion de ces films dans une solution physiologique entraîne leur dégradation, ce qui n'est pas le cas des films construits à pH 10.4.

L'adhésion cellulaire est également fortement influencée par le pH de construction des films. Pour les films multicouches construits à un pH de 7.4 dans l'eau, l'adhésion cellulaire de cellules HCS-2/8 est comparable à celles sur les films construits en présence de 0.15 M en NaCl : l'adhésion est plus élevée sur les films terminés par PLL que sur les films terminés par PGA, bien que les films soient beaucoup plus fins et denses lorsqu'ils sont construits en absence de sels. En revanche, les films construits avec des solutions à un pH de 4.4 sont résistants à l'adhésion cellulaire lorsqu'ils sont terminés soit par une couche de PGA ou par d'une couche terminale de PLL. Ce résultat peut s'expliquer par la forte hydratation des films obtenus dans ces conditions de construction. Enfin, si les films sont construits à un pH de 10.4, lorsque le PLL est peu chargé, l'adhésion cellulaire est importante quelque-soit la

dernière couche déposée. La comparaison des épaisseurs mesurées en solution par spectroscopie optique et estimées à sec par AFM, permet de mettre en évidence un plus fort gonflement (entre l'état sec et l'état hydraté) pour les films construits à pH 4.4 que pour les films construits à un pH de 10.4.

La capacité des films à absorber l'eau serait donc une propriété corrélée à l'adhésion cellulaire sur les films multicouches. Par ailleurs, l'adsorption des protéines sériques sur les films montre que le pH de construction ne modifie pas significativement la masse protéique adsorbée : elle reste toujours faible sur les films terminés par PGA et importante sur les films terminés par PLL .

### 3.2.2. Article 2



## pH dependent growth of poly(L-lysine)/poly(L-glutamic acid multilayer films and their cell adhesion properties

Ludovic Richert <sup>a</sup>, Youri Arntz <sup>a</sup>, Pierre Schaaf <sup>b</sup>  
Jean-Claude Voegel <sup>a</sup>, Catherine Picart <sup>a,\*</sup>

<sup>a</sup> INSERM Unité 595, Faculté de Médecine, Bât 3, Université Louis Pasteur, 11 rue Humann, F-67085 Strasbourg Cedex, France  
<sup>b</sup> Institut Charles Sadron (CNRS-ULP), 6 rue Boussingault, F-67083 Strasbourg Cedex, France

Received 15 December 2003

### Abstract

The short-term interaction of chondrosarcoma cells with (PGA/PLL) polyelectrolyte multilayers was investigated in a serum-containing medium for films built at different pHs and subsequently exposed to the culture medium. The build-up of the films and their stability was first investigated by means of optical waveguide lightmode spectroscopy, quartz crystal microbalance, streaming potential measurements and atomic force microscopy. While film growth is linear at all pHs, after a few layers have been deposited the growth is much larger for the films built at basic pH and even more pronounced for those built at acidic pH. However, these latter films remain stable in the culture medium only if they have been crosslinked prior to the ionic strength and pH jumps. The films built at acidic pH were found to swell in water by about 200% whereas those built at other pHs did not swell in a physiological buffer. For thin films ( $\approx$ 20 nm) built at pH = 7.4, the detachment forces were dependent on the outermost layer, the forces being significantly higher on PLL-ending films than on PGA-ending ones. In contrast, for the thick films built at pH = 4.4 and at pH = 10.4 (thickness of the order of few hundred of nanometers), the detachment forces were independent of the outermost layer of the film. The films built at pH = 10.4, which shrink in contact with salt containing solutions, were highly cell adhesive whereas those built at acidic pH were highly cell resistant. Protein adsorption and film roughness (as measured by AFM) could not explain these striking differences. The high adhesion observed on the film built at pH 10.4 may rather be related to the secondary structure of the film and to its relatively low swellability in water, whereas the cell resistance of the films built at pH 4.4 may be linked to their high swellability. Therefore, for the PGA/PLL films, the cell adhesion properties can be tuned depending on the deposition pH of the polyelectrolyte solutions. This study reveals the importance of the multilayer structure and architecture to control the detachment force of cells onto such films.

© 2004 Published by Elsevier B.V.

\* Corresponding author. Tel.: +33-3-90-24-32-58; fax: +33-3-90-24-33-99.  
E-mail address: catherine.picart@medecine.u-strasbg.fr (C. Picart).

31 **Keywords:** Self-assembly; Biological molecules; Adhesion; Atomic force microscopy; Surface structure, morphology, roughness, and  
32 topography

33

#### 34 1. Introduction

35 There is an increasing interest in developing  
36 new coatings to improve biocompatibility and to  
37 prepare biomaterial surfaces that can either resist  
38 or enhance cellular adhesion by mimicking extra-  
39 cellular matrix components [1,2] or even locally de-  
40 liver drugs. The most important step toward this  
41 end concerns the improvement at the nanometer  
42 to micrometer scales of material surface properties  
43 [3] in order to control cellular responses such as  
44 adhesion, motility, spreading, growth and differen-  
45 tiation. This has been the focus of many studies  
46 since about 40 years. It has been shown that differ-  
47 ent parameters such as hydrophobicity and hydro-  
48 philicity [4], surface charge [5–7], roughness [8],  
49 surface free energy [9,10] and topography [11] af-  
50 fect cellular adhesion. The definition of general  
51 rules is not straightforward and the observed cellu-  
52 lar behaviors probably do not depend on a single  
53 parameter but on a complex combination of sev-  
54 eral factors.

55 In addition to being able to control the physico-  
56 chemical surface properties, it is of interest to  
57 establish easy handling methodologies available  
58 for various types of surfaces and for creating con-  
59 trolled topographical features. Typically, appro-  
60 priate surface chemistries such as ethylene glycol  
61 grafting [12] or monolayer self-assembly [13] can  
62 be used in conjunction with patterning techniques  
63 to create both cell-resistant and cell-adherent sur-  
64 face domains. Alternatively, adhesive ligands such  
65 as RGD can be grafted to the deposited polymers  
66 [14].

67 Polyelectrolyte multilayers (PEM) constitute a  
68 new attractive way for creating biofunctionalized  
69 surface coatings. The layer-by-layer (LbL) tech-  
70 nique consists in the alternate deposition of poly-  
71 anions and polycations from aqueous solutions to  
72 build the multilayered films [15,16]. These films  
73 have tunable properties in the thickness range  
74 from nanometer to micrometer [17,18]. It has been

shown that the film morphology, internal molecu-  
75 lar structure and thickness depend largely on the  
76 processing conditions such as ionic strength [19],  
77 and pH of the polyelectrolyte or rinsing solution  
78 [20]. The films are not only stabilized by electro-  
79 statics interactions but also via hydrogen bonds  
80 [21,22].

81 Of special importance for biomedical applica-  
82 tions is the control of the chemical composition  
83 of the surface that can affect biological activity.  
84 Films made of polyamino-acids, i.e. poly(L-lysine)  
85 (PLL), poly(L-glutamic acid) (PGA), natural poly-  
86 electrolytes (e.g. hyaluronan (HA), alginate, chito-  
87 san, collagen) allow, for example, to create  
88 biomimetic architectures [18,23–25]. Various com-  
89 pounds such as DNA, RNA, drugs, inorganic par-  
90 ticles can be embedded in such films or deposited  
91 on the top of them.

92 A great advantage offered by PEM films is their  
93 ability to coat any type of material with any shape.  
94 Thus, PEM films have recently been deposited  
95 onto stainless steel [26], polydimethylsiloxane  
96 (PDMS) [27], vascular stents made of NiTi [28],  
97 and onto biodegradable poly(L-lactic) acid matri-  
98 ces [29]. The geometry was not necessarily planar  
99 but also curved or spherical, as for titanium beads  
100 [30], or polystyrene and glass microspheres. In the  
101 case of films built on particles, the particle core can  
102 also be subsequently removed to form hollow cap-  
103 sules [25] or the films can be detached from the sur-  
104 face to give self-supported membranes [31].

105 Within the past few years, there has been an  
106 increasing interest for biomedical applications of  
107 PEM films. Fundamental and applied studies of  
108 PEM in terms of biological properties with respect  
109 to biological fluids or cells have been published  
110 (see paragraph 2). This includes, for example, the  
111 fabrication of non-adhesive barriers for vascular  
112 grafts [23], the fabrication of films with pro or  
113 anti-coagulant properties [24], the control of the  
114 cell adhesive properties of a film by varying the  
115 deposition pH [32,33], the preparation of hollow  
116

117 capsules for drug release [25], the preparation of  
 118 bacterial resistant film [34,35]. Moreover and very  
 119 interestingly, a further functionalization of the  
 120 films can be achieved by inserting peptides cova-  
 121 lently bonded to polyelectrolytes [36] or through  
 122 protein embedding [37].

123 For the biomaterial field, biocompatibility is a  
 124 major requirement: the material must be non-toxic  
 125 to any living cell. Another requirement is that the  
 126 material possesses chemical and physical proper-  
 127 ties that promote or avoid specific cell substrate  
 128 interactions, i.e. either cell adhesion or non-adhe-  
 129 sion depending on the final application.

130 Rubner and coworkers [32,33] have recently  
 131 demonstrated that PEM films based on synthetic  
 132 polyelectrolytes (polyacrylic acid, polyacrylamide,  
 133 and poly(allylamine) hydrochloride) can either be  
 134 cell resistant (cytophobic) or cell adhesive (cyto-  
 135 philic) depending on the swelling capacities of  
 136 the films, which are modulated by changing the  
 137 deposition pH of the films. In fact, changing the  
 138 deposition pH is known to considerably change  
 139 the internal properties and thicknesses of the films  
 140 [21,38]. We have already investigated cell interac-  
 141 tion with biodegradable (PGA/PLL) multilayers  
 142 built at physiological pH and containing an  
 143 increasing number of layer pairs. We found that  
 144 the initial adhesion was always very low for  
 145 PGA-ending films whereas it was very high and de-  
 146 creased with the number of deposited layers for  
 147 PLL-ending films. But at the working pH (7.4),  
 148 cells were always strongly adhering to PLL-ending  
 149 films and poorly adhering to PGA-ending films. At  
 150 the cellular scale, it would also be of interest to test  
 151 whether the findings presented by the Rubner and  
 152 coworkers [32,33] remain valid for polyamino-acid  
 153 based films. In other words, can a given polyelec-  
 154 trolyte system such a PGA/PLL, which is capable  
 155 of forming ordered structures ( $\alpha$ -helix and  $\beta$ -  
 156 sheets) [39], be adhesive and anti-adhesive for cells  
 157 depending on the deposition pH of the films?

158 The present study is first aimed at investigating  
 159 the possibilities of building films of synthetic poly-  
 160 peptides, such as (PGA/PLL) films, over a large  
 161 range of pHs in order to change their internal  
 162 properties. Second, we will investigate whether  
 163 these films can be used for cell culture experiments,  
 164 i.e. whether they remain stable in a physiological

medium. The third aim is to quantify by microman-  
 165 ipulation the short-term interaction of chondro-  
 166 sarcoma cells with the (PGA/PLL) films built at  
 167 different pH. 168

## 2. Survey of the literature regarding cell adhesion studies on polyelectrolyte multilayer films

169 Studies dealing with the adhesion properties of  
 170 cells on various PEM films are presented in Table  
 1. Cell adhesion and proliferation assays were ini-  
 171 tially performed on cell lineages [33,36,40,41]. Thin  
 172 films were found to be cell adhesive with some dif-  
 173 ferences depending on the outermost layer of the  
 174 film [40]. Recently, Rubner and coworkers [32,33]  
 175 showed that poly(acrylic acid)/poly(allylamine hy-  
 176 drochloride) (PAH) multilayers can either be  
 177 non-adhesive or adhesive for NR6WT fibroblasts  
 178 depending on the pH of preparation of these films.  
 179 These authors suggested that the non-adhesive  
 180 character of the films with respect to the cells is re-  
 181 lated to their high swelling capacities and softness,  
 182 and is fully independent of the protein uptake  
 183 from serum. In addition, a recent work performed  
 184 on 1  $\mu$ m thick (PLL/HA) films indicated that  
 185 crosslinking the film may dramatically change the  
 186 cell adhesion properties: a soft and native film  
 187 was highly cell resistant whereas a covalently  
 188 crosslinked film was highly cell adhesive [42].  
 189 Crosslinking was not only found to increase cell  
 190 adhesion but also to enhance film stability with re-  
 191 spect to an enzymatic degradation, to dehydration  
 192 and noteworthy to increase film rigidity (Richert,  
 193 personal communication). Similarly, incorpo-  
 194 ration of nanocolloids into PEM films, leading to a  
 195 film rigidification, was also shown to render films  
 196 adherent to cells in the presence of colloids [43].

197 The use of primary cells represents a further step  
 198 to mimic real cell behavior prior to *in vivo* exper-  
 199 iments. Such cells are much more sensitive to exter-  
 200 nal conditions and substrate properties than cell  
 201 lineages. Several works were devoted to primary  
 202 cell adhesion onto PEM films (Table 1). PEM films  
 203 based on poly(styrenesulfonate) (PSS) as polyan-  
 204 ion combined with different polycations, either  
 205 PAH [44], or poly(ethylene imine) (PEI) [45] are  
 206 frequently investigated. For such thin films, a good  
 207 208

Table 1

Summary of the different cell culture studies performed on PEM films for both cell lineages and primary cells cultures; also given are, when available, the film thickness and its refractive index  $n_A$ .

Polyanion	$n_A$	Film thickness <sup>a</sup>	Type of cells	Behavior	Reference	Important parameter
<i>Cell lineages</i>						
PAA/PAH	NA	Depends on buildup conditions	NR6WT (fibroblasts)	Adherent for low swellable films Cell resistant for highly hydrated and swellable films	[32,33]	Film swellability
PAA/PAAm						
PMA/PAAm						
HA/PLL	1.36–1.38	(in liquid) $\approx 1 \mu\text{m}$ for $(\text{PLL}/\text{HA})_{10}$	HCS 2/8 (Chondrosar-comas)	Cell resistant for $(\text{PLL}/\text{HA})_{12}$ highly adhesive after crosslinking	[42]	Film stiffness
PDDA/CdTe-(PAA/COL)	NA	(dried) 15 nm for PDDA-(PAA/COL) <sub>5</sub>	PC12 (neurones)	Cyto-toxicity for (PDDA/CdTe) <sub>5</sub> Cell adhesion for (PAA/COL)	[51]	Surface chemistry
PAA/PDDA	NA	(dried) 20 nm for (PDDA/PAA-TiO <sub>2</sub> ) <sub>6</sub>	PC12 (neurones)	Cell resistant for (PDDA/PAA) <sub>6</sub> cell adhesive after insertion of TiO <sub>2</sub> nanoparticles	[43]	Film stiffness
<i>Primary cells</i>						
PSS/PAH	1.48–1.50	(in liquid) 20–30 nm for PEI-(PSS/PAH) <sub>3</sub>	HUVEC (endothelial cells)	Cell adhesive, better for PAH ending films than PSS ending ones Conservation of phenotype	[44]	Surface charge
Last layer PDL or PAH						
PSS/PAH	1.51–1.52	(in liquid) 16–23 nm for PGA, PGA-PLL or PSS deposited on top of a (PSS/PAH) <sub>2</sub> -film	PDL (Periodontal ligament fibroblasts)	Good cell adhesion and proliferation on PGA and PSS ending films	[46]	Surface chemistry Film construction described in Vautier et al. [40]
Last layer PGA, PSS, PAH, or PLL						
Gelatin/PDL	NA	(dried) 23 nm for (PSS/PEI) <sub>3</sub> -(Gelatin/PDL) <sub>3</sub> -gelatin	BCAEC (coronary artery endothelial cells)	Good adhesion for (PSS/PEI) <sub>3</sub> -(Gelatin/PDL) <sub>3</sub> -gelatin Poor adhesion on (PSS/PEI) films ending by PEI or PSS	[27]	Surface chemistry

SUSC15006  
9 July 2004; Disk used

No. of Pages: 17, pp. 501

L. Richert et al. / Surface Science xxx (2004) xxxx–xxx

5

Fb/PDL Lam/PDL	NA	(dried) $\approx$ 20 nm for (PSS/PEI) <sub>3</sub> -(Fb/PDL) <sub>4</sub> same but with lam	Cerebellar neurons	Good adhesion for all the films after seven days in culture	[45]	Cell receptor
Alg/PLL	NA	(dried) $\approx$ 200 nm for (PLL/Alg) <sub>8</sub>	Human fibroblast cells	Cell resistant for (PLL/Alg) <sub>12</sub>	[23]	Film hydration/ swellability
Dex/CHI HEP/CHI	NA	(dried) $\approx$ 64 nm for (Dex/CHI) <sub>3</sub> , built in 1 M NaCl	Human blood platelets	Alternating activity at ionic strength above 0.5 M: - Anti-coagulation for Dex ending films and coagulation for CHI ending films - Anti-coagulation for CHI/HEP films whatever the outermost surface	[24]	Specific groups
HA/CHI/HA/PLL	1.36–1.38	(in liquid) $\approx$ 300 nm for (CHI/HA) <sub>10</sub> ; $\approx$ 1 $\mu$ m for (PLL/HA) <sub>10</sub>	Bovine chondrocytes	Adhesion decreases as the number of layers in the film is increased (poor adhesion after 10 layer pairs when a film is formed)	[35]	

*Abbreviations:* For polyanions: alginate (Alg), dextran (Dex), hyaluronan (HA), poly(styrene sulfonate) (PSS), poly(acrylic acid) (PAA), poly(methacrylic acid) (PMA), polyacyrlamide (PAAm), poly(allylamine hydrochloride) (PAH), poly(diallyldimethylammonium chloride) (PDDA).

For polycations: chitosan (CHI), poly(L-lysine) (PLL), poly(D-lysine)(PDL), collagen (COL).

NA: non-available.

\* For dried films, thickness is often estimated by means of QCM or ellipsometry but refractive index is often unavailable. For hydrated films, both refractive index and thickness are obtained from optical waveguide lightmode spectroscopy measurements [17].

cellular adhesion could be observed. Refractive index of poly(styrenesulfonate)/poly(allylamine hydrochloride) (PSS/PAH) films was measured *in situ* by OWLS and a value of 1.5 was estimated in physiological conditions [17]. This indicates that such films are relatively dense and contain only around 25% of water (a simple approximation of the water content is based on the following formula:  $n_{\text{PEM}} = 1.3340 \times a + (1 - a) \times 1.56$ , 1.334 being the refractive index of a 0.15 M NaCl solution, 1.56 being the refractive index of a pure polymer film [38], and  $a$  being the fraction of water). Other studies were realized with PLL, poly(D-lysine) (PDL), or even chitosan as polycation in combination with polyanions such as gelatin [27], PGA [46], or hyaluronan [35]. As a general rule emerging from the different studies summarized in Table 1, films made of polypeptides and polysaccharides in comparable ionic strength conditions are more hydrated than films made of synthetic polyelectrolytes such as PSS/PAH. This observation is based on refractive indices that are  $\approx 1.36$ –1.38 for polysaccharide films [18,35] and  $\approx 1.42$  for PGA/PLL films [47] which would correspond to water contents ranging respectively from 95% to 60%. Moreover, the high swelling capacities of the polysaccharides, for instance that of hyaluronan [48], renders the buildup of much thicker film possible, e.g. up to several hundred of nanometers [35] or even several micrometers after deposition of 20–30 layer pairs [42]. These polysaccharide based films were always found to be extremely cell resistant [23,35,42] except when the films were rigidified by covalent crosslinking [42]. Therefore, a trend that seems to emerge from all these cell lineages and primary cell studies is that nanometer thin and dense films formed by few layer pairs are more favorable for cellular adhesion than thick and highly hydrated films.

Such results can be partially related to those found for 3D polyacrylamide gels of different stiffness for which it was shown that cell adhesion is directly related to gel stiffness, i.e. the cells exhibited good adhesion on the stiff gels and poor adhesion on soft gels [49]. The highly swellable, lightly crosslinked films may be too soft and their surface may be too watery for cells to adhere [33].

In term of biocompatibility, layer-by-layer films made of PEI, PSS, and PAH, although favorable to cell adhesion *in vitro*, may not be appropriate for surface modifications of medical devices for *in vivo* purposes [50]. For this reason precisely biocompatible polymers (synthetic polypeptides or natural polysaccharides) could be of higher interest [28].

### 3. Experimental 265

#### 3.1. Polyelectrolyte solutions and coupling agent 266

Anionic PGA (MW = 54 kDa), cationic PLL (MW = 30.3 kDa), PEI (MW = 750 kDa), 1-ethyl-3-(3-dimethylaminopropyl) carbodiimide (EDC) and *N*-hydroxysulfo-succinimide (sulfo-NHS) were purchased from Sigma-Aldrich. Sodium chloride (purity = 99.5%) was purchased from Fluka, and Sodium dodecyl sulfate (SDS) was purchased from Sigma. All solutions were prepared using ultrapure water (Milli-Q-plus system, Millipore) with a resistivity of 18.2 MΩcm. Polyelectrolyte solutions were always freshly prepared by direct dissolution of the polyelectrolytes in filtered water. The final polyelectrolyte concentrations were of 1 mg/mL. The pHs of water and the PLL, PGA and PEI solutions were adjusted with 0.01 M HCl or 0.01 M NaOH. For streaming potential experiments, since the experimental device is extremely sensitive to very slight pH changes, solutions were prepared in a Tris-HCl buffer (0.1 mM Tris) for a given pH.

#### 3.2. Analysis of the film growth, surface $\zeta$ potential and morphology by atomic force microscopy (AFM) 287 288 289

The PEI-(PGA/PLL)<sub>*i*</sub> film buildup process (where *i* corresponds to the number of layer pairs) was followed by optical waveguide lightmode spectroscopy (OWLS) and by quartz crystal microbalance (QCM). Briefly, OWLS is sensitive to the penetration depth of an evanescent wave through the film near the waveguide surface and gives access to the optical properties of the films. Details about the experimental setup and the pro-

299 cedure can be found elsewhere [17]. The structure  
 300 of the multilayers was analyzed using the homoge-  
 301 neous and isotropic monolayer model which al-  
 302 lows the refractive index  $n_A$  and the thickness  $d_A$   
 303 to be determined [17]. Mass data are calcu-  
 304 lated according to the De Feijter's formula [52]  
 305 (adsorbed mass =  $(dn/dc)^{-1} \times (n_A - n_C) \times d_A$  with  
 306  $(dn/dc) = 0.188 \text{ cm}^3/\text{g}$  and  $n_C = 1.3332$  is the  
 307 refractive index of water).

308 At the beginning of the experiment, 100  $\mu\text{L}$  of  
 309 the PEI solution was manually injected in the mea-  
 310 surement cell (37  $\mu\text{L}$ ). When a stable adsorption  
 311 signal was obtained (in about 15 min), the water  
 312 flow was started for about 10 min to rinse the ex-  
 313 cess material. In the same way, we continued with  
 314 the alternate adsorption of PGA and PLL on the  
 315 waveguide.

316 QCM (Q-Sense, Göteborg, Sweden) consists of  
 317 measuring the changes in the resonance frequency  
 318 of a quartz crystal when material is deposited from  
 319 solution. The crystal is excited at its fundamental  
 320 frequency (about 5 MHz) and observation takes  
 321 place at different overtones. In this work, however,  
 322 we will present data corresponding to the 15 MHz  
 323 overtone only. The details of the experimental set-  
 324 up has been previously presented [17], except that  
 325 the crystal used for the present study is coated with  
 326 a thick ( $\approx 100 \text{ nm}$ )  $\text{SiO}_2$  film.

327 The streaming potential method was also used  
 328 to characterize the surface. Measurements were  
 329 carried out on a home made apparatus that has  
 330 been previously described [18,53]. The basic princi-  
 331 ple is to measure the pressure and the potential dif-  
 332 ferences on both sides of a 530  $\mu\text{m}$  radius capillary  
 333 made of fused silica via two flasks containing four  
 334 electrodes. Details about the procedure have been  
 335 given in Picart et. al. [18]. PGA and PLL were ad-  
 336 sorbed in water at a given pH and measurements  
 337 were performed after the rinsing of each layer.  
 338 The rinsing solution (similar to that used for the  
 339 measurements) contained only Tris at  $5 \times 10^{-4} \text{ M}$   
 340 at the adjusted pH (either 4.4, 7.4 or 10.4).

341 Atomic force microscopy images were obtained  
 342 in contact mode in air with the Nanoscope III  
 343 from Veeco (Santa Barbara, CA) [47]. Deflection  
 344 and height mode images are scanned simulta-  
 345 neously at a fixed scan rate (2 Hz) with a resolu-  
 346 tion of  $512 \times 512$  pixels. The mean roughness

of the films was calculated according to:  
 $R = \frac{1}{N_x N_y} \sum_{i=1}^{N_x} \sum_{j=1}^{N_y} |z_{ij} - z_{\text{mean}}|$  where  $z_{ij}$  is the  
 height of a given pixel,  $z_{\text{mean}}$  is the average height  
 of the pixels, and  $N_x$  and  $N_y$  are the number of pix-  
 els in the  $x$  and  $y$  directions.

### 3.3. Preparation of the polyelectrolyte multilayer coated glass slides for cell adhesion experiments

For the cell adhesion experiments, the PEM  
 films were deposited on borosilicate glass slides  
 previously cleaned with both 10 mM SDS and  
 0.1 M HCl for 15 min in boiling water bath and  
 extensively rinsed with ultrapure water. The PEI-  
 (PGA/PLL)<sub>n</sub> films were prepared with an auto-  
 matic dipping machine (Dipping Robot DR3, Kir-  
 stein GmbH, Germany). The 18 × 18 mm glass  
 slides were introduced vertically in a home made  
 holder which was dipped for 15 min into a first  
 PEI solution (PEI). The adsorbed layer was subse-  
 quently rinsed at the same pH as the polyelectro-  
 lyte solutions in three different beakers of water  
 of resp. 350, 45 and 45 mL, resp. for 30 s, 2 min  
 and 2 min. The slides were then dipped into  
 the oppositely charged polyelectrolyte solution  
 (PGA) followed by the same rinsing procedure.  
 The buildup was further pursued by alternate  
 PLL and PGA deposition and rinsing steps. Films  
 were stored at 4 °C for no more than four days un-  
 til use. For the crosslinking, EDC (200 mM) and  
 sulfo-NHS (50 mM) were put in contact with the  
 film for 12 h at room temperature. Experiments  
 using fluorescein isothiocyanate labeled PLL  
 (PLL-FITC, MW = 50.2 kDa, Sigma) were also  
 undertaken: PLL-FITC was adsorbed as the ter-  
 minating layer of a PEI-(PGA/PLL)<sub>n</sub>-PGA-  
 PLL-FITC. Fluorescence images were taken with  
 a 40× objective in different medium (water at a gi-  
 ven pH, then at increasing salt concentration, and  
 finally in the MEM).

### 3.4. Cell culture and micromanipulation experi- ments

HCS-2/8 human chondrosarcoma cell culture  
 and micromanipulation experiments were achieved  
 as previously described [41]. Briefly, it consists of  
 an inverted microscope (Ellipse E200, Nikon)

391 equipped with a 40 $\times$  dry objective, a micromanipulator (Narishige) connected to a pressure controller (DP103, Validyne Eng) and a numeric camera (DXM 1200 Nikon). The cells were first deposited 395 at 25 °C into a homemade chamber containing 396 MEM with 10% FCS. A single chondrosarcoma 397 cell was caught with a small negative pressure 398 ( $\approx$ 50 Pa) within the micropipette ( $\sim$ 10  $\mu$ m inner 399 diameter) and brought horizontally into the vicinity 400 of the polyelectrolyte film. Then, the negative 401 pressure was removed and the cell was left in this 402 position for 15 s to allow it to attach to the film. 403 After the seeding time (30 min), the micropipette 404 was brought in contact with the cell and a small 405 depression was applied to the cellular membrane, 406 then the micropipette was pulled slowly away from 407 the surface at a constant speed ( $\approx$ 10  $\mu$ m/s). If the 408 negative pressure applied to the pipette was not 409 sufficient to create a force that exceeds the cellular 410 adhesion force, the procedure was repeated. The 411 depressurization was successively increased (by  $-120$  412 Pa steps), until the chondrosarcoma cell adhesion 413 force was exceeded. More than 40 cells were tested 414 for adhesion on each type of film. The pipette radius ( $R_p$ ) and the depressurization applied ( $\Delta P$ ) to the 415 cell membrane were collected and the detachment 416 force ( $F$ ) was calculated according to  $F = \pi R_p^2 * \Delta P$  [54,55].

417 Comparison between groups was performed 418 using the Mann–Whitney rank test to determine 419 the existence of significant differences ( $p < 0.05$ ).

#### 422 4. Results and discussion

##### 423 4.1. Physico-chemical characteristics of the PEI- 424 (PGA/PLL)<sub>i</sub> films built at different pHs

425 The buildup of the PEI-(PGA/PLL)<sub>10</sub> multi- 426 layer films at different pH values in water was fol- 427 lowed *in situ* step-by-step by OWLS (Fig. 1A). In a 428 previous work [47], the PEI-(PGA/PLL)<sub>i</sub> multilayers 429 built in a buffer containing 0.15 M NaCl at pH 430 7.4 have been characterized by *in situ* atomic force 431 microscopy and by OWLS. The evolution of the 432 thickness and of the adsorbed mass with the num- 433 ber of deposited layers was exponential. These lay- 434 ers formed extended structures that appear with a

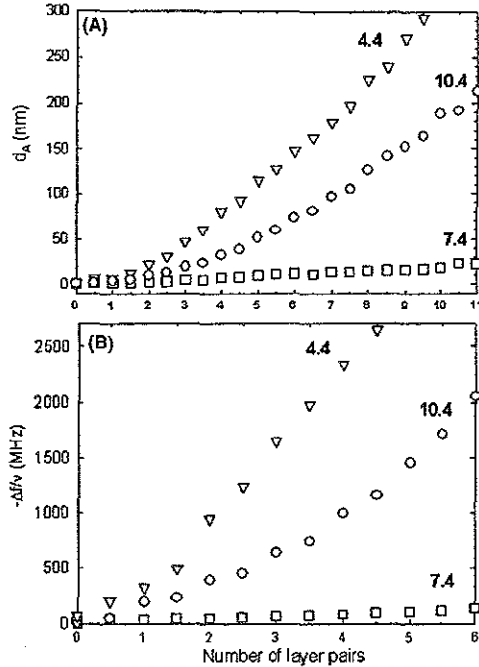


Fig. 1. (A) Thickness  $d_A$  (nm) of PEI-(PGA/PLL)<sub>i</sub> films built at pH = 4.4 ( $\nabla$ ), 7.4 ( $\square$ ) and 10.4 ( $\circ$ ) as a function of the number of layer pairs  $i$  in the film, as measured by the OWLS technique. (B) Frequency shift measured for the same films by QCM-D as a function of  $i$ . For clarity, only the signal obtained at 15 MHz is represented.

vermiculate pattern. In the present experiments, 435 the growth of the film in water is strongly depen- 436 dent on the pH of the buildup. The films are extre- 437 mely thin when built at pH = 7.4 (around 15 nm 438 after deposition of 20 layers). The increase in 439 thickness with the number of layers is linear at this 440 pH. Their refractive index is around 1.5, i.e. simi- 441 lar to that of (PSS/PAH) films and higher than 442 that of the same films built in the presence of 443 0.15 M NaCl ( $\approx$ 1.42) [41,47]. The film growth 444 becomes much more important at the extreme 445 pH values. The thickest films are obtained at 446 pH = 4.4: their thickness could not be estimated 447 by OWLS after the deposition of nine pairs of lay- 448 ers. For these films, the refractive index reaches a 449

450 relatively high value ( $\approx 1.45$ ) for five layer pairs.  
 451 The buildup could not be achieved at lower pH  
 452 due to a precipitation in the PGA solution. For  
 453 the alkaline pHs, the buildup was not successful  
 454 at pH higher than 11, the connection tubes being  
 455 plugged after the injection of the polyelectrolytes.  
 456 The QCM data for the five first layer pairs qualita-  
 457 tively confirm the differences in growth obtained  
 458 by OWLS (Fig. 1B). QCM is sensitive to the whole  
 459 mass of the film, including water, which may ex-  
 460 plain why the growth at pH 4.4 is even more pro-  
 461 nounced than that observed by OWLS. An  
 462 exponential growth of the (PGA/PLL) multilayer  
 463 films has previously been observed for films built  
 464 at pH = 7.4 in a Mes-Tris buffer containing 0.1  
 465 M NaCl. The exponential growth of the multilay-  
 466 ers was explained on the basis of polyelectrolyte  
 467 diffusion [47]: when the architecture is in contact  
 468 with a PLL solution, PLL diffuses in the film  
 469 whereas PGA diffuses out. In the present case, film  
 470 growth appears rather linear for all the investi-  
 471 gated conditions after few layers have been depos-  
 472 ited.

473 Both OWLS and QCM data indicate that the  
 474 growth of (PGA/PLL) films in pure water is highly  
 475 dependent on the pH used for the buildup. Alter-  
 476 nately, one could fix the pH at a given value and  
 477 change the buildup conditions by changing the io-  
 478 nic strength. This was done recently for chitosan/  
 479 hyaluronan multilayer films (built at pH = 5) for  
 480 which it was shown that film growth is linear at  
 481 low ionic strength. The growth becomes expo-  
 482 nential at 0.15 M NaCl [41].

The  $\zeta$  potential of the PEI-(PGA/PLL)<sub>5</sub> multi-  
 483 layer films was also determined after the deposition  
 484 of each new polyelectrolyte layer (Fig. 2 and Table  
 485 2). At pH = 7.4, the  $\zeta$  potential alternates after each  
 486 new PLL and PGA adsorption and becomes posi-  
 487 tive (+50 mV) or negative (-120 mV) respectively.  
 488 The value of the  $\zeta$  potentials are very different at  
 489 pH = 4.4 and 10.4. At acidic pH, PGA-ending lay-  
 490 ers have still a slightly negative  $\zeta$  potential. This can  
 491 be due to a charge decrease on the PGA chains  
 492 when the pH is decreased, even if the effective  
 493

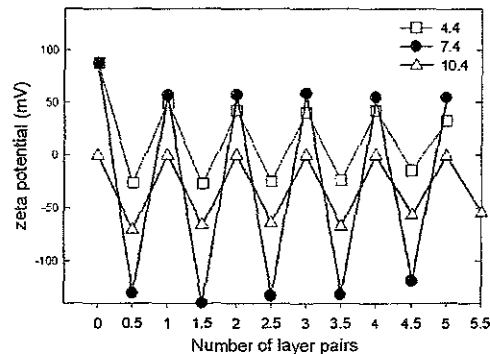


Fig. 2. Evolution of the  $\zeta$  potential (mV) during the alternate deposition of PGA and PLL as a function of the number of deposited layer pairs  $i$  on a fused silica capillary at different pHs. Zero corresponds to the first PEI layer. pH = 4.4 (□), pH = 7.4 (●) pH = 10.4 (△). PGA and PLL were prepared in a 0.5 mM Tris-HCl buffer at the given pHs. The symbols represent the mean and standard deviation of three successive measurements for a given layer (for one single experiment).

Table 2

Refractive index  $n_A$ , optical thickness  $d_A$  (nm), and optical mass  $Q_A$  ( $\mu\text{g}/\text{cm}^2$ ) for the PEI-(PGA/PLL)<sub>5</sub> films ( $i = 5$  and 10) built at different pH 4.4, 7.4 and 10.4, as measured by the OWLS technique

pH	$I$	$n_A$	$Q_A$ ( $\mu\text{g}/\text{cm}^2$ )	$d_A$ (nm) OWLS	$d_A$ (nm) dried AFM	Ra (nm)	$\zeta$ -PGA (mV)	$\zeta$ -PLL (mV)
4.4	5	$1.449 \pm 0.014$	$7.52 \pm 2.96$	$118.2 \pm 32.3$	$180.5 \pm 5$	$32.5 \pm 8.0$	$-14.2 \pm 0.1$	$33.4 \pm 0.9$
	10	NA	NA	NA				
7.4	5	$1.535 \pm 0.013$	$0.81 \pm 0.21$	$8.1 \pm 0.3$	$20.5 \pm 1.5$	$3.5 \pm 0.5$	$-118.5 \pm 0.3$	$55.2 \pm 1.6$
	10	$1.499 \pm 0.013$	$1.56 \pm 0.12$	$15.5 \pm 0.9$				
10.4	5	$1.435 \pm 0.013$	$3.31 \pm 0.16$	$66.1 \pm 13.8$	$254.5 \pm 10.0$	$14.0 \pm 0.5$	$-50.6 \pm 1.3$	$0.3 \pm 0.5$
	10	$1.440 \pm 0.014$	$9.39 \pm 0.26$	$164.3 \pm 3.2$				

For each investigated pH, at least three experiments were performed in order to calculate the means and standard deviations of the optical parameters. The  $\zeta$  potentials of the fifth PGA and PLL layers are also given (means and standard deviations of three successive measurements of a single experiment). Dried thickness and mean roughness (Ra) were also determined by AFM.

494  $pK_a$  of PGA, which is around 2.5 in PGA/PLL  
 495 films built in salt, is lower than that in solution  
 496 [34]. The  $\zeta$  potential of PLL remains highly positive  
 497 since PLL is fully charged. At pH 10.4,  $\zeta$  potential  
 498 of PGA is highly negative although less than at pH  
 499 7.4, but  $\zeta$  potential of PLL is  $\approx 0$ . This is probably  
 500 because PLL is much less charged at this pH [39] as  
 501 it is close to the  $pK_a$  value of PLL in solution,  
 502 which is about 9 [56]. Taken together, the  $\zeta$  poten-  
 503 tial measurements confirm the expected fact that  
 504 the films are tightly ionically linked at physiological  
 505 pH whereas they are much fewer ionic bonds at  
 506 both acidic and basic pH. The  $\zeta$  potential data indi-  
 507 cate clearly that, when both polyelectrolytes are  
 508 fully charged at pH = 7.4, the adsorption of the  
 509 incoming oppositely charged polyelectrolyte occurs  
 510 via electrostatic interactions. When one of the poly-  
 511 electrolytes bears less charges, i.e. either less nega-  
 512 tive (at pH = 4.4) or less positive (at pH = 10.4)  
 513 charges, one can expect that film stabilization can  
 514 also occur via hydrogen bonding [21]. In the partic-  
 515 ular case of PLL and PGA, these polyelectrolytes  
 516 assembled into a film do exhibit a secondary struc-  
 517 ture, which greatly depends on the pH of buildup  
 518 [39]. However, as we will see later, the stability of  
 519 the films when they are subjected to changes in  
 520 the suspending medium (cells experiments have to  
 521 be performed in a physiological medium at pH  
 522 7.4) might be a problem for their use in physiolog-  
 523 ical pH conditions. The different films were also ob-  
 524 served by AFM (Fig. 3). Imaging was performed in  
 525 air due to the strong attraction between the films  
 526 and the tip when imaging the thick films in liquid  
 527 conditions. AFM images confirm the low thickness  
 528 ( $\approx 20$  nm) of the films built at pH 7.4. The dried  
 529 AFM thickness of the films built at pH 10.4 is  
 530 about 40% higher than that measured by OWLS  
 531 in water, which is due to differences in sensing of  
 532 these two techniques. Indeed, the films shrink when  
 533 they are exposed to solutions containing an  
 534 increasing salt concentration, which suggests that  
 535 these films have a low hydration/swellability degree  
 536 in physiological conditions. On the other hand, the  
 537 films built at pH = 4.4 have a dried thickness of 180  
 538 nm, their hydrated thickness being too high to be  
 539 measured by OWLS (a thickness of the order of  
 540 350–400 nm would be obtained). This suggests that

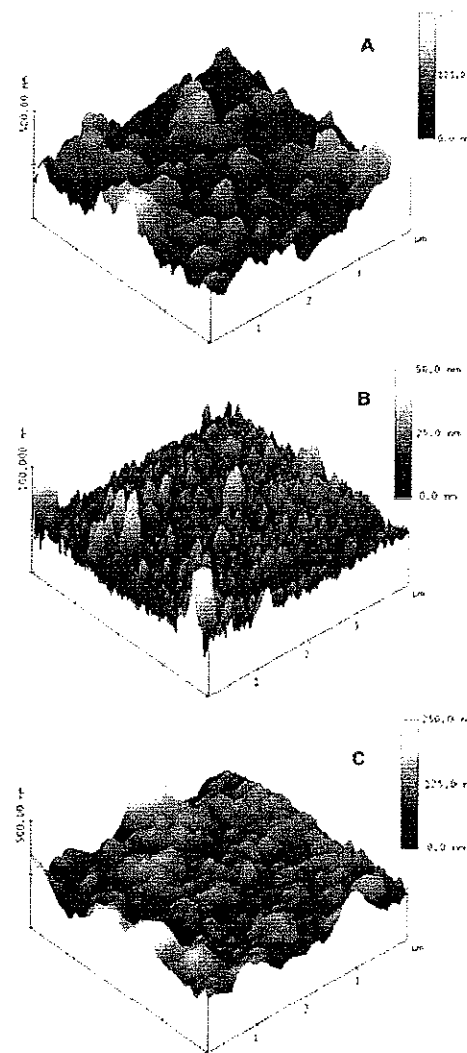


Fig. 3. AFM height mode images in air obtained for PEI-(PGA/PLL)<sub>10</sub> films built at different pHs. (A) 4.4, (B) 7.4, (C) 10.4. The image dimensions are  $4 \times 4 \mu\text{m}^2$  and the maximum z-range is 250 nm for (A) and (C) and 50 nm for (B).

these films are swellable by a factor of at least 541  
 200%. 542

We also tried to build the films at intermediate 543  
 pH values to investigate the transition from very 544

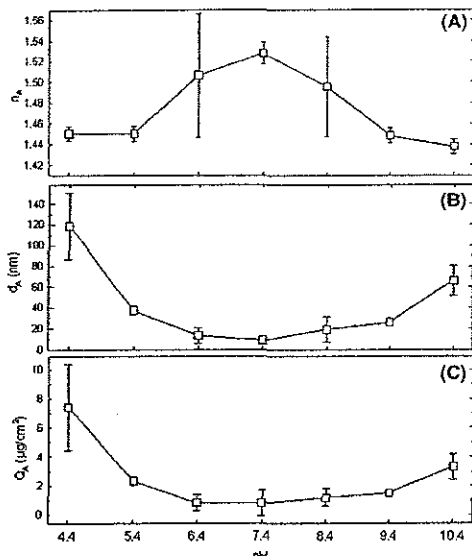


Fig. 4. Refractive index  $n_A$  (A), total thickness  $d_A$  (B) and total adsorbed amount  $Q_A$  ( $\mu\text{g}/\text{cm}^2$ ) (C) of PEI-(PGA/PLL) films as a function of the pH of buildup, for films built at pH varying from 4.4 to 10.4.

thin and dense films to much thicker and hydrated films (Fig. 4). The refractive index, total thickness and adsorbed amount of films made of five layer pairs are given as a function of the pH of the buildup up in Fig. 4. The smallest film thicknesses are obtained at pH = 6.4 and 7.4 where both polyelectrolytes are fully ionized. Then, the thickness and adsorbed mass increase toward a maximum at both acidic and basic pHs where respectively PGA and PLL are less ionized. The increase in thickness as a function of the pH is steeper at acidic pHs. The evolution found for (PGA/PLL) films is qualitatively comparable to that found for other pH sensitive weak polyelectrolyte films, such as PAA/PAH or PLL/HA films [21,38].

#### 4.2. Stability of the films in culture medium

As our ultimate aim was to use these films as substrates for cell adhesion assays, their stability in the culture medium was investigated. A change in suspending medium is expected to introduce

several stresses to the film: the first can be due to the increase in ionic strength from pure water to a medium containing approximately 0.15 M NaCl, the second can be due to the change from the buildup pH to the physiological pH of 7.4 at which the polyelectrolyte will be fully ionized, and the third stress can be due to the presence of ionic species in the culture medium such as phosphate and divalent ions ( $\text{Ca}^{2+}$ ,  $\text{Mg}^{2+}$ ). These ions are particularly known to give rise to certain gelling properties with biopolymers like alginate [57].

In order to test the stability of these films, two types of experiments were performed: OWLS was used to estimate the change in thickness and refractive index of the film and fluorescence microscopy with labeled PLL to visualize the eventual changes in film morphology. To this end, PLL-FITC was added as the last layer of the films. Then, the coated glass slide was introduced in a home made final chamber and subsequently put in contact with the different medium. The films built at pH = 7.4 and 10.4 in water remain stable in the culture medium whereas those built at pH = 4.4 become ruffled (Fig. 5). We then changed the medium composition step-by-step in order to understand the origin of the weak film stability. The films remain stable until a relatively high ionic strength of about 0.5 M (Table 3) while keeping the pH constant (4.4). On the other hand, when the film is put in phosphate buffer saline at pH = 7.4 containing 0.015 M NaCl, ruffles do appear. Divalent cations alone ( $\text{Ca}^{2+}$ ,  $\text{Mg}^{2+}$ ) at a physiological concentration, respectively 2 and 1 mM, do not affect film morphology. More likely, the combination of chloride, phosphate, and calcium ions seem to lead to a film ruffling.

As we recently investigated, polyelectrolyte multilayer films containing carboxyl and amine groups can be covalently crosslinked into amide bounds [42]. This approach was used for the present system. Crosslinking can be achieved on various types of films like PGA/PLL [58], therefore, the crosslinking protocol was applied to PGA/PLL films built in water at pH = 4.4. After a contact of 12 h with the coupling agent (EDC) and the sulfo-NHS (coupling enhancer) prepared in pure water adjusted to pH = 4 with 0.1 M HCl, the films were rinsed and then put in contact with the cul-

565  
566  
567  
568  
569  
570  
571  
572  
573  
574  
575  
576  
577  
578  
579  
580  
581  
582  
583  
584  
585  
586  
587  
588  
589  
590  
591  
592  
593  
594  
595  
596  
597  
598  
599  
600  
601  
602  
603  
604  
605  
606  
607  
608  
609  
610  
611  
612

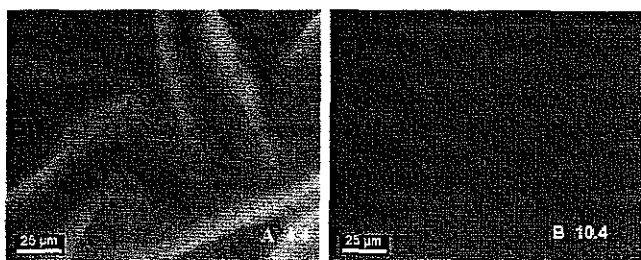


Fig. 5. Stability of the films built at pH 4.4 and 10.4 in water (no salt) when they are put in contact with the culture medium (approximate salt concentration 0.15 M NaCl with  $Mg^{2+}$  and  $Ca^{2+}$  ions, pH = 7.4) as observed by fluorescence microscopy on labeled PEI-(PGA/PLL)<sub>10</sub> films (the last PLL layer is PLL-FITC). The films built at pH = 7.4 are not shown since they are stable (white bar is 25  $\mu$ m). After crosslinking the film built at pH 4.4, it is stable in the culture medium and looks like that in B.

Table 3

Stability of the PEI-(PGA/PLL)<sub>10</sub> films built in water at different pHs (adjusted by addition of few drops of NaOH or HCl) and subsequently exposed to water containing an increasing amount of NaCl, or divalent cations, or a phosphate buffer saline solution at pH = 7.4 (1X corresponds to a solution containing 0.14 M NaCl, 1.5 mM KH<sub>2</sub>PO<sub>4</sub>, 8.1 mM Na<sub>2</sub>HPO<sub>4</sub>, 2.6 mM KCl)

pH	NaCl (same pH)	$Ca^{2+}$ (2 mM) $Mg^{2+}$ (1 mM) pH = 7.4	PBS (0.01X, 0.1X, 1X) pH = 7.4
4.4	- 0.01 M: small holes appear - >0.5 M: ruffling of the film	Stable	- 0.01X: small holes - 0.1X: ruffling of the film <i>Stable when crosslinked</i>
7.4	Stable, no shrinkage observed	Stable	Stable
10.4	Stable with a shrinkage up to 1 M	Stable	Stable

ture medium. As could be evidenced by fluorescence microscopy, the crosslinked films become stable in the medium. Therefore, for films built at pH = 4.4, all the cell experiments were performed after film crosslinking.

#### 4.3. Detachment forces for chondrosarcoma cells

The films built at different pHs in water were then tested in terms of their adhesion properties. To measure the detachment forces of chondrosarcoma cells on top of these films, each cell was individually put into contact with the films and left for 30 min at rest in a serum-containing medium. Then, the cells were progressively aspirated and pulled until they finally detached (Fig. 6). Within this time frame, the cells remained round.

The cell detachment forces were measured on PLL- or PGA-ending films consisting of 10 pair layers built in water at pH = 7.4, 10.4 and 4.4 (fol-

lowed by crosslinking in this latter case). The films were put in contact with the culture medium prior to the experiment for 1 h. The histograms of the adhesion forces obtained on the film architectures (more than 40 cells for a given film) built at different pHs are represented in Fig. 7.

The force distributions are symmetric. It can also be pointed out that, at pH 7.4, the detachment forces are higher for PLL-ending films than for PGA-ending ones. The films built at a physiological pH of 7.4 in water behave like the same films built in a salt containing medium (Mes-Tris buffer containing 0.1 M NaCl) (Fig. 8B). The PGA-ending films are highly cell "repulsive" or cytophobic whereas the PLL-ending films are highly cell "attractive" or cytophilic. For this system, the adhering cells are still sensitive to the ending polyelectrolyte layer even after contact with serum.

The histograms become comparable for PGA- and PLL-ending films when the films were built

631  
632  
633  
634  
635  
636  
637  
638  
639  
640  
641  
642  
643  
644  
645  
646  
647  
648  
649  
650

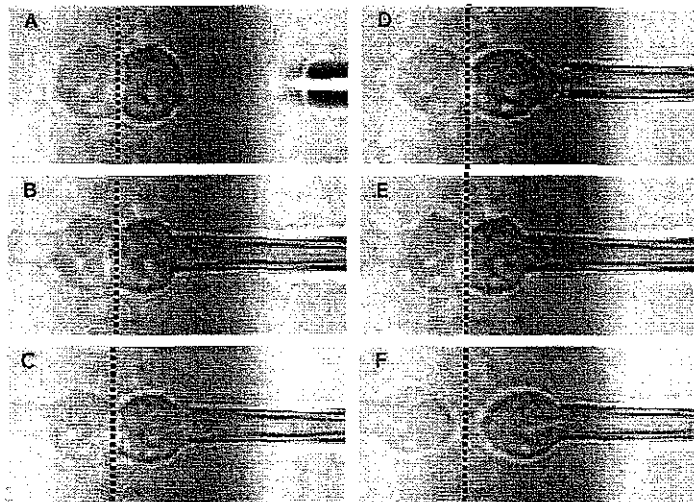


Fig. 6. Cell detachment measurement: after a 30 min seeding time (A), a chondrosarcoma cell was pulled from the multilayer surface with step-by-step increase in the aspiration depression (B–E). The pipette holding the cell with a minimum aspiration depression was moved by micromanipulation until the cell finally became detached from the surface (F) (the dotted line represents the cell/film polyelectrolyte film interface).

651 at pH 4.4 and 10.4. At this pHs, the outermost  
652 layer did not play a significant role in the measured  
653 detachment force. At pH 10.4, histograms were  
654 moreover very close to the force distribution found  
655 for the PLL films built at pH 7.4 (no statistical dif-  
656 ference) and the films were highly cell adhesive. In  
657 contrast, PGA- and PLL-ending films built at pH  
658 4.4 were highly cell resistant. It has to be noticed  
659 that these results are not specific to this short-term  
660 adhesion study since they were confirmed by a  
661 long-term cell culture test performed on the differ-  
662 ent films (data not shown). The average detach-  
663 ment forces are plotted on a single graph (Fig.  
664 8A) where it appears more clearly that films built  
665 at acidic pHs are cytophobic whereas those built  
666 at basic pHs are cytophilic. These observations  
667 are independent of the outermost layer of the  
668 films, except at physiological pH values, for very  
669 thin films for which the detachment force depends  
670 on the outermost layer of the film. In a previous  
671 paper, we have already shown using fluorescently  
672 labeled films that the rupture occurs more likely  
673 at the cell/substrate interface suggesting that there  
674 is no rupture of the cell [41]. It may have been

interesting to use a more sophisticated technique  
to investigate the cell/film interface [59], but this  
was not the aim of this article.

Our findings are in agreement with those of  
Rubner and coworkers for highly swellable films,  
for which the outermost layer does not play a  
determinant role in the cell adhesion properties  
of the film. However, these authors found that  
their polyelectrolyte system had cytophobic prop-  
erties at both basic and acidic pHs, which is not  
the case for the PGA/PLL films. In order to investi-  
gate whether the origin of the observed differ-  
ences for PGA/PLL films at low and high pH  
values may originate from parameters such as pro-  
tein adsorption, secondary structure of the films,  
or films roughness, complementary AFM, OWLS,  
and Fourier transform infrared spectroscopy  
experiments (FTIR) were performed. Adsorbed  
protein amounts were measured by OWLS on  
PGA-ending films and were found to be similar  
for films built at pH = 4.4 and 10.4 ( $\approx 0.37 \mu\text{g}/\text{cm}^2$ ) and undetectable for films built at physiolog-  
ical pH (this latter result was previously found for  
PGA/PLL films built in a Mes-Tris buffer at pH

675  
676  
677  
678  
679  
680  
681  
682  
683  
684  
685  
686  
687  
688  
689  
690  
691  
692  
693  
694  
695  
696  
697  
698

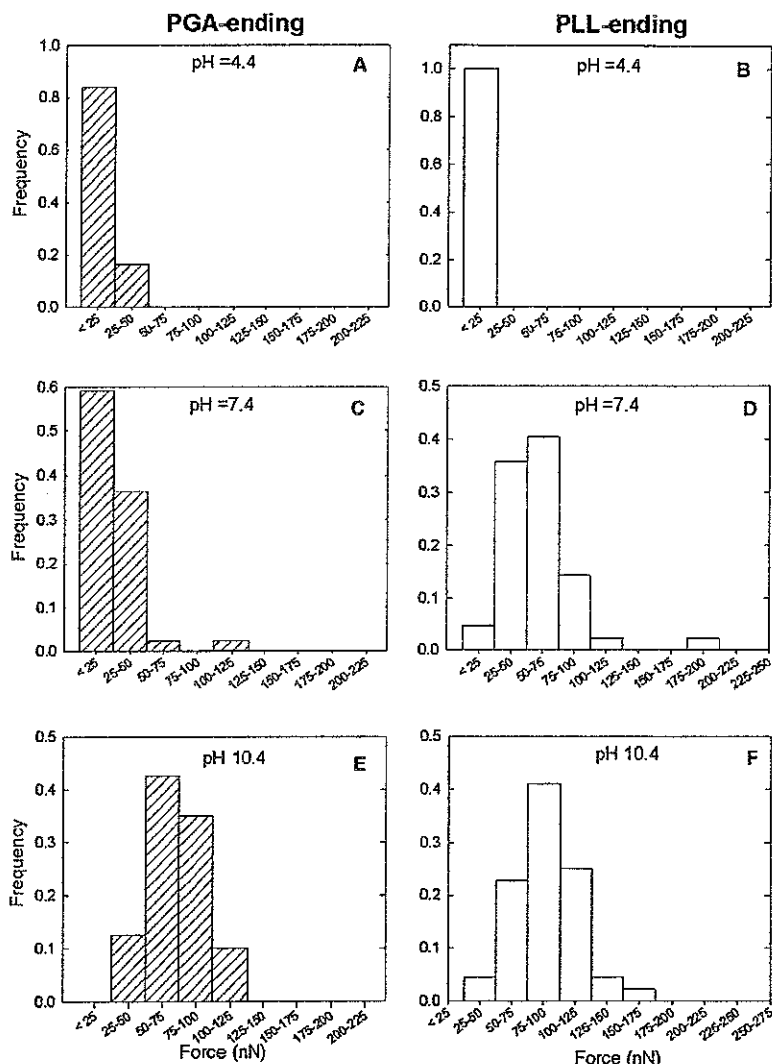


Fig. 7. Histograms of cell detachment forces on PEI-(PGA/PLL)<sub>10</sub>-PGA films or PEI-(PGA/PLL)<sub>10</sub> built in water at pH = 4.4 (A,B) 7.4 (C,D) or at pH = 10.4 (E,F). The histograms for PGA-ending films (hatched bars) are shown on the right hand side and those corresponding to PLL-ending films (white bars) are shown on the left hand side (44 cells for each type of condition).

699 7.4 [41]). Thus, protein adsorption does not seem  
700 to be related to cell adhesion properties, as was  
701 previously suspected [33]. The surface roughness  
702 of the film was estimated by means of AFM (Table  
703 2). The mean roughness is lower for the film built

at pH 10.4 ( $14 \pm 1$  nm) than for that built at pH 4.4 ( $32.5 \pm 8$  nm). Therefore, the higher cell adhesion on the films built at pH = 10.4 cannot be explained by the slightly increased roughness of the surfaces used here. Finally, the secondary structure

704

705

706

707

708

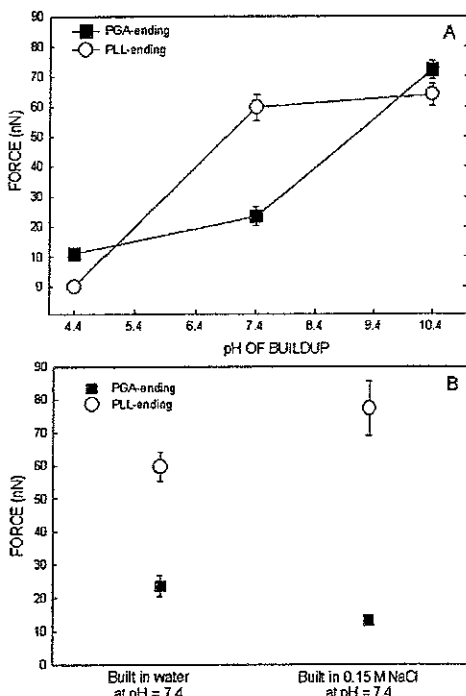


Fig. 8. Average detachment force of chondrosarcoma cells seeded in the presence of serum on PEI-(PGA/PLL)<sub>10</sub> films (A) as a function of the pH of buildup of the film for positively PLL-(○) and negatively PGA-(■) ending films. Films were built in water whose pH was adjusted by means of NaOH or HCl (same cell numbers as in Fig. 7). The lines have been drawn to guide the eyes. (B) for films either built in pure water or in a salt containing solution (0.15 M NaCl) both at pH = 7.4 for positively PLL-(○) and negatively PGA-(■) ending films. Error bars are SEM.

of the films was investigated by means of FTIR. The films built at pH 7.4 and 10.4 exhibit similar structures, both having a high  $\beta$ -sheet content ( $\approx 50\%$ ) and an  $\alpha$ -helix content of about 12% whereas the films built at pH 4.4 have a low  $\beta$ -sheet content ( $\approx 10\%$ ) but a higher percentage of  $\alpha$ -helix (25%).

All these results suggest that neither protein adsorption, nor surface roughness or secondary structure explain the strong differences observed in the cell adhesion properties of the films. A higher water content of films built at pH 4.4 when put

in a physiological medium as compared to those built at pH 10.4 could constitute one possible origin of the “cytophobic” or “cytophilic” character of the films at pH 4.4 and 10.4 respectively.

## 5. Conclusions

The short-term interaction of chondrosarcoma cells with (PGA/PLL) polyelectrolyte multilayers was investigated in a serum-containing medium for films built at different pHs and subsequently exposed to the culture medium. The buildup of the films and their stability was first investigated. Whereas film growth is linear at all pHs after a few layers have been deposited, the growth is much larger for the films built at basic pH and even more for those built at acidic pH. However, these latter films remain stable in the culture medium only if they have been crosslinked prior to ionic strength and pH jumps. The films built at acidic pH were found to swell in water much more than the other films. The detachment forces were significantly higher on PLL-ending films than on PGA-ending ones for thin films ( $\approx 20$  nm) built at pH 7.4 but were independent of the outermost layer of the film for the thick films built at pH = 4.4 and at pH = 10.4 (thickness of the order of few hundred of nanometers). Films built at pH = 10.4 were highly cell adhesive whereas those built at acidic pH were highly cell resistant. The high adhesion on the films built at pH 10.4 may be related to their secondary structure and to their relatively low swellability in water whereas the cell resistance of the films built at pH 4.4 may be linked to their high swellability. Therefore, depending on the deposition pH, the cell adhesion properties of the PGA/PLL films can be tuned. This study reveals the importance of the multilayer structure and architecture to control the detachment force of cells onto such films.

## Acknowledgements

The authors wish to thank Fouzia Boulmedais for her assistance in the FTIR experiments. We also thank Prof. M. Rubner and Dr. S.Y. Yang

763 from the MIT (Boston) for fruitful discussions.  
 764 C.P. is indebted to the “Université Louis Pasteur”  
 765 for financial support to setup the micropipette  
 766 technique. This work was supported by the pro-  
 767 gram “ACI Technologies pour la Santé” from  
 768 the French Ministry of Research.

## 769 References

- 770 [1] K.E. Healy, *Curr. Opin. Solid State Mater. Sci.* 4 (1999)  
 771 381.
- 772 [2] A.K. Dillon, M. Tirrell, *Curr. Opin. Solid State Mater.*  
 773 *Sci.* 3 (1998) 252.
- 774 [3] N. Angelova, D. Hunkeler, *Trends Biotechnol.* 17 (1999)  
 775 409.
- 776 [4] F. Grinnell, M.K. Feld, *J. Biol. Chem.* 257 (1982) 4888.
- 777 [5] B.A. Pethica, *Exp. Cell. Res.* 8 (Suppl.) (1961) 123.
- 778 [6] A.S. Curtis, *Biol. Rev. Camb. Philos. Soc.* 37 (1962) 82.
- 779 [7] Q. Qiu, M. Sayer, M. Kawaja, X. Shen, J.E. Davies, *J.*  
 780 *Biomed. Mater. Res.* 42 (1998) 117.
- 781 [8] Y.F. Dufrêne, T.G. Marchal, P.G. Rouxhet, *Langmuir* 15  
 782 (1999) 2871.
- 783 [9] D.R. Absalom, W. Zingg, A.W. Neumann, *J. Biomed.*  
 784 *Mater. Res.* 21 (1987) 161.
- 785 [10] R. Kapur, A.S. Rudolph, *Exp. Cell. Res.* 244 (1998) 275.
- 786 [11] A.S. Curtis, M. Varde, *J. Natl. Cancer Inst.* 33 (1964) 15.
- 787 [12] J.M. Harris, *Poly(ethylene glycol) Chemistry: Biotechnical*  
 788 *and Biomedical Applications*, Plenum, New York, 1992  
 789 127 pp.
- 790 [13] C.S. Kwock, P.D. Mourad, L.A. Crum, B.D. Ratner,  
 791 *Biomacromolecules* 1 (2000) 139.
- 792 [14] U. Hersel, C. Dahmen, H. Kessler, *Biomaterials* 24 (2003)  
 793 4385.
- 794 [15] G. Decher, J.D. Hong, J. Schmitt, *Thin Solid Films* 1992  
 795 (1992) 831.
- 796 [16] G. Decher, *Science* 277 (1997) 1232.
- 797 [17] C. Picart, G. Ladam, B. Senger, J.-C. Voegel, P. Schaaf,  
 798 F.J.G. Cuisinier, C. Gergely, *J. Chem. Phys.* 115 (2001)  
 799 1086.
- 800 [18] C. Picart, P. Lavalle, P. Hubert, F.G. Cuisinier, G. Decher,  
 801 P. Schaaf, J.-C. Voegel, *Langmuir* 17 (2001) 7414.
- 802 [19] R.A. McAloney, M. Sinyor, V. Dudnik, M.C. Goh,  
 803 *Langmuir* 17 (2001) 6655.
- 804 [20] D. Yoo, S.S. Shiratori, M.F. Rubner, *Macromolecules* 31  
 805 (1998) 4309.
- 806 [21] S.S. Shiratori, M.F. Rubner, *Macromolecules* 33 (2000)  
 807 4213.
- 808 [22] S.L. Clark, P.T. Hammond, *Langmuir* 16 (2000) 10206.
- 809 [23] D.L. Elbert, C.B. Herbert, J.A. Hubbell, *Langmuir* 15  
 810 (1999) 5355.
- 811 [24] T. Serizawa, M. Yamaguchi, M. Akashi, *Biomacromolecules* 3 (2002) 724.
- 812 [25] D.B. Shenoy, A. Antipov, G.B. Sukhorukov, H. Möhwald,  
 813 *Biomacromolecules* 4 (2003) 265.
- [26] Q. Tan, J. Ji, M.A. Barbosa, C. Fonseca, J. Shen, *Biomaterials* 24 (2003) 4699.  
 815  
 [27] H. Ai, Y. Lvov, D. Mills, M. Jennings, J. Alexander, S. Jones, *Cell Biochem. Biophys.* 38 (2003) 103.  
 817  
 [28] B. Thierry, F.M. Winnik, Y. Merhi, J. Silver, M. Tabrizian, *Biomacromolecules* 4 (2003) 1564.  
 819  
 [29] Y. Zhu, C. Gao, T. He, X. Liu, J. Shen, *Biomacromolecules* 4 (2003) 446.  
 821  
 [30] D. Vautier, J. Hemmerlé, C. Vodouhe, G. Koenig, L. Richert, C. Picart, J.-C. Voegel, C. Debry, J. Chluba, J. Ogier, *Cell Motility Cytoskeleton* 56 (2003) 147.  
 823  
 [31] A.A. Mamedov, N.A. Kotov, M. Prato, D.M. Galdi, J.P. Wicksted, A. Hirsch, *Nat. Mater.* 1 (2002) 190.  
 825  
 [32] S.Y. Yang, J.D. Mendelsohn, M.F. Rubner, *Biomacromolecules* 4 (2003) 987.  
 828  
 [33] J.D. Mendelsohn, S.Y. Yang, J. Hiller, A.I. Hochbaum, M.F. Rubner, *Biomacromolecules* 4 (2003) 96.  
 829  
 [34] F. Boulmedais, B. Frisch, O. Etienne, P. Lavalle, C. Picart, J. Ogier, J.-C. Voegel, P. Schaaf, C. Egles, *Biomaterials*, ASAP (2004).  
 831  
 [35] L. Richert, P. Lavalle, E. Payan, J.-F. Stoltz, X.Z. Shu, G.D. Prestwich, P. Schaaf, J.-C. Voegel, C. Picart, Langmuir, ASAP (2003).  
 833  
 [36] J. Chluba, J.C. Voegel, G. Decher, P. Erbacher, P. Schaaf, J. Ogier, *Biomacromolecules* 2 (2001) 800.  
 835  
 [37] N. Jessel, F. Atalar, P. Lavalle, J. Mutterer, G. Decher, P. Schaaf, J.C. Voegel, G. Ogier, *Adv. Mater.* 15 (2003) 692.  
 837  
 [38] S.E. Burke, C.J. Barrett, *Biomacromolecules* 4 (2003) 1773.  
 838  
 [39] F. Boulmedais, M. Bozonnet, P. Schwinté, J.-C. Voegel, P. Schaaf, *Langmuir* 19 (2003) 9873.  
 840  
 [40] D. Vautier, V. Karsten, C. Egles, J. Chluba, P. Schaaf, J.C. Voegel, J. Ogier, *J. Biomater. Sci. Polym. Ed.* 13 (2002) 713.  
 841  
 [41] L. Richert, P. Lavalle, D. Vautier, B. Senger, J.-F. Stoltz, P. Schaaf, J.-C. Voegel, C. Picart, *Biomacromolecules* 3 (2002) 1170.  
 843  
 [42] L. Richert, F. Boulmedais, L. Ph, J. Mutterer, E. Ferreux, G. Decher, P. Schaaf, J.-C. Voegel, C. Picart, *Biomacromolecules*, in press.  
 844  
 [43] D.S. Koktysh, X. Liang, B.G. Yun, I. Pastoriza-Santos, R.L. Matts, M. Giersig, C. Serra-Rodriguez, L.M. Liz-Marzán, N.A. Kotov, *Adv. Funct. Mater.* 12 (2002) 255.  
 845  
 [44] C. Boura, P. Menu, E. Payan, C. Picart, J.-C. Voegel, S. Müller, J.-F. Stoltz, *Biomaterials* 24 (2003) 3521.  
 846  
 [45] H. Ai, H. Meng, I. Ichinose, S.A. Jones, D.K. Mills, Y.M. Lvov, X. Qiao, *J. Neurosci. Meth.* 128 (2003) 1.  
 847  
 [46] P. Tryoen-Toth, D. Vautier, Y. Haikel, J.-C. Voegel, P. Schaaf, J. Chluba, J. Ogier, *J. Biomed. Mater. Res.* 60 (2002) 657.  
 848  
 [47] P. Lavalle, C. Gergely, F. Cuisinier, G. Decher, P. Schaaf, J.-C. Voegel, C. Picart, *Macromolecules* 35 (2002) 4458.  
 849  
 [48] L. Lapčík, L. Lapčík, S. De Smedt, J. Demeester, P. Chabrecek, *Chem. Rev.* 98 (1998) 2663.  
 850  
 [49] C.M. Lo, H.B. Wang, M. Dembo, Y.L. Wang, *Biophys. J.* 79 (2000) 144.  
 851
- [50] L. Richert, P. Lavalle, D. Vautier, B. Senger, J.-F. Stoltz, P. Schaaf, J.-C. Voegel, C. Picart, *Biomacromolecules* 3 (2002) 1170.  
 852  
 [51] L. Richert, F. Boulmedais, L. Ph, J. Mutterer, E. Ferreux, G. Decher, P. Schaaf, J.-C. Voegel, C. Picart, *Biomacromolecules*, in press.  
 853  
 [52] D.S. Koktysh, X. Liang, B.G. Yun, I. Pastoriza-Santos, R.L. Matts, M. Giersig, C. Serra-Rodriguez, L.M. Liz-Marzán, N.A. Kotov, *Adv. Funct. Mater.* 12 (2002) 255.  
 854  
 [53] C. Boura, P. Menu, E. Payan, C. Picart, J.-C. Voegel, S. Müller, J.-F. Stoltz, *Biomaterials* 24 (2003) 3521.  
 855  
 [54] H. Ai, H. Meng, I. Ichinose, S.A. Jones, D.K. Mills, Y.M. Lvov, X. Qiao, *J. Neurosci. Meth.* 128 (2003) 1.  
 856  
 [55] P. Tryoen-Toth, D. Vautier, Y. Haikel, J.-C. Voegel, P. Schaaf, J. Chluba, J. Ogier, *J. Biomed. Mater. Res.* 60 (2002) 657.  
 857  
 [56] P. Lavalle, C. Gergely, F. Cuisinier, G. Decher, P. Schaaf, J.-C. Voegel, C. Picart, *Macromolecules* 35 (2002) 4458.  
 858  
 [57] L. Lapčík, L. Lapčík, S. De Smedt, J. Demeester, P. Chabrecek, *Chem. Rev.* 98 (1998) 2663.  
 859  
 [58] C.M. Lo, H.B. Wang, M. Dembo, Y.L. Wang, *Biophys. J.* 79 (2000) 144.  
 860

SUSC 15066

No. of Pages 17, DTD 5.0.1

9 July 2004 Disk used

L. Richert et al. / Surface Science xxx (2004) xxxx-xxx

17

- 871 [50] H. Ai, S.A. Jones, Y.M. Lvov, Cell Biochem. Biophys. 39  
872 (2003) 23.  
873 [51] V.A. Sinani, D.S. Koktysh, B.-G. Yun, R.L. Matts, T.C.  
874 Pappas, M. Motamedi, S.N. Thomas, N.A. Kotov, Nano  
875 Lett. 3 (2003) 1177.  
876 [52] J.A. De Feijter, J. Benjamins, F.A. Veer, Biopolymers 17  
877 (1978) 1759.  
878 [53] G. Ladam, P. Schaad, J.-C. Voegel, P. Schaaf, G. Decher,  
879 F.G. Cuisinier, Langmuir 16 (2000) 1249.  
[54] H.J. Ra, C. Picart, H. Feng, H.L. Sweeney, D.E. Discher, 880  
J. Cell. Sci 112 (1999) 1425. 881  
[55] E.A. Evans, Method. Enzymol. 173 (1989) 3. 882  
[56] G.D. Fasman, Handbook of Biochemistry and Molecular 883  
Biology, CRC Press, Boca Raton, FL, 1976. 884  
[57] B. Amsden, N. Turner, Biotechnol. Bioeng. 65 (1999) 605. 885  
[58] C. Picart, R. Elkaim, L. Richert, F. Audoin, M. Da Silva 886  
Cardoso, P. Schaaf, J.-C. Voegel, B. Frisch, in preparation. 887  
[59] R.G. Richards, I. ap Gwynn, K.J. Bundy, B.A. Rahn, 888  
Cell. Biol. Int. 19 (1995) 1015. 889  
889  
889

# **Chapitre 4 : Réticulation des films multicouches de (poly(L-lysine)/ Hyaluronane) : conséquences sur les propriétés physico-chimiques, mécaniques et d'adhérence des films.**

Le second volet de ce travail concerne les films à base de poly(L-Lysine) et de hyaluronane. Ces films, qui ne diffèrent des films (PLL/PGA) que par le type de polyanion, sont pourtant très différents dans leur structure et dans leurs propriétés biologiques. En effet, leur épaisseur croît également de façon exponentielle avec le nombre de couches déposées et atteint rapidement 1 µm après l'adsorption de 8 à 10 paires de couches mais ils présentent un degré d'hydratation plus élevé (indice de réfraction mesuré par spectroscopie optique inférieur à 1.38). De plus, ces films sont résistants à l'adhésion de cellules de chondrosarcomes et de chondrocytes, et ce quelque-soit la couche terminale. Le hyaluronane fait pourtant partie de la famille des glucosaminoglycans (GAGs) et se retrouve notamment dans la matrice extracellulaire ainsi que dans le liquide synovial, où il joue un grand rôle, particulièrement dans l'hydratation des tissus ainsi que dans les interactions cellules/matrice extracellulaire puisqu'il se lie aux récepteurs CD44 et RHAMM et à divers composants de la matrice extracellulaire.

Deux hypothèses peuvent être formulées pour expliquer la non-adhérence des cellules : la première repose sur leur forte hydratation et capacité de gonflement, ainsi que Rubner et al. (Mendelsohn et al., 2003) l'ont suggéré pour les films (PAA/PAH), indiquant que les propriétés d'adhésion cellulaire dépendent du taux de gonflement du film. La deuxième repose sur la rigidité du film : les films mous ne permettraient pas un ancrage stable des cellules. Cette hypothèse a déjà été démontrée pour les gels de polyacrylamides pour différents types cellulaires, les cellules préférant les gels durs aux gels mous (Engler et al., 2004a; Lo et al., 2000; Pelham and Wang, 1998).

Afin de modifier la rigidité des films (PLL/HA), nous avons procédé à leur réticulation par un agent de couplage de type carbodiimide (EDC) en présence d'un agent catalyseur

(sNHS). Dans un premier temps (chapitre 4-1), nous avons examiné les changements physico-chimiques induits au sein du film par la réticulation. En particulier, nous avons mis en évidence la formation de liaisons amides associée à la diminution des groupements carboxyliques libres. Les films réticulés sont également stables dans l'eau et dans l'éthanol. De plus, contrairement aux films non réticulés, ils résistent à la dégradation enzymatique par la hyaluronidase. Dans un deuxième temps, nous avons évalué les propriétés d'adhésion des films natifs et réticulés vis-à-vis des cellules de chondrosarcomes.

Nous avons ensuite cherché à caractériser les propriétés mécaniques (chapitre 4-2) des films par des tests de nano-indentation par AFM. Ces propriétés ont été corrélées à l'adhésion cellulaire sur les films (PLL/HA). Enfin, nous avons évalué l'adhésion de cellules de chondrocytes primaires sur les films multicouches (PLL/HA) natifs et réticulés (chapitre 4-3).

## 4.1 : Modification des propriétés physico-chimiques des films multicouches par réticulation.

### 4.1.1. Résumé 3

Dans le chapitre 1, nous avons décrit les différentes techniques de réticulation possibles applicables aux films multicouches de polyélectrolytes. Le PLL et le HA portant respectivement des fonctions amine et carboxyle réactives, il est théoriquement possible de former au sein du film (PLL/HA) des liaisons amides. Cette réaction peut être induite par un agent de couplage de type carbodiimide, comme l'EDC déjà utilisée pour des complexes de (PLL/HA) en solution (Hermanson, 1996). Cette réaction est d'ailleurs souvent utilisée pour le couplage de protéines. Il est également possible d'utiliser un agent catalyseur, le sulfo-NHS. Nous avons pu montrer pour les films multicouches de polyélectrolytes à base de PLL et HA que l'utilisation d'EDC avec le N-hydroxysulfo succinimide (sulfo-NHS) permet la formation contrôlée de liaison covalentes entre les groupements amines de la poly(L-Lysine) et les groupements carboxyles du hyaluronane. Cette réaction a été suivie à l'aide de la spectroscopie infrarouge à transformée de Fourrier (FTIR). Nous avons ainsi observé la diminution des pics correspondants aux groupements carboxyle du hyaluronane et la formation de pics amides témoignant de la réticulation.

Cette réticulation modifie fortement de nombreuses caractéristiques des films (PLL/HA). Ainsi, la microbalance à quartz indiqué une forte augmentation de la dissipation visqueuse après la réticulation, suggérant ainsi une augmentation de la rigidité du film. Par ailleurs, les films (PLL/HA) sont, après réticulation, plus résistants à la dégradation enzymatique (hyaluronidase) ainsi qu'à la déshydratation à l'éthanol alors que ces mêmes produits détruisent les films non réticulés. Les mesures de recouvrement de fluorescence après photo-blanchiment (FRAP), réalisées par microscopie confocale, ont également montré une diffusion de la PLL au sein des films natifs, alors qu'elle ne diffuse plus au sein des films réticulés. Sur le plan biologique, les films de (PLL/HA) à l'état natif sont résistants à l'adhésion cellulaire, alors qu'après réticulation, ils favorisent l'adhésion et à la prolifération de cellules de chondrosarcomes.

#### 4.1.2. Article 3

### Improvement of Stability and Cell Adhesion Properties of Polyelectrolyte Multilayer Films by Chemical Cross-Linking

Ludovic Richert,<sup>†</sup> Fouzia Boulmedais,<sup>†</sup> Philippe Lavalle,<sup>†</sup> Jérôme Mutterer,<sup>‡</sup> Emmanuelle Ferreux,<sup>†</sup> Gero Decher,<sup>§</sup> Pierre Schaaf,<sup>§,||</sup> Jean-Claude Voegel,<sup>†</sup> and Catherine Picart<sup>\*,†,||</sup>

*Institut National de la Santé et de la Recherche Médicale, Unité 595, Faculté de Chirurgie Dentaire, Université Louis Pasteur, 11 rue Humann, 67085 Strasbourg Cedex, France, Ecole Européenne de Chimie, Polymères et Matériaux de Strasbourg, 25 rue Becquerel, 67087 Strasbourg Cedex 2, France, Institut de Biologie Moléculaire des Plantes, 12 rue du Général Zimmer, 67084 Strasbourg Cedex, France, and Institut Charles Sadron, Centre National de la Recherche Scientifique, Université Louis Pasteur, 6 rue Boussingault, 67083 Strasbourg Cedex, France*

Received July 8, 2003; Revised Manuscript Received October 8, 2003

Poly(L-lysine)/hyaluronan (PLL/HA) films were chemically cross-linked with a water soluble carbodiimide (EDC) in combination with a *N*-hydroxysulfo-succinimide (NHS) to induce amide formation. Fourier transform infrared spectroscopy confirms the conversion of carboxylate and ammonium groups into amide bonds. Quartz crystal microbalance-dissipation reveals that the cross linking reaction is accompanied by a change in the viscoelastic properties of the films leading to more rigid films. After the cross-linking reaction, both positively and negatively ending films exhibit a negative zeta potential. It is shown by fluorescence recovery after photobleaching measured by confocal laser scanning microscopy that cross-linking dramatically reduces the diffusion of the PLL chains in the network. Cross linking also renders the films highly resistant to hyaluronidase, an enzyme that naturally degrades hyaluronan. Finally, the adhesion of chondrosarcoma cells on the films terminating either with PLL or HA is also investigated. Whereas the non cross-linked films are highly resistant to cell adhesion, the cells adhere and spread well on the cross-linked films.

#### Introduction

Surface modifications of materials is of primary importance for biomedical applications.<sup>1–3</sup> Among the different techniques used to modify surfaces, the deposition of polyelectrolyte multilayers (PEM) has emerged as a very easy handling and versatile tool.<sup>4–7</sup> Based on the alternate adsorption of polycations and polyanions, this technique allows films to be built-up with tunable properties: by adjusting several parameters such as the chemical nature of the polyelectrolytes, pH and ionic strength, immersion and rinsing times, post-treatment of the film, it is possible to obtain an almost infinite variety of architectures.<sup>8–10</sup> Of special importance for biomedical applications is the control of the chemical composition of the surface which can affect biological activity. Films made from polypeptides, i.e., poly(L-lysine), natural polyelectrolytes, or biopolymers (e.g., hyaluronan, alginate, chitosan, and collagen), allow, for example, biomimetic architectures to be created.<sup>11–14</sup> Ap-

plications include also the fabrication of nonadhesive barriers for vascular grafts,<sup>11</sup> the fabrication of films with pro- or anti-coagulant properties,<sup>12</sup> or the preparation of hollow capsules for drug release.<sup>13</sup> Bioactivity of the films can be achieved by their functionalization by inserting peptides coupled to polyelectrolytes<sup>15</sup> or through the embedding of proteins.<sup>16</sup> For biomaterial applications, biocompatibility is a major requirement: the material must be nontoxic to any living cell. Another requirement is that the material possesses chemical and physical properties that promote specific cell substrate interactions, either cell adhesion or nonadhesion depending on the final application. Along this line, it was shown that primary cells can be grown on poly(styrene-sulfonate)/poly(allylamine hydrochloride) films<sup>17</sup> and on poly(L-lysine)/poly(L-glutamic acid) films for several days while maintaining their phenotype.<sup>18</sup> Recently, Mendelsohn et al.<sup>19</sup> showed that poly(acrylic acid)/poly(allylamine hydrochloride) multilayers can be either nonadhesive or adhesive depending on the pH of preparation of the films. These authors suggested that the nonadhesive character of the films with respect to cells is related to their high swelling capacities and is independent of their adhesive or nonadhesive character with respect to proteins from serum.

For various applications, the preservation of the structural integrity of the film is crucial.<sup>20</sup> Polyelectrolyte multilayers based on biopolymers or polypeptides are hydrogels and must be considered as “soft” and sensitive materials. For example,

\* To whom correspondence should be addressed. Address: INSERM U595, Faculté de Médecine, Bât 3, 11 rue Humann, 67 085 Strasbourg cedex, France. Phone: 33-3-90-24-32-58. Fax: 33-3-90-24-33-79. E-mail: Catherine.Picart@medecine.u-strasbg.fr.

<sup>†</sup> Institut National de la Santé et de la Recherche Médicale, Université Louis Pasteur.

<sup>‡</sup> Institut de Biologie Moléculaire des Plantes.

<sup>§</sup> Institut Charles Sadron, Université Louis Pasteur.

<sup>||</sup> Ecole Européenne de Chimie, Polymères et Matériaux de Strasbourg.

exposure to solvents, pH, and ionic strength jumps can affect their structural integrity,<sup>9,21</sup> and cross-linking constitutes a possible way to stabilize them. Until now, only few cross-linkable PEM systems have been reported. The approaches generally rely on the cross-linking through condensation reaction of complementary groups located on adjacent layer. The different strategies make use of bifunctional aldehydes such as glutaraldehyde,<sup>22,23</sup> incorporation of diazoesters that are subsequently exposed to UV light,<sup>24</sup> and more recently, cross-linking of hybrid clay/polyelectrolyte layers using a photocross-linkable polyelectrolyte<sup>25</sup> and of proteins multilayers<sup>26</sup> by carbodiimide chemistry. Heating the films at high temperature (130 °C) for several hours was also explored.<sup>27–29</sup> Depending on the types of polyelectrolytes used, heating could produce amide<sup>27</sup> or imide bonds.<sup>29</sup> Cross-linking not only enhances the stability of the films but it allows also to change their permeability, conductivity,<sup>28,30</sup> and eventually also their viscoelastic properties. All of these cross-linking methods also present however drawbacks. Introducing linker molecules such as glutaraldehyde may, for example, not only modify the film structure in a noncontrolled manner but also may change its biocompatibility. On the other hand, heating is not always possible depending upon the nature of the substrate.

As an alternative method, we investigate in this article the cross-linking of poly(L-lysine)/hyaluronan multilayers with a water soluble carbodiimide, 1-ethyl-3-(3-dimethylaminopropyl) carbodiimide (EDC), which is commonly used for the covalent attachment of proteins on surfaces.<sup>31</sup> EDC catalyzes the formation of amide bonds between carboxylic groups of HA and amine groups of PLL. The cross linking reaction will be favored by the presence of *N*-hydroxysulfo succinimide (NHS).<sup>32</sup> EDC alone has already been used for the cross-linking of hyaluronan solutions<sup>33</sup> and hyaluronan/collagen sponges.<sup>34</sup> In contrast to conventional agents, such as glutaraldehyde or polyepoxides, carbodiimides do not remain as a part of that linkages but simply change to water soluble urea derivatives that have very low cytotoxicity.<sup>33,35</sup> The cross-linking reaction will be followed by Fourier transformed infrared spectroscopy (FTIR). The quartz crystal microbalance-dissipation (QCM-D) technique will furnish information on the evolution of the viscoelastic properties of the film. The film will also be characterized by zeta potential measurements and confocal laser scanning microscopy (CLSM). Finally, cellular adhesion properties onto the native and on cross-linked (PLL/HA)<sub>n</sub> films will be investigated. These later experiments are motivated by previous results obtained on thick polyacrylamide gels whose elasticity was changed by adjusting the percentage of bis-acrylamide.<sup>36,37</sup> These authors found evidence that cell adhesion strongly depended on the substrate viscoelastic properties and was increased as substrate compliance was decreased.

## Materials and Methods

**Polyelectrolyte Solutions.** The preparation of solutions of poly(L-lysine) (PLL, 30 kDa, Sigma, France), hyaluronan (HA, 400 kDa, Bioiberica, Spain), and the buildup of (PLL/

HA)<sub>n</sub> films was previously described.<sup>14</sup> PLL and HA were dissolved at 1 mg/mL in 0.15 M NaCl at pH 6–6.5. During the film construction, all the rinsing steps were performed with an aqueous solution containing 0.15 M NaCl at pH 6–6.5. Fluorescein isothiocyanate labeled PLL (PLL-FITC), 1-ethyl-3-(3-dimethylaminopropyl) carbodiimide (EDC), *N*-hydroxysulfo-succinimide (sulfo-NHS), and hyaluronidase (Type I) were purchased from Sigma-Aldrich and used without any purification.

**Chemical Cross-Linking of the Films by EDC/NHS.** Cross-linking was performed on films deposited either on the ZnSe coated crystal (for FTIR experiments), on the SiO<sub>2</sub> crystal (for quartz crystal microbalance experiments), or on the 12 mm glass slides introduced in 24 wells culture plates. EDC solution alone (200 mM) or a EDC/sulfo-NHS mixture (EDC at 400 mM and NHS at 100 mM were mixed v/v) were freshly prepared in a 0.15 M NaCl solution at pH 5.5. The coupling chemistry is based on the reaction of activated carboxylic sites with primary amine groups.<sup>38</sup> The film coated substrate was put in contact with the mixed EDC/NHS solution for 12 h (for clarity, the simplified notation EDC/NHS will be used instead of the complete writing EDC/sulfo-NHS). Rinsing was performed three times with a 0.15 M NaCl solution for 1 h. For the FTIR experiments, a similar protocol was used except that the EDC and NHS were dissolved in a deuterated 0.15 M NaCl solution.

**Fourier Transform Infrared Spectroscopy in Attenuated Total Reflection.** The crosslinking of (PLL/HA)<sub>n</sub> films deposited on a ZnSe crystal was investigated by *in situ* Fourier transform infrared (FTIR) spectroscopy in attenuated total reflection (ATR) mode with an Equinox 55 spectrophotometer (Bruker, Wissembourg, France). All the experimental details have been given previously.<sup>39</sup> The experiments were performed in a deuterated 0.15 M NaCl solution at pH ≈ 6. D<sub>2</sub>O is used as the solvent instead of water because the amide I bands of both PLL and HA are affected by the strong water band absorption around 1643 cm<sup>-1</sup> (O–H bending), whereas the corresponding vibration in D<sub>2</sub>O is found around 1209 cm<sup>-1</sup>. During the buildup, the film was continuously in contact with the 0.15M NaCl solution and was never dried. After each polyelectrolyte deposition, rinsing step, and the final contact with the EDC/NHS solution, single-channel spectra from 512 interferograms were recorded between 400 and 4000 cm<sup>-1</sup> with a 2 cm<sup>-1</sup> resolution, using Blackman-Harris three-term apodization and the standard Bruker OPUS/IR software (version 3.0.4). Analysis of the raw spectrum was performed at the end of the film buildup by taking the (PLL/HA)<sub>n</sub> film spectrum and subtracting the contribution of the ZnSe crystal. During the contact of the (PLL/HA)<sub>n</sub> film with the EDC/NHS solution, single-channel spectra from 512 interferograms were recorded every 20 min. To follow the kinetics of the cross-linking reaction, difference spectra were calculated for a given time period by considering the actual raw spectra and subtracting to its value the contribution of the (PLL/HA)<sub>n</sub> film (before contact with the EDC/NHS solution).

**Quartz Crystal Microbalance.** The (PLL/HA)<sub>n</sub> film buildup and the cross-linking process were followed *in situ* optical waveguide lightmode spectroscopy<sup>40,41</sup> and by quartz

crystal microbalance-dissipation (QCM-D, Q-sense AB, Göteborg, Sweden).<sup>42,43</sup> These techniques have already been described and used for the characterization of (PLL/HA)<sub>n</sub> films.<sup>14,44</sup> The quartz crystal is excited at its fundamental frequency (about 5 MHz) as well as at the third, fifth, and seventh overtones (denoted by  $\nu = 3$ ,  $\nu = 5$ ,  $\nu = 7$  and corresponding respectively to 15, 25, and 35 MHz). Changes in the resonance frequencies  $\Delta\nu$  and in the relaxation of the vibration once the excitation is stopped are measured at the four frequencies. The relaxation gives access to the dissipation  $D$  of the vibrational energy stored in the resonator. A decrease in  $\Delta\nu/\nu$  is usually associated, in a first approximation, to an increase of the mass coupled to the quartz and a decrease of  $D$  at constant mass is usually associated to a stiffer (less elastic) film. Both  $\Delta\nu/\nu$  and  $D$  at the four resonance frequencies give thus information on the viscoelastic properties of the film. After the buildup of a (PLL/HA)<sub>n</sub> film or a (PLL/HA)<sub>n</sub>-PLL film, 2 mL of the EDC/NHS solution were injected in the measuring cell, left at rest for 12 h and then rinsed. The QCM and OWLS signals were followed during the whole period.

**Zeta Potential Measurements.** Measurements of the zeta potential of the layers adsorbed on a capillary were carried out on a homemade streaming potential measurement apparatus developed by Zembala and Déjardin.<sup>45</sup> The apparatus has been previously described.<sup>14,46</sup> By measuring the pressure and the potential differences on both sides of a 530  $\mu\text{m}$  radius capillary made of fused silica via two flasks containing four electrodes, one gets access, through the Smoluchowski relation, to the zeta potential of the capillary. Details about the procedure are given in Picart et al.<sup>14</sup> Polyelectrolytes were adsorbed in the 0.15 M NaCl solution, and measurements were performed after the rinsing of each layer at a ionic strength of  $5 \times 10^{-4}$  M ( $\text{pH} = 6$ ). For cross-linking, 8 mL of the EDC/NHS in 0.15 M NaCl were injected in the capillary, left at rest for 12 h and rinsed before measurement.

**Automatic Buildup of the Polyelectrolyte Multilayered Films for CLSM and Cell Culture Experiments.** For CLSM and cell culture experiments, the multilayers were prepared with a dipping machine (Dipping Robot DR3, Kierstein GmbH, Germany) on 12 mm glass slides (VWR Scientific, France) preliminarily cleaned with 10 mM SDS and 0.1 N HCl and extensively rinsed. The glass slides were introduced vertically in a homemade holder which was dipped into a polyelectrolyte solution for 10 min and was subsequently rinsed in three different beakers containing the 0.15 M NaCl solution. The slides were dipped four times (15 s each) in the first beaker and once for five minutes in the two other beakers. The slides were then dipped into the oppositely charged polyelectrolyte solution followed by the same rinsing procedure. Rinsing beakers were changed every three layers. Slides were then stored at 4 °C until use in 24 wells culture plates.

**Confocal Laser Scanning Microscopy (CLSM).** PLL-FITC was used to image the dye labeled film in the green channel. The configuration of the microscope and the parameters used for the CLSM observations on a Zeiss LSM510 microscope have been given elsewhere.<sup>44</sup> The 12 mm glass slides were introduced in a homemade chamber

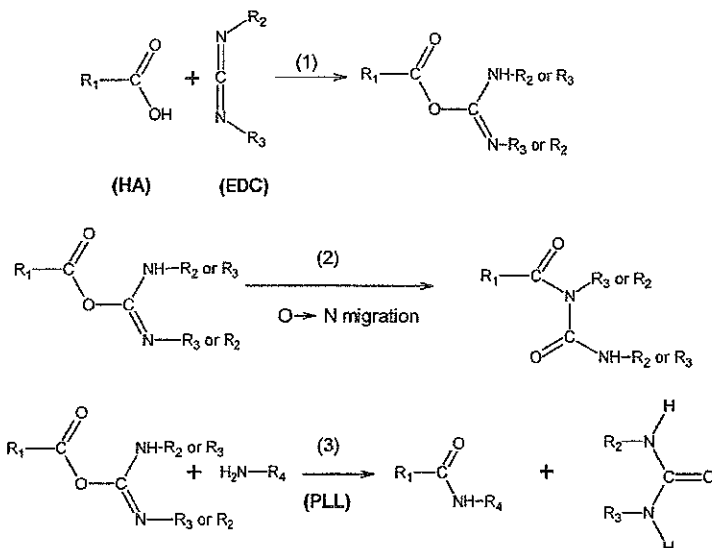
and observed by imaging series of consecutive overlapping optical sections. The thickness of the film was determined by the measurement of the green band (corresponding to the PLL-FITC) in computed orthogonal vertical sections through the imaged volumes. For the fluorescence recovery after photobleaching experiments (FRAP), a circular zone was bleached in the center of the image by iterative illumination at 488 nm. Images were taken before, right after, and 30 min after the bleach process.

**Cell Culture.** HCS-2/8 human chondrosarcoma cells derived from chondrocyte-like cell line<sup>47</sup> were routinely grown in Gibco BRL's minimum essential medium with Eagle's salts (MEM, Life Technologies), 10% fetal calf serum (FCS, Life Technologies), 50 U/mL penicillin, and 50 U/mL streptomycin (Bio-Whittaker) in a 5% CO<sub>2</sub> and 95% air atmosphere at 37 °C. A flask of cells was brought into suspension after incubating for 2.5 min in 0.5% trypsin (Bio-Whittaker). Following trypsinization, cells were washed twice by centrifugation to a pellet at 500 g for 5 min and resuspended in 10 mL of fresh medium containing 10% FCS with serum. The (PLL/HA)<sub>n</sub> or (PLL/HA)<sub>n</sub>-PLL films, either native or cross-linked, with EDC/NHS, were deposited on 12 mm glass slide that were put in a 24 wells culture plate. These twelve bilayers thick films were chosen such as to have a uniform film on the glass substrate as was previously checked by AFM.<sup>14</sup> 3 × 10<sup>4</sup> cells were deposited in each well.

## Results and Discussion

**Comparison of the Action of EDC Alone and EDC Combined to Sulfo-NHS.** In the literature, there are many works aimed at cross-linking HA for biomedical purposes. In fact, the introduction of functional groups on HA is a subject of great interest.<sup>48</sup> An early report claimed that carbodiimide-catalyzed reaction of HA with glycine methyl ester, a monofunctional amine, led to the formation of an amide linkage.<sup>49</sup> More recently, Tomihata et al.<sup>33</sup> showed that EDC mediates an ester bond formation between the hydroxyl and carboxyl groups of HA. These authors also observed that adding L-lysine methyl ester in the HA solution leads to the formation of an amide bond. Indeed, *in vivo* degradation of the cross-linked films in the medium containing lysine ester underwent slower degradation indicating a more stable linkage for the amide bond than for the ester bond. Park et al. also used only EDC for cross-linking their HA gels.<sup>34</sup> For HA solutions only (not containing the methyl ester), the EDC reaction could only be carried out at a very high polysaccharide concentration and at very low water concentration. Beside results obtained on HA molecules, EDC was also found to modify the side-groups on proteins to make them reactive with other side groups. This was the case for collagen/HA sponges, for which amide bonds could be formed between the amine groups of collagen and the carboxyl groups of HA, and ester linkages between the carboxyl groups of HA and the hydroxyl groups of HA or collagen.<sup>34</sup>

However, other studies showed that amide linkages could not be formed for HA alone in the presence of only EDC.<sup>50,51</sup>

**Scheme 1.** Coupling Schéma between PLL and HA in the Presence of Only EDC<sup>a</sup>

<sup>a</sup>EDC reacts with a carboxylic group and activates it to give a *O*-acylisourea intermediate (1). The *O*-acylisourea may rearrange to a stable *N*-acylurea by way of a cyclic electronic displacement (2).<sup>52,53</sup> It may also react with an amine group (such as PLL) to form an amide bond (3).

In fact, EDC reacts with available carboxyl groups to form active *O*-acylisourea intermediates (Scheme 1, step 1). However, under mild acidic conditions and in the absence of nucleophiles, the *O*-acylisourea intermediates can also rearrange by a cyclic electronic displacement to a stable *N*-acylurea (Scheme 1, step 2).<sup>51–54</sup> This irreversible reaction is reported to hinder the formation of the desired amide linkage.<sup>49,54</sup> Eventually, the *O*-acylisourea can react directly with the amine of PLL (Scheme 1, step 3).

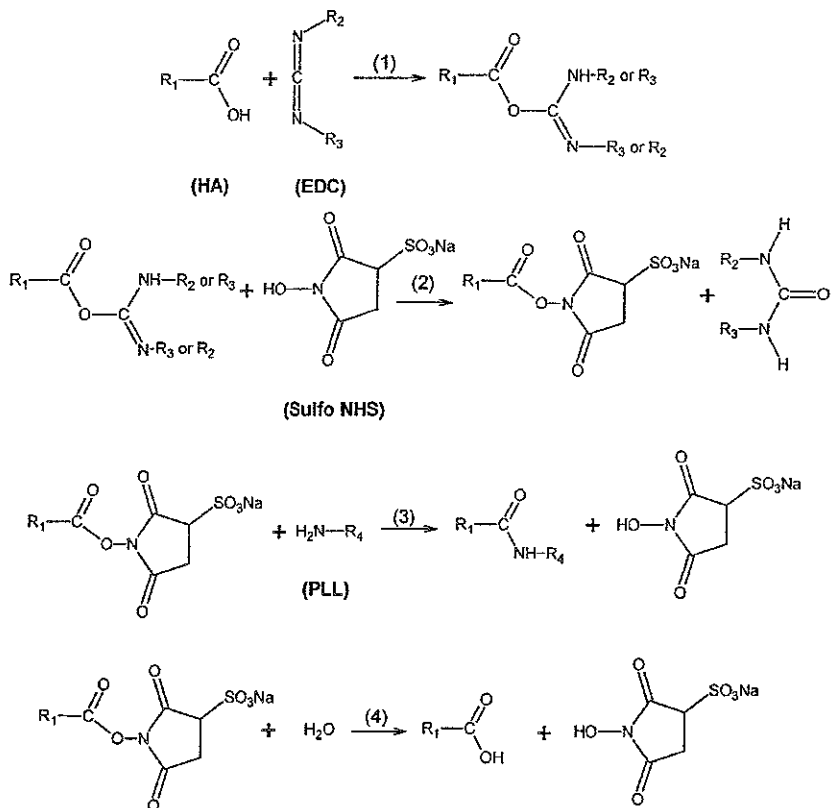
To enhance the efficiency of coupling between HA and primary amines, it is possible to add sulfo-NHS to the reaction, an esterification reagent that is known to enhance the formation of amide bonds.<sup>38</sup> In the presence of both carboxylic and amine groups, the coupling chemistry is based on the following reaction scheme (Scheme 2).<sup>38</sup> Beside the reactions already described in Scheme 1 (step 2 and 3), the *O*-acylisourea intermediates react with sulfo-NHS to give the NHS-ester intermediates (Scheme 2, step 2). For kinetic reasons, this later reaction is strongly preferred. This reaction being faster than O → N migration of *O*-acylisourea, this NHS-ester activated site reacts with primary amine sites to form an amide derivative (Scheme 2, step 3). For these reasons, precisely, the EDC/NHS reaction is more efficient than the EDC reaction alone. Failure to react with an amine results in hydrolysis of the intermediate, regeneration of the carboxyls and the release of sulfo-NHS (Scheme 2, step 4). Moreover, it was recently shown that, in the presence of EDC/NHS, HA could react with different amines to form amide linkages.<sup>53</sup> More generally, this technique was successfully used for coupling amine and carboxyl groups.<sup>55</sup>

Therefore, we chose to use a mixture of EDC/NHS (200 mM/50 mM). Some control experiments have been done using only EDC (200 mM). However, as will be shown below and as anticipated, EDC alone was not sufficient to

fully cross-link PLL to HA and to affect the cellular adhesion properties of the film.

**Cross-Linking Reaction followed by FTIR.** The cross-linking between ammonium groups of PLL and carboxylate groups of HA in the presence of EDC/NHS was first followed by FTIR-ATR. Figure 1A shows a typical spectrum of a (PLL/HA)<sub>n</sub> film deposited on a ZnSe crystal before contact with the EDC/NHS solution. The peaks of HA attributed to  $\text{--COO}^-$  asymmetric and symmetric stretches (1606, 1412 cm<sup>-1</sup> respectively) can be clearly identified.<sup>56</sup> The amide I and amide II bands for HA appear respectively at 1650–1675 and 1530–1565 cm<sup>-1</sup> (in water).<sup>56</sup> For PLL in D<sub>2</sub>O, the amide I is located at 1600–1680 cm<sup>-1</sup> and the amide II band at 1450 cm<sup>-1</sup>.<sup>57,58</sup>

It has to be noticed that all of the frequencies appearing in our spectra correspond closely to those found by FTIR for hyaluronan in water<sup>56,59</sup> although our experiments were performed in D<sub>2</sub>O. This indicates that the HA constituting the multilayer is still highly hydrated. The spectrum evolves as soon as the film is brought in contact with the EDC/NHS solution. The kinetics of the cross-linking reaction emerges more clearly by following the difference between the actual spectrum and the spectrum recorded before contact with EDC/NHS. The evolutions of these difference spectra as a function of the contact time between the film and the EDC/NHS solution are shown in Figure 1B. As the contact time increases, the intensity of the peaks attributed to the carboxylic groups (1606, 1412 cm<sup>-1</sup>) decreases and relatively the intensity of the amide bands increases (1620–1680 cm<sup>-1</sup>). This is a strong indication for the formation of amide bonds between PLL and HA at the expense of carboxylic groups. A stabilization of the spectra is observed after  $\approx$ 6 h of contact with the EDC/NHS solution (see inset of Figure 1B). It has to be noticed that, in the case of EDC

Scheme 2. EDC and Sulfo-NHS Coupling Scheme<sup>a</sup>

<sup>a</sup> EDC reacts with a carboxylic group and activates it (1). The activated complex is converted into an active ester with sulfo-NHS (2). The active ester reacts with primary amine to form an amide bound (3). The unreacted sites are hydrolyzed to give a regeneration of the carboxyls (4).

alone, the FTIR spectrum after contact with the EDC solution for 24 h showed only very slight changes (data not shown).

**Zeta Potential Measurements.** The  $\zeta$  potential of the film prior to and after the cross-linking is presented in Figure 2. It alternates between +50 and -50 mV during the film construction for PLL and HA terminating layers respectively, in accordance with former results.<sup>14,60</sup> Cross-linking was performed both on a negative (PLL/HA)<sub>n</sub> and a positive (PLL/HA)<sub>n</sub>-PLL multilayer. Surprisingly, the zeta potential of the cross-linked films, whether negatively or positively ending, is always negative and of the order of -55 mV. Adding a new positive PLL layer on top of the cross-linked films leads to a charge reversal. Subsequent PLL and HA depositions on the cross-linked film lead again to an alternate charge reversal after each deposition step. It thus seems possible to continue the layer-by-layer buildup on top of a cross-linked film. Moreover, the fact that a PLL ending film becomes negatively charged after cross-linking seems to indicate that the outer layer is essentially formed of HA chains. There may also be some unreacted sulfo-NHS molecules on top of the film.

**Viscoelastic Changes.** We also followed *in situ* the film buildup and the subsequent cross-linking by QCM-D. As found in a previous study,<sup>14</sup> the rescaled frequency shifts  $-\Delta f/\nu$  increase exponentially (data not shown) with the number of deposition steps indicating, as a first approxima-

tion, that the mass of the film also increases exponentially. It has been shown that this exponential growth is related to the "in" and "out" diffusion of PLL through the whole film during each PLL deposition step. Moreover the values of  $-\Delta f/\nu$  do depend on  $\nu$  for a given number of deposition steps, indicating the viscoelastic nature of the material constituting the multilayer. When such a film is brought in contact with the EDC/NHS solution one observes a slight increase in  $-\Delta f/\nu$  and a pronounced decrease of the dissipation factor  $D$  for the four resonance frequencies. These changes are represented in Figure 3. The evolutions take place over roughly 5 h. The decrease of  $D$  is characteristic of the stiffening of the film. Similar results were obtained when PLL was the outermost layer of the film (data not shown). For a thick polyelectrolyte films (thicker than the penetration depth of the evanescent field), it is also possible to determine by OWLS the film refractive index considering the film as an infinite medium.<sup>44</sup> The refractive index noticeably increases as the cross-linking is performed, and it changes from 1.380 before the cross-linking to 1.395 after the cross-linking. This suggests that the film has become more dense.

**Changes in the Diffusion Properties of PLL.** We used confocal laser scanning microscopy (CLSM) to get information on the (PLL/HA)<sub>n</sub> film thickness and on the diffusion process through the native and cross-linked films. This

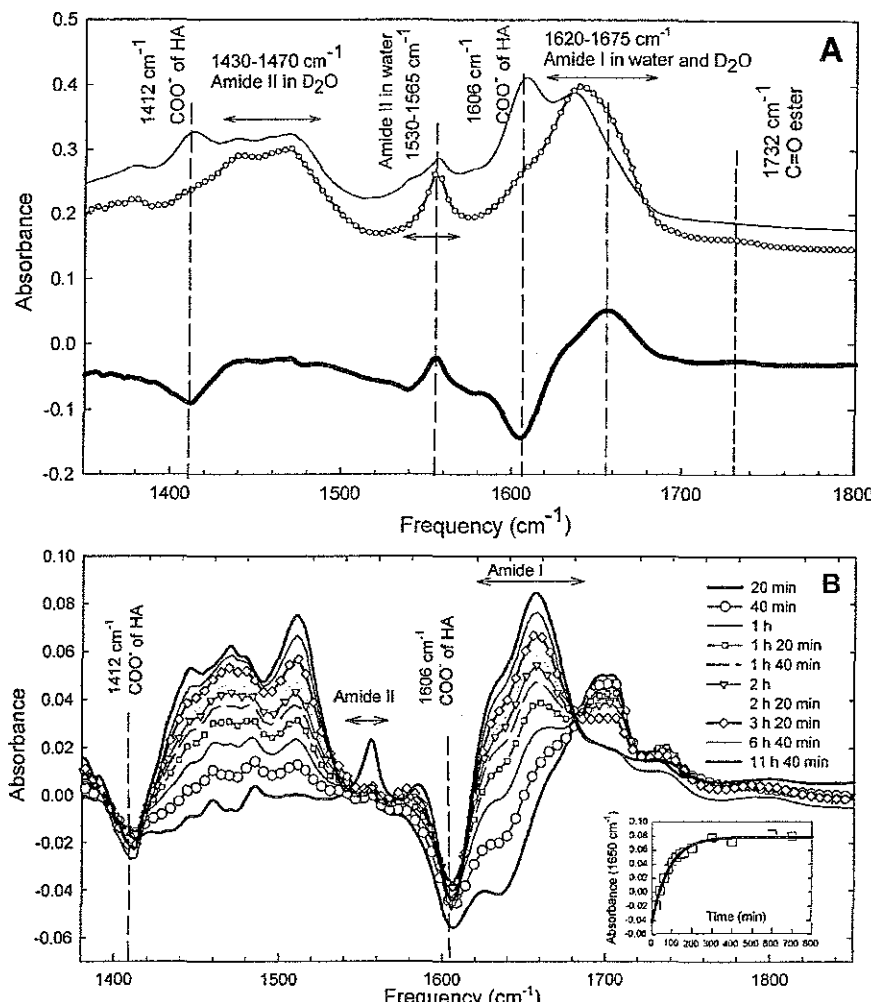


**Figure 1.** ATR-FTIR spectra of a native and a cross-linked  $(\text{PLL}/\text{HA})_8$  film. (A) before (—) and after the cross-linking procedure and the final rinsing step (—O—). Cross-linking was achieved by contact with the EDC/NHS solution for 12 h at room temperature. The difference between the two spectra (before and after cross-linking) is also represented (thick black line). (B) Evolution of the difference between the actual spectra during the contact with the EDC/NHS solution and the spectrum recorded for the  $(\text{PLL}/\text{HA})_8$ , as a function of the contact time (from 20 min to 12 h; the contribution of the multilayer film was subtracted to the actual spectrum at each contact time). (Inset) The evolution of the absorbance at  $1650 \text{ cm}^{-1}$  as a function of time (black square) and the corresponding exponential fit.

technique allowed us previously to prove the existence of the “in” and “out” diffusion process of PLL through the whole film during each PLL deposition step.<sup>44</sup> It also gives access to the thickness of the films for films typically thicker than  $1 \mu\text{m}$ . The use of an automatic dipping machine together with the visualization by CLSM allows us to follow the thickness  $d$  for films made of a large number  $n_b$  of pairs of layers. As can be seen in Figure 4, the behavior of  $d$  with  $n_b$  is fully compatible with an exponential growth, and one reaches a thickness of the order of  $12 \mu\text{m}$  for 30 pairs of layers (native films). As a supplementary experimental proof for the cross-linking of the film, fluorescence recovery after photobleaching (FRAP) experiments were performed by CLSM on un-cross-linked and cross-linked  $(\text{PLL}/\text{HA})_{20}$ –PLL-FITC films. A circular zone was bleached, and images were taken immediately after the bleach and after a 30 min delay (Figure 5, parts A and B). Intensity profiles along the

$X$  axis are plotted for the two images (Figure 5, parts C and D). For un-cross-linked films (Figure 5, parts A and C), one observes a partial recovery of the fluorescence in the bleached zone, whereas for cross-linked films, no recovery is found (Figure 5, parts B and D). This indicates the absence of PLL-FITC diffusion in the cross-linked films. For non cross-linked films, the diffusion coefficient  $D$  of the PLL chains can be estimated to be of the order of  $\langle \text{dist}^2 \rangle / (2 \times t) = 2 \times 10^{-9} \text{ cm}^2 \text{ s}^{-1}$  where  $\text{dist}$  corresponds to half the width of the bleached rectangle ( $\approx 28 \mu\text{m}$ ) and  $t$  the diffusion time ( $t \approx 1800 \text{ s}$ ). This value is largely smaller than the value of  $10^{-7}$ – $10^{-8} \text{ cm}^2 \text{ s}^{-1}$  estimated from the evolution of optical waveguide light mode spectroscopy data during the deposition steps of PLL as the film is built.<sup>14</sup> The difference can be explained by the fact that the CLSM experiments were performed 24 h after the film buildup. During this period of time, “free” PLL-FITC chains present in the film could

## Biomacromolecules

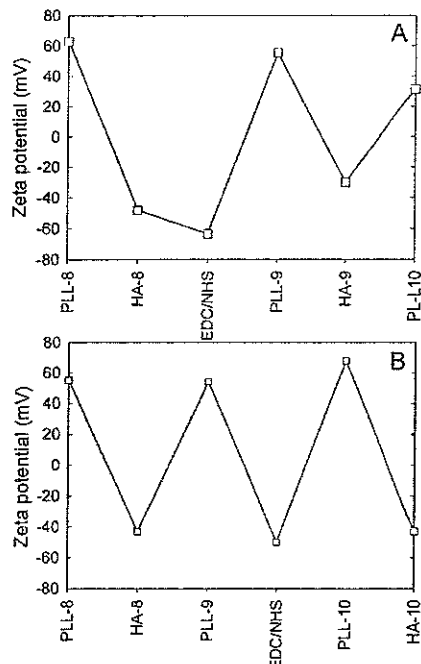


**Figure 2.** Evolution of the zeta potential (mV) for (PLL/HA) films prior to and after the cross-linking with EDC/NHS as a function of the layers deposited (□). PLL (MW  $3 \times 10^4$  Da) and HA (MW  $4 \times 10^5$  Da) were prepared at 1 mg/mL in a 0.15 mM NaCl solution containing 0.15 M NaCl. Each point represents the mean value of three successive measurements. Standard deviations are so small that they are not visible on the graph. Additional PLL and HA layers have been adsorbed on the cross-linked films. (A) Cross-linking of a negatively ending (PLL/HA)<sub>8</sub> film. (B) Cross-linking of a positively ending (PLL/HA)<sub>8</sub>-PLL film. For clarity, the values of the zeta potential for the previous layers (from first until 8 pairs of layers) are not represented.

exchange with PLL chains from the PLL/HA network and could gradually establish links with this network, reducing greatly their mobility. The existence of such an exchange process has been proven in a previous study.<sup>44</sup> The fact that the PLL diffusion within the film is greatly reduced after cross-linking is a supplementary indication for the successful involvement of PLL in the coupling reaction with HA.

Further evidence that cross-linking changes the internal structure of the film comes from the deposition of PLL-FITC onto a previously cross-linked but non labeled (PLL/HA)<sub>20</sub> film. Whereas a (PLL/HA)<sub>20</sub>-PLL-FITC film (which has been cross-linked after the deposition of PLL-FITC) appears uniformly green (Figure 6A), there is no visible fluorescence on a cross-linked (PLL/HA)<sub>20</sub> film on top of which a PLL-FITC layer has been adsorbed using the same adjustment for the detector gain of the CLSM apparatus (Figure 6B). By increasing the detector gain by a factor of 2, a very thin green line becomes visible (Figure 6C), but the noise is also greatly increased, as can be seen by the large number of green pixels over all of the image (and not especially within the film). This thin line, located on the top of the film, has a thickness of the order of 1  $\mu\text{m}$  which is much smaller than the  $\approx 5 \mu\text{m}$  thickness of the (PLL/HA)<sub>20</sub>-PLL-FITC film. This strongly suggests that PLL is no more able to diffuse

## Cross-Linking of Polyelectrolyte Multilayer Films G

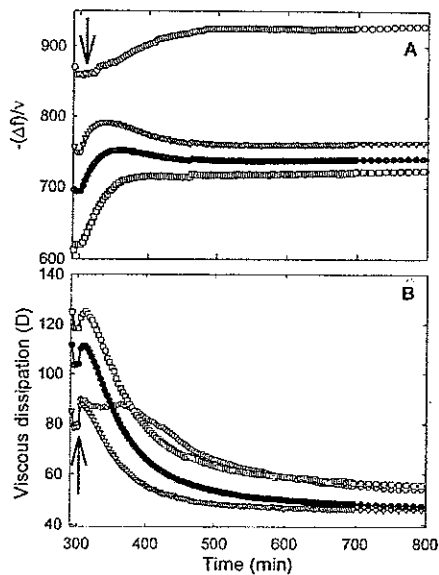


**Figure 3.** In situ cross-linking of a (PLL/HA)<sub>7</sub> film as followed by QCM. (A) Evolution of the frequency shifts ( $-\Delta f/\nu$ ) and (B) of the viscous dissipation  $D$  as a function of time, after the (PLL/HA)<sub>7</sub> film has been put in contact with the EDC/sulfo-NHS solution. The four harmonics are represented (○) 5, (▽) 15, (●) 25, and (□) 35 MHz. The arrows indicate the injection of the EDC/sulfo-NHS solution.

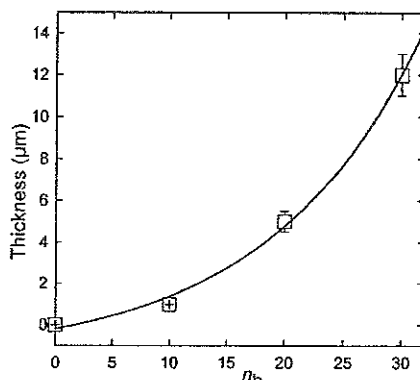


**Figure 4.** Thickness  $d$  of the (PLL/HA) films as a function of the number of pairs of layers  $n_b$ , as measured by AFM (+) and by CSM (□) for films built with the automatic dipping machine on 12 mm glass slides. AFM height measurements were performed by scratching the film (data taken from ref 14), whereas CSM measurements were performed using PLL-FITC as the last layer to label the whole film (observation of a green band). Error bars represent the uncertainty on the CSM measurements.

into a cross-linked film. In the case of EDC alone, when we deposited a PLL-FITC layer on top of a film that had been in contact with EDC, the entire film appeared green suggesting that PLL is still able to diffuse within these films and, thus, that the cross-linking between PLL and HA in the presence of EDC alone is not as efficient as in the presence of EDC/NHS.

This result seems to indicate that PLL-FITC does not diffuse within the cross-linked film during the PLL-FITC deposition step. It could also be due to the absence of exchange process between “free” PLL-FITC chains in the

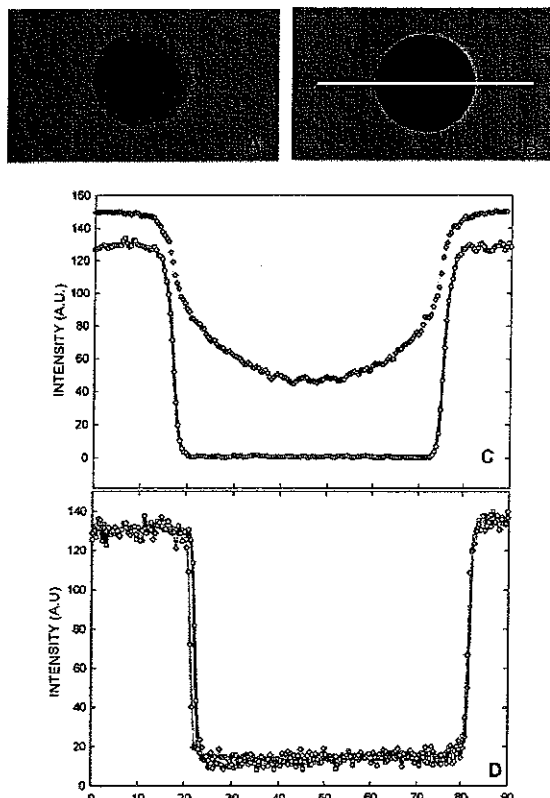


**Figure 5.** CLSM images taken 30 min after the bleach of the circular zone (around 55  $\mu\text{m}$  in diameter). The green fluorescence comes from the (PLL/HA)<sub>20</sub>-PLL-FITC film. (A) Native film; (B) cross-linked film. The corresponding intensity profiles along the white line from images obtained immediately after the bleach (○) and 30 min after the bleach (◊) are given for the (C) native and (D) cross-linked films.

film and PLL chains cross-linked to HA and to the total diffusion (out of the film) of the PLL-FITC during the rinsing step by the aqueous solution. OWLS experiments can bring additional useful information since they were shown to evidence the diffusion of PLL within a thick (PLL/HA) multilayer film.<sup>44</sup> Experiments performed by OWLS on cross-linked films evidence that there is no more signal changes when PLL and HA are adsorbed after the cross-linking procedure has been performed. This suggests that the first hypothesis is to be preferred.

**Stability of the Films: Un-Cross-Linked Versus Cross-Linked Multilayers.** The stability of the non-cross-linked and cross-linked films in contact with water, with different ethanol solutions, and with hyaluronidase was also investigated. This enzyme is able to cleave hyaluronan.<sup>61,62</sup> The non-cross-linked (PLL/HA)<sub>12</sub> multilayers (built in 0.15 M NaCl solution) are stable in the 0.15 M NaCl solution for several months, as checked by CLSM, and for at least two weeks when in contact with cells and culture medium (in an incubator at 37 °C). Longer times have not been tested in this case. On the other hand, observations performed by CLSM indicate that the films tend to lift up from the substrate locally when the multilayer is transferred from the 0.15 M

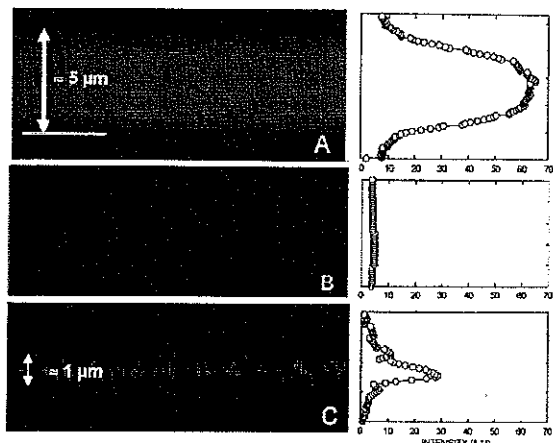


**Figure 6.** Vertical sections through (PLL/HA)<sub>20</sub>-PLL-FITC films (A) a cross-linked (PLL/HA)<sub>20</sub>-PLL-FITC film for which PLL-FITC has been added before the cross-linking. The thickness of the film is around 5  $\mu\text{m}$  as can be seen by the diffusion of the PLL-FITC in the film (white line, image size is 23  $\mu\text{m} \times 10 \mu\text{m}$ ). (B) a cross-linked (PLL/HA)<sub>20</sub> film on top of which PLL-FITC has been deposited and then rinsed. For this image, the gain and the amplification of the detector were unchanged when compared to (A) (image size is 22.5  $\mu\text{m} \times 9.2 \mu\text{m}$ ). (C) same sample as for image (B) but observed with the detector gain increased by a factor of two. A weak green fluorescence is visible over a short distance at the top of the film (white arrow) because PLL-FITC diffuses weakly into the cross-linked film (image size is 22.5  $\mu\text{m} \times 7.2 \mu\text{m}$ ). However, the noise is also greatly increased as can be seen by the large number of green pixels overall the image. On the right side of the images, the corresponding intensity profiles along a section are also given for more clarity.

NaCl solution into pure water (data not shown). This may be due to strong restructuration effects inside the film or to a weakening of the interactions between the film and the substrate during the transfer of the multilayer into water. On the other hand, the cross-linked (PLL/HA)<sub>20</sub>-PLL-FITC films, are very stable when transferred in water or in water/ethanol solutions whatever the ethanol proportion is. The thickness of the film as a function of the ethanol concentration is given in Figure 7. The thickness of the cross-linked film continuously decreases as the ethanol content is increased and reaches in pure ethanol a thickness which represents 50% from its initial value in water. The rehydration of the film is almost fully reversible at the 15 min time period applied here. Such a film thickness decrease as the ethanol content increases may be due to a decrease of the ionic content of the film which would lead to a decrease of the osmotic pressure. Finally, after contact for 42 h at 37 °C with a hyaluronidase solution at 1000 U/mL, the topography of a cross-linked film remained unchanged whereas un-cross-linked films were strongly degraded as can be seen in Figure 8. One also observes that the degradation of un-cross-linked films by hyaluronidase leads to a very porous, spongelike film.

**Cell Adhesion Properties.** The un-cross-linked and cross-linked films were also tested with respect to the adhesion of chondrosarcoma cells, taking bare glass as a reference. These cells were grown on negative (PLL/HA)<sub>12</sub> and positive (PLL/HA)<sub>12</sub>-PLL films, either native or cross-linked (four conditions). Three slides were used for each condition. On the

## Biomacromolecules

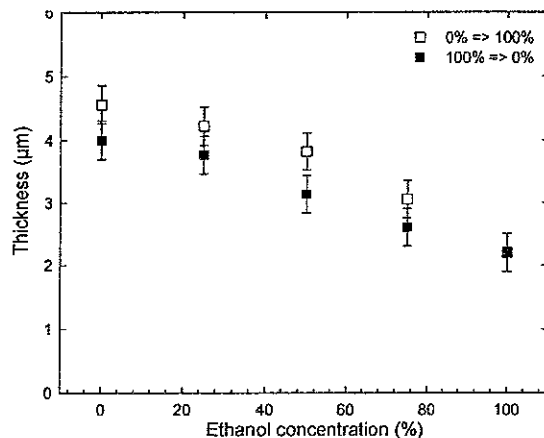


Figure 7. Thickness of a cross-linked  $(\text{PLL}/\text{HA})_{20}$ -PLL-FITC film as a function of the ethanol concentration as measured by CLSM. Films built and cross-linked in the 0.15 M NaCl solution were then put in contact with water followed by solutions at increasing ethanol concentrations (25%, 50%, 75%, and 100%) (□). The rehydration of the films was followed by decreasing ethanol concentration (from pure ethanol to pure water) (■).

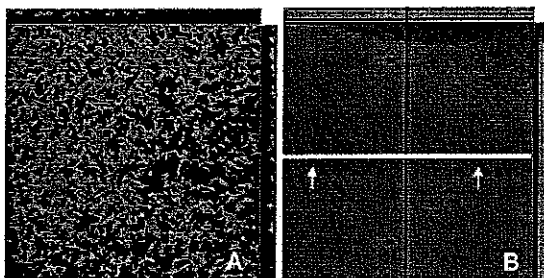


Figure 8. CLSM study of the degradation of a  $(\text{PLL}/\text{HA})_{24}$ -PLL-FITC film that has been in contact with hyaluronidase (type I, 1000U) for 42h at 37 °C. (A) native and (B) cross-linked film. Z sections collected at 0.4  $\mu\text{m}$  interval were taken with the 40  $\times$  oil objective (230  $\mu\text{m} \times 230 \mu\text{m}$ ) in order to image the whole films. The top views of the film are shown. Vertical section along the white line (see white arrows and top view) and along the black line (see black arrows and side view) are also represented. The vertical section scales are respectively 12.9  $\mu\text{m}$  for the left image and 11.8  $\mu\text{m}$  for the right image. From the right image, the cross-linked film thickness can be estimated to be 5.7  $\mu\text{m}$ .

$(\text{PLL}/\text{HA})_{12}$  and  $(\text{PLL}/\text{HA})_{12}$ -PLL films, cells neither adhere nor spread at all after 2–6 days of culture (respectively Figure 9, parts A and C). These results hold for both HA and PLL ending films. An important question arises as to whether any cells ever did initially adhere to and then subsequently detached from the polyelectrolyte films. Such behavior would suggest that the multilayers are potentially cytotoxic. However, this nonadhesion is not due to a toxicity of the films since the cells could adhere at the bottom of the well (on the plastic near the coated glass). Also, if the suspended cells from the un-cross-linked PLL/HA films were transplanted to fresh culture plates, even after 2 days of floating, many cells readily attached and spread similarly to healthy cells. By contrast, cells deposited on the cross-linked HA and PLL ending films adhered and spread well comparably to cells on uncoated glass slides. The surface of the

## Cross-Linking of Polyelectrolyte Multilayer Films |

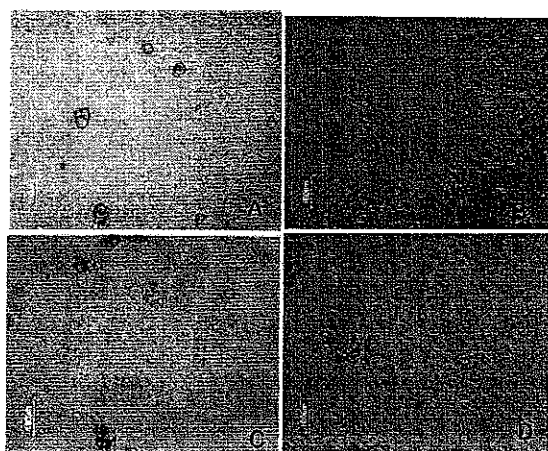


Figure 9. Chondrosarcoma cells (HCS2/8) cultured on native or cross-linked  $(\text{PLL}/\text{HA})_{12}$  and  $\text{PLL}(\text{HA})_{12}$ -PLL films for 6 days, i.e., films terminating either by  $\sim\text{PLL}$  or  $\sim\text{HA}$ : (A)  $\sim\text{HA}$  (B) cross-linked  $\sim\text{HA}$  (C)  $\sim\text{PLL}$  (D) cross-linked  $\sim\text{PLL}$ .

cross-linked film was almost entirely covered over the 6 days period of culture (Figure 9, parts B and D). It has to be noticed that these results were obtained only in the case of the EDC/NHS cross-linking protocol and not when EDC alone was used. In this latter case, the films were still highly cell resistant. These findings further demonstrate that there is no effective cross-linking in the absence of sulfo-NHS.

The change from a nonadhesive to an adhesive character of the  $(\text{PLL}/\text{HA})_n$  films after cross-linking may originate from changes in the film rigidity as evidenced by QCM-D and from the strongly reduced diffusion of PLL. Several studies have demonstrated the influence of the rigidity of a substrate on the cell adhesion and movement. Lo et al.<sup>37</sup> showed, by using polyacrylamide gels coated with collagen, that cell movements can be controlled by purely physical interactions at the cell substrate interface. The rigidity of the gel was adjusted by changing the concentration of the bis-acrylamide cross-linker. These authors evidenced that cells preferred the stiff substrate (what they called the “durotaxis”). This kind of physical rule was further evidenced for neuronal cells.<sup>63</sup> Moreover, it is expected that cross-linking reduces the hydration of the films and their deswelling and swelling ability consecutive to drying and rehydration. Following Mendelsohn et al.,<sup>19</sup> this should favor cellular adhesion on the films. The issue of protein adhesiveness is often simultaneously investigated when performing *in vitro* cell studies with biomaterials. However, recent studies on polyelectrolyte multilayers suggest that differences in protein adhesiveness cannot account for the significant differences in cell-multilayer interactions.<sup>19,64</sup>

Another way to modify film stiffness may be to introduce organic nanocolloids.<sup>65,66</sup> Titania nanoshells introduced in a layer by layer assembly of poly(diallyldimethylammonium chloride) (PDDA)/poly(acrylic acid) (PAA) were found to favor PC12 (a cell lineage) cell attachment onto the films, whereas there was no attachment of the cells to PDDA/PAA multilayers free of particles. The main advantage of the simple cross-linking protocol based on a zero length cross-

linker such as EDC is that it does not introduce additional molecule or particle that may be toxic in *in vivo* applications. Future work is also needed *in vitro* to investigate the properties of native and cross-linked films with respect to primary cells which are much more sensitive than cell lineages.

### Conclusion

We successfully demonstrated that polyelectrolyte multi-layered films containing carboxylic and ammonium groups can be chemically cross-linked by means of a water soluble carbodiimide EDC in combination with sulfo-NHS. We also proved that the use of sulfo-NHS in combination with EDC was necessary for getting an effective cross-linking of the films. Fourier transform infrared spectroscopy evidences the conversion of these groups into amide bonds. The zeta potential of the films becomes negative after the cross-linking. As a first consequence of the cross-linking, the rigidity and the density of the film are increased, as suggested by the decrease in the viscous dissipation observed by QCM and the increase in the film refractive index measured by OWLS. As a second consequence of the cross-linking, CLSM images demonstrate that the diffusion of the PLL-FITC within the (PLL/HA)<sub>n</sub> films has vanished and the cross linking hinders further diffusion of PLL chains within the film when it is brought in contact with a PLL solution. Moreover cross-linked films adhere in a much more stable way than non-cross-linked ones to the substrate. Finally, cross-linked films are stable in ethanol and they are not degraded by hyaluronidase (over a 42 h incubation period at 37 °C), whereas the non-cross-linked films are highly degraded when exposed to this enzyme. As a consequence of the cross-linking, chondrosarcoma cells do adhere very well on the films terminating either with PLL or HA whereas the native films are highly cell anti-adhesive. This effect is explained by an increase of the film rigidity after cross linking.

**Acknowledgment.** We thank Prof. D. E. Discher (University of Pennsylvania, Philadelphia), Dr. R. Richter (Q-Sense), Prof. G. D. Prestwich (University of Utah, Salt Lake City), and Dr. B. Frisch (CNRS, Strasbourg) for fruitful discussions. We also thank G. Marzoff and G. Bonani for their technical help. This work was supported by the programs ACI "Technologies pour la Santé" and ACI "Surfaces, interfaces et conception de nouveaux matériaux" from the Ministère Français de la Recherche. The CLSM platform used in this study was co-financed by the Région Alsace, the CNRS, the Université Louis Pasteur, and the Association pour la Recherche sur le Cancer.

### References and Notes

- (1) Castner, D. G.; Ratner, B. D. *Surf. Sci.* 2002, 500, 28–60.
- (2) Healy, K. E. *Curr. Opin. Solid State Mater. Sci.* 1999, 4, 381–387.
- (3) Ratner, B. D.; Hoffman, A. S.; Schoen, F. J.; Lemons, J. E. *Biomaterials science: an introduction to materials in medicine*; Academic Press: New York, 1996.
- (4) Decher, G.; Hong, J. D.; Schmitt, J. *Thin Solid Films* 1992, 831–835.
- (5) Decher, G. *Science* 1997, 277, 1232–1237.
- (6) Bertrand, P.; Jonas, A.; Laschewsky, A.; Legras, R. *Macromol. Rapid. Commun.* 2000, 21, 319–348.
- (7) Schönhoff, M. *Curr. Opin. Colloid Interface Sci.* 2003, 8, 86–95.
- (8) Shiratori, S. S.; Rubner, M. F. *Macromolecules* 2000, 33, 4213–4219.
- (9) Dubas, S. T.; Schlenoff, J. B. *Macromolecules* 2001, 34, 3736.
- (10) Fery, A.; Schöler, B.; Cassagneau, T.; Caruso, F. *Langmuir* 2001, 17, 3779–3783.
- (11) Elbert, D. L.; Herbert, C. B.; Hubbell, J. A. *Langmuir* 1999, 15, 5355–5362.
- (12) Serizawa, T.; Yamaguchi, M.; Akashi, M. *Biomacromolecules* 2002, 3, 724–731.
- (13) Shenoy, D. B.; Antipov, A.; Sukhorukov, G. B.; Möhwald, H. *Biomacromolecules* 2003, 4, 265–272.
- (14) Picart, C.; Lavalle, P.; Hubert, P.; Cuisinier, F. J. G.; Decher, G.; Schaaf, P.; Voegel, J. C. *Langmuir* 2001, 17, 7414–7424.
- (15) Chluba, J.; Voegel, J. C.; Decher, G.; Erbacher, P.; Schaaf, P.; Ogier, J. *Biomacromolecules* 2001, 2, 800–805.
- (16) Jessel, N.; Atalar, F.; Lavalle, P.; Mutterer, J.; Decher, G.; Schaaf, P.; Voegel, J. C.; Ogier, G. *Adv. Mater.* 2003, 15, 692–695.
- (17) Boura, C.; Menu, P.; Payan, E.; Picart, C.; Voegel, J. C.; Muller, S.; Stoltz, J.-F. *Biomaterials* 2003, 24, 3521–3530.
- (18) Tryoen-Toth, P.; Vautier, D.; Haikel, Y.; Voegel, J.-C.; Schaaf, P.; Chluba, J.; Ogier, J. *J. Biomed. Mater. Res.* 2002, 60, 657–667.
- (19) Mendelsohn, J. D.; Yang, S. Y.; Hiller, J.; Hochbaum, A. I.; Rubner, M. F. *Biomacromolecules* 2003, 4, 96–106.
- (20) Eckle, M.; Decher, G. *Nano Lett.* 2001, 1 (1), 45–49.
- (21) Kovacevic, D.; van der Burgh, S.; de Keizer, A.; Cohen Stuart, M. A. *Langmuir* 2002, 18, 5607–5612.
- (22) Brynda, E.; Houska, M. J. *Colloid Interface Sci.* 1996, 183, 18–25.
- (23) Leporati, S.; Voigt, A.; Mittlöhner, R.; Sukhorukov, G.; Donath, E.; Möhwald, H. *Langmuir* 2000, 16, 4059–4063.
- (24) Chen, J.; Huang, L.; Ying, L.; Luo, G.; Zhao, X.; Cao, W. *Langmuir* 1999, 15, 7208–7212.
- (25) Vuillaume, P. Y.; Jonas, A. M.; André Laschewsky, A. *Macromolecules* 2002, 35, 5004–5012.
- (26) Tengvall, P.; Jansson, E.; Askendal, A.; Thomsen, P.; Gretzer, C. *Colloids Surf. B* 2003, 28, 261–272.
- (27) Harris, J. J.; DeRose, P.; Bruening, M. J. *Am. Chem. Soc.* 1999, 121, 1978.
- (28) Dai, J.; Jensen, A.; Mohanty, D.; Erndt, J.; Bruening, M. *Langmuir* 2001, 17, 931–937.
- (29) Lee, B. J.; Kunitake, T. *Langmuir* 1994, 10, 557–562.
- (30) Anagi, M.; Balachandra, A. M.; Dai, J.; Bruening, M. L. *Macromolecules* 2002, 35, 3171–3178.
- (31) Timkovich, R. *Anal. Biochem.* 1977, 79, 135–143.
- (32) Grabarek, Z.; Gergely, J. *Anal. Biochem.* 1990, 185, 131–135.
- (33) Tomihata, K.; Ikada, Y. *J. Biomed. Mater. Res.* 1997, 37, 243–251.
- (34) Park, S.-N.; Park, J.-C.; Kim, H. O.; Song, M. J.; Suh, H. *Biomaterials* 2002, 23, 1205–1212.
- (35) Taguchi, T.; Ikoma, T.; Tanaka, J. *J. Biomed. Mater. Res.* 2002, 61, 330–336.
- (36) Pellman, R. J., Jr.; Wang, Y. I. *Proc. Natl. Acad. Sci.* 1997, 94, 13661–13665.
- (37) Lo, C. M.; Wang, H. B.; Dembo, M.; Wang, Y. L. *Biophys. J.* 2000, 79, 144–152.
- (38) Hermanson, G. T. In *Bioconjugate techniques*; Hermanson, G. T., Ed.; Academic Press: San Diego, 1996; pp 169–176.
- (39) Schwinté, P.; Voegel, J.-C.; Picart, C.; Haikel, Y.; Schaaf, P.; Szalontai, B. *J. Phys. Chem. B* 2001, 105, 11906–11916.
- (40) Tiefenthaler, K.; Lukosz, W. *J. Opt. Soc. Am. B* 1989, 6, 209–220.
- (41) Picart, C.; Ladam, G.; Senger, B.; Voegel, J.-C.; Schaaf, P.; Cuisinier, F. J. G.; Gergely, C. *J. Chem. Phys.* 2001, 115, 1086–1094.
- (42) Rodahl, M.; Kasemo, B. *Sens. Actuators B (Chem.)* 1996, B37, 111–116.
- (43) Hook, F.; Rodahl, M.; Brzezinski, P.; Kasemo, B. *J. Colloid Interface Sci.* 1998, 208, 63–67.
- (44) Picart, C.; Mutterer, J.; Richert, L.; Luo, Y.; Prestwich, G. D.; Schaaf, P.; Voegel, J.-C.; Lavalle, P. *Proc. Natl. Acad. Sci.* 2002, 99, 12531–12535.
- (45) Zembala, M.; Déjardin, P. *Colloids Surf. B* 1994, 3, 119–129.
- (46) Ladam, G.; Schaad, P.; Voegel, J. C.; Schaaf, P.; Decher, G.; Cuisinier, F. *Langmuir* 2000, 16, 1249–1255.
- (47) Tagikawa, M.; Tajama, K.; Pan, H. O.; Enomoto, M.; Kinoshita, A.; Suzuki, F.; Takano, Y.; Mori, Y. *Cancer Res.* 1989, 49, 3996–4002.
- (48) Laurent, T. C. *The chemistry, biology, and medical applications of hyaluronan and its derivatives*; Cambridge University Press: Cambridge, U.K., 1998; Vol. 72.
- (49) Danishefsky, I.; Siskovic, E. *Carbohydr. Res.* 1971, 16, 199–205.

- (50) Ogano, A.; Matsuzaki, K.; Uchiyama, H.; Nagasawa, K. *Carbohydr. Res.* 1982, **105**, 69–85.
- (51) Kuo, J. W.; Swann, D. A.; Prestwich, G. D. *Bioconjugate Chem.* 1991, **2**, 232–241.
- (52) Kurzer, F.; Douraghi-Zedeh, K. *Chem. Rev.* 1967, **67**, 107–152.
- (53) Bulpitt, P.; Aeschlimann, D. *J. Biomed. Mater. Res.* 1999, **47**, 152–169.
- (54) Pouyani, T.; Kuo, J. W.; Harbison, G. S.; Prestwich, G. D. *J. Am. Chem. Soc.* 1992, **114**.
- (55) Araki, J.; Wada, M.; Kuga, S. *Langmuir* 2001, **17**, 21–27.
- (56) Haxaire, K.; Marechal, Y.; Milas, M.; Rinaudo, M. *Biopolymers* 2003, **72**, 10–20.
- (57) Boulmedais, F.; Ball, V.; Schwinte, P.; Frisch, B.; Schaaf, P.; Voegel, J. C. *Langmuir* 2002, **19**, 440–445.
- (58) Zuber, G.; Prestrelski, S. J.; Benedek, K. *Anal. Biochem.* 1992, **207**, 150–156.
- (59) Haxaire, K.; Marechal, Y.; Milas, M.; Rinaudo, M. *Biopolymers* 2003, **72**, 149–161.
- (60) Rickett, J.; Brecht, A.; Gopel, W. *Biosens. Bioelectron.* 1997, **12**, 567–575.
- (61) Alberts, B.; Bray, D.; Lewis, J.; Raff, M.; Roberts, K.; Watson, J. D. *Molecular biology of the cell*; Garland Publishing Inc: New York, 1994.
- (62) Prestwich, G. D.; Marecak, D. M.; Marecek, J. F.; Vercruyse, K. P.; Ziebell, M. R. *J. Controlled Release* 1998, **53**, 93–103.
- (63) Flanagan, L. A.; Ju, Y. E.; Marg, B.; Osterfield, M.; Jamney, P. A. *Neuroreport* 2002, **13**, 2411–2415.
- (64) Richert, L.; Lavalle, P.; Vautier, D.; Seeger, B.; Stoltz, J.-F.; Schauf, P.; Voegel, J.-C.; Picart, C. *Biomacromolecules* 2002, **3**, 1170–1176.
- (65) Tang, Z.; Kotov, N. A.; Magonov, S.; Ozturk, B. *Nat. Mater.* 2003, **2**, 413–418.
- (66) Koktysh, D. S.; Liang, X.; Yun, B. G.; Pastoriza-Santos, I.; Matts, R. L.; Giersig, M.; Serra-Rodríguez, C.; Liz-Marzáñ, L. M.; Kotov, N. A. *Adv. Funct. Mater.* 2002, **12**, 255–265.

Cross-Linking of Polyelectrolyte Multilayer Films K

BM0342281

## 4.2 : Propriétés mécaniques de films natifs et réticulés : relation à l'adhésion cellulaire.

### 4.2.1. Résumé 4

Comme nous l'avons vu à l'aide des mesures réalisées par QCM-D dans l'étude précédente, la réticulation des films de (PLL/HA) semble entraîner une forte augmentation de la rigidité des films. Etant donné que l'analyse quantitative des propriétés mécaniques est difficile à partir des données obtenues par QCM-D, nous avons cherché une autre approche pour la détermination de ces propriétés. Les techniques existantes s'appliquant en général sur des échantillons « macroscopiques» (comme la rhéométrie, les essais de traction), nous avons utilisé une technique de nano-indentation basée sur l'AFM. Les propriétés mécaniques des films peuvent en effet être déterminées par AFM mode force, en utilisant de préférence une sonde colloïdale pour les matériaux « mous » et fragiles. Cette étude a été réalisée en collaboration avec le Prof D. Discher (Université de Pennsylvanie) sur des films (PLL/HA) d'épaisseur micrométrique comprenant respectivement 20, 40 et 60 paires de couches. Nous avons utilisé le modèle de Hertz modifié et adapté à un objet sphérique, décrit par Dimitriadis (Dimitriadis et al., 2002), pour la mesure du module d'Young pour les films minces et mous. A l'aide de cette technique, nous avons montré que les propriétés mécaniques sont influencées par le nombre de couches déposées. Sur les films natifs, le module d'Young apparent du film diminue avec l'augmentation de l'épaisseur du film même après 20 paires de couches. Cette analyse a également montré une évolution des propriétés mécaniques des films multicouche au cours du temps, suggérant une lente restructuration du film.

Les mesures sur les films réticulés ont montré une forte augmentation du module d'Young (d'un facteur 2 à 10) par rapport aux films natifs, alors qu'après réticulation, le module d'Young est indépendant de l'épaisseur du film. En répétant la procédure de réticulation une seconde fois, le module d'Young du film augmente encore.

Des mesures d'étalement de cellules musculaires lisses après 4h d'adhésion ont également été réalisées sur les différents films de (PLL/HA) natifs et réticulés. Nous avons ainsi pu établir une corrélation entre le module d'Young des films et l'étalement cellulaire.

## 4.2.2. Article 4

### Elasticity of Native and Cross-Linked Polyelectrolyte Multilayer Films

Ludovic Richert,<sup>†</sup> Adam J. Engler,<sup>‡</sup> Dennis E. Discher,<sup>‡</sup> and Catherine Picart<sup>\*§</sup>

*Institut National de la Santé et de la Recherche Médicale, Unité 595, Université Louis Pasteur, 11 rue Humann, 67085 Strasbourg Cedex, France, Departments of Chemical & Biomolecular Engineering, Mechanical Engineering & Applied Mechanics, and the Institute for Medicine and Engineering, University of Pennsylvania, Philadelphia, Pennsylvania 19104, and Ecole Européenne de Chimie, Polymères et Matériaux de Strasbourg, 25 rue Becquerel, 67087 Strasbourg Cedex 2, France*

Received April 3, 2004; Revised Manuscript Received June 16, 2004

Mechanical properties of polyelectrolyte multilayer films were studied by nanoindentation using the atomic force microscope (AFM). Force-distance measurements using colloidal probe tips were systematically obtained for supported films of poly(L-lysine) and hyaluronan that are suited to bio-application. Both native and covalently cross-linked films were studied as a function of increasing layer number, which increases film thickness. The effective Young's modulus perpendicular to the film,  $E_{\perp}$ , was determined to be a function of film thickness, cross-linking, and sample age. Thick PEM films exhibited a lower  $E_{\perp}$  than thinner PEM, whereas the Young's modulus of cross-linked films was more than 10-fold larger than native films. Moduli range from  $\approx 20$  kPa for native films up to  $\approx 800$  kPa for cross-linked ones. Young's moduli increased slightly with sample age, plateauing after  $\sim 4$  weeks. Spreading of smooth muscle cells on these substrates with pre-attached collagen proved to be highly dependent on film rigidity with stiffer films giving greater cell spreading.

#### Introduction

Layer by layer assembly has rapidly become a primary tool for controlled fabrication of thin films.<sup>1,2</sup> These films are being increasingly used in applications ranging from biomaterials<sup>3–5</sup> to antireflection coatings,<sup>6</sup> separation membranes,<sup>7</sup> drug delivery capsules,<sup>8</sup> and tailored films.<sup>9</sup> Controlling internal film architecture is important to tuning properties such as porosity,<sup>10</sup> stability, and, although untested until now, film deformability as well.

Weak polyelectrolytes have become increasingly used since they enable one to obtain films with properties that depend on the pH used during preparation of the films.<sup>11</sup> Biopolymers also open new possibilities for building up biodegradable films<sup>12</sup> or films that can mimic the extracellular matrix, by using polysaccharides such as hyaluronan,<sup>3,13</sup> chitosan,<sup>14</sup> and proteins such as collagen.<sup>15</sup> Also, as some weak polyelectrolytes can diffuse within the films, film thicknesses may reach several micrometers after a reasonable number of layers (few tens) have been deposited.<sup>16</sup>

For many applications, especially when the films are thick and deformed by contact, sheared by a fluid, remodeled by aging, or used as a substrate to promote or inhibit cell growth,<sup>17,18</sup> it would seem important to know the mechanical properties of the film and control them. In particular, one may envision applications in the coating of stents,<sup>3,4</sup> which have a complex and expandable geometry. Proliferation of

smooth muscle cells (SMCs) into and onto stents can be a significant problem leading to stent failure.<sup>19</sup> Therefore, it is interesting to investigate the adhesion of SMCs to PEM films and to investigate whether physical properties, beyond purely chemical interactions, can modulate SMC adhesion. An additional way to modulate stent interaction with blood and tissue cells could indeed be functionalization with bioactive molecules.<sup>3</sup> Covalent cross-linking of a polyelectrolyte film was recently shown to have a dramatic effect on the cell adhesive properties of the film<sup>20</sup> with native films being nonadhesive and covalently cross-linked films proving highly adhesive. Similarly, insertion of titania nanoparticles into PAA/PAH films<sup>21</sup> leads to a dramatic change in cell adhesion. Such results may be related to those found for polyacrylamide (PA) gels of different stiffness, for which it has been shown that cell adhesion is directly related to gel stiffness: cells generally exhibit stable, focal adhesions on stiff gels but poor adhesion on soft gels.<sup>22</sup> An extremely soft gel appears to be perceived by a tissue cell as nearly fluid and therefore inadequate for sustaining an anchorage-dependent response.<sup>23</sup> Translated to PEM films, highly swellable, lightly cross-linked PEM films may simply be too soft and their surface too "watery" for cells to adhere.<sup>17</sup>

Viscoelastic properties of these layer-by-layer polyelectrolyte films are still poorly understood with no systematic attempts to relate mechanical properties to cell adhesion on the films. This is partly due to the lack of available techniques capable of probing the rheology at length scales relevant to these films whose thickness range from nano- to micrometers. The few studies undertaken to date have focused on the elasticity and mechanical stability of hollow capsules of the

\* To whom correspondence should be addressed. E-mail: Catherine.Picart@medecine.u-strasbg.fr.

<sup>†</sup> Université Louis Pasteur.

<sup>‡</sup> University of Pennsylvania.

<sup>§</sup> Ecole Européenne de Chimie, Polymères et Matériaux de Strasbourg.

## B Richert et al.

*Biomacromolecules*

78 polyelectrolytes,<sup>24,25</sup> or self-supported membranes that could  
 79 be studied by microtraction experiments.<sup>26</sup> Gravimetric  
 80 techniques such as quartz crystal microbalance (QCM) could  
 81 also be used in principle for mechanical characterization of  
 82 the film,<sup>13</sup> but the shear modulus extracted from QCM data  
 83 is extremely sensitive to the environment and not well  
 84 worked out in general. Techniques based on colloidal probes  
 85 have recently been developed to study soft thin films,<sup>27</sup> and  
 86 have been complemented by surface force measurements  
 87 with conical tips<sup>28</sup> or with colloidal beads attached to AFM  
 88 tips.<sup>29</sup> For gel samples that can be macroscopically measured,  
 89 good agreement has been obtained with the apparent Young's  
 90 modulus computed from AFM indentation using the Hertz  
 91 model for a conical tip as an approximation for a pyramidal  
 92 tip.<sup>23</sup>

93 Past AFM studies on PEM films have strictly focused on  
 94 imaging thin films to observe the influence on topography  
 95 of preparation parameters such as number of layer pairs, ionic  
 96 strength, pH conditions, and post-assembly treatment.<sup>30,31</sup> No  
 97 studies have yet been done on PEM properties using AFM  
 98 force-indentation measurements and spherical tips. Other thin  
 99 gels have been studied (collagen, poly(vinyl alcohol)) using  
 100 a colloidal probe,<sup>29,32</sup> but studies of PEM supported and  
 101 planar films are lacking. The only recent investigations using  
 102 AFM in force mode have been conducted either with  
 103 common pyramidal tips<sup>33</sup> or very thin PEM shells using a  
 104 colloidal probe.<sup>25</sup> For extremely soft and sensitive samples,  
 105 it seems more appropriate to attach microspheres to the  
 106 cantilevers in order to avoid stress damage to samples. This  
 107 is particularly important when the probed samples are a few  
 108 microns or less<sup>34</sup> as is the case for most PEM films.

109 To test whether mechanical properties of the films can be  
 110 extracted from AFM force measurements, we studied a  
 111 relatively thick PEM system of poly(L-lysine) (PLL) and  
 112 hyaluronan (HA) with  $i$  layers (PLL/HA) $_i$ , supported by an  
 113 underlying glass coverslip.<sup>13,16</sup> (PLL/HA) $_i$  films of different  
 114 thicknesses, either native or cross-linked by means of a water  
 115 soluble carbodiimide are investigated and compared to thinly  
 116 cast polyacrylamide gels from 5 to 70  $\mu\text{m}$  thick.<sup>35</sup> As  
 117 motivated further below, adhesive spreading of smooth  
 118 muscle cells is also investigated and related to the elasticity  
 119 of these layer-by-layer films.

## Materials and Methods.

120 **Substrates.** Glass slides (24  $\times$  24 mm $^2$ , VWR Scientific)  
 121 cleaned with 10 mM sodium dodecyl sulfate (SDS, Sigma)  
 122 for 10 min and 0.1 N HCl for 10 min and extensively rinsed  
 123 with pure deionized water were used as substrates for the  
 124 polyelectrolyte multilayers.

125 **Polyelectrolyte Solutions.** Poly(L-lysine) (PLL, 30 kDa),  
 126 poly(L-lysine)-FITC (PLL-FITC) (0.003–0.01 mol FITC per  
 127 mol lysine monomer), and sodium chloride (purity 99.5%)  
 128 were purchased from Sigma. Sodium hyaluronate (HA, 400  
 129 kDa) was purchased from Bioiberica (Spain). All solutions  
 130 were prepared using ultrapure water (Milli Q-plus system,  
 131 Millipore) with a resistivity of 18.2 M $\Omega$  cm. Polyelectrolyte  
 132 solutions at 1 mg/mL were prepared by dissolution of the  
 133 respective adequate polymer amounts in filtered 0.15 M NaCl  
 134 solution at pH = 6.

135 **Automatic Buildup of the Polyelectrolyte Multilayer  
 136 Films.** (PLL/HA) $_i$  films where  $i$  represents the number of  
 137 layer pairs were prepared with an automatic dipping machine  
 138 (Dipping Robot DR3, Kirstein GmbH, Germany). The glass  
 139 slides were arranged vertically in a custom holder, which  
 140 was immersed for 10 min in a first polyelectrolyte solution  
 141 (PLL). The slides were subsequently rinsed successively in  
 142 three different beakers, containing 0.15 M NaCl solution (pH  
 143 6), of volumes 350, 200, and 200 mL for 1, 5, and 5 min  
 144 respectively. They were then dipped into the oppositely  
 145 charged polyelectrolyte solution (HA) followed by the same  
 146 rinsing procedure. The whole procedure was repeated with  
 147 the PLL solution and so on. Rinsing solutions were changed  
 148 after the deposition of every twentieth layer. Films with  $i$  =  
 149 20, 40, and 60 were prepared and stored in 0.15 M NaCl at  
 150 4 °C. The thickness of the films was determined by confocal  
 151 laser scanning microscopy (CLSM) on a Zeiss LSM 510 by  
 152 measuring the green band in z-sections corresponding to the  
 153 diffusing band of PLL-FITC within the (PLL/HA) films.<sup>16</sup>  
 154 This method gives thicknesses above the micrometer with a  
 155 resolution of about 700 nm.<sup>20</sup>

156 **(PLL/HA) $_i$  Cross-Linking Procedure.** For the chemical  
 157 cross-linking of the films, a previously published protocol  
 158 was applied on the (PLL/HA) $_i$  films.<sup>20</sup> It is based on the  
 159 reaction of activated carboxylic sites with primary amine  
 160 groups<sup>36</sup> in the presence of a water soluble carbodiimide,  
 161 1-ethyl-3-(3-dimethylamino-propyl)carbodiimide (EDC) and of  
 162 *N*-hydroxysulfosuccinimide (sulfo-NHS). EDC and sulfo-  
 163 NHS were purchased from Sigma and prepared at 400 and  
 164 100 mM respectively in 0.15 M NaCl solution at pH 5. 2  
 165 mL of the mixed EDC/Sulfo-NHS solution (v/v) was  
 166 deposited in the Petri dish containing the (PLL/HA) $_i$  coated  
 167 substrates ( $i$  = 20, 40, 60) for 12 h at room temperature.  
 168 Rinsing was performed three times with a 0.15 M NaCl  
 169 solution for 1 h. (For clarity, the simplified notation EDC/  
 170 NHS will be used instead of the complete writing EDC/sulfo-  
 171 NHS.)

172 For the cell adhesion tests, collagen was adsorbed on the  
 173 surface of multilayers, whether cross-linked or not, overnight  
 174 at 37 °C. Excess collagen was rinsed with 0.15 M NaCl and  
 175 attachment was confirmed by immunofluorescence using  
 176 polyclonal anticollagen antibodies.

177 Collagen was adsorbed to the HA terminating multilayers,  
 178 whether the PLL/HA film was cross-linked or not, overnight  
 179 at 37 °C. Excess collagen was rinsed away with 0.15 M  
 180 NaCl, and substrate attachment was measured using 10:1  
 181 collagen/FITC-collagen mixture and comparison to fluores-  
 182 cent collagen standards.<sup>23,37</sup> Z-section confocal microscopy  
 183 was performed to confirm surface localization of collagen  
 184 on the native and cross-linked PLL/HA multilayers.

185 **Gel Substrates.** PA gels were polymerized as homoge-  
 186 neous thin films on rigid glass supports. Gels with homo-  
 187 geneous bis-acrylamide cross-linker concentration were  
 188 prepared per Wang and Pelham,<sup>38</sup> with the addition of glass  
 189 spacer beads of desired diameter. These glass spacer beads  
 190 (5–10  $\mu\text{m}$ ; Duke Scientific; Palo Alto, CA) were used to  
 191 prepare very thin film of known thickness. To induce cross-  
 192 linking, 1/200 volume of 10% ammonium persulfate and  
 193 1/2000 volume of *N,N,N',N'*-tetramethylmethylenediamine

*Biomacromolecules*

## Elasticity of Polyelectrolyte Multilayer Films C

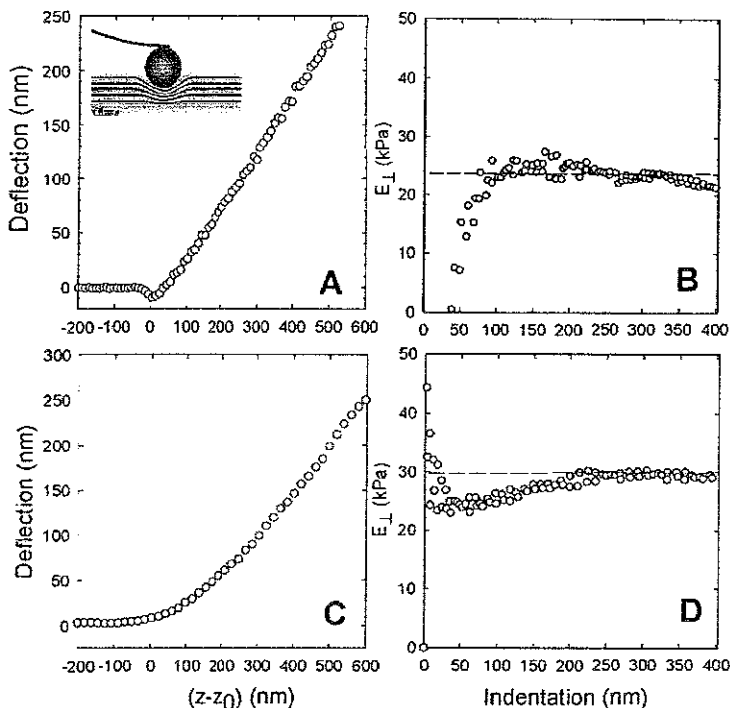


**Figure 1.** Indentation curves obtained by atomic force microscopy and the corresponding Young's Modulus, which was calculated as a function of the indentation by fitting each data point independently with the finite thickness corrected Hertz sphere model (eq 1) after determination of the contact point  $z_0$ : (A, B) determination for a (PLL/HA)<sub>20</sub> film (4  $\mu\text{m}$  thick) and (C,D) for a polyacrylamide gel (70  $\mu\text{m}$  thick). The Young's modulus of the sample was taken to be the plateau value (dashed lines).

were added to PA gel solutions, composed of 5–10% acrylamide monomer, 0.03–0.3% bis-acrylamide cross-linker, and 1% bead spacers, 25  $\mu\text{L}$  drops of polymerizing gel solution were placed on glutaraldehyde-treated aminosilanized coverslips, which covalently bound the gels. Chlorosilanized coverslips were placed on top of the PA, and weights were added to ensure that the gel thickness was defined by the spacer bead diameter. For PA gels between 10 and 70  $\mu\text{m}$  thick, the droplet volume was used to control gel height. All gel heights were confirmed by light microscopy. Substrate attachment of collagen was measured with 10:1 collagen/FITC-collagen mixture and compared to standard slides of known fluorescent collagen<sup>23,37</sup> in order to calibrate the amount of surface bond collagen.

**Atomic Force Microscopy Characterization of Films and Gels.** The force–distances curves were acquired at room temperature with an Asylum 1-D AFM (Asylum Research; Santa Barbara, CA). The PA gels and (PLL/HA)<sub>t</sub> films were tested in liquid (respectively phosphate buffered saline (PBS) for the PA gels and 0.15 M NaCl for the PEM films) with borosilicate sphere tipped cantilever ( $R = 2.5 \mu\text{m}$ ; Bioforce Nanoscience; Ames, IA) having a spring constant of  $\sim 60$  pN/nm, which was confirmed by a thermal fluctuations method.<sup>39</sup> Indentation velocity of the cantilever was kept constant at 2  $\mu\text{m}/\text{s}$ . Indentation ( $\delta$ ) is obtained by subtracting the deflection ( $d$ ) to the movement of the piezoelectric ceramic ( $\Delta z = z - z_0$ ) in  $z$  direction, where  $z_0$  is the contact point. The contact point ( $z_0$ ) was determined following the method proposed by Domke and Radmacher<sup>28</sup> using an

automatic least-squares fitting procedure in the deflection range 10–100 nm.

**Data Analysis.** For each point of the approach curve, the Young modulus ( $E_{\perp}$ ) was determined for PLL/HA and PA gels (Figure 1A,B) by fitting the  $X-Y$  curve using the finite thickness corrected Hertz sphere model (Dimitriadis et al. 2002). According to this model, which is applicable when the sample is bonded to the substrate, the relation between the Young modulus ( $E_{\perp}$ ), force ( $F$ ), indentation ( $\delta$ ), Poisson's ratio ( $\nu$ ), radius of the sphere tip ( $R$ ), and sample thickness ( $h$ ) is the following:

$$F = 4 \frac{4E}{3(1-\nu^2)} R^{1/2} \delta^{3/2} \left[ 1 - \frac{2\alpha_0}{\pi} \chi + \frac{4\alpha_0^2}{\pi^2} \chi^2 - \frac{8}{\pi^3} \left( \alpha_0^3 - \frac{4\pi^2}{15} \right) \chi^3 + \frac{16\alpha_0}{\pi^4} \left( \alpha_0^3 - \frac{3\pi^2}{5} \beta_0 \right) \chi^4 \right]$$

$$\alpha_0 = \frac{1.2876 - 1.4789\nu + 1.3442\nu^2}{1-\nu}$$

$$\beta_0 = \frac{0.6387 - 1.0277\nu + 1.5164\nu^2}{1-\nu}$$

The model is valid for  $\delta \leq 0.1 h$ , e.g., for indentation less than 10% of the sample thickness. In the case of the (PLL/HA) films, sample thickness is at least 3–4  $\mu\text{m}$  and in the range  $\sim 0.1 R_C \leq h \leq \sim 13 R_C$ , where  $h$  is sample thickness and  $R_C$  is the contact radius of the indenter.<sup>29</sup> As the samples

D Richert et al.

were highly hydrated,  $\nu$  is taken equal to 0.5. A mean value of  $E$  was calculated by averaging the values of  $E$  over the plateau zone on the  $E$  versus indentation curve (Figure 1). Four different areas were tested for each sample.

**Cell Culture.** A7r5 smooth muscle cells (SMC) were maintained in polystyrene flasks between passages 2 and 15, and cultured in media containing DMEM, supplemented with 10% of fetal bovine serum and antibiotics. Cells were passed every 3 days, when reaching  $\sim 80\%$  confluence, and plated on various substrates at  $\sim 1 \times 10^4$  cells/dish for experiments. Prior to cell plating, collagen type I adsorbed to all substrates (total adsorbed amounts of 300–3000 ng/cm<sup>2</sup>) for 12 h at 37 °C. Substrates were either glass-bottom 35 mm dishes (Mattek Corporation; Ashland, MA) or coverslips coated with the relevant thin films. Cell images were taken after 4 h of incubation and fixation with a 10% formaldehyde solution and mounting (Biomedica; Foster City, CA).

Cell culture supplies were obtained from Invitrogen, Life Technologies (Carlsbad, CA); all other supplies were from Sigma (St. Louis, MO) unless noted. Image analysis of projected cell area was performed with Scion Image (Frederick, MD), and is displayed as an average ( $\pm$  standard error of the mean (SE)).

## Results

**Film Observation and Thickness Determination.** Multilayers of PLL as the polycation alternating with HA as the polyanion were prepared on glass slides with 20, 40, or 60 layer pairs, i.e., (PLL/HA)<sub>20</sub>, (PLL/HA)<sub>40</sub>, and (PLL/HA)<sub>60</sub>. A large number of layers was chosen in order to build a film several microns thick to minimize the influence of the stiff underlying glass substrate. For AFM indentation measurements with a sphere of radius 2.5  $\mu\text{m}$ , the thickness-corrected Hertz model is valid for films  $>1 \mu\text{m}$  thick. Calculating the Young's modulus of the films using the AFM data and eqs 1 and 2, requires knowing film thickness, which can be easily determined by means of confocal laser scanning microscopy (CLSM) and fluorescently labeled PLL<sup>16,20</sup> on z-section images obtained by CLSM, the green band corresponds to the diffuse PLL (Figure 2). As a function of layer number, the thickness is found to increase exponentially up to about 40 pairs of layers and then growth slows down. This is although immersion time and rinsing times are kept constant (respectively 10 and 5 min). Cross-linked films, which appear dimmer, are thicker than un-cross-linked films by up to 20%. This is most evident for films with a large number of layers and can be explained perhaps by a pH change within the films during cross-linking: the films are prepared at pH 6.5 and then cross-linked at pH 5. Such a change can swell these films as recently reported for (PLL/HA) films built in water at different pHs.<sup>40</sup> Once cross-linked, however, the film thickness remains stable.

**Young's Moduli on Native PEM Films.** The AFM has long been used as a nanoindenter<sup>41</sup> to measure the elastic properties on a wide range of materials.<sup>42,43</sup> Quantitative measurements are not straightforward due to factors such as nonnormal loading conditions, difficulty in determining the geometric interaction area on nano/microscale and possibili-

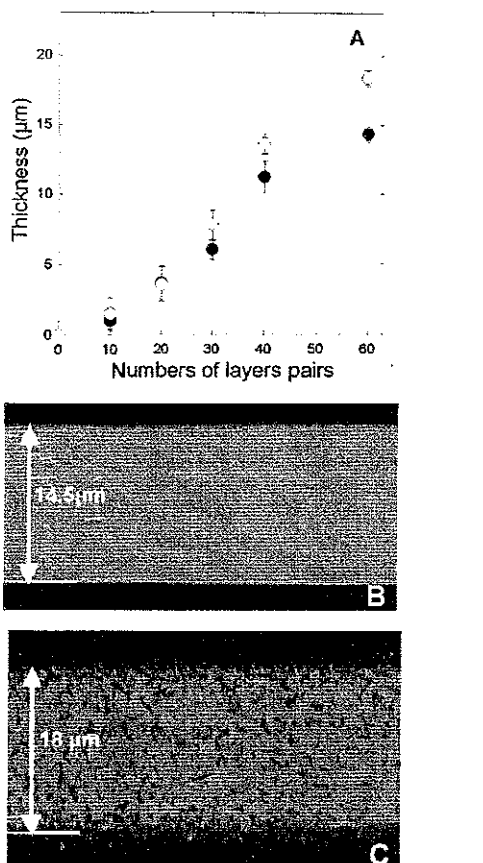


**Figure 2.** (A) Thickness of (PLL/HA)<sub>n</sub> films as a function of the number of layer pairs, as measured by CLSM for native (I) and cross-linked (O) films. Error bars are SE of the mean. The thickness was measured using PLL-FITC as the last layer for visualizing the diffusion of PLL-FITC in z sections through native (B) and cross-linked (C) films (in this example for (PLL/HA)<sub>20</sub> films). The glass substrate is indicated by a white line. For the cross-linked films, the images were systematically noisier.

ties of irreversible deformation due to large pressures developed at the indenting tip. Measuring the elasticity of polymeric films of various types may not seem difficult when compared to the complex structure, loading conditions, and viscoelasticity of biological systems such as tissues. However, in the thin film limit, defects, rigid supports, and surface forces can all prove a significant complication. In this study, relatively thin films of several microns, which are considered thick for PEM, were tested with borosilicate sphere-tipped cantilevers ( $R = 2.5 \mu\text{m}$ ) having a suitable spring constant (60 pN/m).<sup>35</sup> Force-indentation profiles from these samples were fit with a Hertz sphere model using a thin film correction appropriate when  $h \leq 13 R_c$ ,  $R_c$  being the contact radius of the indenter.<sup>29</sup> In this limit, the importance of a thickness correction and larger contact area increased exponentially relative to the semi-infinite substrate usually assumed for the sphere model.<sup>28,44–46</sup> In a recent work, Engler et al.<sup>35</sup> acquired force indentation profiles on homogeneous polyacrylamide gels using pyramid-tipped cantilevers and sphere tips cantilevers. In the former case, the Hertz cone

*Biomacromolecules*

model was used for the analysis whereas the Hertz sphere model was used in the latter. However, both models agreed. Recently, Uricanu et al.<sup>32</sup> determined the Young's modulus of gelatin gels using the Hertz model. They also used the Johnson, Kendall, and Robert (JKR) theory of adhesion mechanics to estimate the adhesion force between a silicone nitride tip and gelatin. This theory generally accounts for the short-range attractive forces local to the region of contact which typically can increase the contact area of the probe. However, they found a very weak adhesion (of the order of 2 nN) and concluded that the contact is limited only to the indentation region. The JKR model is particularly used for stiff substrates (GPa) and stiff probes ( $k > 0.5$  N/m). The probes used in our study have a low stiffness of 0.06 N/m. In the present case, samples were indented at rates of  $\sim 2 \mu\text{m/s}$ , which is generally sufficient to explore relatively reversible and elastic rather than viscoelastic properties of cells, matrix, or substrates.<sup>34</sup> Slower indentations on time scales of minutes or even hours are likely to be more relevant to sustained cell tractions in cell spreading. For this reason and also because PEM have layer symmetry, i.e., they are orthotropic, we refer to the elastic modulus obtained from fits of the Hertz model as an apparent or effective perpendicular Young's modulus in the z direction,  $E_1$ . Qualifications on this modulus arise in part because the layer-by-layer formation process leads to orthotropic rather than isotropic symmetry; hence, measurements perpendicular to the layer symmetry give only a modulus in that direction. Additionally, the PLL molecules have been found to reorganize as PLL diffuses throughout the film.<sup>16,20</sup>  $E_{\text{app}}$  for PLL/HA films is thus an apparent modulus with an implicit time scale.

The Young's moduli of the various  $(\text{PLL}/\text{HA})_i$  films (with  $i = 20, 40, 60$ ) were obtained by fitting the raw data per the Hertz sphere model as shown in Figure 3. In the first part of the indentation curve, there was always a transition zone in which the Young's modulus deviates from the plateau value. This kind of behavior has also been observed for other types of gels, such as poly(vinyl alcohol)<sup>29</sup> and gelatin.<sup>32</sup> Therefore,  $E_1$  was taken at the plateau value.  $E_1$  is of the order of 40–90 kPa for the un-cross-linked films. The modulus decreases as the number of layers in the films increases, suggesting that the films become softer as their thickness is increased, potentially due to greater hydration of the upper layers of the film. These effective values appear around 10-fold stiffer than the typical range of PA gel elasticity at similar thickness (8 kPa for a gel of 5% acrylamide).<sup>35</sup> For these latter gels,  $E_{\text{gel}}$  proves independent of thickness over the 5–70  $\mu\text{m}$  range of film thickness, but the modulus determination by AFM on 5  $\mu\text{m}$  substrates required a correction for film thickness.

The decrease in Young's modulus as a function of thickness for the PEM films cannot be attributed to a change in surface structure, nor to an increased heterogeneity or roughness of the surface. In fact, in contrary to other films whose exponential growth has been related to an increased surface roughness,<sup>47,48</sup> AFM images on  $(\text{PLL}/\text{HA})_i$  films showed that the films have a nanometer roughness. Indeed, for these films, the exponential growth was attributed to the diffusion of the PLL.<sup>16</sup> The decrease can neither be attributed

## Elasticity of Polyelectrolyte Multilayer Films E

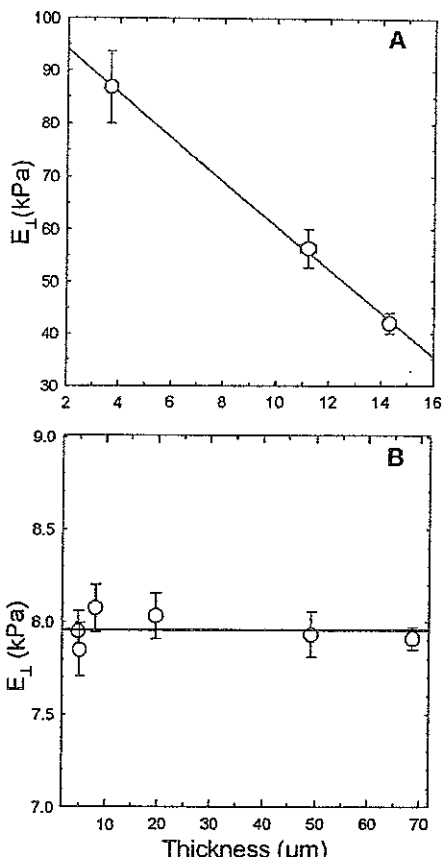


Figure 3. Young's Modulus as a function of film thickness for native  $(\text{PLL}/\text{HA})_i$  films (A) and polyacrylamide gels (B) as measured by colloidal probe AFM with a sphere tip of radius 2.5  $\mu\text{m}$  as indenter. Films of various thicknesses were obtained by varying the number of layer pairs for the PEM films and the spacer beads for the PA gels. The data were analyzed using the finite thickness corrected Hertz sphere model (eq 1). Error bars are the SE of the mean.

to the Hertz model used for data analysis, since the moduli prove independent of the height of PA gels in this thickness range.

Yet, this kind of multilayer, based on a highly swellable polysaccharide such as HA, is a swollen hydrogel as are PA gels. Differences in density, pore size, hydration, and cross-linking between monomer units are all likely to lead to very different properties. Nonetheless, the range of values are comparable to those found by AFM measurements on other soft biological gels, such as gelatin, collagen, or agarose as listed in Table 1.

Such AFM measurements contain several possible sources of error that include calibration of the cantilever, determination of the contact point, inadequacy of the model used to analyze the data, heterogeneity of the surface, and variability between samples. The calibration is done repeatedly (5–10 times) and averaged, giving a value generally within 10% of the manufacturer's value and thus affecting the Young's modulus by a similar amount. The error in the determination of the contact point is minimized by a least-squares fit fitting, and the  $(\text{PLL}/\text{HA})_i$  films have just nanometer scale rough-

F Richert et al.

Biomacromolecules

**Table 1.** Young's Modulus of Various Soft Polymers, Either Synthetic or Natural, Including Cells and of Polyelectrolyte Multilayer Films as Determined by AFM in Force Mode<sup>a</sup>

	film	geometry of indenter	Young's modulus	ref
polymer gels	poly(vinyl alcohol) concentration 1.6%	sphere	5.8 kPa	29
	polyacrylamide gels various bis-acrylamide content	sphere	1–35 kPa	35
biological gels	gelatin in water at various pH	sphere	1–9 kPa	49
	gelatin (10%) in dodecane	pyramidal	100 kPa	32
	gelatin (0.5%) thin films (1.1 $\mu\text{m}$ ) dried overnight	pyramidal	20 kPa	28
	chitosan/gelatin in buffer solution	cone	0.14–1.2 MPa	50
	agarose (3%)	pyramidal/sphere	25 kPa	51
cells	fibroblasts, endothelial cells, macrophages	cone/pyramidal tip	1–7 kPa	34,52,53
	cartilage	parabolic cone	0.16–0.6 MPa	54
other PEM films	(PSS/PAH) hollow capsules	sphere tip combined with RICM	1.3–1.9 GPa	25
	(PAH/P-azo) 1 $\mu\text{m}$ thick	cone	100 kPa–10 MPa	33

<sup>a</sup>The geometry of the indenter is also indicated.

396 ness. Finally, several locations were probed in one sample,  
 397 so as to average the values obtained for a given sample. All  
 398 together, one can estimate an uncertainty of about 30% for  
 399 the measured values. As a systematic error, this would not  
 400 change the trends, such as the differences between different  
 401 film types.

402 Few other studies have dealt with determination of  
 403 polyelectrolyte multilayer mechanical properties. Mermut et  
 404 al.<sup>33</sup> reported a Young's modulus in the range of 100 kPa to  
 405 10 MPa for poly(allylamine hydrochloride) (PAH)/azoben-  
 406 zene-containing polyelectrolyte films. This is of the same  
 407 order of magnitude or even higher than (PLL/HA)<sub>n</sub> films,  
 408 which may be explained by the increased rigidity of PAH  
 409 as compared to PLL or HA. Hollow shells of dense (PSS/  
 410 PAH)<sub>n</sub> multilayers have been investigated by osmotic defla-  
 411 tion and swelling<sup>24</sup> or by AFM colloidal probes in combi-  
 412 nation with reflection interference contrast microscopy.<sup>25</sup> In  
 413 either case, the values of  $E$  reported for the (PSS/PAH) films  
 414 were 4 orders of magnitude higher than for the (PLL/HA)<sub>n</sub>  
 415 films here. Besides differences in experimental techniques,  
 416 differences may be explained by the small shell thicknesses  
 417 and high density of (PSS/PAH)<sub>10</sub> films which lowers their  
 418 hydration relative to our PLL/HA films. These PSS/PAH  
 419 films are ~50 nm in thickness with a refractive index of  
 420 about 1.5 (determined by optical waveguide lightmode  
 421 spectroscopy<sup>55,56</sup>), as compared to thick and watery micron-  
 422 thick (PLL/HA)<sub>10</sub> films whose refractive index of ~1.37 is  
 423 obviously very close to that of water.<sup>13</sup> It was also recently  
 424 shown by QCM applied to a binary mixture of polyanions  
 425 (poly(L-glutamic acid) and PSS) and PAH as the polycation<sup>57</sup>  
 426 that the films are much stiffer than those made of a single  
 427 mixture of polyelectrolytes. Mamedov et al.<sup>58</sup> have also  
 428 shown by micro-traction experiments that the Young's  
 429 modulus of free-standing membranes made of single wall  
 430 nanotubes (SWNT)/polyelectrolyte can reach 250 MPa. This  
 431 is well above our estimates and is probably due to rigidifi-  
 432 cation of the membrane by the SWNT.

433 **Aging of the Films.** Figure 4 shows the evolution of  $E_{\perp}$   
 434 for (PLL/HA)<sub>40</sub> film over a period of 1–8 weeks after the  
 435 buildup of the films (the film being kept at 4 °C meanwhile).  
 436 The Young's modulus has doubled from 29 to 57 kPa  
 437 between the first and second weeks. Then, its value tends to  
 438 a plateau at around 40 kPa. Similar behaviors were found  
 439 for films containing 20 and 60 pairs of layers. This evolution

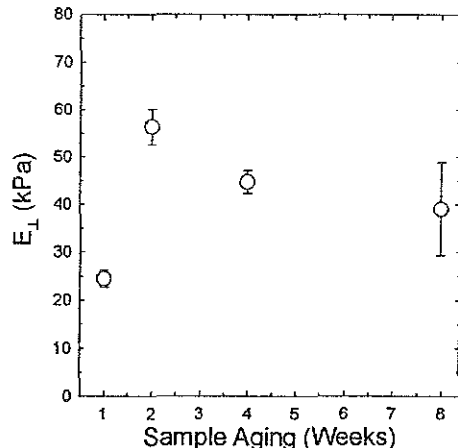
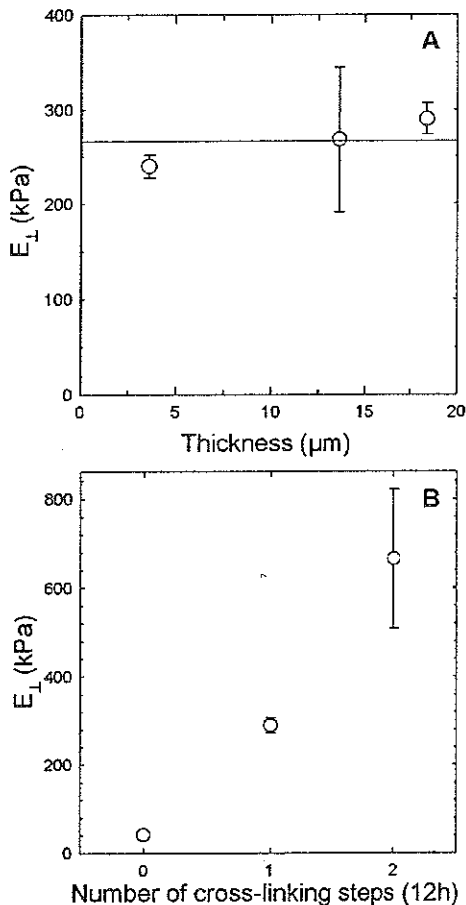


Figure 4. Evolution of the Young's modulus as a function of sample aging (in weeks) for a native (PLL/HA)<sub>40</sub> film. The films were built up in 0.15 M NaCl and stored at 4 °C in the same solution until use. Error bars are SE of the mean.

is not due to a change in film thickness, as was checked by CLSM over a month period. As PLL and HA are weak polyelectrolytes and as PLL is able to diffuse within the films,<sup>16</sup> the change in  $E_{\perp}$  is likely due to a reorganization or thinning of the film's layers. This is not at all surprising given comparisons with the creeping flow known for soft, wet polymers. In addition, recent work on the structure of poly(L-lysine)/poly(L-glutamic) films investigated by means of surface force apparatus<sup>59</sup> demonstrated that film structure evolves in time, with the outermost portions of the film being a "brush" whose thickness decreases with age.

**Influence of Film Cross-Linking.** PLL/HA films can be covalently cross-linked with a water soluble carbodiimide, EDC, in combination with sulfo-NHS.<sup>20</sup> Recently, EDC alone has also been used to cross-link hollow capsules made of poly(acrylic acid)/PAH (PAA/PAH).<sup>60</sup> This chemical cross-linking leads to the formation of amide bonds between primary amines in PLL and carboxylate groups in HA. Cross-linking reduces the diffusivity of PLL in the films to nearly zero, but it may not limit viscoelastic mechanisms involving solvent flow or unbound polyelectrolytes. Thus, the multilayer maintains a more orthotropic symmetry where the elastic modulus has an *apparent*  $E_{\perp}$  normal to the layer. It



**Figure 5.** Young's modulus as a function of film thickness for cross-linked  $(\text{PLL}/\text{HA})_i$  films (A). Film thickness was varied by increasing the number of layer pairs ( $i = 20, 40, 60$ ). For these measurements, the cross-linking protocol was performed only once. (B) Evolution of the Young modulus of a native  $(\text{PLL}/\text{HA})_{60}$  that was subsequently cross-linked once or twice. Cross-linking was achieved by putting the film in contact with the EDC/sNHS solution at room temperature for 12 h and was repeated a second time with fresh reagents. Error bars are SE of the mean.

also leads to a dramatic change in chondrosarcoma cell adhesion: the native films are not adhesive whereas as the cross-linked ones are highly adhesive.<sup>20</sup> To quantify the change in the rigidity of the films after cross-linking, the native  $(\text{PLL}/\text{HA})_i$  films containing an increasing number of layers were cross-linked and studied again by AFM indentation.

In Figure 5A,  $E_{\perp}$  is shown for films of different thickness. Based again on CLSM observations, we determine cross-linked film thicknesses, which proved slightly higher than the native films.  $E_{\perp}$  for all of the cross-linked films lies in the range 250–300 kPa. This 4–6-fold increase in stiffness relative to native films is undoubtedly due to the covalent bonds that supplement the purely physical ionic cross-links of native films. However, for the cross-linked films,  $E_{\perp}$  did not depend on the film thickness ( $p = 0.637$ ). Stiffening from these covalent bonds implies that polymer chains in the

pristine PEM are not so strongly cross-linked to each other, which mirrors the cross-link-dependent stiffness of PA gels.<sup>35</sup>

As a consequence of film cross-linking, the force–distance curve exhibited a different profile particularly during the retraction phase of AFM indentation. Whereas tip adhesion<sup>44</sup> or capillary bridges<sup>32</sup> to native films held the cantilever back from returning its initial position, no hysteresis was seen during tip retraction off of a cross-linked film. Hysteresis might also originate from viscous dissipation,<sup>61</sup> but since the surface zeta potential of the HA ending films remains negative upon cross-linking, the difference in hysteresis cannot be explained by a change in surface zeta potential. The present thin film model used for data analysis here does not account for any viscous component in film rheology, but such a response may be relevant at the typical tip velocities used in indentation.

We also investigated the influence of the number of cross-linking steps on the effective Young's modulus. As can be seen in Figure 5B for a  $(\text{PLL}/\text{HA})_{40}$  film, the cross-linking is incomplete after the first cross-linking cycle, since the modulus increases 2-fold between the first and second step. A similar trend was observed for films containing 20 and 60 layer pairs. The variance in  $E_{\perp}$  grows with cross-linking steps, indicating that the local surface heterogeneity of the films is higher after cross-linking.

The effect of film cross-linking on  $E_{\perp}$  is not especially surprising, since the degree of cross-linking is known to influence  $E$  for other gel systems. For PA gels, the Young's modulus increases with cross-linker concentration; for example,  $E_{\perp}$  doubles as bis-acrylamide concentration is increased from 0.1% to 0.3%.<sup>23</sup> Likewise, the Young's modulus of poly-*N*-isopropylamide hydrogels strongly depends on the cross-linker concentration.<sup>62</sup>

**Spreading of SMCs on Native and Cross-Linked Multilayer Films.** PEM films are being widely considered and applied in biomaterial applications, with one envisioned application being the coating of stents used to reexpand blocked blood vessels. Stents have a complex and cylindrically expandable geometry, and the idea is that a deformable coating would modulate stent interactions with blood as well as tissue cells. Proliferation of vascular smooth muscle cells (SMC) into and onto stents can be a significant problem in stent failure, and so adhesive interactions of SMC with candidate PEM films is an important criteria for qualification. How cells respond to physical properties of constant chemistry films is also an open and active issue of wide importance.

For PA gel substrates of varied stiffness, it has been shown that cell adhesion and spreading depends on gel stiffness for a wide range of collagen surface densities.<sup>23,63,64,65</sup> This “substrate stiffness” dependence has been reported for cell types ranging from fibroblasts and neurons to muscle cells. In the experiments here, A7r5 smooth muscle cells (aorta-derived cell line) were plated on collagen-coated substrates of varying stiffness to address the influence of the elastic modulus on cell spreading.

To study cell spreading on these multilayers, we first adsorbed collagen-I onto the surface of both the native and cross-linked multilayers. Surface concentrations similar to

H Richert et al.

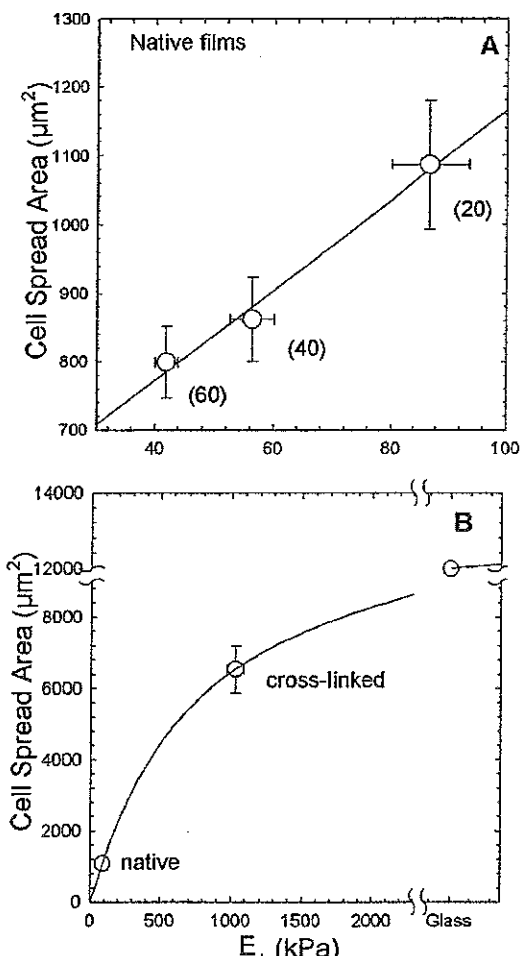
*Biomacromolecules*

Figure 6. Comparison of smooth muscle cell spread area on native (PLL/HA)<sub>60</sub> films and on cross-linked films of different stiffness after 4 h of adhesion: (A) for the native films of increased stiffness (B) for native and cross-linked (PLL/HA)<sub>i2</sub> films, as compared to a glass substrate. All the substrates have been coated with collagen prior to cell plating. Error bars are SE of the mean.

PA gels that gave “optimal” spreading were sought (i.e., 200–700 ng/cm<sup>2</sup>). These surface concentrations were readily achieved by overnight incubations and were verified, as with the PA gels, by use of calibrated imaging of fluorescent collagen (see Methods). Z-section imaging by confocal microscopy suggested slightly higher surface-average densities of collagen on the native multilayer films as compared to the cross-linked ones.

Projected cell area (4 h after plating and incubation) was used as a simple measure of adhesion and quantified from cell images of 10% formaldehyde fixed cells plus mounting media. Results are displayed in Figure 6 as an average ( $\pm$  standard error of the mean) with paired t-tests to determine significance.

As shown in Figure 6A, the projected cell area of the SMC is greater when the film stiffness is higher, e.g., for films containing 20 layer pairs. However, in all cases, most of the cells had a round morphology. On (PLL/HA)<sub>60</sub> films, cell

spreading is around ~40% more than on the softer (PLL/HA)<sub>60</sub> films. These results may be related to the decrease in adhesion force of chondrosarcoma cells already measured on poly(L-lysine)/poly-L-glutamic films when the film thickness increased.<sup>66</sup> Interestingly, these results also look similar to those found for much thicker PA gels, for which it was shown that SMC spreading generally increase with  $E$ .<sup>23</sup>

With increasing stiffness, thin, collagen-coated PLL/HA substrates promoted spreading analogous to PA gels.<sup>35</sup> The apparent elasticity scale for the multilayer results is not equivalent: multilayers are stiffer than PA gels but less adhesive. The difference may be attributed to the slow polymer diffusion within the multilayers on long time scales. It should be kept in mind that elasticity measurements here take just several seconds (at rates of  $\mu\text{m/sec}$ ). Longer time scales of minutes to hours seem more relevant for cell spreading. For films that have been cross-linked twice, cell spread area is increased by a factor of about ~10 (Figure 6B); cells spread nicely on these latter films, likely due to cells “feeling” the underlying solidity of the substrate through stable cross-links within the film that are lacking in the hydrated, native films.

Parallel studies on primary chondrocytes assessed cell viability on (PLL/HA)<sub>12</sub> films after 6 days in culture using the MTT test. The results obtained by the MTT test for the primary chondrocytes after 6 days in culture agreed with those found on the SMC cell line: the cross-linked films are more favorable for the long term adhesion of viable cells. These results support what we already very qualitatively observed for HCS 2/8 (a chondrosarcoma cell line) adhesion on (PLL/HA)<sub>12</sub>: after few hours of plating, the cells kept a round shape on the native films whereas they had already began to nicely spread on the cross-linked ones.<sup>20</sup>

## Conclusion

Surface probe measurements of local elasticity allow the effective perpendicular Young's modulus  $E_{\perp}$  of micrometer thick polyelectrolyte multilayers to be determined. The Young's modulus for native films was found to be dependent on the thickness of the films, with thicker films being softer. PA gels of a constant formulation have, in contrast, a constant elasticity. The evolution of PEMs'  $E_{\perp}$  as a function of the time could be followed over several weeks. Once the films were covalently cross-linked using water soluble carbodiimide, the films appear 6–8-fold stiffer. The number of cross-linking steps also has an influence, with the Young's modulus increasing with the number of steps. Finally, the spread area of smooth muscle cells was found to increase with the film stiffness. Stiffer films are thus preferred in terms of cell adhesion. The differences are most striking if one compares native versus cross-linked films. Altogether, these results not only show that PEM films vary in stiffness but also that cells can sense this, consistent with emerging ideas that cells are very tactile in their adhesive processes.

**Acknowledgment.** The authors thank Dr. Jean-Claude Voegel for access to all of the facilities of his laboratory as

## Biomacromolecules PAGE EST: 8.9

612 well as for financial support and Dr. Bernard Senger for  
 613 fruitful discussion regarding data analysis.

## References and Notes

- (1) Decher, G.; Hong, J. D.; Schmitt, J. *Thin Solid Films* 1992, 210–211, 831–835.
- (2) Decher, G. *Science* 1997, 277, 1232–1237.
- (3) Thierry, B.; Winnik, F. M.; Merli, Y.; Silver, J.; Tabrizian, M. *Biomacromolecules* 2003, 4, 1564–1571.
- (4) Tan, Q.; Ji, J.; Barbosa, M. A.; Fonseca, C.; Shen, J. *Biomaterials* 2003, 24, 4699–4705.
- (5) Vautier, D.; Hemmerlé, J.; Vodouhe, C.; Koenig, G.; Richert, L.; Picart, C.; Voegel, J.-C.; Debry, C.; Chluba, J.; Ogier, J. *Cell Motility Cytoskeleton* 2003, 56, 147–158.
- (6) Hiller, J.; Mendelsohn, J. D.; Rubner, M. F. *Nat. Mater.* 2002, 1, 59–63.
- (7) Rmaile, H. H.; Schlenoff, J. B. *J. Am. Chem. Soc.* 2003, 125, 6602–6603.
- (8) Ge, L.; Mohwald, H.; Li, J. *Chemistry* 2003, 9, 2589–2594.
- (9) Jessel, N.; Schwinté, P.; Falvey, P.; Darcy, R.; Harkel, Y.; Schaaf, P.; Voegel, J.-C.; Ogier, J. *Adv. Funct. Mater.* 2004, 14, 174–182.
- (10) Fery, A.; Schönler, B.; Cassagnau, T.; Caruso, F. *Langmuir* 2001, 17, 3779–3783.
- (11) Shiratori, S. S.; Rubner, M. F. *Macromolecules* 2000, 33, 4213–4219.
- (12) Serizawa, T.; Yamaguchi, M.; Akashi, M. *Macromolecules* 2002, 35, 8656.
- (13) Picart, C.; Lavalle, P.; Hubert, P.; Cuisinier, F. G.; Decher, G.; Schaaf, P.; Voegel, J.-C. *Langmuir* 2001, 17, 7414–7424.
- (14) Richert, L.; Lavalle, P.; Payan, E.; Stoltz, J.-F.; Shu, X. Z.; Prestwich, G. D.; Schaaf, P.; Voegel, J.-C.; Picart, C. *Langmuir* 2004, 1, 284–294.
- (15) Sinani, V. A.; Koktysh, D. S.; Yun, B.-G.; Matts, R. L.; Pappas, T. C.; Motamedi, M.; Thomas, S. N.; Kotov, N. A. *Nano Lett.* 2003, 3, 1177–1182.
- (16) Picart, C.; Mutterer, J.; Richert, L.; Luo, Y.; Prestwich, G. D.; Schaaf, P.; Voegel, J.-C.; Lavalle, P. P. *Natl. Acad. Sci. USA* 2002, 99, 12531–12535.
- (17) Mendelsohn, J. D.; Yang, S. Y.; Hiller, J.; Hochbaum, A. I.; Rubner, M. F. *Biomacromolecules* 2003, 4, 96–106.
- (18) Boura, C.; Menu, P.; Payan, E.; Picart, C.; Voegel, J.-C.; Muller, S.; Stoltz, J.-F. *Biomaterials* 2003, 24, 3521–3530.
- (19) Fattori, R.; Piva, T. *Lancet* 2003, 361, 247–249.
- (20) Richert, L.; Boulimedais, F.; Lavalle, P.; Mutterer, J.; Ferreux, E.; Decher, G.; Schaaf, P.; Voegel, J.-C.; Picart, C. *Biomacromolecules* 2004, 5, 284–294.
- (21) Koktysh, D. S.; Liang, X.; Yun, B. G.; Pastoriza-Santos, I.; Matts, R. L.; Giersig, M.; Serra-Rodríguez, C.; Liz-Marzáñ, L. M.; Kotov, N. A. *Adv. Funct. Mater.* 2002, 12, 255–265.
- (22) Lo, C. M.; Wang, H. B.; Dembo, M.; Wang, Y. L. *Biophys. J.* 2000, 79, 144–152.
- (23) Engler, A.; Bacakova, L.; Newman, C.; Hategan, A.; Griffin, M.; Discher, D. E. *Biophys. J.* 2004, 86, 617–628.
- (24) Gao, C.; Donath, E.; Moya, S.; Dudnik, V.; Mohwald, H. *Eur. Phys. J. E* 2001, 5, 21–27.
- (25) Dubreuil, F.; Elsner, N.; Fery, A. *Eur. Phys. J. E* 2003, 12, 215–221.
- (26) Tang, Z.; Kotov, N. A.; Magonov, S.; Ozturk, B. *Nat. Mater.* 2003, 2, 413–418.
- (27) Mukhopadhyay, A.; Steve, G. *Curr. Opin. Colloid Interface Sci.* 2001, 6, 423–429.
- (28) Domke, J.; Radmacher, M. *Langmuir* 1998, 14, 3320–3325.
- (29) Dimitriadis, E. K.; Horkay, F.; Maresca, J.; Kachar, B.; Chadwick, R. S. *Biophys. J.* 2002, 82, 2798–2810.
- (30) McAloney, R. A.; Dudnik, V.; Goh, M. C. *Langmuir* 2003, 19, 3947–3952.
- (31) Lavalle, P.; Gergely, C.; Cuisinier, F.; Decher, G.; Schaaf, P.; Voegel, J.-C.; Picart, C. *Macromolecules* 2002, 35, 4458–4465.
- (32) Uricaru, V. I.; Duits, M. H. G.; Nelissen, R. M. F.; Bennink, M.; Mellema, J. *Langmuir* 2003, 19, 8182–8194.
- (33) Mermut, O.; Lefebvre, J.; Gray, D. G.; Barrett, C. J. *Macromolecules* 2003, 36, 8819–8824.
- (34) Mahaffy, R. E.; Shit, C. K.; MacKintosh, F. C.; Kas, J. *Phys. Rev. Lett.* 2000, 85, 880–883.
- (35) Engler, A.; Richert, L.; Wong, J. Y.; Picart, C.; Discher, D. E. *Surf. Sci.* 2004, in press.
- (36) Hermanson, G. T. In *Bioconjugate techniques*; Academic Press: New York, 1996; pp 169–176.
- (37) Gaudet, C.; Marganski, W. A.; Kim, S.; Brown, C. T.; Gunderia, V.; Dembo, M.; Wong, J. Y. *Biophys. J.* 2003, 85, 3329–3335.
- (38) Wang, Y. L.; Pelham, R. J., Jr. *Methods Enzymol.* 1998, 298, 489–496.
- (39) Thundat, T.; Warrack, R. J.; Chen, G. Y.; Allison, D. P. *Appl. Phys. Lett.* 1994, 64, 2894–2896.
- (40) Burke, S. E.; Barrett, C. J. *Biomacromolecules* 2003, 4, 1773–1783.
- (41) Burnham, N. A.; Colton, R. J. *J. Vac. Sci. Technol.* 1989, A7, 2906–2913.
- (42) Chudoba, T.; Schwarzer, N.; Richter, F.; Beck, U. *Thin Solid Films* 2000, 377–378, 366–372.
- (43) Bhushan, B. *Wear* 2001, 250, 1105–1123.
- (44) Heinz, W. F.; Hoh, J. H. *Trends Biotechnol.* 1999, 17, 143–150.
- (45) Sneddon, I. N. *Int. J. Eng. Sci.* 1965, 3, 47–57.
- (46) Vinckier, A.; Semenza, G. *FEBS Lett.* 1998, 430, 12–16.
- (47) Ruths, J.; Essler, F.; Decher, G.; Riegler, H. *Langmuir* 2000, 16, 8871–8878.
- (48) DeLongchamp, D. M.; Kastantin, M.; Hammond, P. T. *Chem. Mater.* 2003, 15, 1575–1586.
- (49) Benmouna, F.; Johannsmann, D. *Langmuir* 2004, 20, 188–193.
- (50) Yao, K. D.; Liu, W. D.; Lin, Z.; Qiu, X. H. *Polym. Int.* 1998, 48, 794–798.
- (51) Costa, K. D.; Ho, M. M. Y.; Hung, C. T. In *Summer Bioengineering Conference*; Key Biscayne, Florida, 2003; pp 285–286.
- (52) Kataoka, N.; Kanso; Hashimoto, K.; Mochizuki, S.; Ogasawara, Y.; Sato, M.; Tsujioka, K.; Kajiya, F. *Proc. Natl. Acad. Sci. U.S.A.* 2002, 99, 15638–15643.
- (53) Reitsch, C.; Braet, F.; Wisse, E.; Radmacher, M. *Cell. Biol. Int.* 1997, 21, 685–696.
- (54) Weisenhorn, A. L.; Khorsandi, M.; Kasas, S.; Gotzos, V.; Butt, H. J. *Nanotechnology* 1993, 4, 106.
- (55) Picart, C.; Gergely, C.; Arntz, Y.; Schaaf, P.; Voegel, J.-C.; Cuisinier, F. G.; Senger, B. *Biosens. Bioelectron.* 2004, ASAP.
- (56) Picart, C.; Ladam, G.; Senger, B.; Voegel, J.-C.; Schaaf, P.; Cuisinier, F. J. G.; Gergely, C. *J. Chem. Phys.* 2001, 115, 1086–1094.
- (57) Hübsch, E.; Ball, V.; Senger, B.; Decher, G.; Voegel, J.-C.; Schaaf, P. *Langmuir* 2004, 20, 1980–1985.
- (58) Mamedov, A. A.; Kotov, N. A.; Prato, M.; Guldi, D. M.; Wicksted, J. P.; Hirsch, A. *Nat. Mater.* 2002, 1, 190–194.
- (59) Kulcsár, A.; Lavalle, P.; Voegel, J.-C.; Schaaf, P.; Kékicheff, P. *Langmuir* 2004, 20, 282–286.
- (60) Schuetz, P.; Caruso, F. *Adv. Funct. Mater.* 2003, 13, 929–937.
- (61) Mathur, A. B.; Collinsonworth, A. M.; Reichert, W. M.; Kraus, W. E.; Truskey, G. A. *J. Biomech.* 2001, 34, 1545–1553.
- (62) Matzelle, T. R.; Geuskens, G.; Kruse, N. *Macromolecules* 2003, 36, 2926–2931.
- (63) Flanagan, L. A.; Ju, Y. E.; Marg, B.; Osterfield, M.; Janmey, P. A. *Neuroreport* 2002, 13, 2411–2415.
- (64) Pelham, R. J., Jr.; Wang, Y. L. *Proc. Natl. Acad. Sci. U.S.A.* 1997, 94, 13661–13665.
- (65) Wong, J. Y.; Velasco, A.; Rajagopalan, P.; Pham, Q. *Langmuir* 2003, 19, 1908–1913.
- (66) Richert, L.; Lavalle, P.; Vautier, D.; Senger, B.; Stoltz, J.-F.; Schaaf, P.; Voegel, J.-C.; Picart, C. *Biomacromolecules* 2002, 3, 1170–1176.

## Elasticity of Polyelectrolyte Multilayer Films 1

- (67) BM0498023
- (68)
- (69)
- (70)
- (71)
- (72)
- (73)
- (74)
- (75)
- (76)
- (77)
- (78)
- (79)
- (80)
- (81)
- (82)
- (83)
- (84)
- (85)
- (86)
- (87)
- (88)
- (89)
- (90)
- (91)
- (92)
- (93)
- (94)
- (95)
- (96)
- (97)
- (98)
- (99)
- (100)
- (101)
- (102)
- (103)
- (104)
- (105)
- (106)
- (107)
- (108)
- (109)
- (110)
- (111)
- (112)
- (113)
- (114)
- (115)
- (116)
- (117)
- (118)
- (119)
- (120)
- (121)
- (122)
- (123)
- (124)
- (125)
- (126)
- (127)
- (128)
- (129)
- (130)
- (131)
- (132)
- (133)
- (134)
- (135)
- (136)
- (137)
- (138)
- (139)
- (140)
- (141)
- (142)
- (143)
- (144)
- (145)
- (146)
- (147)
- (148)
- (149)
- (150)
- (151)
- (152)
- (153)
- (154)
- (155)
- (156)
- (157)
- (158)
- (159)
- (160)
- (161)
- (162)
- (163)
- (164)
- (165)
- (166)
- (167)
- (168)
- (169)
- (170)
- (171)
- (172)
- (173)
- (174)
- (175)
- (176)
- (177)
- (178)
- (179)
- (180)
- (181)
- (182)
- (183)
- (184)
- (185)
- (186)
- (187)
- (188)
- (189)
- (190)
- (191)
- (192)
- (193)
- (194)
- (195)
- (196)
- (197)
- (198)
- (199)
- (200)
- (201)
- (202)
- (203)
- (204)
- (205)
- (206)
- (207)
- (208)
- (209)
- (210)
- (211)
- (212)
- (213)
- (214)
- (215)
- (216)
- (217)
- (218)
- (219)
- (220)
- (221)
- (222)
- (223)
- (224)
- (225)
- (226)
- (227)
- (228)
- (229)
- (230)
- (231)
- (232)
- (233)
- (234)
- (235)
- (236)
- (237)
- (238)
- (239)
- (240)
- (241)
- (242)
- (243)
- (244)
- (245)
- (246)
- (247)
- (248)
- (249)
- (250)
- (251)
- (252)
- (253)
- (254)
- (255)
- (256)
- (257)
- (258)
- (259)
- (260)
- (261)
- (262)
- (263)
- (264)
- (265)
- (266)
- (267)
- (268)
- (269)
- (270)
- (271)
- (272)
- (273)
- (274)
- (275)
- (276)
- (277)
- (278)
- (279)
- (280)
- (281)
- (282)
- (283)
- (284)
- (285)
- (286)
- (287)
- (288)
- (289)
- (290)
- (291)
- (292)
- (293)
- (294)
- (295)
- (296)
- (297)
- (298)
- (299)
- (300)
- (301)
- (302)
- (303)
- (304)
- (305)
- (306)
- (307)
- (308)
- (309)
- (310)
- (311)
- (312)
- (313)
- (314)
- (315)
- (316)
- (317)
- (318)
- (319)
- (320)
- (321)
- (322)
- (323)
- (324)
- (325)
- (326)
- (327)
- (328)
- (329)
- (330)
- (331)
- (332)
- (333)
- (334)
- (335)
- (336)
- (337)
- (338)
- (339)
- (340)
- (341)
- (342)
- (343)
- (344)
- (345)
- (346)
- (347)
- (348)
- (349)
- (350)
- (351)
- (352)
- (353)
- (354)
- (355)
- (356)
- (357)
- (358)
- (359)
- (360)
- (361)
- (362)
- (363)
- (364)
- (365)
- (366)
- (367)
- (368)
- (369)
- (370)
- (371)
- (372)
- (373)
- (374)
- (375)
- (376)
- (377)
- (378)
- (379)
- (380)
- (381)
- (382)
- (383)
- (384)
- (385)
- (386)
- (387)
- (388)
- (389)
- (390)
- (391)
- (392)
- (393)
- (394)
- (395)
- (396)
- (397)
- (398)
- (399)
- (400)
- (401)
- (402)
- (403)
- (404)
- (405)
- (406)
- (407)
- (408)
- (409)
- (410)
- (411)
- (412)
- (413)
- (414)
- (415)
- (416)
- (417)
- (418)
- (419)
- (420)
- (421)
- (422)
- (423)
- (424)
- (425)
- (426)
- (427)
- (428)
- (429)
- (430)
- (431)
- (432)
- (433)
- (434)
- (435)
- (436)
- (437)
- (438)
- (439)
- (440)
- (441)
- (442)
- (443)
- (444)
- (445)
- (446)
- (447)
- (448)
- (449)
- (450)
- (451)
- (452)
- (453)
- (454)
- (455)
- (456)
- (457)
- (458)
- (459)
- (460)
- (461)
- (462)
- (463)
- (464)
- (465)
- (466)
- (467)
- (468)
- (469)
- (470)
- (471)
- (472)
- (473)
- (474)
- (475)
- (476)
- (477)
- (478)
- (479)
- (480)
- (481)
- (482)
- (483)
- (484)
- (485)
- (486)
- (487)
- (488)
- (489)
- (490)
- (491)
- (492)
- (493)
- (494)
- (495)
- (496)
- (497)
- (498)
- (499)
- (500)
- (501)
- (502)
- (503)
- (504)
- (505)
- (506)
- (507)
- (508)
- (509)
- (510)
- (511)
- (512)
- (513)
- (514)
- (515)
- (516)
- (517)
- (518)
- (519)
- (520)
- (521)
- (522)
- (523)
- (524)
- (525)
- (526)
- (527)
- (528)
- (529)
- (530)
- (531)
- (532)
- (533)
- (534)
- (535)
- (536)
- (537)
- (538)
- (539)
- (540)
- (541)
- (542)
- (543)
- (544)
- (545)
- (546)
- (547)
- (548)
- (549)
- (550)
- (551)
- (552)
- (553)
- (554)
- (555)
- (556)
- (557)
- (558)
- (559)
- (560)
- (561)
- (562)
- (563)
- (564)
- (565)
- (566)
- (567)
- (568)
- (569)
- (570)
- (571)
- (572)
- (573)
- (574)
- (575)
- (576)
- (577)
- (578)
- (579)
- (580)
- (581)
- (582)
- (583)
- (584)
- (585)
- (586)
- (587)
- (588)
- (589)
- (590)
- (591)
- (592)
- (593)
- (594)
- (595)
- (596)
- (597)
- (598)
- (599)
- (600)
- (601)
- (602)
- (603)
- (604)
- (605)
- (606)
- (607)
- (608)
- (609)
- (610)
- (611)
- (612)
- (613)
- (614)
- (615)
- (616)
- (617)
- (618)
- (619)
- (620)
- (621)
- (622)
- (623)
- (624)
- (625)
- (626)
- (627)
- (628)
- (629)
- (630)
- (631)
- (632)
- (633)
- (634)
- (635)
- (636)
- (637)
- (638)
- (639)
- (640)
- (641)
- (642)
- (643)
- (644)
- (645)
- (646)
- (647)
- (648)
- (649)
- (650)
- (651)
- (652)
- (653)
- (654)
- (655)
- (656)
- (657)
- (658)
- (659)
- (660)
- (661)
- (662)
- (663)
- (664)
- (665)
- (666)
- (667)
- (668)
- (669)
- (670)
- (671)
- (672)
- (673)
- (674)
- (675)
- (676)
- (677)
- (678)

## 4.3 : Adhésion de chondrocytes sur des films natifs et réticulés : observations microscopiques.

### 4.3.1. Résumé 5

L'ensemble des résultats obtenus sur des films (PLL/HA) réticulés indique que leurs propriétés physico-chimiques et biologiques sont fortement modifiées par rapport aux films natifs. Dans le but d'utiliser de tels films comme traitement de surface d'implant, nous avons étudié plus précisément l'influence de la réticulation des films sur l'adhésion de cellules primaires de type chondrocytes plus exigeantes que les lignées cellulaires étudiées précédemment. Nous avons également étudié leur dégradation par des macrophages (THP-1). Nous avons également cherché à visualiser l'interaction cellule/film au moyen de techniques optiques comme la microscopie confocale et la microscopie à force atomique. Les films (PLL/HA) natifs sont dégradés par les macrophages. Les films natifs et réticulés ne sont pas cytotoxiques pour les chondrocytes. Cependant, les films natifs sont très peu favorables à l'adhésion cellulaire. Au contraire, les films réticulés permettent une prolifération de l'ordre de 75 % par rapport au verre alors qu'elle est inférieure à 10% pour les films natifs. Ces résultats sont indépendants de la couche terminale du film multicouche, les films terminés par PLL ou HA donnant des résultats similaires.

La dégradation du film par les macrophages (THP-1) a également été suivie par microscopie confocale. Après 48 h de contact, les macrophages ont internalisé la PLL et de nombreuses zones d'attaques sont visibles en microscopie confocale. En revanche, les films réticulés résistent à la dégradation par les macrophages sans pour autant être cytotoxiques.

Ces résultats ont été confirmés par des observations morphologiques du cytosquelette d'actine par microscopie de fluorescence. Le marquage immunologique du collagène de type II a également permis de confirmer le phénotype des chondrocytes. La structure des cellules a été aussi observée par microscope à force atomique. Les cellules s'étaient fortement sur les films réticulés et présentent une morphologie polygonale. Sur les films natifs, très peu de cellules restent adhérentes et elles sont rondes. De plus les observations en microscopie confocale associé à un marquage du cytosquelette permet de visualisé la déformation du film au niveau des cellules

#### 4.3.2. Article 5

## Primary chondrocytes adhesion onto native and cross-linked polyelectrolyte multilayer.

Ludovic Richert<sup>1</sup>, Dominique Vautier<sup>1</sup>, Laurent Grossin<sup>2</sup>, Elisabeth Payan<sup>2</sup>, Nadia Jessel<sup>1</sup>,  
Pierre Schaaf<sup>3,4</sup>, Jean-Claude Voegel<sup>1</sup>, Catherine Picart<sup>1,4\*</sup>

<sup>1</sup> Institut National de la Santé et de la Recherche Médicale, Unité 595, Faculté de Chirurgie Dentaire, Université Louis Pasteur, 11 rue Humann, 67085 Strasbourg Cedex, France

<sup>2</sup> Laboratoire de Physiopathologie et Pharmacologie Articulaires, UMR 7561 et IFR 111, Faculté de Médecine, 54 505 Vandoeuvre-les-Nancy, France

<sup>3</sup> Institut Charles Sadron, Centre National de la Recherche Scientifique, Université Louis Pasteur, 6 rue Boussingault, 67083 Strasbourg Cedex, France

<sup>4</sup> Ecole Européenne de Chimie, Polymères et Matériaux de Strasbourg, 25 rue Becquerel, 67087 Strasbourg Cedex 2, France

AUTHOR EMAIL ADDRESS : Catherine.Picart@medecine.u-strasbg.fr

#### TITLE RUNNING HEAD :

CORRESPONDING AUTHOR FOOTNOTE. Catherine Picart, INSERM U595, Faculté de Médecine, Bât 3, 11 rue Humann, 67 085 Strasbourg cedex, France. Tel : 33-3-90-24-32-58 ; Fax : 33-3-90-24-33-79.

#### INTRODUCTION

There is an increasing interest in developing new coatings to improve biocompatibility and to prepare biomaterial surfaces that can either resist or enhance cellular adhesion by mimicking extracellular matrix components (Dillow and Tirrell 1998; Healy 1999) or even locally deliver drugs. The most important step toward this end concerns the improvement at the nanometer to micrometer scales of material surface properties (Angelova and Hunkeler 1999) in order to control cellular responses such as adhesion, motility, spreading, growth and differentiation.

Polyelectrolyte multilayers (PEM) constitute a new attractive way for creating biofunctionalized surface coatings. The layer-by-layer (LbL) technique consists in the

alternate deposition of polyanions and polycations from aqueous solutions to build the multilayered films (Decher 1997; Decher *et al.* 1992). These films possess tunable properties in the thickness range from nanometer to micrometer. (Picart *et al.* 2001a; Picart *et al.* 2001b). It has been shown that the film morphology, internal molecular structure and thickness depend largely on the processing conditions such as ionic strength (McAloney *et al.* 2001), and pH of the polyelectrolyte or rinsing solution (Yoo *et al.* 1998).

Of special importance for biomedical applications is the control of the chemical composition of the surface that can affect biological activity. Films made of polyaminoacids, i.e. poly(L-lysine) (PLL), poly(L-glutamic acid) (PGA), natural

polyelectrolytes (eg hyaluronan (HA), alginate, chitosan, collagen) allow, for example, to create biomimetic architectures (Elbert *et al.* 1999; Picart *et al.* 2001c; Serizawa *et al.* 2002; Shenoy *et al.* 2003). Various compounds such as DNA, RNA, drugs, inorganic particles, proteins (Jessel *et al.* 2003), or peptides covalently bound to polyelectrolytes (Chluba *et al.* 2001), can be embedded in such films or deposited on the top of them. A further main advantage offered by PEM films concerns their ability to be deposited on any type of material with any shape, including stainless steel (Tan *et al.* 2003), polydimethylsiloxane (PDMS) (Ai *et al.* 2003a), vascular stents made of NiTi (Thierry *et al.* 2003), and biodegradable poly(L-lactic) acid matrices (Zhu *et al.* 2003).

A great number of fundamental and applied studies devoted to PEM focused on the interaction of PEM with biological fluids or cells. These were motivated by the fact that cell/substrate interactions are of prime importance in several key biological processes. These studies include, for example, the fabrication of non adhesive barriers for vascular grafts (Elbert *et al.* 1999), the fabrication of films with pro or anti-coagulant properties (Serizawa *et al.* 2002), the control of the cell adhesive properties of a film by varying the film deposition pH (Mendelsohn *et al.* 2003; Yang *et al.* 2003), the preparation of bacterial resistant film (Boulmedais *et al.*; Richert *et al.* 2003b)....

Cell adhesion and proliferation assays were initially performed on cell lineages (Chluba *et al.* 2001; Mendelsohn *et al.* 2003; Richert *et al.* 2002; Vautier *et al.* 2002). Thin films were usually found to be cell adhesive with however some differences depending on the outermost layer of the film (Vautier *et al.* 2002). Recently, Rubner and coworkers (Mendelsohn *et al.* 2003; Yang *et al.* 2003) showed that poly(acrylic acid) (PAA) /poly(allylamine hydrochloride) (PAH) multilayer films can either be non adhesive or adhesive for NR6WT fibroblasts depending on the pH of preparation of such films. These authors suggested that the non-adhesive character of the films with respect to cells is related to their high swelling capacities. In addition, a recent work performed on 1  $\mu\text{m}$  thick (PLL/HA) films indicated that these

hydrated films were highly resistant toward adhesion of chondrosarcoma cells (Richert *et al.* 2003a). After covalent cross-linking, the film became not only highly adhesive, but also more stable with respect to enzymatic degradation and to dehydration (Richert *et al.* 2004a). Similarly, incorporation of nanocolloids into PEM films leading to a film rigidification was also shown to change their cell adhesive properties and to render them adherent to cells only in the presence of colloids (Koktysh *et al.* 2002).

The use of primary cells, which are much more sensitive to external conditions and substrate properties, represents a further step to mimic real cell behavior prior to *in vivo* experiments. For thin and dense (refractive index of about 1.5) films based on poly(styrenesulfonate) (PSS) as polyanion combined with different polycations, either PAH (Boura *et al.* 2003), or poly(ethylene imine) (PEI) (Ai *et al.* 2003b), a good cellular adhesion could be observed. For more hydrated films containing PLL, poly(D-lysine) (PDL), or chitosan as polycation in combination with polyanions such as gelatin (Ai *et al.* 2003a), PGA (Tryoen-Toth *et al.* 2002), or hyaluronan (Richert *et al.* 2003b), thin films ( $\approx$  20-30 nm) were found to be cell adhesive in certain conditions (Ai *et al.* 2003b; Tryoen-Toth *et al.* 2002), depending on the cell type whereas micrometer thick and probably very soft and water containing films made of polysaccharides were cell adhesion resistant (Elbert *et al.* 1999; Richert *et al.* 2004a). Taken all together, the results obtained with cell lineages and primary cells suggest that purely physical properties, eg film stiffening, may importantly influence cell adhesion. As biocompatible and biodegradable polymers are of interest for *in vivo* applications and as they can be used in a layer-by-layer process to build micrometer thick films of controlled thickness, one may seek for a way to render them cell adhesive for primary cells.

In this work, the aim was to evaluate whether a change in film stiffness by chemical cross-linking could change the cell adhesive properties of primary chondrocytes. In particular, we focused on cellular adhesion onto the native and cross-linked films in order to characterize the interaction of cells with the film, by means of optical microscopy, confocal

laser scanning microscopy, and atomic force microscopy.

## Material / Methods

**Polyelectrolyte solutions.** The preparation of solutions of poly(L-lysine) (PLL, 30 kDa, Sigma, France), hyaluronan (HA, 400 kDa, Bioiberica, Spain) and the buildup of (PLL/HA)<sub>i</sub> films (where *i* corresponds to the number of layer pairs) was previously described (Picart *et al.* 2001c). PLL and HA were dissolved at 1 mg/mL in 0.15 M NaCl at pH 6-6.5. During the film construction all the rinsing steps were performed with an aqueous solution containing 0.15 M NaCl at pH 6-6.5. Fluorescein isothiocyanate labeled PLL (PLL <sup>FITC</sup>), 1-ethyl-3-(3-dimethylaminopropyl) carbodiimide (EDC), N-Hydroxysulfo-succinimide (sulfo-NHS), and hyaluronidase (Type I) were purchased from Sigma-Aldrich and used without any purification.

**Automatic buildup of the polyelectrolyte multilayered films for CLSM and cell culture experiments.** For CLSM and cell culture experiments, the multilayers made of either 12 or 24 layer pairs were prepared with a dipping machine (Dipping Robot DR3, Kierstein GmbH, Germany) on 12 mm glass slides (VWR Scientific, France) preliminarily cleaned with 10 mM SDS and 0.1 N HCl and extensively rinsed with ultrapure water. The glass slides were introduced vertically in a home made holder which was then dipped into a polyelectrolyte solution for 10 min. and was subsequently rinsed in three different beakers containing the 0.15 M NaCl solution (for respectively one min., five min. and five min.). The slides were then dipped into the oppositely charged polyelectrolyte solution followed by the same rinsing procedure.

### Chemical cross-linking of the films by EDC/NHS.

Cross-linking was performed on the 12 mm glass slides introduced in 24 wells culture plates as previously described (Richert *et al.* 2004a). Briefly, EDC at 400 mM and NHS at 100 mM were freshly prepared in 0.15 M NaCl solution at pH 5.5 and mixed v/v. The coupling chemistry is based on the reaction of activated carboxylic sites with primary amine groups (Hermanson 1996). The film coated substrate was put in contact with the mixed EDC/NHS

solution for 12 hours. Rinsing was performed three times with a 0.15 M NaCl solution for one hour. The efficiency of the crosslinking, e.g. the formation of amine bonds between the ammonium groups of PLL and the carboxylate groups of HA was checked on (PLL/HA)<sub>8</sub> films by *in situ* Fourier Transform Infrared (FTIR) Spectroscopy in Attenuated Total Reflection (ATR) mode with an Equinox 55 spectrophotometer (Bruker, Wissembourg, France). With this technique, we could follow versus time the intensity of the peaks attributed to the carboxylic groups (1606, 1412 cm<sup>-1</sup>) and those of the amide bands (1620-1680 cm<sup>-1</sup>) which respectively decreased and increased as the reaction went on (Richert *et al.* 2004a). This is a strong indication for the formation of amide bonds between PLL and HA at the expense of carboxylic groups.

### Cell culture

Rat chondrocytes were isolated from femoral head caps of Wistar rats. Femoral head caps were respectively digested in 2 mg/mL pronase (Sigma, P-5147, France) diluted in physiological serum for 2 h at 37°C, 5% CO<sub>2</sub> incubator and in 1.5 mg/mL B collagenase (Boehringer) diluted in 1/1 DMEM/Ham's F12 medium in presence of 1 mM L-glutamine, 50 U/mL penicillin (all from Life Technologies) for 15 h at 37°C, 5% CO<sub>2</sub> incubator. The supernatant was collected and gentle centrifugated (3 min. at 1000g) and suspended in 1/1 DMEM/Ham's F12 medium supplemented with 10% FBS, 1 mM glutamine, 50U/mL penicilline, 50 µg/mL Fungizone and then seeded in a culture flask (Falcon). After reaching confluence, cells were passed and only cells from the 1st and 2nd passages were used.

### Primary cells

**Cell viability (MTT assay).** Chondrocytes were isolated from femoral head caps and cultured as previously described (Miralles *et al.* 2001). MTT is a common assay for testing the cellular viability based on the reductive cleavage of yellow tetrazolium salt to a purple formazon compound by the dehydrogenase activity of intact mitochondria (Denizot and Lang 1986). Consequently, this conversion only occurs in living cells. 100 µL of dye was added to each well (in addition to the 1 mM DMEM). The film coated slides were

incubated at 37°C for 4h in CO<sub>2</sub> incubator. The medium was gently aspirated and 300 µL of acidic propanol (500 mL propanol + 3.5 mL of 6N HCl) were added. The plates were slightly shaken for 2 hours to ensure crystal dissolution. Aliquot of 150µL from each well were put into 96-well plates and absorbance was measured into a Multiplate Reader (Biotek) at the wavelength of 550 nm and 630 nm. The adsorbance difference ( $A_{550\text{nm}} - A_{630\text{nm}}$ ) was calculated for each type of film. Mean value obtained for chondrocytes adhered on glass slides was taken as a reference (100%). The experiments were performed in triplicate.

**THP-1 macrophages.** Human promonecytic THP-1 cells (American Type Culture Collection) were maintained in Roswell Parc Memorial Institute (RPMI) 1640 medium containing 10% fetal bovine serum (FBS), 2 mM L-glutamine and antibiotics (all from Life Technologies, Paisley, UK). Differentiated THP-1 cells were obtained by treatment with 5 nM TPA for two days and then starved overnight in 0.5% FBS-RPMI in the presence of 5 nM TPA before stimulation (Jessel *et al.* 2003).

#### Observation of cell/film interaction by Confocal Laser Scanning Microscopy (CLSM).

PLL<sup>FITC</sup> was used to image the dye labeled film in the green channel and Rhodamin-Phalloïdin (RP) was used to image the actin cytoskeleton of the chondrocytes in the red channel. The configuration of the microscope and the parameters used for the CLSM observations on a Zeiss LSM510 microscope have been described elsewhere (Picart *et al.* 2002). Prior to the cell observation, the cells attached on the films were rinsed briefly in PBS for 15 min. at room temperature were fixed with 4% paraformaldehyde and stained with RP (P1951, Sigma, France). The 12 mm glass slides were introduced in a home-made chamber and observed by imaging series of consecutive overlapping optical sections. The thickness of the film was determined by the measurement of the green band (corresponding to the PLL<sup>FITC</sup>) in computed orthogonal vertical sections through the imaged volumes.

#### Observations of cell morphology by Atomic Force Microscopy

After reaching confluence, the primary rat chondrocytes at the 2<sup>nd</sup> passage were dissociated with trypsin/EDTA solution (Gibco BRL, UK) and cells were seeded on PEM coated slides placed into 24-well plastic plates (NUNC) (10<sup>4</sup> cells/mL per well). After 48 hours of culture, cells attached to the substrate were washed in PBS (37°C, two washes of two min.) and fixed for 20 min. in 2.5% glutaraldehyde (TAAB, Berkes) in PBS at room temperature. Samples were rinsed in PBS (three washes of ten minutes each) and dehydrated in solutions with increasing ethanol content (50, 70, 90, 100 and 100%, 10 minutes each). Atomic force images were obtained in contact mode in air with the Multimode Nanoscope IV from Veeco (Santa Barbara, CA, USA). Cantilevers with a spring constant of 0.03 N/m and with silicon nitride tips were used (Model MLCT-AUHW Park Scientific, Sunnyvale, CA, USA). Deflection and height mode images were scanned simultaneously at a fixed scan rate (between 2 and 4 Hz) with a resolution of 512 x 512 pixels. For the cross-linked films, observations were performed on three independent experiments, ten cells being observed in each experiment. For the control glass slide, the observations were performed in duplicate.

## Results and discussion

#### Native and cross-linked (PLL/HA) films : film morphology and degradability

In recent works, we showed that PLL/HA multilayer films can be built under physiological conditions. The growth is initially characterized by islets formation that progressively coalesce up to the formation of a homogeneous and uniform film after ≈ 8 polyelectrolyte layer pairs have been deposited (Picart *et al.* 2001b). The thickness of a (PLL/HA)<sub>10</sub> film is about one micrometer as observed by atomic force microscopy. Thicker films containing more than 10 layer pairs could not be observed due to strong film/cantilever tip interactions. As film growth is exponential (Picart *et al.* 2001b), film thickness rapidly reaches several micrometers. It is therefore possible to determine the film thickness by

means of CLSM using fluorescently labeled polyelectrolytes. Typically, PLL can be labeled with FITC and  $\text{PLL}^{\text{FITC}}$  can be deposited as the ending layer of the film, thus allowing the visualization of the whole film thickness which corresponds to the green diffuse band of  $\text{PLL}^{\text{FITC}}$ , since PLL diffuses through the whole film. For instance, the thickness of a  $(\text{PLL}/\text{HA})_{20}$  film is around 4 micrometers. Recently, we evidenced that such PEM films can be covalently cross-linked using EDC and sulfo-NHS to form amide bonds between the ammonium groups of PLL and the carboxylate groups of HA (Engler et al., 2004b). Both types of film can be observed by CLSM (Figure 1), with however an increased detector gain and noise for the cross-linked films.

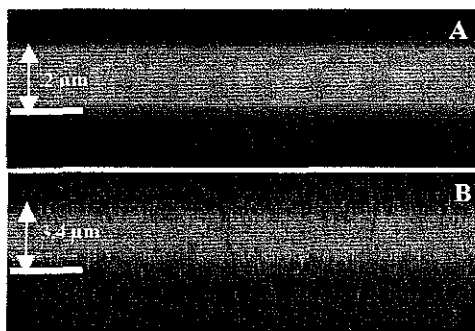


FIGURE 1. CLSM of the  $(\text{PLL}/\text{HA})_{24}$  films : (A) native (image size  $23 \mu\text{m} \times 10.5 \mu\text{m}$ ) and (B) cross-linked (image size  $23 \mu\text{m} \times 9 \mu\text{m}$ ). The films were observed after adding  $\text{PLL}^{\text{FITC}}$  as ending layer. The detector gain had to be increased for the cross-linked films and images became more noisy. Films thickness are respectively of  $3.2 \mu\text{m}$  (A) and of  $3.4 \mu\text{m}$  (B).

For the  $(\text{PLL}/\text{HA})_{20}$  films, cross-linking does not change significantly the film thickness. However, in contrary to the native films, the cross-linked films can be observed by AFM (Figure 2). The surface of the cross-linked film is smooth and homogeneous. When the film is brought in contact with the medium containing serum, some proteins do adsorb on top of it, as materialized by the presence of the white dots.

In a previous work, we showed that the cross-linked films are very stable when transferred in water or in water/ethanol solutions for any ethanol content (Richert et al. 2004a). The thickness of the cross-linked film continuously decreased as the ethanol content was increased and reached in pure ethanol

about 50% from its initial value in pure water. The film re-hydration was almost fully reversible. Also, after a 42 hours contact at  $37^\circ\text{C}$  with a hyaluronidase solution at 1000 U/mL, the topography of a cross-linked film remained unchanged whereas native films became strongly degraded (Richert et al. 2004a).

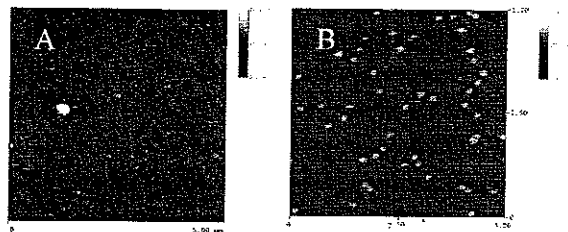


FIGURE 2 : AFM height mode images in liquid obtained (A) for a  $(\text{PLL}/\text{HA})_{12}$  film that has been cross-linked by means of EDC/sulfo-NHS, (B) for the same film that has been in contact with the culture medium containing 10% bovine serum proteins. The image dimensions are  $5 \times 5 \mu\text{m}^2$  and the maximum z-range are respectively of 60 (A) nm and 200 nm (B).

In the present work, we further investigated the cellular interactions with native and cross-linked films. As a evaluation of film degradability and stability in contact to cells, THP-1 macrophages cells were deposited on top of native and cross-linked  $(\text{PLL}/\text{HA})_{24}$  films that had been fluorescently labeled (the last deposited PLL layer was  $\text{PLL}^{\text{FITC}}$ ). This number of layer pairs was chosen to reach a sufficient thickness to get a clear visualization of the film by CLSM. After one day of culture, macrophages have partly degraded the native film and have become fluorescent. Holes are visible in the film (Figure 3A) and the cells do exhibit some green fluorescence. As can be seen on the side view of the film (Figure 3C), it was preferentially degraded at locations corresponding precisely to the presence of the macrophages. This indicates that they were able to induce film degradation and to incorporate the  $\text{PLL}^{\text{FITC}}$ . The digestion of the  $\text{PLL}^{\text{FITC}}$  by the macrophages can be also clearly seen (green fluorescence extending out of the film) (Fig. 3C). On the other hand, the cross-linked films were not degraded at all at least up to a 48 hours time period and the macrophages did not exhibit any fluorescence (Figure 3D).

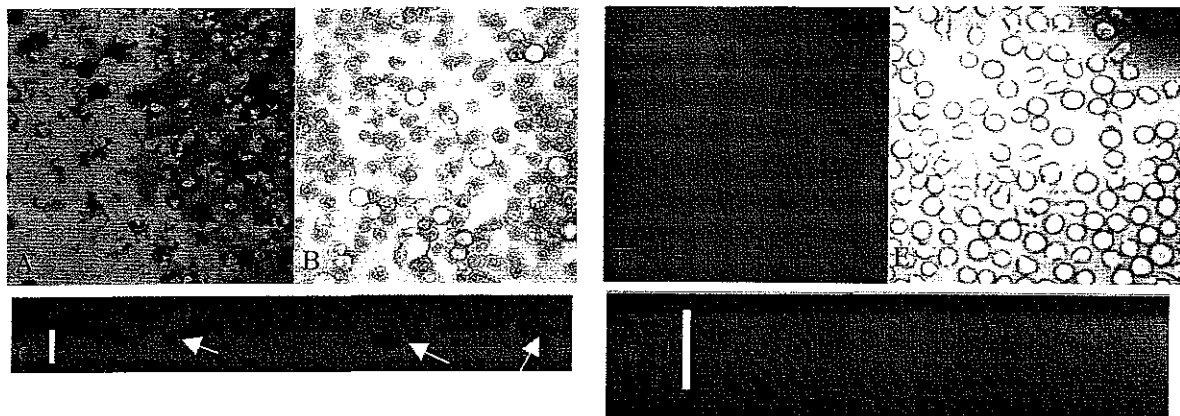


FIGURE 3 : CLSM study of the degradation of a  $(\text{PLL}/\text{HA})_{24}$ -PLL-FITC film that has been in contact with THP-1 macrophages for 24 hours at  $37^\circ\text{C}$ . Top view of the films observed in fluorescence (A, D), and corresponding images in brightfield (B, E) (image size :  $230\mu\text{m} \times 230\mu\text{m}$ ). Cross-sections of the films on which THP-1 macrophages were deposited are also shown (C, F). scale bar :  $5\mu\text{m}$ . The images A,B,C corresponds to a native film whereas images D,E,F corresponds to a cross-linked film.

They appeared healthy and round (Figure 3E) and they remained highly mobile even in the time scale of the z-series acquisition (three to four min.). The film has remained as a continuous green band (Figure 3F) of  $\approx 6\mu\text{m}$  in thickness and no holes in the film were visible.

### Primary chondrocyte adhesion onto native and cross-linked films

Primary chondrocytes were also grown on the native and cross-linked films made of twelve layer pairs ( $\approx 1\mu\text{m}$  thick) and ending either by PLL or HA. After 24 hours of culture, one can already observe by light microscopy that native films behave quite unfavorably with respect to cellular adhesion whereas the cross-linked ones were extremely favorable (data not shown). This is even more noticeable after six days in culture. Cells neither adhere nor spread on the native films (Figure 4A and 4C). These results hold for both HA and PLL ending films. This non-adhesion is not due to a toxicity of the films since the cells could adhere at the bottom of the well (on the plastic near the coated glass). Also, if the suspended cells from the uncross-linked PLL/HA films were transplanted to fresh culture plates, after 12 hours of “floating”, many cells readily attached and spread similarly to healthy cells. By contrast, cells do adhere and proliferate well on the cross-linked PLL and HA ending films (Figure 4B and 4D).

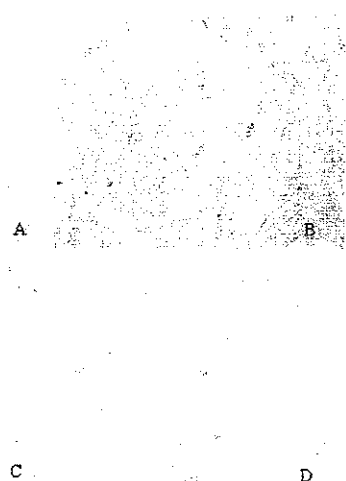
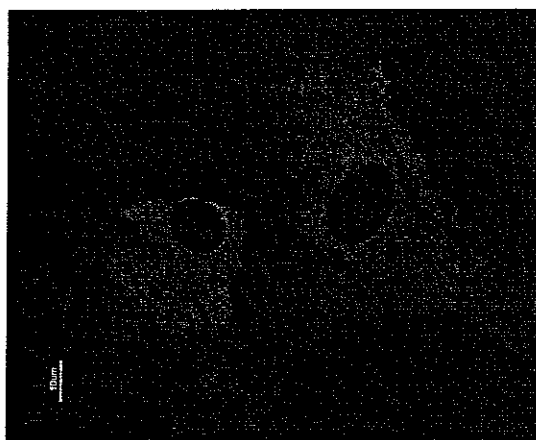


FIGURE 4. Microscopic observation of primary chondrocytes cultured on native or cross-linked  $(\text{PLL}/\text{HA})_{12}$  and  $(\text{PLL}/\text{HA})_{12}$ -PLL films for six days, ie films terminating either by  $\sim\text{PLL}$  or by  $\sim\text{HA}$  : (A)  $\sim\text{HA}$  (B) cross-linked  $\sim\text{HA}$  (C)  $\sim\text{PLL}$  (D) cross-linked  $\sim\text{PLL}$ .

It has to be noticed that the outermost layer of the film had no significant incidence in this later case. Results are similar whether the ending layer is positive or negative. Type II collagen production was also controlled. As shown in Figure 5, the chondrocytes were stained by the anti-type II collagen (about 50 to 60% of the total cell population) whereas Rat 1 fibroblasts were not stained by this antibody. The surface of the cross-linked film was nicely covered over the six days period of culture. We did not follow the phenotype over a long period of time (two weeks), but chondrocytes

generally dedifferentiate when grown on monolayers (Brodkin *et al.* 2004)



**FIGURE 5.** Observation of the collagen II staining on the chondrocytes by fluorescence microscopy (x60 objective). The chondrocytes have been cultured on the (PLL/HA)<sub>12</sub>-PLL films for three days.

These qualitative cell adhesion observations and results were confirmed by the MTT test performed on the primary cells after six days in culture (Figure 6). By taking glass as reference (100%), one observes that CL films are favorable to cell proliferation (73 to 77% of the reference) as compared to native ones (5 to 9%). This represents a ten fold increase in terms of cellular adhesion and proliferation. These results confirm preliminary data obtained for chondrosarcoma cells, a cell lineage, on the native and cross-linked (PLL/HA)<sub>12</sub> films (Richert *et al.* 2004a), and extend them to primary cells which are much more sensitive. As another evaluation of the strong change in the film adhesive properties between native or cross-linked architectures, another primary cell types, primary motoneurons, was tested.

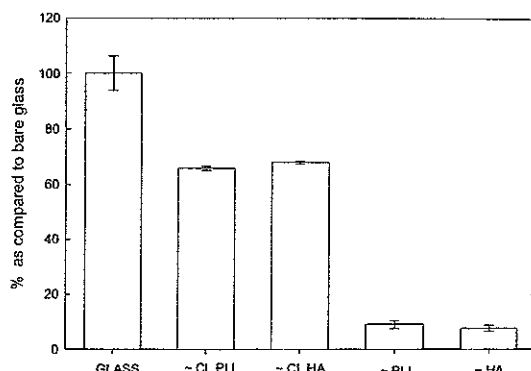


**FIGURE 6.** Results of the MTT test for primary rat chondrocytes cultured on native or cross-linked (PLL/HA)<sub>12</sub> and (PLL/HA)<sub>12</sub>-PLL films for six days, ie films terminating either by ~PLL or ~HA, as compared to the results for cells grown on bare glass (value for the glass slides is adjusted at 100%).

After two days in culture on the native and cross-linked (PLL/HA)<sub>12</sub> films, cells were observed by fluorescence microscopy after labeling  $\beta$ -tubulin. As for chondrocytes, but with even more striking differences, strong differences were observed for neurons grown on native films and neurons grown on CL films (data not shown). No neuron adhered on the native films (no motoneuron could be observed by fluorescence microscopy after two days in culture), whereas the neurons on the CL films developed neurites

### Microscopic observation of cell/film contact

In order to get a better understanding of the origin of these differences in adhesion for the native films compared to cross-linked ones, primary chondrocytes that have adhered on top of the different films were imaged by CLSM and AFM. For CLSM experiments, the terminating PLL layer of the film was labeled prior to cross-linking. After 48 hours of culture, the chondrocytes were fixed and their cytoskeletal actin was labeled with Texas Red. This allowed a dual visualization in both green and red channels. It has to be noticed that it was only possible to observe only few chondrocytes on native films after this time period due to their lack of adherence. As can be seen in Figure 7 (A and B), the film was deformed in the cell contact zone. This suggests that the

chondrocytes have been able to pull on the film such as to deform it and to “imprint” it. They also incorporated some PLL<sup>FITC</sup>, as can be seen by the observation in the green channel. The incorporation of PLL by the chondrocytes may be explained by the diffusion of PLL within the native films (Picart *et al.* 2002; Richert *et al.* 2004a). The film may be too soft and too deformable such that the cells are unable to create strong anchors. On the other hand, the chondrocytes grown on the cross-linked film have fully different shapes (Figure 7, C and D). They are well spread and lie above the film, with however some anchoring to the film. This can be evidenced by the yellow fluorescence areas, which correspond to the presence of both PLL (green) and actin (red). However, at this microscopic scale, no film deformation is visible and no green fluorescence is visible within the cells : this indicates that the PLL<sup>FITC</sup> in the cross-linked films is fully maintained in a stable position and does not diffuse at all toward the cell membrane.

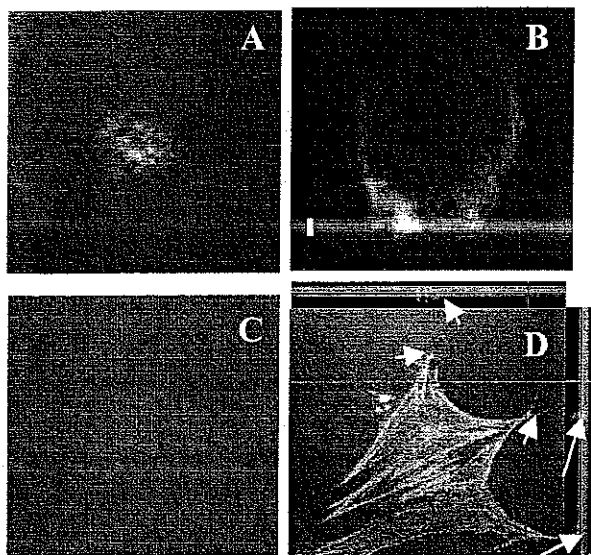


**FIGURE 7. CLSM observations of the adhesion of primary chondrocytes on top of native and cross-linked (PLL/HA)<sub>2a</sub>-PLL-FITC films.** Native film : (A) View in a z-section in the film, near the glass substrate, two channels being superposed. The green fluorescence comes from the film and the three red areas come from the cells. The cell has been able to deform the film, as can be seen by the imprints of the cell in the film (see arrowheads). (B) Side view of a cell reconstructed from a z-stack acquisition. Some green fluorescence is visible over the cell membrane

and also insight the cell suggesting the diffusion of the PLL-FITC. Cross-linked films : (C) Similar view of the film near the glass substrate : the film appears uniformly green and no holes are visible. (D) View in a z-section inside the cell together with two (X,Y) sections overall the z-stack performed along the two lines drawn on the image. On the upper image and on the side image are shown the projected sections, showing the (PLL/HA) film in green and the contact points of the cell in yellow (green and red co-localization). These images show the cell anchoring in the film. The z section images are 230 μm x 230 μm; film thickness is ≈ 5 μm.

The confocal images clearly evidence that differences in stiffness exist between the films. The native films are presumably deformed by the cells due to their very low rigidity. As a consequence of the film softness and of the diffusivity of the PLL molecules within the native films, cells do incorporate some PLL<sup>FITC</sup>, which is able to be internalized (membrane is negative, whereas PLL is positive). Under such conditions, cells are not able to adhere and spread. Therefore, very few cells (less than 5%) do remain anchored. A totally different behavior occurs on the cross-linked films. First, PLL is no more able to diffuse within the films (Richert *et al.* 2004a) and second the film seems to be more rigid.

A more precise insight of the microscopic adhesion of the cells onto the cross-linked films could be observed by AFM. It has to be noticed that such information could not be gained for cells grown on the native films due to the very low number of cells remaining on the top of films after fixation and dehydration. Also, their round shape hindered the observation due to their large height compared to well spread cells. The observations are therefore difficult to perform because of the cantilevers tip effects.

On the cross-linked films, primary chondrocytes are able to widely spread and they exhibit typical “polygonal” shapes, whether terminated by HA (data not shown) or PLL (Figure 8). The cell edges were well defined. Similar images were obtained on the control glass substrate (Figure 8A), with however slightly more fibers at the cell edges (Fig 8B). On the cross-linked films, cells develop

Pour la thèse de Ludovic RICHERT,  
il n'y a pas de Page 130.

explain why other bio-polymeric films were found to be highly non-adhesive for cells, such as PLL/alginate (Elbert *et al.* 1999) or Poly(acrylic acid). Poly(allyalamine hydrochloride) (Berg *et al.* 2004; Yang *et al.* 2003) for fibroblasts or chitosan/hyaluronan (Richert 2004) for chondrocytes. The high swellability of all these films may be associated to a softness, which has to be avoided for cell adhesion. It would be of high interest to build films with gradients in the percentage of extremely interesting to create a film with a gradient in cross-linking, similarly to what has been done for PA gels (Lo *et al.* 2000) and to investigate whether a gradient in cell adhesion is also observed. But this would require some preliminary careful analysis of the cross-linking method on which we are currently working on.

In the past years, several studies demonstrated the influence of purely physical properties on cell adhesion and differentiation. For instance, the matrix stiffness become increasingly recognized as playing a role in many cellular processes ranging from motility (Lo *et al.* 2000; Pelham and Wang 1997) to phagocytosis (Beningo *et al.* 2002) and differentiation (Deroanne *et al.* 2001). Cells display an apparent spreading preference for stiffer substrates, a phenomenon referred to as *durotaxis* (Lo *et al.* 2000). This was shown on polyacrylamide gels with adjustable rigidity by changing the concentration of the bis-acrylamide cross-linker. The effect was checked for different cell types, such as fibroblasts, neurons (Flanagan *et al.* 2002), and more recently smooth muscle cells (Engler *et al.* 2004a). These observations could be analyzed on the basis of gel softness : to a cell, an extremely soft gel could be perceived as nearly fluid and therefore inadequate for sustaining an anchorage-dependent response (Engler *et al.* 2004a). Recently, the effect of substrate mechanics was also evidenced for chondrocytes grown on alginate gels over a modulus range of 10 to 130 kPa (Genes *et al.* 2004). However, it has to be noticed that such matrix stiffness effects have always been investigated for relatively "thick" gels, eg gels of at least 70 micrometers in thickness. Whether this would remain valid on thin gels (ranging from nanometer to micrometer thicknesses) was never investigated, because of

the difficulty to prepare thin gels of controlled thickness and of different stiffness. The polyelectrolyte multilayers in general and the  $(\text{PLL}/\text{HA})_{12}$  films in particular represents a new way to address this question. As we observed, the native and soft films were too soft to allow cell adhesion whereas the cross-linked and much stiffer films were preferred for cell adhesion. We are now working toward preparing films of controlled rigidity, which can also be further functionalized by adhesion peptides, to see whether a chemical grafting can compete with a pure physical stimulus.

## CONCLUSION

In this work, we showed that primary chondrocytes only adhere on top of  $(\text{PLL}/\text{HA})$  multilayer films once these films have been cross-linked. As evidenced in an earlier study, cross-linking modifies the physico-chemical properties of the film and PLL diffusion within the film is also hindered. Whereas the native films can be degraded by THP-1 macrophages over a two days period, the cross-linked ones are not degraded over the same period by the macrophages. Confocal images allowed us to visualize the deformation of the native films by cells and the diffusion of  $\text{PLL}^{\text{FITC}}$  within the cell. Also, the anchoring of the cell in the cross-linked films and their spreading was observed. The AFM images confirm the nice aspect and spreading of the chondrocytes onto the cross-linked films.

## ACKNOWLEDGMENTS

The authors are grateful to Dominique Baptiste for her help in the chondrocytes culture. This work was supported by the programs ACI "Technologies pour la Santé" and ACI "Surfaces, interfaces et conception de nouveaux matériaux" from the Ministère Français de la Recherche. The CLSM platform used in this study was co-financed by the Région Alsace, the CNRS, the Université Louis Pasteur, and the Association pour la Recherche sur le Cancer.

## REFERENCES

- Ai H, Lvov Y, Mills D, Jennings M, Alexander J, Jones S. 2003a. Coating and selective deposition of nanofilm on silicone rubber for cell adhesion and growth. *Cell Biochem Biophys.* 38(2):103-14.
- Ai H, Meng H, Ichinose I, Jones SA, Mills DK, Lvov YM, Qiao X. 2003b. Biocompatibility of layer-by-layer self-assembled nanofilm on silicone rubber for neurons. *J. Neursci. Meth.* 128(1-2):1-8.
- Angelova N, Hunkeler D. 1999. Rationalizing the design of polymeric biomaterials. *Trends Biotechnol.* 17(10):409-421.
- Beningo KA, Lo CM, Wang YL. 2002. Flexible polyacrylamide substrata for the analysis of mechanical interactions at cell-substratum adhesions. *Methods in Cell Biology* 69:325-39.
- Berg MC, Yang SY, Hammond PT, Rubner MF. 2004. Controlling mammalian cell interactions on patterned polyelectrolyte multilayer surfaces. *Langmuir* 20(4):1362-1368.
- Boulmedais F, Frisch B, Etienne O, Lavalle P, Picart C, Ogier J, Voegel J-C, Schaaf P, Egles C. 2004. Polyelectrolyte multilayer films with pegylated polypeptides as a new type of anti-microbial protection for biomaterials. *Biomaterials ASAP*.
- Boura C, Menu P, Payan E, Picart C, Voegel J-C, Muller S, Stoltz J-F. 2003. Endothelial cells grown on thin polyelectrolyte multilayered films: An evaluation of a new versatile surface modification. *Biomaterials* 24(20):3521-3530.
- Brodkin KR, Garcia AJ, Levenston ME. 2004. Chondrocyte phenotypes on different extracellular matrix monolayers. *Biomaterials* 25(28):5929-38.
- Chluba J, Voegel JC, Decher G, Erbacher P, Schaaf P, Ogier J. 2001. Peptide Hormone Covalently Bound to Polyelectrolytes and Embedded into Multilayer Architectures Conserving Full Biological Activity. *Biomacromolecules* 2(3):800-805.
- Decher G. 1997. Fuzzy nanoassemblies: Toward layered polymeric multicomposites. *Science* 277(5330):1232-1237.
- Decher G, Hong JD, Schmitt J. 1992. Buildup of ultrathin multilayer films by a self-assembly process. Consecutively alternating adsorption of anionic and cationic polyelectrolytes on charges surface. *Thin Solid Films* 1992(210):831-835.
- Denizot F, Lang R. 1986. Rapid colorimetric assay for cell growth and survival : Modifications to the tetrazolium dye procedure giving improved sensitivity and reliability. *J. Immunol. Methods* 89(2):271-277.
- Deroanne CF, Lapierre CM, Nusgens BV. 2001. In vitro tubulogenesis of endothelial cells by relaxation of the coupling extracellular matrix-cytoskeleton. *Cardiovascular Research* 49(3):647-58.
- Dillow AK, Tirrell M. 1998. Targeted cellular adhesion at biomaterial interfaces. *Curr. Opin. Solid State Mater. Sci.* 3(3):252-259.
- Elbert DL, Herbert CB, Hubbell JA. 1999. Thin polymer layers formed by polyelectrolyte multilayer techniques on biological surfaces. *Langmuir* 15(16):5355-5362.
- Engler A, Bacakova L, Newman C, Hategan A, Griffin M, Discher DE. 2004a. Substrate compliance versus ligand density in cell on gel responses. *Biophys. J.* 86(1):617-628.
- Engler A, Richert L, Wong JY, Picart C, Discher DE. 2004b. Surface probe measurements of the elasticity of sectioned tissue, thin gels, and polyelectrolyte multilayer films : correlations between substrate stiffness and cell adhesion. *Surface Science* in press.
- Flanagan LA, Ju YE, Marg B, Osterfield M, Janmey PA. 2002. Neurite branching on deformable substrates. *Neuroreport* 13(18):2411-2415.
- Genes NG, Rowley JA, Mooney DJ, Bonassar LJ. 2004. Effect of substrate mechanics on chondrocyte adhesion to modified alginate surfaces. *Archives of Biochemistry and Biophysics* 422(2):161-7.
- Healy KE. 1999. Molecular engineering of materials for bioreactivity. *Curr. Opin. Solid State Mater. Sci.* 4(4):381-387.
- Hermanson GT. 1996. Zero-length cross-linkers. In: Hermanson GT, editor. *Bioconjugate techniques*. San Diego: Academic Press. p 169-176.
- Jessel N, Atalar F, Lavalle P, Mutterer J, Decher G, Schaaf P, Voegel JC, Ogier G. 2003. Bioactive coatings based on

- polyelectrolyte multilayer architecture functionalised by embedded proteins. *Advanced Materials* 15(9):692-695.
- Koktysh DS, Liang X, Yun BG, Pastoriza-Santos I, Matts RL, Giersig M, Serra-Rodríguez C, Liz-Marzán LM, Kotov NA. 2002. Biomaterials by design: Layer-by-layer assembled ion-selective and biocompatible films of TiO<sub>2</sub> nanoshells for neurochemical monitoring. *Adv. funct. mater.* 12(4):255-265.
- Lapčík L, Lapčík L, De Smedt S, Demeester J, Chabrecek P. 1998. Hyaluronan: Preparation, Structure, properties, and applications. *Chem. Rev.* 98(8):2663-2684.
- Lo CM, Wang HB, Dembo M, Wang YL. 2000. Cell movement is guided by the rigidity of the substrate. *Biophys. J.* 79(1):144-152.
- McAloney RA, Sinyor M, Dudnik V, Goh MC. 2001. Atomic force microscopy studies of salt effects on polyelectrolyte multilayer film morphology. *Langmuir* 17(21):6655-6663.
- Mendelsohn JD, Yang SY, Hiller J, Hochbaum AI, Rubner MF. 2003. Rational design of cytophilic and cytophobic polyelectrolyte multilayer thin films. *Biomacromolecules* 4(1):96-106.
- Miralles G, Baudoin R, Dumas D, Baptiste D, Hubert P, Stoltz JF, Dellacherie E, Mainard D, Netter P, Payan E. 2001. Sodium alginate sponges with or without sodium hyaluronate: in vitro engineering of cartilage. *J Biomed Mater Res* 57(2):268-78.
- Pelham RJ, Jr, Wang YL. 1997. Cell locomotion and focal adhesions are regulated by substrate flexibility. *P. Natl. Acad. Sci. USA.* 94(25):13661-13665.
- Picart C, Ladam G, Senger B, Voegel J-C, Schaaf P, Cuisinier FJG, Gergely C. 2001a. Determination of structural parameters characterizing thin films by optical methods: A comparison between scanning angle reflectometry and optical waveguide lightmode spectroscopy. *J. Chem. Phys.* 115(2):1086-1094.
- Picart C, Lavalle P, Hubert P, Cuisinier FG, Decher G, Schaaf P, Voegel J-C. 2001b. Buildup mechanism for poly(L-lysine)/hyaluronic acid films onto a solid surface. *Langmuir* 17(23):7414-7424.
- Picart C, Lavalle P, Hubert P, Cuisinier FJG, Decher G, P S, Voegel JC. 2001c. Buildup mechanism for poly(L-lysine)/hyaluronic acid films onto a solid surface. *Langmuir* 17(23):7414-7424.
- Picart C, Mutterer J, Richert L, Luo Y, Prestwich GD, Schaaf P, Voegel J-C, Lavalle P. 2002. Molecular basis for the explanation of the exponential growth of polyelectrolyte multilayers. *Proceedings of the National Academy of Sciences of the United States of America* 99(20):12531-12535.
- Richert L, Boulmedais F, Lavalle P, Mutterer J, Ferreux E, Decher G, Schaaf P, Voegel J-C, Picart C. 2004a. Improvement of stability and cell adhesion properties of polyelectrolyte multilayer films by chemical cross-linking. *Biomacromolecules* 5(2):284-294.
- Richert L, Boulmedais F, Ph L, Mutterer J, Ferreux E, Decher G, Schaaf P, Voegel J-C, Picart C. 2003a. Improvement of stability and cell adhesion properties of polyelectrolyte multilayer films by chemical cross-linking. *Biomacromolecules* in press.
- Richert L, Engler AJ, Discher DE, Picart C. 2004b. Elasticity of native and cross-linked polyelectrolyte multilayer. *Biomacromolecules* in press.
- Richert L, Lavalle P, Payan E, Stoltz J-F, Shu XZ, Prestwich GD, Schaaf P, Voegel J-C, Picart C. 2003b. Layer by layer buildup of polysaccharide films : Physical chemistry and cellular adhesion aspects. *Langmuir* ASAP.
- Richert L, Lavalle P, Vautier D, Senger B, Stoltz J-F, Schaaf P, Voegel J-C, Picart C. 2002. Cell interactions with polyelectrolyte multilayer films. *Biomacromolecules* 3(6):1170-1176.
- Serizawa T, Yamaguchi M, Akashi M. 2002. Alternating Bioactivity of Polymeric Layer-by-Layer Assemblies: Anticoagulation vs Procoagulation of Human Blood. *Biomacromolecules* 3(4):724-731.
- Shenoy DB, Antipov A, Sukhorukov GB, Möhwald H. 2003. Layer-by-Layer Engineering of Biocompatible, Decomposable Core-Shell Structures. *Biomacromolecules* 4(2):265-272.
- Tan Q, Ji J, Barbosa MA, Fonseca C, Shen J. 2003. Constructing thromboresistant surface on biomedical stainless steel via layer-by-

- layer deposition anticoagulant. *Biomaterials* 24(25):4699-705.
- Thierry B, Winnik FM, Merhi Y, Silver J, Tabrizian M. 2003. Bioactive coatings of endovascular stents based on polyelectrolyte Multilayers. *Biomacromolecules* 4(6):1564-1571.
- Tryoen-Toth P, Vautier D, Haikel Y, Voegel J-C, Schaaf P, Chluba J, Ogier J. 2002. Viability, adhesion, and bone phenotype of osteoblast-like cells on polyelectrolyte multilayer films. *J. Biomed. Mater. Res.* 60(4):657-667.
- Vautier D, Karsten V, Egles C, Chluba J, Schaaf P, Voegel JC, Ogier J. 2002. Polyelectrolyte multilayer films modulate cytoskeletal organization in chondrosarcoma cells. *Journal of Biomaterials Science. Polymer Edition* 13(6):713-32.
- Yang SY, Mendelsohn JD, Rubner MF. 2003. New class of ultrathin, highly cell-adhesion-resistant polyelectrolyte multilayers with micropatterning capabilities. *Biomacromolecules* 4(4):987-94.
- Yoo D, Shiratori SS, Rubner MF. 1998. Controlling bilayer composition and surface wettability of sequentially adsorbed multilayers of weak polyelectrolytes. *Macromolecules* 31:4309-4318.
- Zhu Y, Gao C, He T, Liu X, Shen J. 2003. Layer-by-Layer assembly to modify poly(L-lactic acid) surface toward improving its cytocompatibility to human endothelial cells. *Biomacromolecules* 4(2):446-452.

# **Chapitre 5 : Films multicouches à bases de polysaccharides (chitosane/hyaluronane) : propriétés physico-chimiques et biologiques.**

---

Dans le but de réaliser un film multicouche entièrement à base de polyélectrolytes naturels, biocompatibles et biodégradables, nous avons étudié la réalisation de films multicouches construits avec le chitosane (CHI) et le hyaluronane (HA). Le chitosane est un copolymère cationique de N-acetylglucosamine partiellement déacétylé généralement obtenu à partir de l'exosquelette de crustacés. Il est non toxique, biodégradable et biorésorbable (Denuziere et al., 1996). Le chitosane présente aussi des fonctions thérapeutiques. Il est ainsi utilisé dans le domaine médical notamment pour ses propriétés hémostatiques (Malette et al., 1983), antibactériennes (Jia et al., 2001) ou encore analgésiques (Okamoto et al., 2002). Comme le hyaluronane, il est beaucoup utilisé pour fabriquer des hydrogels et des membranes, notamment pour la reconstruction du cartilage et de la peau (Francis Suh and Matthew, 2000). Il est possible d'associer ces deux polysaccharides pour former des gels destinés à prolonger la libération de médicament comme la gentamicine (Lim et al., 2000). La formation de complexe entre ces deux polyélectrolytes a par ailleurs déjà été étudiée et entraîne une modification de leurs caractéristiques biologiques individuelles et les protège partiellement de la dégradation enzymatique (Denuziere et al., 1998).

Tout d'abord, nous avons dans un premier temps étudié la construction des films à base de chitosane et de hyaluronane dans différentes conditions. Nous avons particulièrement analysé l'influence du taux de sel et du pH des solutions lors de la construction. Nous avons ensuite étudié *in vitro* le comportement de tels films en présence de chondrocytes et de bactéries afin d'évaluer leur propriété d'adhésion cellulaire et d'évaluer si ces films permettent de limiter l'adhésion bactérienne.

## 5.1 : Résumé 6

La construction des films (CHI/HA) a été suivie *in situ* à l'aide de la spectroscopie optique et de la microbalance à quartz. Le pH des solutions de chitosane et de hyaluronane a été fixé à 5 car le chitosane à un pKa voisin de 6.5 aux degrés de déacetylation utilisés (Denuziere et al., 1996). Des essais ont également été réalisés en déposant le chitosane à un pH de 5.0 et le hyaluronane à un pH de 7.4, mais dans ce cas, le film se construit mal. En présence de 0.15 M en NaCl, le film construit à pH 5 possède des caractéristiques comparables aux films à base de (PLL/HA). La croissance du film avec le nombre de couches est exponentielle avec une épaisseur voisine de 300 nm après le dépôt de 10 paires de couches. Les observations des films de (CHI/HA) en microscopie confocale après le marquage avec le chitosane chitosane-FITC et le hyaluronane-TR mettent en évidence la diffusion de CHI à travers l'ensemble du film du film, de manière comparable à la PLL au sein du film (PLL/HA).

Lorsque le film est construit dans une solution saline à un taux de sels inférieur, la cinétique de croissance des films est ralentie. Les observations par AFM mettent en évidence une formation rapide d'un film uniforme après le dépôt d'une dizaine de paires de couches, lorsque le taux de sel est de 0.15 M, alors que des gouttelettes sont toujours visibles sur la surface pour des taux de sels  $10^{-2}$  M et  $10^{-4}$  M pour un nombre équivalent de couches déposées. A  $10^{-2}$  M NaCl, il faut une vingtaine de paires de couches pour obtenir un film continu et à  $10^{-4}$  M, le dépôt est toujours constitué de gouttelettes et leur épaisseur est très faible (moins de 10 nm), même après le dépôt de cinquante paires de couches.

Les films construits à 0.15 M ont été mis en contact avec des chondrocytes et l'on observe un comportement des cellules identique à celui observé sur les films de (PLL/HA), avec une absence d'adhésion. La nature du polycation((CHI au lieu de PLL) ne semble pas modifier les propriétés d'adhésion cellulaire, alors que les propriétés mécaniques et le degré d'hydratation semblent jouer un rôle prépondérant. Nous avons aussi testé l'adhésion bactérienne (*Escherichia coli*) sur des films élaborés à 0.15 M et 0.01 M en NaCl. Elle est très faible, particulièrement sur les films construit à 0.15 M se terminant par le chitosane. Des perspectives intéressantes apparaissent pour l'utilisation de tels films, notamment pour la réalisation de surface ayant des propriétés anti-microbiennes.

## 5.2 : Article 6

### Layer by Layer Buildup of Polysaccharide Films: Physical Chemistry and Cellular Adhesion Aspects

Ludovic Richert,<sup>†</sup> Philippe Lavalle,<sup>†</sup> Elisabeth Payan,<sup>‡</sup> Xiao Zheng Shu,<sup>§</sup> Glenn D. Prestwich,<sup>§</sup> Jean-François Stoltz,<sup>||</sup> Pierre Schaaf,<sup>†,‡</sup> Jean-Claude Voegel,<sup>†</sup> and Catherine Picart<sup>\*†,‡</sup>

*Institut National de la Santé et de la Recherche Médicale, Unité 595, Université Louis Pasteur, 11 rue Humann, 67085 Strasbourg Cedex, France, Laboratoire de Physiopathologie et Pharmacologie Articulaires, UMR 7561 et IFR 111, Faculté de Médecine, 54 505 Vandoeuvre-les-Nancy, France, Department of Medical Chemistry, The University of Utah, Salt Lake City, Utah 84112-5820, Laboratoire de Mécanique et Ingénierie Cellulaire et Tissulaire, UMR 7563 et IFR 111, Faculté de Médecine, 9 avenue de la forêt de Haye, 54 505 Vandoeuvre-les-Nancy, France, Institut Charles Sadron, Centre National de la Recherche Scientifique, Université Louis Pasteur, 6 rue Boussingault, 67083 Strasbourg Cedex, France, and Ecole Européenne de Chimie, Polymères et Matériaux de Strasbourg, 25 rue Becquerel, 67087 Strasbourg Cedex 2, France*

Received August 3, 2003. In Final Form: October 8, 2003

The formation of polysaccharide films based on the alternate deposition of chitosan (CHI) and hyaluronan (HA) was investigated by several techniques. The multilayer buildup takes place in two stages: during the first stage, the surface is covered by isolated islets that grow and coalesce as the construction goes on. After several deposition steps, a continuous film is formed and the second stage of the buildup process takes place. The whole process is characterized by an exponential increase of the mass and thickness of the film with the number of deposition steps. This exponential growth mechanism is related to the ability of the polycation to diffuse "in" and "out" of the whole film at each deposition step. Using confocal laser microscopy and fluorescently labeled CHI, we show that such a diffusion behavior, already observed with poly(L-lysine) as a polycation, is also found with CHI, a polycation presenting a large persistence length. We also analyze the effect of the molecular weight (MW) of the diffusing polyelectrolyte (CHI) on the buildup process and observe a faster growth for low MW chitosan. The influence of the salt concentration during buildup is also investigated. Whereas the CHI/HA films grow rapidly at high salt concentration (0.15 M NaCl) with the formation of a uniform film after only a few deposition steps, it is very difficult to build the film at 10<sup>-4</sup> M NaCl. In this latter case, the deposited mass increases linearly with the number of deposition steps and the first deposition stage, where the surface is covered by islets, lasts at least up to 50 bilayer deposition steps. However, even at these low salt concentrations and in the islet configuration, CHI chains seem to diffuse in and out of the CHI/HA complexes. The linear mass increase of the film with the number of deposition steps despite the CHI diffusion is explained by a partial redissolution of the CHI/HA complexes forming the film during different steps of the buildup process. Finally, the uniform films built at high salt concentrations were also found to be chondrocyte resistant and, more interestingly, bacterial resistant. Therefore, the (CHI/HA) films may be used as an antimicrobial coating.

#### Introduction

Polyelectrolyte multilayer (PEM) coatings have become a new and general way to functionalize surfaces, and their applications range from optical devices to biomaterial coatings.<sup>1,2</sup> The technique is based on the

alternate deposition of polyanions and polycations.<sup>3,4</sup> Film functionalization can be achieved by incorporating particles<sup>5</sup> or active molecules<sup>6,7</sup> into it. The film physico-chemical properties can be controlled by changing the deposition conditions (pH, salt concentration, etc.)<sup>8–10</sup> or the outermost layer of the film.<sup>11</sup> For example, it has been shown that poly(acrylic acid)/poly(allylamine) films can be rendered nonadhesive to cells by suitably selecting the pH during the construction.<sup>12</sup> Cells can also react with

\* To whom correspondence should be addressed. Catherine Picart, INSERM U595, Faculté de Médecine, Bât 3, 11 rue Humann, 67 085 Strasbourg cedex, France. Tel: 33-3-90-24-32-58. Fax: 33-3-90-24-33-79. E-mail: Catherine.Picart@medecine.u-strasbg.fr.

<sup>†</sup> Institut National de la Santé et de la Recherche Médicale, Unité 595, Université Louis Pasteur.

<sup>‡</sup> Laboratoire de Physiopathologie et Pharmacologie Articulaires, UMR 7561 et IFR 111, Faculté de Médecine.

<sup>§</sup> Department of Medical Chemistry, The University of Utah.

<sup>||</sup> Laboratoire de Mécanique et Ingénierie Cellulaire et Tissulaire, UMR 7563 et IFR 111, Faculté de Médecine.

<sup>1</sup> Institut Charles Sadron, Centre National de la Recherche Scientifique, Université Louis Pasteur.

<sup>\*</sup> Ecole Européenne de Chimie, Polymères et Matériaux de Strasbourg.

(1) Hammond, P. T. *Curr. Opin. Colloid Interface Sci.* 1999, 4, 430–442.

(2) Bertrand, P.; Jonas, A.; Laschewsky, A.; Legras, R. *Macromol. Rapid. Commun.* 2000, 21, 319–348.

(3) Decher, G.; Hong, J. D.; Schmitt, J. *J. Thin Solid Films* 1992, 1992, 831–835.

(4) Decher, G. *Science* 1997, 277, 1232–1237.

(5) Koktysh, D. S.; Liang, X.; Yun, B. G.; Pastoriza-Santos, I.; Matts, R. L.; Giersig, M.; Serra-Rodríguez, C.; Liz-Marzáñ, L. M.; Kotov, N. A. *Adv. Funct. Mater.* 2002, 12, 255–265.

(6) Chluba, J.; Voegel, J. C.; Decher, G.; Erbacher, P.; Schaaf, P.; Ogier, J. *Biomacromolecules* 2001, 2, 800–805.

(7) Jessel, N.; Atalar, F.; Lavalle, P.; Mütterer, J.; Decher, G.; Schaaf, P.; Voegel, J. C.; Ogier, G. *Adv. Mater.* 2003, 15, 692–695.

(8) Shiratori, S. S.; Rubner, M. F. *Macromolecules* 2000, 33, 4213–4219.

(9) Steitz, R.; Leiner, V.; Siebrecht, R.; Klitzing, R. V. *Colloids Surf. B* 2000, 163, 63–70.

(10) Yoo, D.; Shiratori, S. S.; Rubner, M. F. *Macromolecules* 1998, 31, 4309–4318.

(11) Xie, A. F.; Granick, S. *Macromolecules* 2002, 35, 1805–1813.

proteins embedded in poly(L-lysine)/poly(glutamic acid) multilayers.<sup>7</sup>

Described by Decher and co-workers,<sup>3</sup> the first investigated polyelectrolyte systems exhibit a linear growth of both the mass and the thickness of the films with the number of deposition steps. Poly(styrene sulfonate)/poly(allylamine hydrochloride) is one of the most prominent examples of linearly growing systems.<sup>13–18</sup> These films present a stratified structure, each polyelectrolyte layer interpenetrating only its neighboring ones. The growth mechanism involves mainly electrostatic interactions between the polyelectrolytes from the solution and the polyelectrolytes of opposite charge forming the outer layer of the film. Each new polyelectrolyte deposition leads to a charge overcompensation that is the actual motor for the film growth and to a change in the  $\xi$  potential.<sup>13</sup> More recently, using polysaccharides and polypeptides, Elbert and co-workers<sup>19</sup> and Picart and co-workers<sup>20,21</sup> described a new type of polyelectrolyte multilayers which are characterized by an exponential growth of both the mass and the thickness of the film with the number of deposition steps. Poly(L-lysine)/alginate<sup>19</sup> and poly(L-lysine)/hyaluronan<sup>20,21</sup> were the first reported examples. Whereas the typical thickness of a linearly growing film constituted of 20 bilayers is of the order of 100 nm, the thickness of exponentially growing films can reach 10  $\mu\text{m}$  or more after the deposition of a similar number of layers. Other exponentially growing films have been reported.<sup>22,23</sup> Two explanations for these exponential growth mechanism have been proposed: one relies on the diffusion of polyelectrolyte "in" and "out" of the film during each bilayer step,<sup>21,22</sup> whereas the second one relies on the increase in film surface roughness as the film builds up.<sup>14,24</sup> However, no change in surface roughness was observed for the exponentially growing films made of polypeptides.<sup>20,22,25</sup> A deep investigation of the poly(L-lysine)/hyaluronan (PLL/HA) system allowed a better understanding of the processes underlying such a growth mechanism.<sup>21</sup> For this investigated system, the growth mechanism relies on the diffusion in and out of the whole structure during each "bilayer" deposition step of one type of the polyelectrolytes constituting the films.<sup>21,22</sup> Even if the exponential growth mechanism begins to be understood, many fundamental questions remain unanswered: for example, one is not able to predict which systems will grow linearly or exponentially. Most, but not all, of the reported expo-

nentially growing films contain PLL as the polycation (poly(L-glutamic acid)/poly(allylamine) (PGA/PAH) is an example of exponentially growing film which does not contain PLL<sup>25</sup>). Do polyelectrolytes presenting other physicochemical characteristics (persistence length, hydration, etc.) also give this type of films? Does the mass of the polyelectrolytes play a role in their ability to diffuse? Can a polyanion/polycation system that grows exponentially under certain conditions become linearly growing when the deposition conditions are changed? Could polyelectrolyte also diffuse in a linearly growing film? All the reported exponentially growing films were constructed from high salt concentration solutions that favor the buildup of thick films. By reducing the salt concentration of the polyelectrolyte solutions during the buildup, it is expected that the films become thinner (for a given number of deposition steps) and more dense thereby hindering polyelectrolyte diffusion into the film. It would therefore be of interest to investigate the influence of the salt concentration (during buildup) on the growth mechanism. These questions will be addressed in this study where we investigate the buildup of chitosan/hyaluronan (CHI/HA) multilayers. Both polyelectrolytes are polysaccharides, chitosan being a polycation at acidic pH, and both present relatively high intrinsic chain stiffness (a persistence length of the order of 6–12 nm for chitosan<sup>26,27</sup> and 6 nm for hyaluronan<sup>28</sup>) which should influence their diffusion abilities.

This study is however not only of fundamental interest. For biomedical applications, the buildup of multilayered films entirely constituted of natural polysaccharides has emerged within the past years.<sup>29,30</sup> Polysaccharides differ from most of the synthetic polyelectrolytes by their multifunctional monomers. Serizawa et al.<sup>31</sup> prepared dextran/chitosan films at high ionic strength (>0.5 M NaCl) that possess alternated activity with anti- and procoagulation for the dextran sulfate and chitosan ending films, respectively. Shenoy et al.<sup>32</sup> prepared also hollow capsules made of multilayers of sodium alginate/chitosan films for controlled drug release applications. Chitosan shows also several advantages over other synthetic polycations: Chitosan is obtained after N-deacetylation of chitin by alkaline treatment (Figure 1), chitin being the second most abundant naturally occurring polysaccharide.<sup>33</sup> It is found in crustacean shells and insects and is also synthesized by some unicellular organisms. Hyaluronan (HA) (Figure 1) is also a highly hydrated polysaccharide of great biological interest.<sup>34</sup> It possesses lubricating functions in the cartilage and participates in the control of tissue hydration, in water transport, and in the inflammatory response after a trauma. It is widely used in cosmetic formulation and seems promising in tissue engineering applications.<sup>35,36</sup> Chitosan and hyaluronan are biocompatible and nontoxic. These polysac-

- (12) Mendelsohn, J. D.; Yang, S. Y.; Hiller, J.; Hochbaum, A. I.; Rubner, M. F. *Biomacromolecules* 2003, 4, 96–106.
- (13) Ladam, G.; Schaad, P.; Voegel, J.-C.; Schaad, P.; Decher, G.; Cuisinier, F. *Langmuir* 2000, 16, 1249–1255.
- (14) Ruths, J.; Essler, F.; Decher, G.; Riegler, H. *Langmuir* 2000, 16, 8871–8878.
- (15) Caruso, F.; Lichtenfeld, H.; Donath, E.; Mohwald, H. *Macromolecules* 1999, 32, 2317–2328.
- (16) Caruso, F.; Furlong, D. N.; Ariga, K.; Ichinose, I.; Kunitake, T. *Langmuir* 1998, 14, 4559–4565.
- (17) Caruso, F.; Niikura, K.; Furlong, D. N.; Okahata, Y. *Langmuir* 1997, 13, 3422–3426.
- (18) Picart, C.; Ladam, G.; Senger, B.; Voegel, J.-C.; Schaad, P.; Cuisinier, F. J. G.; Gergely, C. *J. Chem. Phys.* 2001, 115, 1086–1094.
- (19) Elbert, D. L.; Herbert, C. B.; Hubbell, J. A. *Langmuir* 1999, 15, 5355–5362.
- (20) Picart, C.; Lavalle, P.; Hubert, P.; Cuisinier, F. J. G.; Decher, G.; Schaad, P.; Voegel, J. C. *Langmuir* 2001, 17, 7414–7424.
- (21) Picart, C.; Mutterer, J.; Richert, L.; Luo, Y.; Prestwich, G. D.; Schaad, P.; Voegel, J.-C.; Lavalle, P. *Proc. Natl. Acad. Sci. U.S.A.* 2002, 99, 12531–12535.
- (22) Lavalle, P.; Gergely, C.; Cuisinier, F.; Decher, G.; Schaad, P.; Voegel, J.-C.; Picart, C. *Macromolecules* 2002, 35, 4458–4465.
- (23) DeLongchamp, D. M.; Kastantin, M.; Hammond, P. T. *Chem. Mater.* 2003, 15, 1575–1586.
- (24) McAloney, R. A.; Sinyor, M.; Dudnik, V.; Goh, M. C. *Langmuir* 2001, 17, 6655–6663.
- (25) Boujmedais, F.; Ball, V.; Schwinte, P.; Frisch, B.; Schaad, P.; Voegel, J.-C. *Langmuir* 2003, 19, 440–445.

- (26) Berth, G.; Dautzenberg, H. *Carbohydr. Polym.* 2002, 47, 39–51.
- (27) Colfen, H.; Berth, G.; Dautzenberg, H. *Carbohydr. Polym.* 2001, 45, 373–383.
- (28) Fouassac, E.; Milas, M.; Rinaudo, M.; Borsali, R. *Macromolecules* 1992, 25, 5613–5617.
- (29) Berth, G.; Voigt, A.; Dautzenberg, H.; Donath, E.; Möhwald, H. *Biomacromolecules* 2002, 3, 579–590.
- (30) Lu, C.; Luo, C.; Cao, W. *Colloids Surf., B* 2002, 25, 19–27.
- (31) Serizawa, T.; Yamaguchi, M.; Akashi, M. *Biomacromolecules* 2002, 3, 724–731.
- (32) Shenoy, D. B.; Antipov, A.; Sukhorukov, G. B.; Möhwald, H. *Biopolymers* 2003, 4, 265–272.
- (33) Kumar, M. N. V. R. *React. Funct. Polym.* 2000, 46, 1–27.
- (34) Laurent, T. C. *The chemistry, biology, and medical applications of hyaluronan and its derivatives*; Cambridge University Press: Cambridge, U.K., 1998; Vol. 72.
- (35) Lapčík, L.; Lapčík, L.; De Smedt, S.; Demeester, J.; Chabrecek, P. *Chem. Rev.* 1998, 98, 2663–2684.

## Layer by Layer Buildup of Polysaccharide Films

## Langmuir C

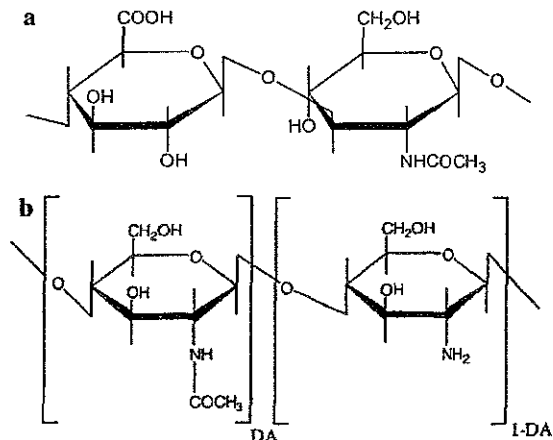


**Figure 1.** Molecular structures of the (a) hyaluronan and (b) chitosan repeating units. DA is the degree of acetylation of chitosan.

charides are biodegradable by enzymatic hydrolysis with chitosanase,<sup>37</sup> lysozyme and hyaluronidase.<sup>38</sup> Both have already been widely used in biomedical applications and have interesting intrinsic properties.<sup>39</sup> Chitosan is used particularly in pharmaceutical drug formulation, in sustained release of water-soluble drugs,<sup>40</sup> and in antibacterial treatment.<sup>41</sup> Tissue engineering based on chitosan and hyaluronan hydrogels seems also promising.<sup>42</sup> As another advantage, chitosan and hyaluronan can be easily chemically modified<sup>43–45</sup> and coupled to various molecules such as cell-targeted prodrugs<sup>46</sup> and carbohydrates.<sup>47</sup> Last, the low cost of chitosan compared to PLL (around 10 times cheaper) makes it a better candidate for industrial applications. Up to now, both polysaccharides have mostly been used in a hydrogel or membrane form.<sup>41,48,49</sup> An alternative application which we will investigate here would be to build thin films of chitosan and hyaluronan for the coating of biomaterial surfaces.

## Materials and Methods

**Polyelectrolyte Solutions.** HA (as sodium hyaluronate,  $4 \times 10^5$  g/mol) was purchased from Bioiberica (Spain). HA is a polyanionic macromolecule with  $pK_a \approx 2.9^{35}$  and has a negative

charge at pH = 5. It has a low charge density since only one residue from two is charged.<sup>50</sup> Hyaluronan labeled with Texas Red (TR) was prepared according to a previously published procedure.<sup>21</sup> Chitosan (CL113 of MW =  $1.1 \times 10^5$  g/mol, CL213 of MW =  $2.7 \times 10^5$  g/mol, and G213 of MW =  $4.6 \times 10^5$  g/mol) was purchased from FMC-Biopolymers/Novamatrix (Norway). The degree of acetylation (DA) given by the manufacturer is 13%, 16%, and 14%, respectively, for the three samples. CHI is a weak base, a positively charged polyelectrolyte in acidic conditions with  $pK_a \approx 6$ .<sup>50,51</sup> Sodium dodecyl sulfate (SDS) was purchased from Sigma, and sodium chloride (purity, 99.5%) was obtained from Fluka (St. Quentin Fallavier, France). All solutions were prepared using ultrapure water (Milli-Q plus system, Millipore) with a resistivity of  $18.2 \text{ M}\Omega \text{ cm}$ . Fresh polyelectrolyte solutions at 1 mg/mL were always prepared by dissolution of the respective adequate polymer amounts in filtered saline solutions. CHI and HA were dissolved at 1 mg/mL in 0.15 M NaCl (respectively  $10^{-2}$ ,  $10^{-3}$ , and  $10^{-4}$  M NaCl) in water and were gently stirred for several hours. The pH of the polyelectrolyte solutions in the NaCl solution was adjusted to 5 with a 0.1 M acetic acid solution. For both polyelectrolytes, taking into account their molecular weight, the concentrations were below the critical concentration  $c^*$ ,<sup>28,52</sup> (CHI/HA), architectures where  $i$  corresponds to the number of bilayer were then built.

**Fluorescein Isothiocyanate (FITC) Labeled Chitosan.** CHI (250 mg of MW =  $1.1 \times 10^5$  g/mol) was dissolved in 25 mL of distilled water to give 0.1% (w/v) solution, and then 10 mg of fluorescein 5-isothiocyanate (0.026 mmol, Sigma, St. Louis, MO) in 25 mL of DMSO was added under magnetic stirring. The pH of the solution was adjusted to 6.0, and the solution was stirred for 24 h at room temperature. The reaction mixture was then gel filtered on a Sephadex G-25. The homogeneity of the CHI–FITC was determined by gel permeation analysis by monitoring absorption at 494 nm (FITC) and 210 nm (CHI absorption). The aqueous eluate was adjusted to pH 2.0 with 0.1 N HCl and then lyophilized to give CHI–FITC in the chloride salt form. The degree of substitution was determined to be 6.5 mmol FITC per CHI saccharide unit.

**Automatic Buildup of the Polyelectrolyte Multilayered Films.** For atomic force microscopy (AFM) imaging and bacterial adhesion experiments, the (CHI/HA) films were prepared with an automatic dipping machine (Dipping Robot DR3, Kirstein and Riegler GmbH, Germany) on 12 mm glass slides (VWR Scientific, France) preliminarily cleaned with 10 mM SDS and 0.1 N HCl and extensively rinsed. The glass slides were introduced vertically in a homemade holder which was dipped for 15 min into the first polyelectrolyte solution (CHI, 15 mL) and was subsequently rinsed in three different beakers containing a 0.15 M NaCl solution at pH = 5 (or other ionic strengths depending on the working conditions). The slides were dipped in the first rinsing beaker (350 mL) and once for 6 min in the two other rinsing beakers (40 mL each). The slides were then dipped into the oppositely charged polyelectrolyte solution (HA, 15 mL) followed by the same rinsing procedure. The robot was programmed to move to fresh rinsing beakers every three layers. Slides were then stored at 4 °C until use in 24-well culture plates.

**Analysis of the Film Growth and of Its Surface Charge.** The (CHI/HA) film buildup process was followed *in situ* by optical waveguide lightmode spectroscopy (OWLS) and by *in situ* quartz crystal microbalance (QCM-Dissipation, Q-sense, Sweden).<sup>53,54</sup> Briefly, OWLS is sensitive to the penetration depth of an evanescent wave through the film near the waveguide surface (roughly over 200–300 nm) and gives access to the optical properties of the films.<sup>55,56</sup> Details about the experimental setup and the procedure can be found elsewhere.<sup>18</sup> The polyelectrolyte

- (36) Kirker, K. R.; Luo, Y.; Nielsen, J. H.; Shelby, J.; Prestwich, G. D. *Biomaterials* 2002, 23, 3661–3671.
- (37) Serizawa, T.; Yamaguchi, M.; Akashi, M. *Macromolecules* 2002, 35, 8656.
- (38) Menzel, E. J.; Farr, C. *Cancer Lett.* 1998, 131, 3–11.
- (39) Denuziere, A.; Ferrier, D.; Domard, A. *Biomaterials* 1998, 19, 1275–1285.
- (40) Kumar, M. N. V. R.; Kumar, N.; Domb, A. J.; Arora, M. In *Filled elastomers drug delivery systems*; Advances in Polymer Science, Vol. 160; Springer-Verlag: Berlin, 2002; pp 45–117.
- (41) Ikinci, G.; Senel, S.; Akincibay, H.; Kas, S.; Ercis, S.; Wilson, C. G.; Hincal, A. A. *Int. J. Pharm.* 2002, 235, 121–127.
- (42) Suh, J. K. F.; Matthew, H. W. T. *Biomaterials* 2000, 21, 2589–2598.
- (43) Desbridores, J.; Martinez, C.; Rinaudo, M. *Int. J. Biol. Macromol.* 1996, 19, 21–28.
- (44) Sabinis, S.; Block, L. H. *Int. J. Biol. Macromol.* 2000, 27, 181–186.
- (45) Prestwich, G. D.; Marecak, D. M.; Marecek, J. F.; Vercruyse, K. P.; Ziebell, M. R. *J. Controlled Release* 1998, 53, 93–103.
- (46) Luo, Y.; Prestwich, G. D. *Bioconjugate Chem.* 1999, 10, 755–763.
- (47) Morimoto, M.; Saimoto, H.; Usui, H.; Okamoto, Y.; Minami, S.; Shigemasa, Y. *Biomacromolecules* 2001, 2, 1133–1136.
- (48) Jentsch, H.; Pomowski, R.; Kundt, G.; Gacke, R. *J. Clin. Periodontol.* 2003, 30, 159–164.
- (49) Pelletier, S.; Hubert, P.; Payan, E.; Marchal, P.; Choplin, L.; Dellacherie, E. *J. Biomed. Mater. Res.* 2001, 54, 102–108.

- (50) Denuziere, A.; Ferriera, D.; Domard, A. *Carbohydr. Polym.* 1996, 29, 317–323.
- (51) Rinaudo, M.; Milas, M.; Le Dung, P. *Int. J. Biol. Macromol.* 1993, 15, 281–285.
- (52) Desbridores, J. *Biomacromolecules* 2002, 3, 342–349.
- (53) Höök, F.; Rodahl, M.; Brzezinski, P.; Kasemo, B. *J. Colloid Interface Sci.* 1998, 208, 63–67.
- (54) Rodahl, M.; Kasemo, B. *Rev. Sci. Instrum.* 1996, 67, 3238–3241.
- (55) Tiefenthaler, K.; Lukosz, W. *J. Opt. Soc. Am. B* 1989, 6, 209–220.
- (56) Vörös, J.; Ramsden, J. J.; Csucs, G.; Szendro, I.; De Paul, S. M.; Textor, M.; Spencer, N. D. *Biomaterials* 2002, 23, 3699–3710.

solutions ( $100\text{ }\mu\text{L}$ ) were injected and rinsed under constant flow rate ( $7\text{ mL/h}$ ) for 12 min with the NaCl solution. The QCM-D technique has already been described and used for the characterization of (PLL/HA) films at four different frequencies.<sup>20</sup> The quartz crystal is excited at its fundamental frequency (about 5 MHz) as well as at the third, fifth, and seventh overtones (denoted by  $\nu = 3$ ,  $\nu = 5$ , and  $\nu = 7$  and corresponding respectively to 15, 25, and 35 MHz). Changes in the resonance frequencies  $\Delta\nu$  once the excitation is stopped are measured at the four frequencies. The apparatus gives also access to the dissipation  $D$  of the vibrational energy stored in the resonator. However, as great care has to be taken with the analysis of this parameter, we will not use it in this work. The films were built by successive injections of  $500\text{ }\mu\text{L}$  of the polyelectrolyte solutions in the measuring cell (15 min adsorption for each layer) and a subsequent rinsing with  $500\text{ }\mu\text{L}$  of the NaCl solution. The  $500\text{ }\mu\text{L}$  aliquots of solution were injected within 10 s.

**ξ Potential Measurements.** Measurements of the  $\xi$  potential of the layers adsorbed on a capillary were carried out on a homemade streaming potential measurement apparatus developed by Zembala and Déjardin.<sup>57</sup> The apparatus has been previously described.<sup>13,20</sup> By measuring the pressure and the potential differences on both sides of a  $530\text{ }\mu\text{m}$  radius capillary made of fused silica via two flasks containing four electrodes, one gets access, through the Smoluchowski relation, to the  $\xi$  potential of the capillary. Details about the procedure are given in Picart et al.<sup>20</sup> Polyelectrolytes were adsorbed in the  $0.15$  or  $10^{-4}\text{ M}$  NaCl solution, and measurements were performed after the rinsing of each layer. The rinsing solution (also that used for the measurements) contained only Tris at  $5 \times 10^{-4}\text{ M}$  (pH = 5).

**Atomic Force Microscopy.** The images were obtained in contact mode in liquid conditions with the Nanoscope IV from Veeco (Santa Barbara, CA).<sup>22</sup> Cantilevers with a spring constant of  $0.03\text{ N/m}$  and with silicon nitride tips were used (model MSCT-AUHW, Veeco, CA). Several scans were performed over a given surface area. These scans had to give reproducible images to ascertain that there is no sample damage induced by the tip. Deflection and height mode images are scanned simultaneously at a fixed scan rate (2 Hz) with a resolution of  $512 \times 512$  pixels. For all the observations, the samples were kept under liquid.

**Confocal Laser Scanning Microscopy (CLSM).** For the CLSM experiments, the film-coated glass slides were prepared with the dipping robot. The dye-conjugated polyelectrolytes, respectively HA-TR and CHI-FITC, were adsorbed in the same way at a certain stage of the buildup. As an example, (CHI/HA)<sub>19</sub>-(CHI<sub>20</sub>-FITC) corresponds to a film composed of 19 bilayers on the top of which a final layer of CHI<sub>20</sub>-FITC has been adsorbed. Each film observed at a given stage of the construction corresponds to a totally new buildup. The configuration of the microscope and the parameters used for the CLSM observations on a Zeiss LSM510 microscope have been given elsewhere.<sup>21</sup> The 12 mm glass slides were introduced in a homemade chamber and observed by imaging a series of consecutive overlapping optical sections ( $x-y$  images at different depth  $z$ ). Orthogonal vertical sections were computed in order to image a ( $x-z$ ) section of the film.

**Proliferation of Chondrocytes.** Chondrocytes were isolated from femoral head caps and cultured as previously described.<sup>58</sup>  $^3\text{H}$ -thymidine uptake was used to evaluate cell proliferation. Briefly, cells were distributed into 24-well plates containing the film-coated glass slides ( $10^6/\text{well}/\text{slide}$ ) in a total volume of  $2\text{ mL}$  of DMEM supplemented. The medium was changed after 3 days; then at 4 days, the cultures were pulsed with thymidine-methyl- $^3\text{H}$  (Perkin-Elmer Sciences, Belgium) ( $5\text{ }\mu\text{Ci/mL}$ ) for 24 h and the cells that were partially adherent were harvested by PBS washing ( $2\text{ mL}$ ). After washing, the adherent cells were trypsinized and lysed by freeze/thaw cycles. The cell lysates were transferred into liquid scintillation vials. Total radioactivity was quantified by liquid scintillation counting (Packard-Perkin-Elmer, France). Data are expressed as mean percent  $\pm$  standard error of the mean (SEM) of cell binding, the reference being the noncoated glass slides.

**Bacterial Adhesion Assay.** The *Escherichia coli* Gram-negative strain used for the study has been kindly provided by Dr. Ph. Bocquet (Centre d'Etudes Nucléaires, Saclay, France). To obtain fluorescent bacteria, the *E. coli* were transformed using a plasmide bearing the GFPmut3 (Green Fluorescent protein mutant 3) gene under the control of the *Salmonella typhimurium* ribosomal protein promoter (a generous gift of Dr. B. Lemaitre, CNRS -CCM, Gif-sur-Yvette, France). The transformed bacteria expressing GFP were grown aerobically in Luria Broth (LB) and selected with ampicillin. For the adhesion tests, the bacteria were harvested in midexponential phase, diluted in LB to an optical density of 0.1 at a wavelength of 600 nm, and plated on the (CHI/HA) films. After 30 min, the films were rinsed three times with PBS. The bacteria adsorbed on the substrate were visualized using an inverted fluorescence microscope (Nikon, Eclipse TE200) and photographed using a digital camera (DXM-1200, Nikon).

The experiment was reproduced three times. For each experiment, three different slides were prepared per condition. Fifteen randomly chosen fields were taken per slide at a magnification of  $\times 400$ , and the mean number of bacteria per counting area was derived for each slide. Later on, the mean number and the SEM were calculated for each experimental condition. With this method, each condition generated at least  $3 \times 3 \times 10 = 90$  counting areas.

### Exponential Growth Mechanism

Before discussing the results, let us briefly summarize the mechanism of the exponential growth which is necessary for a good understanding of the present work. For the system (PLL/HA), it is known that PLL is the diffusing species whereas HA seems to be unable to diffuse through the multilayer.<sup>21</sup> We will discuss the mechanism for this particular system with the understanding that it is much more general. The deposition of one bilayer for this system is summarized schematically in Figure 2. Figure 2A represents the state of the film at the end of a HA deposition step, the multilayer being in contact with the buffer. Due to the charge overcompensation that takes place when a film is in contact with a polyanion solution, an excess of negative charge is present at the outer layer of the film. This negative charge excess creates a negative electrostatic barrier which extends into the solution typically over the Debye length. When this film is brought in contact with a PLL solution (Figure 2B), PLL chains first interact with the outer negative charges forming PLL/HA complexes, rendering the outer surface positive. PLL chains from the solution can however cross this energy barrier and diffuse into the film. These PLL chains will be called "free" chains. As they diffuse into the film, the chemical potential of the free PLL chains increases and diffusion into the film stops when the chemical potential of the free PLL chains in the film becomes equal to that of the PLL chains in the solution (Figure 2C). For the PLL/HA films, it was shown by OWLS that the diffusion of PLL into the film is accompanied by a swelling of the film. When this film is then brought in contact with a pure buffer solution, free PLL chains from the film can again cross the electrostatic energy barrier in the reverse direction and diffuse out of the film (Figure 2D). As this process takes place, the concentration of free PLL chains diminishes and their chemical potential diminishes as well. Therefore, the PLL chains have to cross an increasing energy barrier in order to diffuse out of the film. As soon as this barrier becomes larger than  $kT$ , the diffusion process out the film stops. Consequently, all the free PLL chains within the film do not diffuse out of it during the rinsing step. When this film is further brought in contact with a HA solution, HA interacts with the outer PLL layer to form PLL/HA complexes. The outer surface becomes then negatively charged so that the positive electrostatic

(57) Zembala, M.; Déjardin, P. *Colloids Surf., B* 1994, 3, 119–129.  
(58) Miralles, G.; Baudoin, R.; Dumas, D.; Baptiste, D.; Hubert, P.; Stoltz, J.-F.; Dellacherie, E.; Mainard, D.; Netter, P.; Payan, E. *J. Biomed. Mater. Res.* 2001, 57, 268–278.

*Layer by Layer Buildup of Polysaccharide Films*

*Langmuir E*

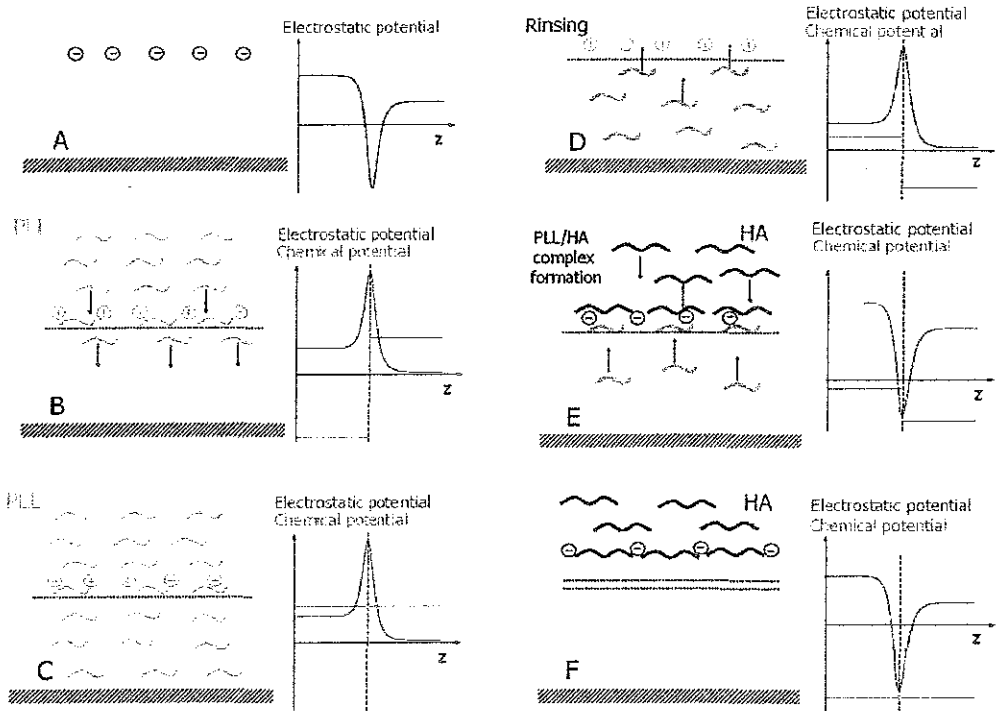


**Figure 2.** Drawing of the buildup mechanism of PLL/HA film. (A) At the end of a HA deposition step with a negative electrostatic potential at the top of the film. (B) PLL interaction with the surface renders it positive; PLL chains can cross the energy barrier and diffuse into the film. As they diffuse into the film, the chemical potential of free PLL chains increases and (C) diffusion stops when the chemical potential of the free PLL chains in the film is equal to that of the PLL chains in the solution. (D) During the rinsing phase with pure buffer, the free PLL chains can cross the electrostatic energy barrier in the reverse direction and diffuse out of the film. During this process, the chemical potential of these chains diminishes as well. (E) When this film is further brought in contact with a HA solution, HA chains interact with the outer PLL layer to form PLL/HA complexes which form the new outer layer of the film. The positive electrostatic barrier totally disappears. The remaining free PLL chains can thus diffuse out of the film. (F) The diffusion process stops when all the free PLL chains inside of the film have diffused out of it.

barrier totally disappears. The remaining free PLL chains can thus diffuse out of the film. As soon as they reach the film/solution interface, they interact with HA chains from the solution and form new HA/PLL complexes that form the new outer layer of the film (Figure 2E). The process stops when all the free PLL chains present inside of the film have diffused out of it (Figure 2F). The film is further rinsed and recovers a state similar to that described in Figure 2A with an additional PLL/HA layer on top of it. Both the PLL diffusion into and out of the film and the nondiffusion of HA into the film have directly been demonstrated by means of confocal laser microscopy using fluorescently labeled PLL and HA.<sup>21</sup> Moreover, the mass of the new PLL/HA deposited layer must be proportional to the amount of free PLL chains present in the film at the end of the rinsing step represented in Figure 2D. This amount is therefore approximately proportional to the film thickness itself before the given deposition step. As a consequence, the mass of the new deposited layer grows exponentially with the number of deposition steps. The growth mechanism outlined above seems to apply to several reported exponentially growing films with some variations. For the poly(L-lysine)/poly(L-glutamic acid) system, both polyelectrolytes seem to diffuse in and out of the film during each bilayer deposition step.<sup>22</sup> In the above description, we assumed that the positive electrostatic barrier builds up almost instantaneously, as soon as the film is brought in contact with the PLL solution. However, this is not absolutely needed and a gradual electrostatic barrier could build up. In such a case, the

polycation diffusion into the film could stop before the chemical potentials of the free polycations in the film and in the solution are equal. Then, when the film is further brought in contact with pure buffer, the energy barrier can be higher than  $kT$ . As a consequence, no free polyelectrolyte diffuses out of the film during the rinsing step. This has been observed for the system PGA/PAH<sup>23</sup> where PGA diffuses into the film but does not diffuse out of the film during the rinsing step.

## Results and Discussion

**Buildup Mechanism for Film Constructed at 0.15 M NaCl.** All the experiments described in this section were performed with CHI of mass  $1.1 \times 10^5$  g/mol, and the films were constructed at pH 5 with polyelectrolyte and rinsing solutions containing 0.15 M NaCl. The stepwise adsorption of CHI and HA was first monitored by *in situ* OWLS and QCM experiments (Figure 3). A typical raw  $N_{TM}$  signal observed during the alternate adsorption of CHI and HA is given in Figure 3A. The effective refractive index  $N_{TM}$  increases after each new CHI and HA deposition up to the 6th layer pair, indicating that CHI and HA adsorb in a layer by layer process. The typical evolution of the optical signal changes by further increasing the number of adsorption cycles. Whereas it continues to increase during each HA deposition, the signal decreases when CHI is adsorbed and increases during the following rinsing step. At the end of the CHI adsorption step, the signal remains lower than at the end of the previous HA rinsing step, and after the deposition of the 9th bilayer the

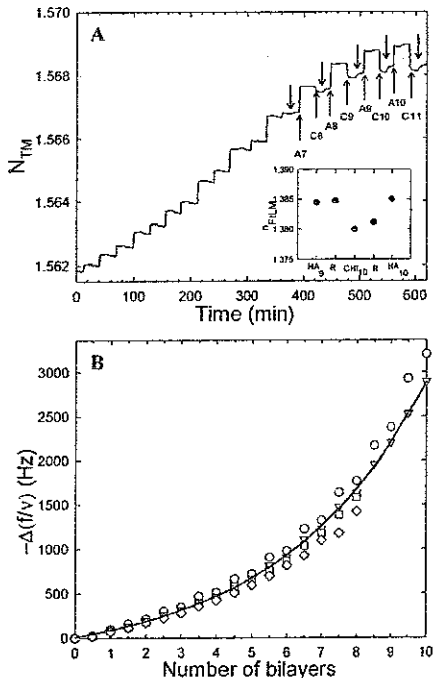


**Figure 3.** (A) Raw  $N_{TM}$  signals obtained in 0.15 M NaCl during a (CHI/HA)<sub>11</sub> film buildup as measured by the OWLS technique, as a function of time (CHI, MW =  $1.1 \times 10^5$  g/mol; HA, MW =  $4.0 \times 10^5$  g/mol). Upward thin long arrows indicate polyelectrolyte injection (respectively  $C_i$  for the  $i$ -th cation layer and  $A_i$ , for the  $i$ -th anion layer), and downward arrows indicate rinsing phases. (Inset) Evolution of  $n_{FILM}$ , the refractive index of the film near the waveguide at the end of each buildup step during one buildup cycle. (B) QCM frequency shifts ( $-\Delta f/v$ ) during the alternate deposition of CHI and HA layers on a SiO<sub>2</sub> crystal obtained at four different harmonics [○ 5 MHz, □ 15 MHz, ▨ 25 MHz, and ◊ 35 MHz] as a function of the number of deposition cycles.

evolution of the signal becomes fully cyclic:  $N_{TM}$  takes similar values at the end of each CHI addition, CHI rinsing, HA addition, and HA rinsing step. By analyzing the raw data using the homogeneous and isotropic bilayer model, we found thicknesses of the order of 150–200 nm at the end of the first 8 deposited layer pairs. Similar observations were already made for (PLL/HA) films built in water containing 0.15 M NaCl.<sup>20</sup> They were explained by the fact that OWLS is an optical technique that senses the film with an evanescent wave (the penetration depth is of the order of 200–300 nm). When the film becomes thicker than the penetration length, the signal is no longer sensitive to the evolution of the outer part of the film but is sensitive to the changes of the refractive index of the film near the substrate. For PLL/HA, the cyclic behavior was explained by changes in the refractive index of the film consecutive to the PLL diffusion in and out of the film during the different buildup steps. A similar explanation may hold for the CHI/HA system. It is thus expected that CHI/HA films reach thicknesses larger than 200–300 nm after the deposition of 9 bilayers. Close similarity of the evolutions of the OWLS signals during the (CHI/HA) and the (PLL/HA) multilayer constructions strongly indicates that CHI seems to diffuse in and out of the film at each deposition step whereas HA does not. The decrease of the  $N_{TM}$  signal when the film is brought in contact with a CHI solution further indicates that the diffusion of CHI into

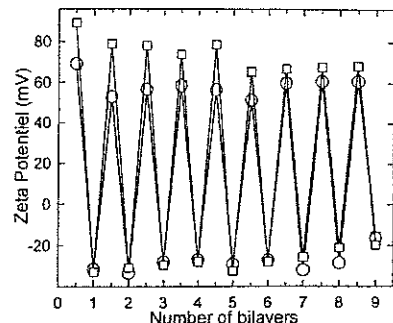


**Figure 4.** Evolution of the  $\xi$  potential (mV) during the alternate deposition of CHI and HA layers as a function of the number of deposition cycles. CHI (MW =  $1.1 \times 10^5$  g/mol) and HA (MW =  $4.0 \times 10^5$  g/mol) were prepared at 1 mg/mL in a 0.5 mM Tris-HCl buffer (pH = 5) containing 0.15 M NaCl (○) or  $10^{-4}$  M NaCl (□). The lines have no physical meanings but were added to guide the eyes. Each point represents the mean value of three successive measurements. Standard deviations are so small that they are not visible on the graph.

the film must be accompanied by a swelling of the film in such a way that its mean refractive index decreases. This is indeed seen in the inset of Figure 3A where the refractive index of the film is evaluated by considering an infinitely thick film. The values of the refractive indexes calculated independently from the  $N_{TE}$  and  $N_{TM}$  closely match. This confirms the validity of the thick film assumption.

Figure 3B shows the evolution of the normalized frequency shifts  $-\Delta f/v$  measured by QCM-D at the fundamental resonance frequency (5 MHz,  $v = 1$ ) of the quartz crystal and at three overtones (15 MHz,  $v = 3$ ; 25 MHz,  $v = 5$ ; and 35 MHz,  $v = 7$ ). The only slight dependence of  $-\Delta f/v$  with  $v$  indicates that the Sauerbrey relation should hold within a good approximation. The exponential increase of  $-\Delta f/v$  with the number of deposited bilayers then demonstrates the exponential character of the CHI/HA buildup process. An exponential growth was also observed for shorter deposition times (10 min and also 5 min). The frequency shifts are higher in the case of the (CHI/HA) film than for the (PLL/HA) film (Figure 2 from Picart et al.<sup>21</sup>) suggesting an increased adsorbed mass. Also, the small differences in  $-\Delta f/v$  for the four harmonics measured for the (CHI/HA) film compared to the (PLL/HA) film suggest that the (CHI/HA) films are more rigid than the latter one. Thus, the (CHI/HA) film is expected to be thinner and more rigid than the investigated (PLL/HA) multilayer which was of the order of 1  $\mu$ m after the deposition of 10 bilayers. Previously, (CHI/polystyrene-sulfonate)<sup>59</sup> and (CHI/dextran) films<sup>31</sup> were found to grow linearly with the number of adsorption cycles (respectively at 0.25 M and at 0.2 M NaCl), but the measurements were performed on dried films in air. It is thus difficult to compare the experiments performed under such different conditions.

The  $\xi$  potential of the film after each new polyelectrolyte deposition from a Tris-HCl buffer (containing 0.15 M NaCl) is presented in Figure 4. After deposition of the first CHI layer, the surface becomes positively charged (ca. +70 mV). The deposition of the following HA layer leads to a charge reversal (ca. -35 mV). Subsequent depositions show comparable behaviors indicating that each new CHI and HA adsorption leads to an overcompensation of the previous charge excess. The potentials

(59) Lvov, Y.; Onda, M.; Ariga, K.; Kunitake, T. *J. Biomater. Sci. Polym. Ed.* **1998**, 9, 345–355.

## Layer by Layer Buildup of Polysaccharide Films

## Langmuir G

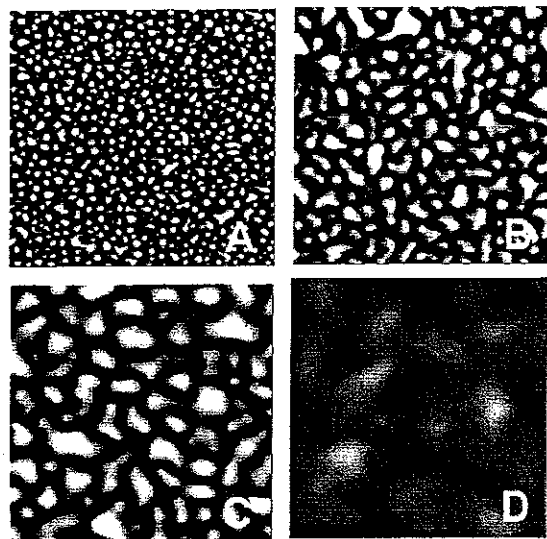


**Figure 5.** AFM height mode images in liquid obtained at the different steps of the alternate deposition of CHI and HA layers on a glass substrate. The polyelectrolytes CHI ( $MW = 1.1 \times 10^6$  g/mol) and HA ( $MW = 4.0 \times 10^5$  g/mol) were prepared at 1 mg/mL in 0.15 M NaCl adjusted to pH = 5 by means of acetic acid. Different stages during the buildup process are visualized: (A)  $(\text{CHI/HA})_3$ , (B)  $(\text{CHI/HA})_5$ , (C)  $(\text{CHI/HA})_7$ , and (D)  $(\text{CHI/HA})_{10}$ . The image dimensions are  $3 \times 3 \mu\text{m}^2$ , and the maximum Z-ranges are 20 nm for image A, 40 nm for image B, and 80 nm for images C and D.

oscillate between ca.  $-30$  mV for HA-terminating layers and ca.  $+60$  mV for CHI-ending layers. These variations of the  $\zeta$  potential confirm that the effective surface charge alternates after the deposition of each new polyelectrolyte layer.

The various steps of a  $(\text{CHI/HA})_n$  film buildup process were also imaged by AFM as a function of the number of deposited bilayers (Figure 5). At the early stages of the deposition, for  $(\text{CHI/HA})_1$ , small islets are seen with a characteristic width of the order of 60 nm. As the number of deposited bilayers increases, the islets coalesce and become larger, respectively 100 nm for  $(\text{CHI/HA})_3$  and 250 nm for  $(\text{CHI/HA})_5$ . After the deposition of approximately 10 bilayers, the surface becomes fully coated and a homogeneous film is observed. Scratching the film at this step indicates that its thickness is of the order of 300 nm with a maximum rugosity of the order of 35 nm. These results confirm the conclusions drawn from the OWLS experiments as far as the film thickness is concerned (after 9 bilayers have been deposited, the OWLS signal becomes cyclic). Even if the film is not fully homogeneous but is made of CHI/HA complexes, the evolution of the film mass is still well approximated by an exponential. QCM-D provides therefore useful information on the buildup process even at this early stage. We will make use of this observation in the following section. From cross-sectional AFM images, it was possible to estimate the contact angles of the nodules on the surface during the buildup of the film (Table 1). One can first observe that for a given number of deposited layers, the range of the measured angles is narrow ( $\pm 5^\circ$ ), indicating that the composition of the islets should be similar. However, contact angles increase with the number of deposited layers, suggesting an evolution of the polyelectrolyte composition in the islands as the buildup process goes on. The AFM images of the  $(\text{CHI/HA})$  system resemble

**Table 1.** Contact Angles (deg) of the Islands<sup>a</sup> on the Surface during the Alternate Deposition of the Layers Built in 0.15 M NaCl and in  $10^{-4}$  M NaCl Solution Determined from AFM Images

	contact angle	standard deviation
	0.15 M NaCl	
$(\text{CHI/HA})_1$	6.6	4.2
$(\text{CHI/HA})_3$	12.0	4.1
$(\text{CHI/HA})_5$	15.2	4.0
$(\text{CHI/HA})_7$	21.3	4.7
	$10^{-4}$ M NaCl	
$(\text{CHI/HA})_{30}$	19.6	4.3
$(\text{CHI/HA})_{50}$	24.7	5.4

<sup>a</sup> Average of at least 35 measurements.



**Figure 6.** Vertical section through a  $(\text{CHI/HA})_{36}$  multilayer containing two labeled layers,  $\text{CHI}_{36}\text{-FITC}$  (green) and  $\text{HA}_{36}\text{-TR}$  (red), obtained from CLSM observations (same polyelectrolytes as for Figure 5). The glass substrate (bottom of the chamber) is indicated with a white line. The image size is  $20.2 \mu\text{m} \times 6.0 \mu\text{m}$ . Green fluorescence (corresponding to  $\text{CHI-FITC}$ ) is visible over a total thickness of around  $2.4 \mu\text{m}$  (white arrow).

those obtained for  $(\text{PLL/HA})_n$  films in the presence of 0.15 M NaCl<sup>20</sup> except that the observed nodules for these latter films were much higher ( $\approx 900$  nm) and wider (a few micrometers wide). However, these former images were obtained with HA or  $MW = 1.5 \times 10^6$  g/mol. Indeed, even if the thickness of the  $(\text{PLL/HA})_{10}$  film was around 1  $\mu\text{m}$  compared to 300 nm for the  $(\text{CHI/HA})_{10}$  films, the transition from nodules to a continuous film takes place in both cases at around the same number of deposited bilayers (8 for  $(\text{PLL/HA})$  and 9 for  $(\text{CHI/HA})$ ).

To get more direct information on the diffusion ability of CHI or HA, we imaged such architectures by CLSM. To this aim, CHI-FITC and HA-TR were incorporated in the film architecture. Figure 6 represents a  $(\text{CHI/HA})_{36}$  film where CHI-FITC and HA-TR constitute the final 36th deposited layer. The green fluorescent zone constitutes a large and continuous band demonstrating that the CHI-FITC, although added at the outermost layer of the film, diffused through the whole film up to the substrate. The thickness of the  $(\text{CHI/HA})_{36}$  film could be estimated to be around  $2.4 \mu\text{m}$ . On the other hand, the red band at the top of the film clearly shows that HA does not diffuse within the film but remains deposited on the outer top layer. The fact that the film appears green after being in contact with HA needs some complementary explanations to the simple picture outlined in the introduction of the exponential growth mechanism. Indeed, when the film containing free CHI-FITC chains is brought in contact with an HA solution, it is expected from the simple model that the entire free CHI-FITC chains diffuse out of the film and remain present only in the outer layer formed by CHI-FITC/HA complexes. This is clearly not the case. Indeed, during the CHI-FITC deposition step, the free CHI-FITC molecules, present in the film, exchange with nonlabeled CHI chains that are involved in the matrix of the CHI/HA film. "Fixed" CHI chains exchange with free CHI-FITC chains so that when the film is further brought in contact with an HA solution, the free CHI chains that

diffuse out of the film are both labeled and nonlabeled chains and the matrix of the film contains both species too. A similar effect was previously observed for the (PLL/HA)<sub>n</sub> films.<sup>21</sup> CHI and PLL constitute in both cases the diffusing species whereas HA does not diffuse. Shenoy et al.<sup>32</sup> observed (sodium alginate/CHI) hollow capsules by CLSM using CHI-rhodamine as the fluorescent polyelectrolyte. The wall thickness of their capsules was around 1.5 μm and appeared homogeneous. One may thus deduce that (alginate/CHI) multilayers also grow exponentially and that CHI is able to diffuse through these films too.

**Effect of the Salt Concentration on the Buildup Process.** We also investigated the influence of the salt concentration on the diffusion process and on the buildup process of the (CHI/HA) films. Salt concentrations above 0.15 M were not explored since HA solubility decreases when the ionic strength is increased and since, in our previous OWLS studies, we found that (PLL/HA) films could not be built in 0.5 M NaCl solutions (the OWLS signal remaining almost flat after each polyelectrolyte adsorption). The formation of (CHI/HA)<sub>n</sub> films from solutions containing respectively 10<sup>-2</sup> and 10<sup>-4</sup> M NaCl was followed *in situ* by QCM-D (Figure 7). The frequency shifts become lower when the NaCl concentration is decreased, indicating that the deposited amounts per bilayer decrease with the salt concentration. A progressive transition from an exponential to a linear growth regime is observed when the ionic strength decreases from 0.15 to 10<sup>-4</sup> M. We also found a linear growth for a (CHI/HA)<sub>8</sub> film built at 10<sup>-4</sup> M NaCl on top of an exponentially growing (CHI/HA)<sub>9</sub> film (built in 0.15 M NaCl) (Figure 1, Supporting Information). The film constructions performed from 10<sup>-2</sup> and 10<sup>-4</sup> M NaCl solutions were also observed by AFM. In all three cases, the surface is covered by islets after the first deposition steps. As a general trend and for a given number of deposition steps, the surface coverage and the size of the islets decrease with the NaCl concentration. At 10<sup>-2</sup> M NaCl, the transition from the islets to the uniform film takes place after the deposition of 20 (CHI/HA) bilayers with a film thickness of the order of 120 nm (Supporting Information, Figure 2) compared to the ≈300 nm in the presence of 0.15 M NaCl. For 10<sup>-4</sup> M NaCl solutions, we could not experimentally reach the islet/film transition even after the deposition of 50 bilayers. Although the surface is only covered by islets, we found previously that QCM-D provides useful information about the buildup mechanism. Figure 7 focuses also on the evolution of  $-\Delta f/v$  over three deposition cycles at 0.15, 10<sup>-2</sup>, and 10<sup>-4</sup> M NaCl. This parameter is, in first approximation, proportional to the deposited mass on the surface. At 0.15 M NaCl (Figure 7B), the mass increase is very rapid as soon as the surface is brought in contact with the CHI or HA solutions. A slight desorption is observed during the rinsing steps. At 10<sup>-2</sup> and 10<sup>-4</sup> M (Figure 7C), the evolution of the deposited mass is more complex. For films constructed from 10<sup>-4</sup> M NaCl solutions, it increases rapidly when brought in contact with a CHI solution. During the rinsing step, the signal decreases slightly. When this surface is further brought in contact with a HA solution, the signal first increases rapidly, peaks, and then decreases steadily. The decrease of the signal continues during the rinsing steps and levels off at a value slightly higher than before contact with the HA solution. When the film is constructed from 10<sup>-2</sup> M solutions, one observes such a "peaked" evolution during contact with the CHI solution. Here too, the signal continues to decrease during the rinsing step and reaches even a value smaller than before contact with the CHI

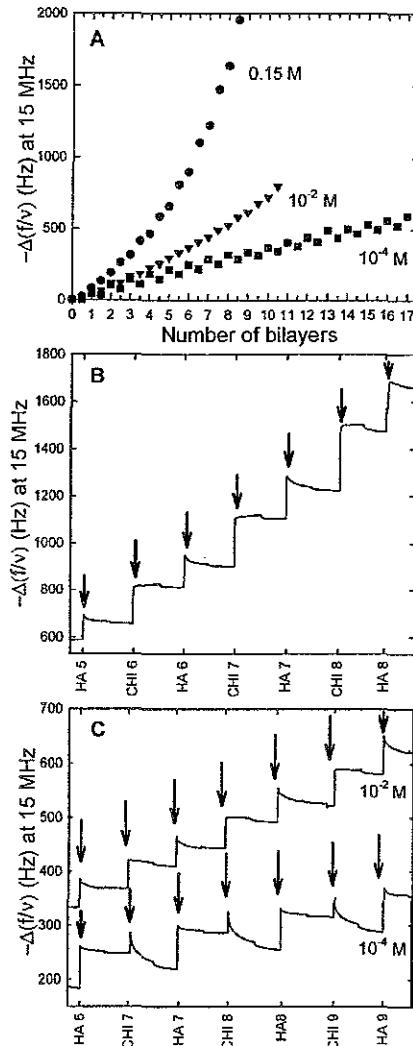


Figure 7. (A) Differences in the QCM frequency shifts  $-\Delta f/v$  for each CHI and HA layer during the layer by layer deposition of CHI/HA multilayer films. CHI ( $MW = 1.1 \times 10^5$  g/mol) and HA ( $MW = 4.0 \times 10^5$  g/mol) solutions were prepared at 1 mg/mL at pH 5 in 0.15 M NaCl (●), 10<sup>-2</sup> M NaCl (▼), and 10<sup>-4</sup> M NaCl (■) solution. For clarity, only the 15 MHz harmonic is given. Focus on the kinetics of the frequency shifts obtained at different ionic strengths during the adsorption of CHI and HA over three adsorption cycles, as a function of time: (B) 0.15 M NaCl; (C) 10<sup>-2</sup> and 10<sup>-4</sup> M NaCl. Thin arrows indicate each polyelectrolyte injection.

solution. However, the evolution of the  $\zeta$  potential during the buildup of (CHI/HA) films from 10<sup>-4</sup> M NaCl solutions exhibits a behavior similar to that of films built in the presence of 0.15 M NaCl (Figure 4). The sign of the  $\zeta$  potential alternates after each CHI or HA addition with values apparently independent of the ionic strength. This suggests an adsorption of CHI molecules on top of the HA layers.

A similar evolution is observed when the surface is brought in contact with the HA solution but to a much smaller extent, the signal remaining almost constant after the initial large increase and during the rinsing step. Such a peaked evolution was already reported by Cohen Stuart

## Layer by Layer Buildup of Polysaccharide Films

## Langmuir I

and co-workers<sup>60</sup> who attributed it to a polyelectrolyte deposition and redissolution of the polyelectrolyte complexes following the contact between the film and the polyelectrolyte solution. In their example, the mass decrease always stopped during the rinsing step when the film was in contact with a pure buffer solution. This is not the case in our system where the mass steadily decays during the rinsing steps.

OWLS experiments performed in the cyclic regime at  $10^{-2}$  M NaCl (see Figure 3, Supporting Information) strongly suggest that CHI diffuses in and out of the film during each bilayer deposition step whereas HA does not. Such experiments were not doable at  $10^{-4}$  M NaCl due to the fact that a film is still not formed after 50 bilayer deposition steps. Let us thus assume that CHI can still diffuse into the CHI/HA nodules and that HA does not at  $10^{-4}$  M NaCl as we demonstrated for films constructed at 0.15 M NaCl and strongly suggested at  $10^{-2}$  M NaCl. The evolutions of the QCM-D signals can then be explained in the following way: at  $10^{-2}$  M, when the surface is brought in contact with the CHI solution, CHI interacts strongly with the outer HA layer of the nodules and diffuses into them. The diffusion process is however slower than at 0.15 M NaCl due to a larger persistence length of the polyelectrolyte, as seen by the slow signal stabilization. When the surface is further brought in contact with the HA solution, after rinsing, HA first interacts strongly with the outer CHI layer and with the free CHI chains that diffuse out of the nodules. The first chains that diffuse out of the nodules form stable complexes with HA which constitutes the new outer layer. However, as the diffusion process of CHI out of the nodule continues, the CHI/HA complexes from the outer layer become richer in CHI and finally start to become unstable, as suggested by Cohen Stuart.<sup>60</sup> These complexes forming the outer layer start to dissolve. When the HA solution is rinsed by pure buffer before the nodules are empty of free CHI chains, the diffusion process out of the nodules continues as well as the redissolution of the CHI/HA complexes. Only part of the initially formed CHI/HA complexes thus remain on the outer layer of the nodules. This explains the slower increase of the deposited mass per bilayer at  $10^{-2}$  M when compared to the 0.15 M NaCl case. At  $10^{-4}$  M, when the surface is brought in contact with the HA solution, HA chains interact directly with the outer CHI layer and then form complexes with the free CHI chains that diffuse out of the nodules. Only a little redissolution is observed in this case. However, when this surface is further brought in contact with a CHI solution, CHI first interacts with the outer HA layer but strong redissolution of the previously formed CHI/HA complexes seems to take place. A large part of the CHI/HA complexes formed in the previous step during the interaction between the free CHI chains (diffusing out of the nodules) and the HA chains present in the solution are redissolved. Only the complexes formed by the interaction of the HA chains from the solution with the outer CHI layer remain. These complexes are expected to be of a different nature than the ones formed between HA and the free diffusing CHI chains and may also become more cohesive. In the case of  $10^{-4}$  M salt concentration, the deposited mass will increase linearly with the number of deposition steps as is observed experimentally. At very low salt concentration ( $10^{-4}$  M), interactions occur strongly, and at higher ionic concentration (0.15 M NaCl) electrostatic screening has to be considered. Hence it may be assumed that strong interac-

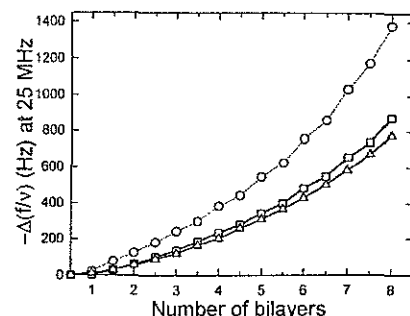


Figure 8. Influence of the molecular weight of chitosan on the CHI/HA film growth as followed by QCM. The frequency shifts  $-\Delta f/v$  measured at 25 MHz are shown for HA of constant MW =  $4.0 \times 10^5$  g/mol and CHI of  $1.1 \times 10^5$  g/mol (○),  $2.7 \times 10^5$  g/mol (□), and  $4.6 \times 10^5$  g/mol (△).

tions at low ionic strength between CHI and HA lead to a low diffusion. Moreover, persistence length is larger in low salt concentration solutions, which may decrease also diffusion.

**Effect of the Mass of CHI.** The exponential growth of the CHI/HA system is related to the ability of CHI to diffuse in and out of the whole film during each deposition step and to the nondesorption of the CHI/HA complexes formed. This ability may be influenced by the mass of the CHI chains. Additionally, the mass of the diffusing polyelectrolyte may also influence the buildup rate. To investigate this point, we performed experiments with CHI of MW =  $1.1 \times 10^5$ ,  $2.7 \times 10^5$ , and  $4.6 \times 10^5$  g/mol, the mass of HA remaining fixed at  $4.0 \times 10^5$  g/mol. These experiments were performed by OWLS and by QCM-D at 0.15 M NaCl at pH 5. For the three systems, the frequency shifts  $-\Delta f/v$  exhibit an exponential growth with the number  $i$  of deposited bilayers (Figure 8). This indicates that the CHI chains are able to diffuse through the film at least up to a mass of  $4.6 \times 10^5$  g/mol. Indeed,  $-\Delta f/v$  increases more rapidly with  $i$  for the smaller CHI mass compared to the films constructed with CHI of MW =  $2.7 \times 10^5$  and  $4.6 \times 10^5$  g/mol. For these two latter MWs, the mass increases with  $i$  are difficult to distinguish within experimental errors even if the increase is slightly steeper for the smaller mass. These results suggest that the film buildup is more rapid when the mass of the diffusing polyelectrolyte is smaller. On the other hand, whereas  $-\Delta f/v$  is rather independent of  $v$  for the films constructed with the  $1.1 \times 10^5$  g/mol CHI, it becomes strongly  $v$  dependent for the larger CHI masses (data not shown). Thus, the viscoelastic properties of the films depend on the mass of the diffusing polyelectrolyte. The film seems to be more rigid when the mass of CHI is smaller. The observed effect is not at all obvious since the mass increase with  $i$  is essentially of thermodynamic and not of kinetic origin and since it is not possible, up to now, to predict the amount of polyelectrolyte that can diffuse into a film.

**Biological Properties of CHI/HA Films.** This physicochemical study allowed us to precisely determine the conditions which lead to the formation of a uniform (CHI/HA) film, for example, after the deposition of around 10 bilayers at 0.15 M NaCl and 20 bilayers at  $10^{-2}$  M NaCl. At lower ionic strengths, we could not get a uniform film up to 50 bilayers. To test such (CHI/HA) uniform films with respect to cell and bacterial adhesion, we will now test the two conditions (at  $10^{-2}$  M NaCl and at 0.15 M NaCl) where uniform films and full substrate coverage were reached. The cell adhesion measurements were performed only at 0.15 M NaCl, whereas the bacterial

(60) Kovacevic, D.; van der Burgh, S.; de Keizer, A.; Cohen Stuart, M. A. *Langmuir* 2002, 18, 5607–5612.

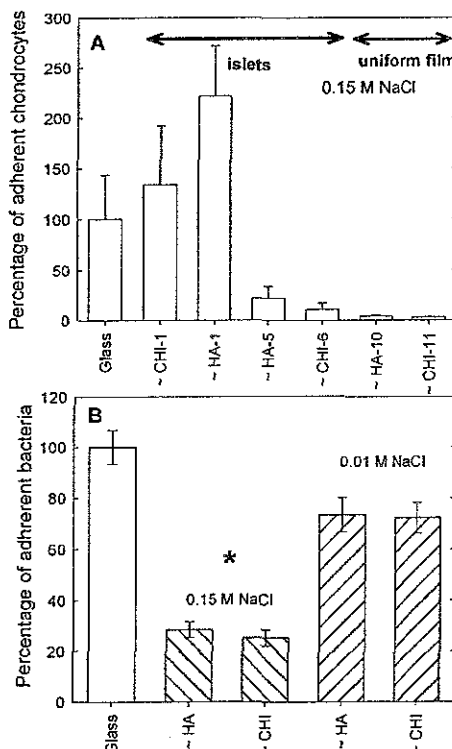


**Figure 9.** (A) Adhesion of primary rat chondrocytes as measured by  $^3\text{H}$ thymidine after 4 days of contact with (CHI/HA)<sub>n</sub> films built in 0.15 M NaCl and containing an increasing number of layers (1, 5, and 10) and either terminated by -CHI or -HA. (B) Bacterial adhesion per mm<sup>2</sup> on bare silica for a (CHI/HA)<sub>10</sub>, a (CHI/HA)<sub>10</sub>-CHI multilayer film built in 0.15 M NaCl at pH = 5, a (CHI/HA)<sub>20</sub>, and a (CHI/HA)<sub>20</sub>-CHI multilayer film built in 10<sup>-2</sup> M NaCl at pH = 5. The fluorescence images were obtained after 30 min of contact with the bacteria and a gentle rinse with PBS. Each multilayer film was generating at least 30 counting areas. The numbers represent the mean  $\pm$  standard deviation of at least three experiments. The adhesion was statistically different on the (CHI/HA) films built at 0.15 M NaCl as compared to glass and to those built in 10<sup>-2</sup> M NaCl (Student's test  $P < 0.01$ ).

adhesion experiments were done for films built both in 0.15 M NaCl and in 10<sup>-2</sup> M NaCl solutions.

Primary chondrocytes were cultured for 4 days on (CHI/HA)<sub>n</sub> films built at 0.15 M NaCl and containing an increasing number of layers (Figure 9). These cells possess a specific receptor for hyaluronan.<sup>61</sup> However, it appeared that the cell adhesion (as measured by the incorporation of  $^3\text{H}$ thymidine) decreased when the number of layers of the film increased. Adhesion was higher for a CHI monolayer and a (CHI/HA) bilayer than for the control. The higher adhesion found on the HA-terminating bilayer may be explained by the presence on the cell of specific HA receptors. Adhesion was much lower after the deposition of five pairs of layers, but again better for the HA-ending film. After the deposition of 10 pairs of layers, the step at which a homogeneous film was formed, adhesion was extremely low (less than 4% of the control). One can relate the nonadhesion of the chondrocytes to the formation of a uniform film. When the films are still of the "islet" type, the cells can still, although poorly, adhere.

(61) Isacke, C. M.; Yarwood, H. *Int. J. Biochem. Cell Biol.* 2002, 34, 718–721.

These (CHI/HA)<sub>n</sub> films seem to behave like the (PLL/alginate) films described by Elbert et al.<sup>19</sup> for which cell adhesion was strongly decreased when the number of layers of the film increased. These authors attributed the "cell resistant" effect to the "gel-like" character of the (PLL/alginate) films. They did not try to relate the nonadhesion of the cells to the full coverage of the surface (uniform film) since they did not image the coated surfaces. Similarly, the (CHI/HA) films may be too gel-like and soft, thus rendering the adhesion unfavorable. As was suggested by a previous study on polyacrylamide-based cross-linked hydrogels, the cells spread if the surface exhibits a critical level of mechanical support.<sup>62</sup> The hydration of the films may also play a great role in this nonadhesion.<sup>63</sup> A recent study by Mendelsohn et al. also suggested that cell "cytotoxicity" is directly related to the swelling and hydrating properties of the polyelectrolyte multilayer films.<sup>12</sup> If the surface is highly hydrated, the cells may see the interface as essentially water and hence will not attach.

Besides chondrocyte adhesion, we investigated bacterial adhesion (Figure 9) on the uniform (CHI/HA) films. Toward this end, two types of films were tested: (CHI/HA)<sub>10</sub> built in 0.15 M NaCl and (CHI/HA)<sub>20</sub> films built in 10<sup>-2</sup> M NaCl. It appears that the (CHI/HA)<sub>10</sub> films are highly resistant to bacterial adhesion and lead to a  $\approx$ 80% decrease in bacterial adhesion as compared to bare glass. On the other hand, the (CHI/HA)<sub>20</sub> films built in 10<sup>-2</sup> M NaCl are less resistant to bacterial adhesion (40% less than the control on the CHI-ending films and 20% less on the HA-ending films). The observed differences may be explained by the lower thickness of the (CHI/HA) films built in 10<sup>-2</sup> M NaCl (120 nm as compared to 300 nm for those built in 0.15 M NaCl) and also probably an increased film rigidity. The (CHI/HA)<sub>10</sub> films built in the presence of 0.15 M NaCl could thus be used as antimicrobial coatings for biomaterials.

### Conclusion

The growth of thin films made of two polysaccharides, chitosan and hyaluronan, was possible at acidic pH. This system behaves similarly to the system PLL/HA; that is, it is characterized by an exponential growth whose mechanism is related to the ability of the polycation to diffuse in and out of the whole film at each deposition step. This study shows that such a diffusion behavior is not only observed with PLL as the polycation but also with a polycation presenting a large persistence length. We also show that the buildup process is faster, with respect to the number of deposited bilayers, when the mass of the diffusing polyelectrolyte, CHI in our case, is smaller. The influence of the salt concentration of the polyelectrolyte solutions during buildup is also investigated. Whereas the CHI/HA films grow rapidly at high salt concentration (0.15 M NaCl), it is very difficult to build the film at 10<sup>-4</sup> M NaCl. In the latter case, the deposited mass increases linearly with the number of deposition steps but the CHI/HA complexes remain in the shape of small islets on the surface and do not form a uniform film. However, even at these low salt concentrations and in the islet configuration, CHI chains seem to be able to diffuse in and out of the CHI/HA complexes but, as they diffuse out of the islets and reach the surface, they form complexes with HA that do not stay on the islet interface. The islet growth is thus entirely due to the direct interactions, related to the charge overcompensation,

(62) Yamato, M.; Kondo, C.; Utsumi, M.; Kikuchi, A.; Okano, T. *Biomaterials* 2002, 23, 561–567.

(63) Morra, M. *J. Biomater. Sci., Polym. Ed.* 2000, 11, 547–569.

between CHI and HA on the outer surface of the islets. For higher salt concentrations, the islets are only present at the first deposition steps, and the higher the salt concentration, the earlier the islet/film transition takes place. Finally, the uniform films built at high salt concentrations were also found to be chondrocyte resistant but also, and more interestingly, bacterial resistant: bacterial adhesion was reduced by 80% as compared to that on a glass substrate. Therefore, the (CHI/HA) films may be used as an antimicrobial coating.

**Acknowledgment.** We thank Dr. F. Cuisinier for his help in the OWLS experimental setup and A. Fritz for OWLS technical help. We also thank Dr. C. Egles and O. Etienne for fruitful discussions about the bacterial adhesion experiments. We are grateful to Dominique Batiste for her help in the chondrocyte culture. This work was supported by the programs ACI "Technologies pour la

Santé" and ACI "Surfaces, interfaces et conception de nouveaux matériaux" from the Ministère Français de la Recherche (2001). We also thank Jerome Mutterer for the access to the CLSM platform used in this study which was cofinanced by the Région Alsace, the CNRS, the Université Louis Pasteur, and the Association pour la Recherche sur le Cancer.

**Supporting Information Available:** Difference in the QCM frequency shifts  $-\Delta f/f$  for each CHI and HA layer during the layer by layer deposition of CHI/HA multilayer films; AFM height mode images in liquid obtained at the different steps of the alternate deposition of CHI and HA layers on a glass substrate; raw  $N_{\text{FM}}$  signals as measured by the OWLS technique during the adsorption of CHI and HA over three adsorption cycles, as a function of time at  $10^{-2}$  M NaCl. This material is available free of charge via the Internet at <http://pubs.acs.org>.

LA035415N

## Conclusion et perspectives.

---

Au cours de ce travail, nous avons étudié et cherché à comprendre les interactions entre un milieu biologique et plusieurs films multicoques de polyélectrolytes. Ce traitement de surface simple et versatile permet de préparer des surfaces possédant des propriétés « à la carte ». Nous avons tout d'abord étudié les relations existant entre les conditions de constructions des films et leurs propriétés physico-chimiques. Nous disposions pour cela de différentes techniques permettant de caractériser ces propriétés sur des films d'épaisseur nano et micrométriques. Ensuite, les différents travaux ont montré l'influence de ces propriétés, notamment de l'hydratation des films et de leurs propriétés mécaniques, sur l'adhésion cellulaire. Il nous a été ainsi possible de corrélérer le module d'Young des films multicoques à base de (PLL/HA) à l'adhésion cellulaire.

Dans un premier temps, nous avons étudié l'évolution des paramètres physico-chimiques lors de la construction des films (PLL/PGA) dans différentes conditions. Le caractère exponentiel de la croissance des films de (PLL/PGA) a ainsi été mis en évidence ainsi que l'influence du taux de sels et du pH des solutions lors de la construction. De plus, l'analyse de l'adhésion cellulaire à court terme a fait ressortir le rôle important de la couche terminale sur le comportement cellulaire ainsi que l'épaisseur du film déposé. En effet, lorsque la couche terminale est favorable à l'adhésion cellulaire (PLL), l'adhésion décroît avec l'épaisseur du film. Toutefois d'autres propriétés du film influencent également l'adhésion. Ainsi deux films d'épaisseur comparable mais construits à des pH différents (10.4 et 4.4) seront respectivement favorables ou non à l'adhésion cellulaire. De plus, ces études indiquent que l'adsorption des protéines sériques par les films multicoques influence l'adhésion cellulaire mais que son un rôle est limité. En effet, les caractéristiques mécaniques et l'hydratation des films multicoques prévalent sur l'adsorption de protéines dans la résistance à l'adhésion cellulaire.

Pour étudier plus précisément le rôle des propriétés mécaniques, des tests de réticulation ont été réalisés afin de rigidifier des films de (PLL/HA). Ces films multicoques sont très épais (d'épaisseur micrométrique) et très hydratés. La réticulation est obtenue par voie chimique en formant des liaisons amides entre les fonctions amines du PLL et les groupements carboxyles du HA. Cette réticulation a été mise en évidence par FTIR. Les mesures par QCM-D et AFM ont montré une augmentation de la rigidité des films après

réticulation et notamment du module d'Young. Les mesures du module d'Young avant réticulation ont également mis en évidence une dépendance de la rigidité du film à son épaisseur : plus le film est fin, plus il est rigide. Toutefois, la réticulation estompe ces différences. Outre le changement de leurs propriétés mécaniques, les films réticulés sont plus résistants aux changements de milieux et à la dégradation enzymatique : ils résistent ainsi à la déshydratation à l'éthanol et à la hyaluronidase. D'autre part, les films réticulés sont favorables à la culture cellulaire alors que les films natifs de (PLL/HA) sont résistants à l'adhésion cellulaire. L'adhésion de cellules musculaires lisses a ainsi pu être corrélates au module de Young de ces films.

Enfin, nous avons montré la possibilité de construire des films multicouches à partir de polysaccharides naturels, en utilisant le chitosan comme polycation et le hyaluronane comme polyanion. L'étude de ces films montre de fortes similitudes avec les films de (PLL/HA), avec notamment une croissance exponentielle du film en fonction du nombre de couche. De plus les observations en microscopie confocale ont montré la diffusion du chitosan au sein du film de façon similaire à la PLL dans les films (PLL/HA). L'étude des conditions de construction a mis en évidence l'influence du taux de sel sur la cinétique de croissance de ces films, mais aussi sur la formation du film. Ainsi les films construits à faible taux de sel ( $10^{-4}$  M NaCl) se présentent sous forme de gouttelettes. Plus généralement, l'obtention d'un film continu de (CHI/HA) rend la surface résistante à l'adhésion cellulaire. Le film limite également l'adhésion d'*Escherichia Coli*. Toutefois, cette caractéristique dépend du taux de sels utilisés lors de la construction. Ainsi, plus le taux de sels est élevé lors de la construction du film, plus ce dernier est résistant à l'adhésion d'*Escherichia Coli*.

L'une des perspectives intéressantes de ce travail serait l'utilisation des films multicouches comme traitement anti-adhésifs. En effet nous avons montré qu'avec les films à base de (PLL/HA) et de (CHI/HA), il est possible de limiter l'adhésion d'*Escherichia Coli* et cellulaire. Ces phénomènes sont préjudiciables et peuvent être source de complications, notamment lors de l'utilisation de cathéters ou de membranes de dialyse. Des tests *in vivo* sur les films étudiés dans le cadre de cette thèse permettraient de tester leur dégradation et la colonisation cellulaire. Ils permettraient également d'optimiser les films notamment dans le choix des polyélectrolytes utilisés (masse molaire, taux de deacetylation par exemple pour le chitosan) et des conditions de construction (pH, taux de sels...).

Un autre point important à étudier dans le cadre d'une application biomédicale est la nécessité ou non d'un traitement préalable de la surface du biomatériau avant le dépôt du film

multicouche (nettoyage, activation chimique, silanisation, couches précurseurs). En effet à la suite de quelques essais préliminaires, ce paramètre semble avoir une grande influence sur les propriétés des films multicouches et plus particulièrement sur leur stabilité en milieu physiologique : une faible interaction entre le film multicouche et son substrat peut entraîner un décollement du film en conditions physiologiques. Le couplage covalent de la première couche de polyélectrolyte ou l'utilisation de couches précurseurs très stables du type PEI-(PSS/PAH) semblent des voies à développer notamment pour les films très hydratés du type (PLL/HA) ou (CHI/HA).

D'un point de vue physico-chimique et notamment afin de mieux comprendre le mécanisme de construction et la structuration des films multicouches, il semble intéressant d'étudier plus précisément les propriétés de diffusion des polyélectrolytes au sein des films pendant et après leur construction. L'utilisation de techniques de fluorescence basées sur le recouvrement de fluorescence après photoblanchiment (FRAP) et de transfert d'énergie par résonance de fluorescence (FRET) associé à des polyélectrolytes marqués permettraient, ainsi, de suivre l'évolution de leur diffusion à l'échelle micro et nanoscopique et ainsi de connaître précisément les interactions entre les différentes chaînes de polyélectrolytes. Ces études permettraient notamment de comprendre et ainsi de maîtriser les phénomènes de maturation des films multicouches au cours du temps.

D'autre part, la réticulation nous a permis de modifier les propriétés biologiques des films multicouches ainsi que leur dégradation. Le contrôle de cette propriété est particulièrement intéressant pour la délivrance localisée et contrôlée de principes actifs fonctionnels au niveau de la zone d'implantation. Toutefois, le procédé actuel de réticulation pourrait encore dénaturer les principes actifs internalisés. Ceci reste encore à vérifier sur quelques molécules tests, mais limiterait les possibilités de fonctionnalisation des films multicouches. L'optimisation de différents paramètres de réticulation (temps, température, concentration) voire l'utilisation d'autres agents de réticulation, doivent permettre de moduler précisément les propriétés des films (vitesse de dégradation, propriétés mécaniques...) mais aussi préserver l'activité biologique de principes actifs insérés dans les films.

Nous avons montré qu'il est possible d'obtenir des surfaces favorables à la prolifération cellulaire comme les films multicouches de (PLL/HA) réticulés. Ces films pourraient également servir de substrat pour la construction de films multicouches bioactifs. On peut ainsi envisager de déposer un film non réticulé sur un film réticulé : le film non réticulé se

dégradant rapidement et ayant ainsi qu'une action à court terme tandis que le film réticulé, plus stable, agira sur l'environnement d'implantation plus longtemps.

Afin d'optimiser l'activité biologique des films multicouches, il semble particulièrement intéressant d'associer les films multicouches, notamment les films (CHI/HA), à des principes actifs agissant en surface et en profondeur du film. Par exemple on peut envisager de greffer des facteurs d'adhésion de type RGD et d'insérer des facteurs de croissance de type VGF ou BMP. Il est également envisageable de combiner ces différents principes actifs par exemple en fonctionnalisant la surface du film avec un agent anti-inflammatoire (par exemple :  $\alpha$ -MSH) et d'immobiliser un facteur de croissance (par exemple : VGF) au sein du film. Cette association sur un implant permettra d'obtenir une action anti-inflammatoire dès l'implantation suivie d'une activation cellulaire à plus long terme permettant de moduler l'environnement de l'implant.

Afin de contrôler plus précisément l'activité des films multicouches, il semble également possible de construire des architectures sensibles aux propriétés du milieu, notamment par l'intégration d'enzymes inactives dans le film, comme l' $\alpha$ -amylase ou la DNase (activée par les ions  $Mg^{2+}$ ). L'augmentation de  $Mg^{2+}$  à proximité d'une telle architecture devrait induire la dégradation du film. Cette augmentation locale de la concentration en  $Mg^{2+}$  est en particulier présente lors de l'inflammation, précurseur de la resténose. Ainsi, dans le cas où le film contient un principe anti-inflammatoire, celui-ci sera libéré lors de la dégradation du film et permettra de limiter l'inflammation et, par conséquent, les risques de resténose. Une telle architecture pourrait notamment s'appliquer aux prothèses vasculaires.

Les possibilités d'applications ouvertes par les films multicouches entièrement biodégradables, par les films réticulés (et dont on pourrait contrôler le taux de réticulation), ainsi que par les propriétés d'adhérence ou de non-adhérence des (vis-à-vis des cellules ou de bactéries) sont donc nombreuses.

# Bibliographie.

---

- Ahrens, H., T.R. Baekmark, R. Merkel, J. Schmitt, K. Graf, R. Raiteri and C.A. Helm. 2000. Hydrophilic/hydrophobic nanostripes in lipopolymer monolayers. *Chemphyschem* 1(2):101-106.
- Ai, H., H. Meng, I. Ichinose, S.A. Jones, D.K. Mills, Y.M. Lvov and X. Qiao. 2003. Biocompatibility of layer-by-layer self-assembled nanofilm on silicone rubber for neurons. *Journal of Neuroscience Methods* 128(1-2):1-8.
- Baldwin, S. and W. Saltzman. 1998. Materials for protein delivery in tissue engineering. *Advanced Drug Delivery Reviews* 33(1-2):71-86.
- Bataille, S., P. Portalier, P. Coulon and J.-P. Ternaux. 1998. Influence of acetylcholinesterase on embryonic spinal rat motoneurones growth in culture: a quantitative morphometric study. *European Journal of Neuroscience* 10(2):560-572.
- Berg, M.C., J. Choi, P.T. Hammond and M.F. Rubner. 2003. Tailored micropatterns through weak: Polyelectrolyte stamping. *Langmuir* 19(6):2231-2237.
- Binnig, G., C.F. Quate and C. Gerber. 1986. Atomic force microscope. *Physical Review Letters* 56(9):930-933.
- Binning, G., H. Rohrer, C. Gerber and E. Weibel. 1982. Surface studies by scanning tunneling microscopy. *Physical Review Letters* 49:57-61.
- Bos, G.W., N.M. Scharenborg, A.A. Poot, G.H. Engbers, T. Beugeling, W.G. van Aken and J. Feijen. 1999. Endothelialization of crosslinked albumin-heparin gels. *Thrombosis and Haemostasis* 82(6):1757-1763.
- Boulmedais, F., B. Frisch, O. Etienne, P. Lavalle, C. Picart, J. Ogier, J.-C. Voegel, P. Schaaf and C. Egles. 2004. Polyelectrolyte multilayer films with pegylated polypeptides as a new type of anti-microbial protection for biomaterials. *Biomaterials* 25(11):2003-2011.
- Boura, C., P. Menu, E. Payan, C. Picart, J.-C. Voegel, S. Muller and J.-F. Stoltz. 2003. Endothelial cells grown on thin polyelectrolyte multilayered films: an evaluation of a new versatile surface modification. *Biomaterials* 24(20):3521-3530.
- Brissova, M., I. Lacik, A.C. Powers, A.V. Anilkumar and T. Wang. 1998. Control and measurement of permeability for design of microcapsule cell delivery system. *Journal of Biomedical Materials Research* 39(1):61-70.
- Brynda, E. and M. Houska. 1996. Multiple alternating molecular layers of albumin and heparin on solid surfaces. *Journal of Colloid and Interface Science* 183(1):18-25.
- Brynda, E. and M. Houska. 2000. In Protein architecture: Interfacing molecular assemblies and immobilization biotechnology. Möhwald H, editor. Marcel Dekker, New York. 251-285.
- Burnham, N.A., D.D. Dominguez, R.L. Mowery and R.J. Colton. 1990. Probing the surface forces of monolayer films with an atomic-force microscope. *Physical Review Letters* 64(16):1931-1934.
- Caruso, F., K. Niikura, D.N. Furlong and Y. Okahata. 1997. 2. Assembly of alternating polyelectrolyte and protein multilayer films for immunosensing. *Langmuir* 13(13):3427-3433.
- Caruso, F., D. Furlong, K. Ariga, I. Ichinose and T. Kunitake. 1998. Characterization of polyelectrolyte-protein multilayer films by atomic force microscopy, scanning electron microscopy, and Fourier transform infrared reflection-absorption spectroscopy. *Langmuir* 14:4559-4565.
- Chapman, D.L. 1913. A contribution to the theory of electrocapillarity. *Phil. Mag.* 25:475-481.
- Chen, J., L. Huang, L. Ying, G. Luo, X. Zhao and W. Cao. 1999. Self-assembly ultrathin films based on diazoxyresins. *Langmuir* 15(21):7208-7212.
- Chen, W. and T.J. McCarthy. 1997. Layer-by-layer deposition: A tool for polymer surface modification. *Macromolecules* 30:78-80.
- Cheng, Y., M. Robert and R.M. Corn. 1999. Ultrathin polypeptide multilayer films for the fabrication of model liquid/liquid electrochemical interfaces. *Journal of Physical Chemistry B* 103(41):8726-8731.
- Chiarelli, P., M.S. Johal, J.L. Casson, B.L. Roberts, J.M. Robinson and H.L. Wang. 2001. Controlled fabrication of polyelectrolyte multilayer thin films using spin-assembly. *Advanced Materials* 13:1167-1170.
- Chluba, J., J.-C. Voegel, G. Decher, P. Erbacher, P. Schaaf and J. Ogier. 2001. Peptide Hormone Covalently Bound to Polyelectrolytes and Embedded into Multilayer Architectures Conserving Full Biological Activity. *Biomacromolecules* 2(3):800-805.
- Cho, J., K. Char, J.D. Hong and K.B. Lee. 2001. Fabrication of highly ordered multilayer films using a spin self-assembly method. *Advanced Materials* 13(14):1076-1078.
- Clark, S.L. and P.T. Hammond. 2000. The role of secondary interactions in selective electrostatic multilayer deposition. *Langmuir* 16(26):10206-10214.

- Cochin, D. and A. Laschewsky. 1999. Layer-by-layer self-assembly of hydrophobically modified polyelectrolytes. *Macromol. Chem. Phys.* 200:609-615.
- Cooper, L.F. 2000. A role for surface topography in creating and maintaining bone at titanium endosseous implants. *Journal of Prosthetic Dentistry* 84(5):522-534.
- Dai, J., A.M. Balachandra, J.I. Lee and M.L. Bruening. 2002. Controlling ion transport through multilayer polyelectrolyte membranes by derivatization with photolabile functional groups. *Macromolecules* 35(8): 3164-3170.
- Dalby, M.J., S.J. Yarwood, M.O. Riehle, H.J.H. Johnstone, S. Affrossman and A.S.G. Curtis. 2002. Increasing fibroblast response to materials using nanotopography: morphological and genetic measurements of cell response to 13 nm high polymer demixed islands. *Experimental Cell Research* 276(1):1-9.
- De Feijter, J.A., J. Benjamins and F.A. Veer. 1978. Ellipsometry as a tool to study the adsorption behavior of synthetic and biopolymers at the air-water interface. *Biopolymers* 17(7):1759-1772.
- Decher, G. and J. Hong. 1991. Buildup of ultrathin multilayer films by a self-assembly process. II: Consecutive adsorption of anionic and cationic bipolar amphiphiles and polyelectrolytes on charged surfaces. *International Journal of Physical Chemistry* 12:1430-1434.
- Decher, G., J.D. Hong and J. Schmitt. 1992. Buildup of ultrathin multilayer films by a self-assembly process. Consecutively alternating adsorption of anionic and cationic polyelectrolytes on charges surface. *Thin Solid Films* 1992(210):831-835.
- Decher, G., Y. Lvov and J. Schmitt. 1994. Proof of multilayer structural organization in self-assembled polycation-polyanion molecular films. *Thin Solid Films* 244(1-2):772-777.
- Decher, G. 1997. Fuzzy nanoassemblies: Toward layered polymeric multicomposites. *Science* 277:1232-1237.
- Decher, G., M. Eckle, J. Schmitt and B. Struth. 1998. Layer-by-layer assembled multicomposite films. *Current Opinion in Colloid and Interface Science* 3(1):32-39.
- Delcorte, A., P. Bertrand, E. Wischerhoff and A. Laschewsky. 1997. Adsorption of polyelectrolyte multilayers on polymer surfaces. *Langmuir* 13:5125-5136.
- Denuziere, A., D. Ferrier and A. Domard. 1996. Chitosan-chondroitin sulfate and chitosan-hyaluronate polyelectrolyte complexes. Physico-chemical aspects. *Carbohydrate Polymers* 29(4):317-323.
- Denuziere, A., D. Ferrier, O. Damour and A. Domard. 1998. Chitosan - chondroitin sulfate and chitosan - hyaluronate polyelectrolyte complexes: Biological properties. *Biomaterials* 19(14):1275-1285.
- Diaspro, A., D. Silvano, S. Krol, O. Cavalleri and A. Gliozzi. 2002. Single living cell encapsulation in nano-organized polyelectrolyte shells. *Langmuir* 18(13):5047-5050.
- Dimitriadis, E.K., F. Horkay, J. Maresca, B. Kachar and R.S. Chadwick. 2002. Determination of elastic moduli of thin layers of soft material using the atomic force microscope. *Biophysical Journal* 82(5):2798-2810.
- Domke, J. and M. Radmacher. 1998. Measuring the elastic properties of thin polymer films with the atomic force microscope. *Langmuir* 14(12):3320-3325.
- Donath, E., D. Walther, V.N. Shilov, E. Knippel, A. Budde, K. Lowack, C.A. Helm and H. Möhwald. 1997. Nonlinear hairy layer theory of electrophoretic fingerprinting applied to consecutive layer by layer polyelectrolyte adsorption onto charged polystyrene latex particles. *Langmuir* 13(20):5294-5305.
- Ducker, W., T. Senden and R. Pashley. 1992. Measurement of forces in liquids using a force microscope. *Langmuir* 8(7):1831-1836.
- Elbert, D., C. Herbert and J. Hubbell. 1999. Thin polymer layer formed by polyelectrolyte multilayer techniques on biological surfaces. *Langmuir* 15: 5355-5362.
- Elbert, D.L. and J.A. Hubbell. 1998. Self-assembly and steric stabilization at heterogeneous, biological surfaces using adsorbing block copolymers. *Chemistry and Biology* 5(3):177-183.
- Engler, A., L. Bacakova, C. Newman, A. Hategan, M. Griffin and D. Discher. 2004a. Substrate compliance versus ligand density in cell on gel responses. *Biophysical Journal* 86(1 Pt 1):617-628.
- Engler, A., L. Richert, J.Y. Wong, C. Picart and D.E. Discher. 2004b. Surface probe measurements of the elasticity of sectioned tissue, thin gels, and polyelectrolyte multilayer films : correlations between substrate stiffness and cell adhesion. *Surface Science* in press.
- Francis Suh, J.-K. and H.W.T. Matthew. 2000. Application of chitosan-based polysaccharide biomaterials in cartilage tissue engineering: a review. *Biomaterials* 21(24):2589-2598.
- Gao, C., S. Leporatti, S. Moya, E. Donath and H. Möhwald. 2001. Stability and mechanical properties of polyelectrolyte capsules obtained by stepwise assembly of poly(styrenesulfonate sodium salt) and poly(diallyldimethyl ammonium) chloride onto melamine resin particles. *Langmuir* 17(11):3491-3495.
- Gergely, C., S. Bahi, B. Szalontai, H. Flores, P. Schaaf, J.-C. Voegel and F.J.G. Cuisinier. 2004. Human serum albumin self-assembly on weak polyelectrolyte multilayer films structurally modified by pH changes. *Langmuir ASAP Article*.
- Gölander, C.-G., H. Arwin, J.C. Ericksson, I. Lundstrom and R. Larsson. 1982. Heparin surface film formation through adsorption of colloidal particles studied by ellipsometry and scanning electron microscopy. *Colloids and Surfaces* 5:1-16.

- Graham, D.C. 1947. The electrical double layer and the theory of electrocapillarity. *Chemical Reviews* 41:441-501.
- Grant, G.G.S., D.S. Koktysh, B. Yun, R.L. Matts and N.A. Kotov. 2001. Layer-by-layer assembly of collagen thin films: Controlled thickness and biocompatibility. *Biomedical Microdevices* 3(4):301-306.
- Greene, G., G. Yao and R. Tannenbaum. 2004. Deposition and wetting characteristics of polyelectrolyte multilayers on plasma-modified porous polyethylene. *Langmuir* 20(7):2739-2745.
- Gristina, A. 1994. Implant failure and the immuno-incompetent fibro-inflammatory zone. *Clinical Orthopaedics and Related Research* 298:106-118.
- Guo, T.F., S.C. Chang, S. Pyo and Y. Yang. 2002. Vertically integrated electronic circuits via a combination of self-assembled polyelectrolytes, Ink-Jet printing, and electroless metal plating processes. *Langmuir* 18:8142-8147.
- Harris, J.J., P.M. DeRose and M.L. Bruening. 1999. Synthesis of passivating, nylon-like coatings through cross-linking of ultrathin polyelectrolyte films. *Journal of the American Chemical Society* 121(9):1978-1979.
- Healy, K.E. 1999. Molecular engineering of materials for bioreactivity. *Current Opinion in Solid State and Materials Science* 4(4):381-387.
- Hermanson, G.T. 1996. Zero-length cross-linkers. In *Bioconjugate techniques*. Press A, editor. 169-176.
- Hiller, J., J.D. Mendelsohn and M.F. Rubner. 2002. Reversibly erasable nanoporous anti-reflection coatings from polyelectrolyte multilayers. *Nature Materials* 1(1):59-63.
- Hoogeveen, N.G., M.A. Cohen Stuart, G.J. Fleer and M.R. Bohmer. 1996. Formation and stability of multilayers of polyelectrolytes. *Langmuir* 12(15):3675-3681.
- Huang, N.-P., R. Michel, J. Voros, M. Textor, R. Hofer, A. Rossi, D.L. Elbert, J.A. Hubbell and N.D. Spencer. 2001. Poly(L-lysine)-g-poly(ethylene glycol) layers on metal oxide surfaces: Surface-analytical characterization and resistance to serum and fibrinogen adsorption. *Langmuir* 17(2):489-498.
- Hubbell, J.A. 1999. Bioactive biomaterials. *Current Opinion in Biotechnology* 10:123-129.
- Huglin, M.B. 1972. Light scattering from polymer solutions. M.B. Huglin E, editor. Academic Press, London, New York.
- Iller, R. 1966. Multilayers of colloidal particles. *Journal of Colloid and Interface Science* 21:569-594.
- Jessel, N., F. Atalar, P. Lavalle, J. Mutterer, G. Decher, P. Schaaf, J.-C. Voegel and J. Ogier. 2003. Bioactive coatings based on a polyelectrolyte multilayer architecture functionalized by embedded proteins. *Advanced Materials* 15(9):692-695.
- Jia, Z., D. Shen and W. Xu. 2001. Synthesis and antibacterial activities of quaternary ammonium salt of chitosan. *Carbohydrate Research* 333(1):1-6.
- Kasemo, B. 1998. Biological surface science. *Current Opinion in Solid State and Materials Science* 3(5):451-459.
- Kim, D.K., S.W. Han, C.H. Kim, J.D. Hong and K. Kim. 1999. Morphology of multilayers assembled by electrostatic attraction of oppositely charged model polyelectrolytes. *Thin Solid Films* 350(1-2):153-160.
- Kim, M. and D.J. Sandman. 2001. Polycation effects on electronic spectra of conjugated polymers in programmed electrostatic assemblies. *Journal of Macromolecular Science-Pure and Applied Chemistry* 38:1291-1304.
- Kotov, N.A. 1999. Layer-by-layer self-assembly: the contribution of hydrophobic interactions. *Nanostructured Materials* 12:789-796.
- Krol, S., O. Cavalleri, P. Ramoino, A. Gliozzi and A. Diaspro. 2003. Encapsulated yeast cells inside *Paramecium primaurelia*: a model system for protection capability of polyelectrolyte shells. *Journal of Microscopy* 212(3):239-243.
- Kyte, J. 1995. Structure in protein chemistry. Garland Publishing, Inc., New-York & London.
- Ladam, G., C. Gergely, B. Senger, G. Decher, J.-C. Voegel, P. Schaaf and F.J.G. Cuisinier. 2000a. Protein interactions with polyelectrolyte multilayers: Interactions between human serum albumin and polystyrene sulfonate/polyallylamine multilayers. *Biomacromolecules* 1(4):674-688.
- Ladam, G., P. Schaad, J.C. Voegel, G. Decher, P. Schaaf and F. Cuisinier. 2000b. In situ determination of the structural properties of initially deposited polyelectrolyte multilayers. *Langmuir* 16: 1249-1255.
- Ladam, G., P. Schaad, F.J.G. Cuisinier, G. Decher and J.-C. Voegel. 2001. Protein adsorption onto auto-assembled polyelectrolyte films. *Langmuir* 17(3):878-882.
- Lapčík, L., L. Lapčík, J. De Smedt, J. Demeester and P. Chabrecek. 1998. Hyaluronan: Preparation, structure, properties, and applications. *Chemical Reviews* 98(8):2663 -2684.
- Lavalle, P., C. Gergely, F.J.G. Cuisinier, G. Decher, P. Schaad, J.-C. Voegel and C. Picart. 2002. Comparison of the structure of polyelectrolyte multilayer films exhibiting a linear and an exponential growth regime: An in situ atomic force microscopy study. *Macromolecules* 35((11)):4458 -4465.

- Lavalle, P., C. Picart, J. Mutterer, C. Gergely, H. Reiss, J.-C. Voegel, B. Senger and P. Schaaf. 2004. Modeling the Buildup of Polyelectrolyte Multilayer Films Having Exponential Growth. *Journal of Physical Chemistry B* 108(2):635-648.
- Lee, B.J. and T. Kunitake. 1994. Two-Dimensional Polymer Networks of Maleic Acid Copolymers and Poly(allylamine) by the Langmuir-Blodgett Technique. *Langmuir* 10(2):557-562.
- Li, C., S. Ke, Q.-P. Wu, W. Tansey, N. Hunter, L.M. Buchmiller, L. Milas, C. Charnsangavej and S. Wallace. 2000. Potentiation of ovarian OCa-1 tumor radioresponse by poly (L-glutamic acid)-paclitaxel conjugate. *International Journal of Radiation Biology* 48(4):1119-1126.
- Lim, S.T., G.P. Martin, D.J. Berry and M.B. Brown. 2000. Preparation and evaluation of the in vitro drug release properties and mucoadhesion of novel microspheres of hyaluronic acid and chitosan. *Journal of Controlled Release* 66(2-3):281-292.
- Lo, C.M., H.B. Wang, M. Dembo and Y.L. Wang. 2000. Cell movement is guided by the rigidity of the substrate. *Biophysical Journal* 79(1):144-152.
- Lösche, M. 1997. Protein monolayers at interfaces. *Current Opinion in Solid State and Materials Science* 2(5):546-556.
- Lulevich, V., D. Andrienko and O. Vinogradova. 2004. Elasticity of polyelectrolyte multilayer microcapsules. *Journal of Chemical Physics* 120(8):3822-3826.
- Lvov, Y., G. Decher and H. Möhwald. 1993. Assembly, structural characterization, and thermal behavior of layer-by-layer deposited ultrathin films of poly(vinyl sulfate) and poly(allylamine). *Langmuir* 9:481-486.
- Lvov, Y., K. Ariga, I. Ichinose and T. Kunitake. 1995. Assembly of multicomponent protein films by means of electrostatic layer-by-layer adsorption. *Journal of the American Chemical Society* 117:6117-6123.
- Lvov, Y., A. Katsuhiko, I. Izumi and K. Toyoki. 1996. Molecular film assembly via layer-by-layer adsorption of oppositely charged macromolecules (linear polymer, protein and clay) and concanavalin A and glycogen. *Thin Solid Films* 284-285:797-801.
- Malette, W.G., H.J. Quigley, R.D. Gaines, N.D. Johnson and W.G. Rainer. 1983. Chitosan: a new hemostatic. *Annals of Thoracic Surgery* 36(1):55-58.
- Margel, S., E.A. Vogler, L. Firment, T. Watt, S. Haynie and D.Y. Sogah. 1993. Peptide, protein, and cellular interactions with self-assembled monolayer model surfaces. *Journal of Biomedical Materials Research* 27(12):1463-1476.
- Martin, Y., D. Abraham and H. Wickramasinghe. 1988. High-resolution capacitance measurement and potentiometry by force microscopy. *Applied Physics Letters* 52(13):1103-1105.
- McAloney, R.A., M. Sinyor, V. Dudnik and M.C. Goh. 2001. Atomic force microscopy studies of salt effects on polyelectrolyte multilayer film morphology. *Langmuir* 17:6655-6663.
- McAloney, R.A., V. Dudnik and M.C. Goh. 2003. Kinetics of salt-induced annealing of a polyelectrolyte multilayer film morphology. *Langmuir* 19(9):3947-3952.
- Mendelsohn, J.D., C.J. Barrett, V.V. Chan, A.J. Pal, A.M. Mayes and M.F. Rubner. 2000. Fabrication of microporous thin films from polyelectrolyte multilayers. *Langmuir* 16(11):5017-5023.
- Mendelsohn, J.D., S.Y. Yang, J. Hiller, A. Hochbaum and M.F. Rubner. 2003. Rational design of cytophilic and cytophobic polyelectrolyte multilayer thin films. *Biomacromolecules* 4(1):96-106.
- Müller, M., T. Rieser, P.L. Dubin and K. Lunkwitz. 2001. Selective interaction between proteins and the outermost surface of polyelectrolyte multilayers: Influence of the polyanion type, pH and salt. *Macromolecular Rapid Communications* 22(6):390-395.
- Ohgaki, M., T. Kizuki, M. Katsura and K. Yamashita. 2001. Manipulation of selective cell adhesion and growth by surface charges of electrically polarized hydroxyapatite. *Journal of Biomedical Materials Research* 57(3):366-373.
- Okamoto, Y., K. Kawakami, K. Miyatake, M. Morimoto, Y. Shigemasa and S. Minami. 2002. Analgesic effects of chitin and chitosan. *Carbohydrate Polymers* 49(3):249-252.
- Onda, M., Y. Lvov, K. Ariga and T. Kunitake. 1996. *Journal of Fermentation Technology* 82:502-506.
- Park, K.D., Y.S. Kim, D.K. Han, Y.H. Kim, E.H. Lee, H. Suh and K.S. Choi. 1998. Bacterial adhesion on PEG modified polyurethane surfaces. *Biomaterials* 19(7-9):851-859.
- Pelham, R.J., Jr. and Y.L. Wang. 1998. Cell locomotion and focal adhesions are regulated by the mechanical properties of the substrate. *Biological Bulletin* 194(3):348-349; discussion 349-350.
- Picart, C., G. Ladam, B. Senger, J.-C. Voegel, P. Schaaf, F.J.G. Cuisinier and C. Gergely. 2001a. Determination of structural parameters characterizing thin films by optical methods: A comparison between scanning angle reflectometry and optical waveguide lightmode spectroscopy. *Journal of Chemical Physics* 115(2):1086-1094.
- Picart, C., P. Lavalle, P. Hubert, F.J.G. Cuisinier, G. Decher, P. Schaaf and J.-C. Voegel. 2001b. Buildup mechanism for poly(L-lysine)/hyaluronic acid films onto a solid surface. *Langmuir* 17(23):7414-7424.

- Picart, C., J. Mutterer, L. Richert, Y. Luo, G.D. Prestwich, P. Schaaf, J.C. Voegel and P. Lavalle. 2002. Molecular basis for the explanation of the exponential growth of polyelectrolyte multilayers. *Proceedings of the National Academy of Sciences of the United States of America* 99(20):12531-12535.
- Picart, C., C. Gergely, Y. Arntz, J.-C. Voegel, P. Schaaf, F.J.G. Cuisinier and B. Senger. sous presse. Measurement of film thickness up to several hundreds of nanometers using optical waveguide lightmode spectroscopy. *Biosensors and Bioelectronics ASAP*.
- Qiu, Q., M. Sayer, M. Kawaja, X. Shen and J.E. Davies. 1998. Attachment, morphology, and protein expression of rat marrow stromal cells cultured on charged substrate surfaces. *Journal of Biomedical Materials Research* 42(1):117-127.
- Ra, H.J., C. Picart, H. Feng, H.L. Sweeney and D.E. Discher. 1999. Muscle cell peeling from micropatterned collagen: direct probing of focal and molecular properties of matrix adhesion. *Journal of Cell Science* 112:1425-1436.
- Radmacher, M., M. Fritz, C. Kacher, J. Cleveland and P. Hansma. 1996. Measuring the viscoelastic properties of human platelets with the atomic force microscope. *Biophysical Journal* 70(1):556-567.
- Ratner, B.D., A.S. Hoffman, F.J. Schoen and J.E. Lemons. 1996. Biomaterials science : an introduction to materials in medicine. Academic Press, San Diego.
- Rezania, A. and K.E. Healy. 1999. Biomimetic peptide surfaces that regulate adhesion, spreading, cytoskeletal organization, and mineralization of the matrix deposited by osteoblast-like cells. *Biotechnology Progress* 15(1):19-32.
- Rodahl, M. and B. Kasemo. 1996. A simple setup to simultaneously measure the resonant frequency and the absolute dissipation factor of a quartz crystal microbalance. *Review of Scientific Instruments* 67(9):3238-3241.
- Rouse, J.H., B.A. MacNeill and G.S. Ferguson. 2000. Sol-gel processing of ordered multilayers to produce composite films of controlled thickness. *Chemistry of Materials* 12(8):2502-2507.
- Ruths, J., F. Essler, G. Decher and H. Riegler. 2000. Polyelectrolytes I: Polyanion/polycation multilayers at the air/monolayer/water interface as elements for quantitative polymer adsorption Studies and preparation of hetero-superlattices on solid surfaces. *Langmuir* 16(23):8871-8878.
- Ryser, H.J. and W.C. Shen. 1978. Conjugation of methotrexate to poly(L-lysine) increases drug transport and overcomes drug resistance in cultured cells. *Proc Natl Acad Sci U S A* 75(8):3867-3870.
- Salomaki, M., P. Tervasmaki, S. Areva and J. Kankare. 2004. The Hofmeister anion effect and the growth of polyelectrolyte multilayers. *Langmuir* 20(9):3679-3683.
- Salthouse, T.N. 1984. Some aspects of macrophage behavior at the implant interface. *Journal of Biomedical Materials Research* 18(4):395-401.
- Sauerbrey, G. 1959. Verwendung von Schwingquarzen zur Wägung dünner Schichten und zur Mikrowägung. *Zeitschrift für physikalische chemie* 155:206-222.
- Schlenoff, J.B., S.T. Dubas and T. Farhat. 2000. Sprayed polyelectrolyte multilayers. *Langmuir* 16:9968-9969.
- Schmitt, J., T. Grünwald, K. Kjaer, P. Pershan, G. Decher and M. Lösche. 1993. The internal structure of layer-by-layer adsorbed polyelectrolyte films: a neutron and x-ray reflectivity study. *Macromolecules* 26:7058-7063.
- Schneider, S., P.J. Feilen, V. Slotty, D. Kampfner, S. Preuss, S. Berger, J. Beyer and R. Pommersheim. 2001. Multilayer capsules: a promising microencapsulation system for transplantation of pancreatic islets. *Biomaterials* 22(14):1961-1970.
- Schönhoff, M. 2003. Self-assembled polyelectrolyte multilayers. *Current Opinion in Colloid and Interface Science* 8(1):86-95.
- Schuetz, P. and F. Caruso. 2002. Multilayer thin films based on polyelectrolyte-complex nanoparticles. *Colloids and Surfaces A* 207(1-3):33-40.
- Schuetz, P. and F. Caruso. 2003. Copper-assisted weak polyelectrolyte multilayer formation on microspheres and subsequent film crosslinking. *Advanced Functional Materials* 13(12):929-937.
- Schultz, P., D. Vautier, L. Richert, N. Jessel, Y. Haikel, P. Schaaf, J.-C. Voegel, J. Ogier and C. Debry. In Press. Polyelectrolyte multilayers functionalized by alpha-MSH as bioactive coatings for tracheal prosthesis. *Biomaterials*.
- Schwinté, P., J.-C. Voegel, C. Picart, Y. Haikel, P. Schaaf and B. Szalontai. 2001. Stabilizing effects of various polyelectrolyte multilayer films on the structure of adsorbed/embedded fibrinogen molecules: An ATR-FTIR study. *Journal of Physical Chemistry B* 105:11906-11916.
- Schwinté, P., V. Ball, B. Szalontai, Y. Haikel, J.-C. Voegel and P. Schaaf. 2002. *Biomacromolecules* 3:1135-1143.
- Serizawa, T., M. Yamaguchi and M. Akashi. 2003. Time-controlled desorption of ultrathin polymer films triggered by enzymatic degradation. *Angewandte Chemie-International Edition* 42(10):1115-1118.

- Shi, X., R.J. Sanedrin, F. Zhou and R. M. 2002. Structural characterization of multilayered DNA and polylysine composite films: Influence of ionic strength of DNA solutions on the extent of DNA incorporation. *Journal of Physical Chemistry B* 106(6):1173-1180.
- Shiratori, S.S. and M.F. Rubner. 2000. pH-dependent thickness behavior of sequentially adsorbed layers of weak polyelectrolytes. *Macromolecules* 33(11):4213-4219.
- Shu, X.Z., K. Ghosh, Y. Liu, F.S. Palumbo, Y. Luo, R.A. Clark and G.D. Prestwich. 2004. Attachment and spreading of fibroblasts on an RGD peptide-modified injectable hyaluronan hydrogel. *Journal of Biomedical Materials Research* 68A(2):365-375.
- Smoluchowski, M.v. 1903. *Bull. Akad. Sci. Cracovie, Classe Sci. Math. Narur.* 1:182.
- Smoluchowski, M.v. 1921. In *Handbuch der Electrizität und des Magnetismus*. Graetz, editor. Barth, Leipzig. 306.
- Stelzer, E.H.K. and S. Lindek. 1994. Fundamental reduction of the observation volume in far-field light microscopy by detection orthogonal to the illumination axis: confocal theta microscopy. *Optics Communications* 111:536-547.
- Sukhishvili, S.A. and S. Granick. 1998. Polyelectrolyte adsorption onto an initially-bare solid surface of opposite electrical charge. *Journal of Chemical Physics* 109(16):6861-6868.
- Sukhorukov, G.B., H. Möhwald, G. Decher and Y.M. Lvov. 1996a. Assembly of polyelectrolyte multilayer films by consecutively alternating adsorption of polynucleotides and polycations. *Thin Solid Films* 284-285:220-223.
- Sukhorukov, G.B., M.M. Montrel, A.I. Petrov, L.I. Shabarchina and B.I. Sukhorukov. 1996b. Multilayer films containing immobilized nucleic acids. Their structure and possibilities in biosensor applications. *Biosensors and Bioelectronics* 11(9):913-922.
- Tan, Q., J. Ji, M.A. Barbosa, C. Fonseca and J. Shen. 2003. Constructing thromboresistant surface on biomedical stainless steel via layer-by-layer deposition anticoagulant. *Biomaterials* 24(25):4699-4705.
- Thierry, B., F.M. Winnik, Y. Merhi, J. Silver and M. Tabrizian. 2003. Bioactive coatings of endovascular stents based on polyelectrolyte multilayers: Nanocoatings onto arteries via layer-by-layer deposition: toward the in vivo repair of damaged blood vessels. *Biomacromolecules* 4(6):1564-1571.
- Thundat, T., R.J. Warmack, G.Y. Chen and D.P. Allison. 1994. Thermal and ambient-induced deflections of scanning force microscope cantilevers. *Applied Physics Letters* 64(21):2894-2896.
- Tiefenthaler, K. and W. Lukosz. 1989. Sensitivity of grating couplers as integrated-optical chemical sensors. *Journal of the Optical Society of America B* 6:209-220.
- Tosatti, S., Z. Schwartz, C. Campbell, D.L. Cochran, S. VandeVondele, J.A. Hubbell, A. Denzer, J. Simpson, M. Wieland, C.H. Lohmann, M. Textor and B.D. Boyan. 2004. RGD-containing peptide GCRGYRGDSPG reduces enhancement of osteoblast differentiation by poly(L-lysine)-graft-poly(ethylene glycol)-coated titanium surfaces. *Journal of Biomedical Materials Research* 68A(3):458-472.
- Tryoen-Toth, P., D. Vautier, Y. Haikel, J.-C. Voegel, P. Schaaf, J. Chluba and J. Ogier. 2002. Viability, adhesion, and bone phenotype of osteoblast-like cells on polyelectrolyte multilayer films. *Journal of Biomedical Materials Research* 60(4):657-667.
- Van Loosdrecht, M.C., J. Lyklema, W. Norde and Z.A. J. 1990. Influence of interfaces on microbial activity. *Microbiology Review* 54(1):75-87.
- Vautier, D., J. Hemmerle, C. Vodouhe, G. Koenig, L. Richert, C. Picart, J.C. Voegel, C. Debry, J. Chluba and J. Ogier. 2003. 3-D surface charges modulate protrusive and contractile contacts of chondrosarcoma cells. *Cell Motility and the Cytoskeleton* 56(3):147-158.
- Viallis-Terrisse, H. 2000. Interaction des silicates de calcium hydratés, principaux constituants du ciment, avec les chlorures d'alcalins. Analogie avec les argiles. In UFR des Sciences et Techniques. Université de Bourgogne, Dijon.
- Vogler, E.A., S. Margel, L. Firment, T. Watt, S. Haynie and D.Y. Sogah. 1999. Water and the acute biological response to surfaces  
Structure and reactivity of water at biomaterial surfaces
- Peptide, protein, and cellular interactions with self-assembled monolayer model surfaces. *Journal of Biomaterials Science, Polymer Edition* 10(10):1015-1045.
- Voinova, M.V., M. Rodahl, M. Jonson and B. Kasemo. 1999. Viscoelastic acoustic response of layered polymer films at fluid-solid interfaces : continuum mechanics approach. *Physica Scripta* 59:391-396.
- Vörös, J., J.J. Ramsden, G. Csucs, I. Szendro, S.M. De Paul, M. Textor and N.D. Spencer. 2002. Optical grating coupler biosensors. *Biomaterials* 23(17):3699-3710.
- Vuillaume, P.Y., A.M. Jonas and A. Laschewsky. 2002. Ordered polyelectrolyte "multilayers". 5. Photo-cross-linking of hybrid films containing an unsaturated and hydrophobized poly(diallylammonium) salt and exfoliated clay. *Macromolecules* 35:5004-5012.

- Wang, L.Y., S.X. Cui, Z.Q. Wang, X. Zhang, M. Jiang, L.F. Chi and H. Fuchs. 2000. Multilayer assemblies of copolymer PSOH and PVP on the basis of hydrogen bonding. *Langmuir* 16(26):10490-10494.
- Yamada, M. and S.S. Shiratori. 2000. Smoke sensor using mass controlled layer-by-layer self-assembly of polyelectrolytes films. *Sensors and Actuators B* 64:124-127.
- Yang, S.Y., J.D. Mendelsohn and M.F. Rubner. 2003. New class of ultrathin, highly cell-adhesion-resistant polyelectrolyte multilayers with micropatterning capabilities. *Biomacromolecules* 4(4):987-994.
- Yoo, D., S.S. Shiratori and M.F. Rubner. 1998. Controlling bilayer composition and surface wettability of sequentially adsorbed multilayers of weak polyelectrolytes. *Macromolecules* 31(13):4309-4318.
- Zhang, J., B. Seeger, P. Schaaf, J.-C. Voegel and P. Lavalle. 2004. Studing polyelectrolyte multilayer films by QCM-D. In QNews.
- Zhang, M., T. Desai and M. Ferrari. 1998. Proteins and cells on PEG immobilized silicon surfaces. *Biomaterials* 19(10):953-960.
- Zhong, Q., D. Inniss, K. Kjoller and V.B. Elings. 1993. Fractured polymer/silica fiber surface studied by tapping mode atomic force microscopy. *Surface Science* 290(1-2):688-L692.
- Zhu, H., J. Ji and J. Shen. 2004. Construction of multilayer coating onto poly(D-lactide) to promote cytocompatibility. *Biomaterials* 25(1):109-117.

# Articles publiés au cours de la thèse

## Articles publiés dans des revues avec comité de lecture

1. Richert L, Lavalle P, Vautier D, Senger B, Stoltz J-F, Schaaf P, Voegel J-C, Picart C: Cell Interactions with Polyelectrolyte Multilayer Films. *Biomacromolecules* 2002, 3:1170-1178.
2. Picart C, Mutterer J, Richert L, Luo Y, Prestwich GD, Schaaf P, Voegel J-C, Lavalle P: Molecular basis for the explanation of the exponential growth of polyelectrolyte multilayers. *Proc. Natl Acad. Sci.* 2002, 99:12531-12535.
3. Vautier D, Hemmerlé J, Vodouhe C, Koenig G, Richert L, Picart C, Voegel J-C, Debry C, Chluba J, Ogier J: 3-D surface charges modulate protrusive and contractile contacts of chondrosarcoma cells. *Cell Motility and the Cytoskeleton*, 2003, 56:147 - 158.
4. Richert L, Lavalle P, Payan E, Shu X, Prestwich G, Stoltz J, Schaaf P, Voegel J, Picart C: Layer by layer buildup of polysaccharide films: Physical chemistry and cellular adhesion aspects. *Langmuir* 2004, 20:448-458.
5. Richert L, Boulmedais F, Lavalle P, Mutterer J, Ferreux E, Decher G, Schaaf P, Voegel J, Picart C: Improvement of Stability and Cell Adhesion Properties of Polyelectrolyte Multilayer Films by Chemical Cross-Linking. *Biomacromolecules* 2004, 5:284-294.
6. Richert L, Arntz Y, Schaaf P, Voegel J, Picart C: pH dependent growth of Poly(L-lysine)/Poly(L-glutamic) acid multilayer films and their cell adhesion properties. *Surface Science, sous presse*
7. Engler A, Richert L, Wong J, Picart C, Discher D: Surface probe measurements of the elasticity of sectioned tissue, thin gels and polyelectrolyte multilayer films: correlations between substrate stiffness and cell adhesion. *Surface Science, sous presse*
8. Richert L, Engler A, Senger B, Discher D, Picart C: Surface measurement of the elasticity of native and cross-linked polyelectrolyte multilayer films. *Biomacromolecules, ASAP*.
9. Schultz P, Vautier D, Richert L, Jessel N, Haikel Y, Schaaf P, Voegel J, Ogier J, Debry C: Polyelectrolyte multilayers functionalized by  $\alpha$ -MSH as bioactive coatings for tracheal prosthesis.. *Biomaterials, sous presse*
10. Picart C., Elkaim R, Richert L, Audoin L, Arntz Y, Da Silva-Cardoso M, Schaaf P, Voegel J, Frisch B : Primary cell adhesion on RGD functionalized and covalently cross-linked thin polyelectrolyte multilayer films. *Advanced Functional Materials, sous presse*.

## Conférences:

### Internationales

1. Richert L., Vautier D., Senger B., Schaaf P., Voegel J-C, Picart C. Quantification of adhesiveness of cell to polyelectrolyte multilayer in vitro by the micropipette technique, Poster, *Gordon Conference on Organic Thin Films*, May 18-23 2003, Il Cosa, Italia.
2. Richert L., Lavalle Ph., Schaaf P., Voegel J.-C., Picart C., Multilayered films of polysaccharides : influences of ionic strength on the buildup and on bacterial adhesion, Poster, *BioSurf V* 25-26 September, Zurich Switzerland, *European Cells and Materials* Vol. 6. Suppl. 1, 2001, p45

### Nationales

1. Richert L., Schaaf P., Voegel J.C., Picart C, Quantification of adhesiveness of chondrosarcoma to modified surfaces in vitro by the micropipette technique, Oral , *XXVIème Congrès de la Société de Biomécanique*, 13-14 September 2001, Marseille, France, *Archives of Physiology and Biochemistry*, 109 suppl (sep 2001) p102.
2. Richert L., Lavalle Ph , Schaaf P., Voegel J.-C., and Picart C., Cell interaction with polyelectrolyte multilayer films, Poster, *6<sup>ème</sup> Forum des jeunes chercheurs en odontologie*, 19-20 June 2002, Reims, France.
3. Picart C., Richert L., Lavalle Ph., Gergely C., Mutterer J., Cuisinier F., Schaaf P., Voegel J-C., Characterization of micro and nano-metric polymers films by optical waveguide light spectroscopy and confocal microscopy, Oral, *4<sup>ème</sup> colloque francophone du club Société Française d'Optique*, 17-21 November 2003.



Nom : Monsieur RICHERT  
Prénom : Ludovic

DOCTORAT DE L'UNIVERSITÉ HENRI POINCARÉ, NANCY 1

en BIOLOGIE SANTÉ ENVIRONNEMENT

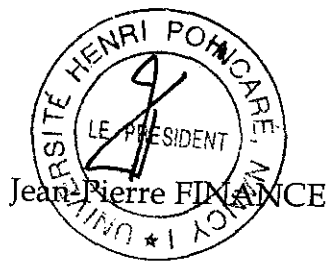
Spécialité : BIOINGÉNIERIE



VU, APPROUVÉ ET PERMIS D'IMPRIMER N°965

Nancy, le 8 décembre 2004

Le Président de l'Université



UNIVERSITÉ HENRI POINCARÉ · NANCY 1

24-30, rue Lionnois B.P. 60120 54003 Nancy cedex · Tél. 03 83 68 20 00 · Fax 03 83 68 21 00

Adresse électronique : \_\_\_\_\_ @uhp-nancy.fr

---

**Résumé :** Dans le domaine des biomatériaux, les films de multicouches de polyélectrolytes représentent une nouvelle voie possible de modification de surface : Ces films sont édifiés par adsorption successive de polyanions et de polycations. Dans le cadre de cette étude, nous avons travaillé sur différents types de films pour d'une part caractériser leurs propriétés physico-chimiques par spectroscopie optique par guide d'onde, par microbalance à cristal de quartz, par microscopie confocale et par la microscopie à force atomique et d'autres part pour étudier les interactions des cellules avec les films.

Une première partie de mon travail a consisté à caractériser les films élaborés à base de poly(L-Lysine) et d'acide poly(L-Glutamique). Plusieurs paramètres de constructions ont été testés (pH, taux de sels, nombres de couches déposées,...). L'adsorption de protéines sériques sur les films a également été évaluée, de même que l'adhésion cellulaire à court terme par des expériences de micromanipulation.

Dans une deuxième partie, nous nous sommes focalisés sur des films à base de polysaccharides, notamment le chitosan et le hyaluronan. Après avoir caractérisé la croissance et la structure de ces films, nous avons ensuite étudié la propriété d'adhésion vis à vis des cellules et des bactéries. Nous avons notamment mis en évidence qu'une rigidification chimique des films change considérablement les propriétés d'adhésion cellulaire: la réticulation des films augmentant l'adhésion cellulaire.

---

**Title:** Study of Multilayers Films build-up with biodegradable polyelectrolytes: chemo-physical properties and cells interactions

**Summary:** In the field of the biomaterials, the films multilayer of polyelectrolytes represent a new possible way of modification of surface: These films are built by successive adsorption of polyanions and polycations. Within the framework of this study, we worked on various types of films to characterize their physico-chemical properties by optical waveguide light spectroscopy, quartz crystal microbalance, confocal microscopy and atomic force microscopy. Other share, we have evaluated the interactions of the cells with films.

A first part of my work consisted in characterizing films worked out containing poly(L-Lysine) and of poly(L-Glutamique acid). Several parameters of constructions were tested (pH, salt rate, numbers of layers deposited...). The adsorption of serum proteins on films was also evaluated, as cellular adhesion in the short run by experiments of micromanipulation. In a second part, we focused ourselves on films multilayer containing polysaccharides, in particular chitosan and hyaluronan.

After having characterized the growth and the structure of these films, we then studied the cellular and bacterial adhesion. We in particular highlighted that a stiffness of films changes significantly the adhesion properties: the reticulation of films increasing the cellular adhesion.

---

**Discipline :** Bioingénierie, Traitement de surface , Biomatériaux

---

**Mots-clés :** Traitement de surface, Auto-assemblage, Multicouche de polyélectrolytes, Adhésion cellulaire, Biodégradable, Hyaluronane, Poly(L-Lysine), Chitosane, Réticulation, Biomatériaux, Module d'Young

---

**Adresse :** Institut National de la Santé et de la Recherche Médical, Unité 595, Faculté de Médecine , 11 rue Humann, 67085 Strasbourg Cedex, France